

Accepted for publication in ApJS

THE *SPITZER* INFRARED SPECTROGRAPH SURVEY of PROTOPLANETARY DISKS IN ORION A: I. DISK PROPERTIES

K. H. Kim^{1,2}, Dan M. Watson², P. Manoj^{2,13}, W. J. Forrest², Elise Furlan³, Joan Najita⁴, Benjamin Sargent⁵, Jesús Hernández⁶, Nuria Calvet⁷, Lucía Adame⁸, Catherine Espaillat⁹, S. T. Megeath¹⁰, James Muzerolle¹¹, M. K. McClure¹²

ABSTRACT

We present our investigation of 319 Class II objects in Orion A observed by *Spitzer*/IRS. We also present the follow-up observation of 120 of these Class II objects in Orion A from IRTF/SpeX. We measure continuum spectral indices, equivalent widths, and integrated fluxes that pertain to disk structure and dust composition from IRS spectra of Class II objects in Orion A. We estimate mass accretion rates using hydrogen recombination lines in the SpeX spectra of our targets. Utilizing these properties, we compare the distributions of the disk and dust properties of Orion A disks

¹Korea Astronomy and Space Science Institute, Korea Astronomy and Space Science Institute (KASI), 776, Daedeokdae-ro, Yuseong-gu, Daejeon 305-348, Republic of Korea; quarkosmos@kasi.re.kr

²Department of Physics and Astronomy, University of Rochester, Rochester, NY 14627, USA

³Infrared Processing and Analysis Center, Caltech, 770 S. Wilson Ave., Pasadena, CA, 91125, USA

⁴National Optical Astronomy Observatory, 950 North Cherry Avenue, Tucson, AZ 85719, USA

⁵Center for Imaging Science and Laboratory for Multiwavelength Astrophysics, Rochester Institute of Technology, 54 Lomb Memorial Drive, Rochester, NY 14623, USA

⁶Centro de Investigaciones de Astronomía, Apdo. Postal 264, Mérida 5101-A, Venezuela

⁷Department of Astronomy, University of Michigan, 830 Dennison Building, 500 Church St, Ann Arbor, MI 48109, USA

⁸Facultad de Ciencias Físico-Matemáticas, Universidad Autónoma de Nuevo León, Av. Universidad S/N, San Nicolás de los Garza, Nuevo León, C.P. 66451, México

⁹Department of Astronomy, Boston University, 725 Commonwealth Avenue, Boston, MA 02215, USA

¹⁰Ritter Astrophysical Research Center, Department of Physics and Astronomy, University of Toledo, 2801 W. Bancroft St., Toledo, OH 43606, USA

¹¹Space Telescope Science Institute, 3700 San Martin Dr., Baltimore, MD 21218, USA

¹²ESO, Karl-Schwarzschild-Str. 2, D-85748, Garching bei München, Germany

¹³Department of Astronomy and Astrophysics, Tata Institute of Fundamental Research, Homi Bhabha Road, Mumbai 400 005, India

to those of Taurus disks with respect to position within Orion A (ONC and L1641) and to the sub-groups by the inferred radial structures, such as transitional disks vs. radially continuous full disks. Our main findings are as follows. (1) Inner disks evolve faster than the outer disks. (2) Mass accretion rate of transitional disks and that of radially continuous full disks are statistically significantly displaced from each other. The median mass accretion rate of radially continuous disks in ONC and L1641 is not very different from that in Taurus. (3) Less grain processing has occurred in the disks in ONC compared to those in Taurus, based on analysis of the shape index of the 10 μm silicate feature ($F_{11.3}/F_{9.8}$). (4) The 20–31 μm continuum spectral index tracks the projected distance from the most luminous Trapezium star, θ^1 Ori C. A possible explanation is the effect of UV ablation of the outer part of the disks.

Subject headings: accretion, accretion disk — protoplanetary disks — stars: pre-main sequence — infrared: stars — surveys

1. INTRODUCTION

In the process of star formation, young stars have circumstellar disks called “protoplanetary disks”. Protoplanetary disks evolve from optically thick flared disks toward optically thin, flat, tenuous disks, and these disks are known as the birth-places of planets. The infrared-based classification of the spectral energy distributions (SEDs) of young stellar objects (YSOs) by Lada (1987) divides this evolution into three stages, Classes I-II-III. These classifications are based on the spectral slope (α) of the infrared SEDs between near- ($\sim 2 \mu\text{m}$) and mid- ($\sim 25 \mu\text{m}$) infrared. Class I objects ($\alpha > 0$) have SEDs with increasing infrared emission dominated by the envelope, as expected from protostars. Class II objects ($-2 < \alpha < 0$) have relatively flat or negative SED slopes, corresponding to excess emission over infrared wavelength ranges produced by a dusty and optically thick disk around a pre-main sequence star. Class III objects ($\alpha < -2$) have SEDs with very little or no disk emission at infrared wavelengths indicating that a disk is much evolved and settled toward to the midplane with large sized grains or has largely or completely dissipated.

Andre et al. (1993) extended the classification to an earlier Class 0 based on millimeter wavelength emission. Adams et al. (1988) modeled T Tauri stars with flat infrared spectrum and Greene et al. (1994) classified spectra with spectral indices between -0.3 and 0.3 as flat spectrum (FS) sources since their spectral slopes are between Class I and II. The SED classes are closely, though not perfectly, matched to evolutionary stages (cf. Robitaille et al. 2006). Classes 0, I and FS correspond to the progress of the accretion and dispersal of the protostellar envelope, and the reduction of the central star’s average accretion rate through the range 10^{-4} – $10^{-7} M_\odot \text{yr}^{-1}$. In the Class II phase, the disk’s gaseous and small-grain components evolve and dissipate, while the central star’s accretion rate decreases from 10^{-7} to $10^{-10} M_\odot \text{yr}^{-1}$. Effects of orientation can make an object from one *evolutionary* stage appear to be in a different SED class; for example, a pro-

protoplanetary disk without an envelope, viewed edge on, may belong to the Class I SED type as in case of DG Tau B (Watson et al. 2004).

Throughout a disk’s life, its material is accreted toward the central star. A classification based on accretion indicators (for instance, H_{α} equivalent width being greater/less than 10 Å) divides T Tauri stars into classical T Tauri stars (CTTS) and weak-lined T Tauri stars (WTTS), which generally correspond closely to Class II and Class III, respectively.

The transitional disks (TDs) have the appearance of a Class III YSOs at shorter infrared wavelengths and Class II YSOs at longer wavelengths (e.g. Espaillat et al. 2014). Therefore, TDs are young systems which have AU-scale radial gaps or central clearing in their dust distribution while they still have optically thick and gas-rich outer disks. There are several mechanisms, such as photoevaporation, dust coagulation and grain growth, MRI instability, and giant planet formation, to explain the origin of gaps and holes in TDs. An interesting finding from the previous studies is that recent observations (e.g. Andrews et al. 2011; Olofsson et al. 2011; Casassus et al. 2013) of TDs and the statistical study of the properties of TDs (Kim et al. 2009, 2013) support the idea that giant planet formation produces the gaps of TDs. Kim et al. (2013) presented observationally and statistically significant trends in mass accretion rates (\dot{M}) showing that mass accretion rates of TDs are reduced by about one order of magnitude compared to the typical \dot{M} of CTTS (Najita et al. 2007; Espaillat et al. 2012). This strongly suggests gap opening and disk clearing by newly-formed planets in disks (Lubow & D’Angelo 2006).

The direction of evolution of protoplanetary disks does not proceed in one universal way. Some disks with weak mid-IR excess suggest that their disk material depleted in a global and homologous manner (e.g. Hernández et al. 2007; Currie et al. 2009). YSOs are also known to evolve along different tracks depending on their masses. A young star called a Herbig Ae/Be star has spectral type of A or B, with masses between 2 and $10 M_{\odot}$. T Tauri star has spectral type between F and M, with masses less than $2 M_{\odot}$. The more massive Herbig Ae/Be stars and their disks evolve much faster than T Tauri stars. T Tauri stars will end up as stars similar to the Sun.

In this paper, we focus on Class II YSOs including TDs, associated with T Tauri stars, because the seeds of planets are thought to be formed in the dusty and massive disks present during this phase of evolution. Especially we will explore the characteristics of Class II YSOs in the Orion A star-forming region, and we will compare their properties with those of YSOs in other nearby star-forming regions, such as NGC 1333, Chamaeleon I and Taurus.

The entire Orion A molecular cloud appears to be a filament that is roughly perpendicular to the line of sight at a distance of 414 pc (Menten et al. 2007). Fits of stellar-evolution models to the color-magnitude diagrams of their member stars give ages of <1 Myr in the Orion Nebular Cluster (ONC) (Hillenbrand 1997) and ~ 1 Myr for the southern part of Orion A LDN 1641 (L1641) (Gálfalk & Olofsson 2008). YSO association age is a difficult subject. We will assume that the ages of the young clusters addressed in this paper lie in the range 0.5–5 Myr, and that the color-magnitude diagrams correctly rank the typical ages, with ONC, L1641 and NGC 1333 being the youngest

regions, Chamæleon I being the on the oldest, and Taurus star-forming region in between. Orion A differs from other nearby (≤ 500 pc) YSO associations studied with *Spitzer*, in that it is the only one that harbors an OB association. Yet it also includes regions in the L1641 molecular cloud with stellar density and UV intensity as low as in the fiducial low-mass star-formation region, Taurus.

To reveal the evolutionary characteristics of protoplanetary disks in Orion A, we use Spitzer-IRS observations of 319 protoplanetary disks in Orion A and follow-up observations of 120 objects with IRTF/SpeX. To explore the effects of environment on disk evolution and planet formation, we compare the structural and dust properties of Orion A disks to those of the much sparser Taurus association (Furlan et al., 2006, 2009, 2011).

This paper is organized as the following ways. In Section 2, we describe the observations and data reduction process. We report the basic stellar properties and disk properties derived from IRS spectra in Section 3 and Section 4. Then, we compare the observed and derived stellar and disk properties of Orion A young members to those of Taurus members in Section 5. The main purpose of this paper is to make available measurements of the properties we measure from IRS spectra and conduct basic analysis to find how Orion A disks differ from disks in other regions. We will discuss many detailed correlations between properties as key clues of disk evolution in a forthcoming paper (Kim et al. 2016, in preparation). In Section 6, we discuss how the evolution of protoplanetary disks is affected by the ultraviolet radiation field, by comparing disk properties by the distance from θ^1 Ori C, the most luminous O star in ONC. Finally, we summarize our results in Section 7.

2. OBSERVATIONS AND DATA REDUCTION

We present 319 objects observed with *Spitzer*/IRS in the Orion A star-forming region in this paper. Some of the objects classified as TDs in section 4.3.2 of this paper were presented in Kim et al. (2013). We described the *Spitzer*/IRS and IRTF/SpeX observations and data reduction process in Kim et al. (2013). Therefore, here, we will describe our observations and data reduction process more briefly.

2.1. *Spitzer*/IRS

The Orion A objects in this paper were selected based on the identification of young stars with disks by IRAC/2MASS color-color diagrams (Megeath et al. 2012). We observed them using *Spitzer*/IRS during campaigns 36, 39, 40, and 44 between 2006 November and 2007 October. We include 303 Class II objects which we classified based on their Spitzer 4.5 to 22 μm spectral index. Of these, we observed 241 with full IRS wavelength coverage of 5-37 μm (SL and LL modules). In addition, 62 objects located close to Trapezium region were observed with partial wavelength coverage (5-14 μm ; SL only) because the detectors for the longer wavelengths would have been

saturated by bright background emission. To this group we added 16 additional objects (5 in ONC; 11 in L1641) which were reclassified as Class II from Class 0/I sources observed in the Orion A protostar survey by Poteet et al. (2016, in preparation). 14 of these 16 were observed during campaigns 39 and 40, but 2 sources were observed in campaign 56. This gives us a total of 319 sources with 62 near the Trapezium, 132 in the ONC, and 125 in L1641 in this paper. Table 1 gives the IRS observation log, including coordinates, observation date, observing mode, AOR ID, and campaign numbers. The positions of these IRS targets in ONC, L1641, and the Trapezium are indicated in Figure 1, Figure 2, and Figure 3, respectively.

We began with version S15.3 of the basic calibrated data (BCD) product from the Spitzer Science Center IRS pipeline for both SL and LL. As described in detail by Kim et al. (2013), we first fix bad, hot and rogue detector-array pixels before extracting objects from the 2D spectral images. Since the spectral extraction of Orion objects needs very careful background subtraction due to the complex and strong sky emission varying spatially and the high stellar density, we used four different source extraction methods to optimize the rejection of emission from background sky and nearby sources. The first method is to extract the spectral source using an automated extractor (“auto”) with two versions of sky subtractions: sky subtraction of the two nods (“off-nod”) and sky subtraction of the sky spectrum in each grating order obtained while the target was being observed in the other order (“off-order”). If the sky subtracted 2D images and the reduced spectra have artifacts attributable to sky-subtraction and/or contamination from nearby sources, we re-extract the source by removing the sky with 0th or 1st order polynomial fitting to the background emission on either side of the target. We call this method “man” because we selected the sky manually. In both “auto” and “man”, we extracted sources from the uniformly-weighted signal along a tapered column, 3-5 pixels wide using the Spectral Modeling, Analysis and Reduction Tool (SMART; Higdon et al. 2004).

The other two methods are to reduce spectra from optimal point-source extraction. One is the AdOpt routine in SMART (Lebouteiller et al. 2010). It uses an empirical point response function (PRF) and can fit multiple objects along the slit. The other script is OPSE, developed separately from SMART (Tayrien & Forrest 2016, in preparation). OPSE uses an analytical PRF and accounts for pointing errors along the slit. The sky is modeled as a linear function of distance in the 5-9 pixel long extraction window.

We calibrated the flux of spectra by multiplication with relative spectral response functions (RSRFs), which were generated by dividing a template of a calibration star’s intrinsic spectrum by the calibrator’s spectrum obtained from its raw spectral extraction, extracted in the same way as the target spectrum. Our photometric standards were α Lac (A1V; M. Cohen 2003, private communication) for SL, ξ Dra (K2III; M. Cohen 2003, private communication) for the part of LL at wavelength less than 32 μm , and Mrk 231 (J.Marshall 2007, private communication) for LL beyond 32 μm .

After comparing the spectra reduced from the different source extraction methods for each

object, we selected the final spectrum with the fewest artifacts. To obtain such a spectrum, we combined spectra extracted in different ways to create the spectrum adopted here, if necessary. For example, we use the combined spectrum for OriA-19, which is mixed and matched with SL1 and SL2 from AdOpt and LL1 and LL2 from OPSE. We list the reduction choices for the final selection of spectra in Table 1.

Not all of our sources have been cited in the literature. We list some selected identifications of the targets in Table 2. In many cases, objects are primarily identified by their coordinates, and it is convenient to name the object according to its coordinates. However, to discuss the sources more easily, we cite the ID number given in Table 1 throughout this paper (e.g., OriA-123 or 123 if the list of objects is long).

2.2. IRTF/SpeX

Of our 257 IRS targets observed in both SL and LL modules in Orion A with *Spitzer*/IRS, we observed 120 at near-IR ($0.8\text{--}2.4 \mu\text{m}$) wavelengths with the medium resolution spectrograph SpeX (Rayner et al. 2003), on the NASA Infrared Telescope Facility (IRTF) on Mauna Kea during the 2010A, 2011A, and 2011B semesters.

We observed all of the SpeX targets with the Short-wavelength Cross-Dispersed mode (SXD). We obtained spectra with various slit widths of $0.3''$, $0.5''$ and $0.8''$ for observations depending on the seeing conditions of each night. We used only the $0.8''$ slit width for the observations of 2011 February because the weather and seeing were generally poor.

During the SpeX observations, we discovered that some of the IRS targets are multiple systems. Among the SpeX targets with close companions, the companions of four objects, OriA-38, OriA-173, OriA-208, and OriA-290, were observed separately from the primary targets. For targets with very close neighbors, OriA-4, OriA-26, OriA-47, OriA-98, and OriA-280, we oriented the slit so as to observe both simultaneously and extracted the spectra of primary and secondary separately during the data reduction process. We also found that OriA-22, OriA-125, OriA-154, OriA-213, and OriA-233 were potential binary systems because they appeared elongated and peanut-shaped in the K-band guider images. The components of these systems were not clearly resolved, so we present their SpeX spectra as combined spectrum from both primary and secondary of the binary. Among those close and/or suspicious binaries observed with SpeX, OriA-26 is the only one identified as a spectroscopic binary based on radial velocity measurement by Tobin et al. (2009, 2013).

We observed an A0V star, HD 37887, every 30–60 minutes for flux calibration and telluric absorption correction (Vacca et al. 2003). To allow for changing the slit orientation to avoid including nearby sources, we also observed the calibrator source with the same slit position angle as the target’s slit position angle. The IRTF/SpeX observation log is given in Table 3. We reduced our spectra with the Spextool package (Cushing et al. 2004), and flux calibration and telluric absorption correction (Vacca et al. 2003) were done with a spectrum of HD 37887, observed near

in time and air mass to each object. In a few exceptional cases, we used a telluric calibration spectrum taken later in time and made a light loss correction to correct a target spectrum for slit losses relative to the flux calibrator, HD 37887.

2.3. Ancillary Photometry

We compiled broadband photometry to construct SEDs in addition to IRS and SpeX spectra. We gathered optical photometry from the Naval Observatory Merged Astrometric Dataset (NOMAD: Zacharias et al. (2005)) with B, V, and R bands at 0.44, 0.55, and 0.64 μm , respectively. For ONC sources, we acquired additional data from da Rio et al. (2010) at U, B, V, TiO, and I bands centered at 0.347, 0.454, 0.538, 0.6217, 0.862 μm , respectively. More optical and near-IR photometry were added from the Sloan Digital Sky Survey (SDSS) photometric catalog (release 8, Adelman-McCarthy & et al. (2011)) at u, g, r, i, and z bands centered on 0.31, 0.48, 0.62, 0.76, and 0.91 μm , respectively. We also take I, J, and K bands at 0.8, 1.25, and 2.16 μm , respectively, from DENIS database (DENIS Consortium 2005). We collected 2MASS J (1.25 μm), H (1.65 μm), and K_s (2.17 μm) magnitudes from 2MASS catalog (Skrutskie et al. 2006). Most of our targets (except OriA-146, OriA-158, OriA-302, and OriA-306) have 2MASS photometry. We adopt J, H, and K magnitudes from Prisinzano et al. (2008) for OriA-306. Additionally, photometry at bands Z (0.88 μm), Y (1.03 μm), J (1.25 μm), H (1.63 μm), and K (2.20 μm) from the UKIRT Infrared Deep Sky Survey (UKIDSS DR8, UKIDSS Consortium (2012)) were collected. IRAC (3.6, 4.5, 5.8, and 8.0 μm) and MIPS (24 μm) photometry of our sources had been acquired prior to the IRS observations (Megeath et al. 2012), and we included them. We also include near- to mid-IR observations at 3.4, 4.6, 12, and 22 μm from the Wide-field Infrared Survey Explorer (WISE) all-sky data release (Cutri & et al. 2012). It is recommended to use WISE photometry with caution due to the source extraction methods used in the pipeline (e.g., Koenig & Leisawitz 2014). We include WISE photometry only if a corresponding observation has a “ex” tag value of zero, i.e., not an extended source, to avoid including neighboring objects because WISE has relatively coarse resolution. We find these criteria eliminate WISE data which show spurious jump compared to IRAC and MIPS photometry in their SEDs.

In case there are multiple (mostly two or three) sets of UKIDSS and SDSS for an object within a distance of 3 arcsec from our target position, we include the combined photometric points of multiple sets for the corresponding SEDs, as we cannot ignore the possibility of multiple system. Tobin et al. (2009, 2013) identified 89 spectroscopic binaries (SBs) in the ONC with high/moderate confidence. Among those 89 SBs, 13 objects match with our objects in ONC. The corresponding objects are OriA-5, 26, 37, 45, 60, 88, 91, 111, 142, 148, 180, 189, and 205. Five of them are double-line binaries (OriA-37, 45, 60, 91, and 111), and the remaining sources are single-lined binaries. We have checked if 13 SBs have multiple UKIDSS and/or SDSS photometry. OriA-26 is the only object with multiple sets both by SDSS and UKIDSS. OriA-37 and OriA-60 have multiple sets of UKIDSS. However, we do not discuss multiplicity further here. A comprehensive discussion of the

multiplicity of these objects awaits higher spatial and spectral resolution observations.

3. BASIC CHARACTERISTICS OF THE STARS

3.1. Spectral Types and Effective Temperatures

For the most part, we gathered the spectral type (SpT) of our targets from the literature (Hillenbrand 1997; Rebull et al. 2000; Allen 1995; da Rio et al. 2010; Fang et al. 2009; Parihar et al. 2009a; Hsu et al. 2012). We also added unpublished results kindly provided by John Tobin and Jesús Hernández. We utilized SpeX spectra to determine spectral types for objects without spectral type information from the literature. As we have described (Kim et al. 2013), to determine spectral type from SpeX spectra, we compared absorption features of Na I, Al I, Mg I, Ca I and CO in source spectra to those of template spectra (Rayner et al. 2009; Cushing et al. 2005). In addition, we have updated spectral types adopted in Kim et al. (2013) with spectral types for L1641 young stars from Hsu et al. (2012). Spectral types of OriA-230, OriA-271, and OriA-294 derived previously from SpeX spectra (M0.0, M2.0, and M2.5 respectively) were replaced with the spectral types of Hsu et al. (2012) (M3.5, M0.2, and M2.0 respectively). These modest differences in spectral types between our determination and Hsu et al. (2012) ($\Delta(\text{SpT}) = 3.5, 1.8, \text{ and } 0.5$, respectively) prove that our spectral type derivation using SpeX spectra is sufficient to narrow the spectral type range down to 2–3 sub-types. Hence, we still adopt spectral types derived from SpeX spectra for 7 objects (OriA-11, 16, 29, 34, 249, and 302) because there is no alternative in the literature for them. The spectral types reported in the literature and the adopted spectral types are listed in Table 4. Most cases, the reported spectral types for an object agree in few sub-types. Less than 10% of the objects with known spectral types have broad range of reported spectral types.

The spectral type distribution for objects with available spectral type information is shown in Figure 4. The distribution shape of the histograms generally agree with the previous studies of objects in ONC (Hillenbrand et al. 2013) and in L1641 (Fang et al. 2013; Hsu et al. 2013), even though we do not have complete spectral type information. The total number of objects with known spectral type is 229: 48 objects in Trapezium with partial IRS spectra, and 181 objects for which we have the full range of IRS spectra in ONC (89 objects) and L1641 (92 objects). The fractions of our IRS targets for which we have spectral types are 77%, 67%, and 74% for the Trapezium, ONC and L1641, respectively. The median spectral type of Class II objects in Orion A is M0: M1 for objects in the Trapezium; M0 for objects in the ONC; and M1 for objects in L1641 (see Figure 4).

We adopted the effective temperature (T_{eff}) and bolometric correction (BC) scale for pre-main sequence (MS) stars derived by Pecaut & Mamajek (2013). They found that pre-MS T_{eff} are ~ 250 K cooler than MS T_{eff} for G5 through K6 types while other spectral types T_{eff} agree in ~ 100 K between pre-MS and dwarfs. The accounted systematic plus statistical uncertainty of pre-MS T_{eff} is less than 1% of T_{eff} (Pecaut & Mamajek 2013). These new scales for pre-MS stars are fully available only for spectral types F0 to M5 in Table 5 in Pecaut & Mamajek (2013). For

spectral types earlier than F0 and later than M5, we consulted with Pecaut & Mamajek (private communication) to find the best way, and we adopted the following combination. For spectral types earlier than F0, we took the T_{eff} and BC scales for dwarfs in Table 5 in it. For spectral types later than M5, we adopted the T_{eff} of dwarfs for spectral types later than M5, and we used the BC scale of pre-MS. For the objects of unknown spectral types, we adopted an effective temperature of 3770 K, which is the temperature of the mean spectral type (M0) of Class II sources with known SpT in Orion A. The uncertainty of T_{eff} lies within the typical uncertainty of spectral types, which can be translated into about 345 K as a median temperature difference between few (~ 3) sub-spectral type differences. We adopt it as a typical uncertainty of T_{eff} .

3.2. Extinction Correction

We correct for extinction toward our sources to minimize the extinction effects on disk classification and interpretation of our data. The way of estimating visual extinction (A_V) toward our targets is described in detail in Kim et al. (2013). Basically, we use the relationship

$$A_V = \frac{\frac{A_V}{A_{\lambda_2}}}{\frac{A_{\lambda_1}}{A_{\lambda_2}} - 1} \times E(\lambda_1 - \lambda_2), \quad (1)$$

where $E(\lambda_1 - \lambda_2)$ is the color excess between two wavelengths (λ_1 and λ_2) which is equal to $([\lambda_1] - [\lambda_2])_{obs} - ([\lambda_1] - [\lambda_2])_{int}$. To derive the color excess, $E(\lambda_1 - \lambda_2)$, we take J, H, and K bands from 2MASS and I and J bands from DENIS and adopt $I - J$, $J - H$, and $H - K$ photospheric colors from Pecaut & Mamajek (2013). For sources without available spectral type information, we adopt an intrinsic color from $J - H$ and $H - K$ of the Classical T Tauri Star (CTTS) locus of colors from Meyer et al. (1997). The CTTS locus is indicated over the color-color diagram of our sample using 2MASS photometry in Figure 5. In Equation 1, A_λ is the extinction at a wavelength of λ . We assume the optical total-to-selective extinction ratio, R_V , to be 5 because (1) R_V values of dense clouds are usually between 4 and 6 (Mathis 1990) and (2) measures of R_V for lines of sight in Orion have confirmed that $R_V \sim 5$ (Cardelli et al. 1989). Therefore, we make use of the extinction curve with $R_V = 5.0$ from Mathis (1990) to obtain A_λ at the wavelengths of the I, J, H, and K band.

We employ extinction laws depending on the A_V values inferred from Equation 1. We take the Mathis (1990) extinction curve with $R_V = 5.0$ in the case of $A_V < 3$. If $A_V > 3$, we used the extinction curve corrected for standard-star photospheric SiO absorption near 8 μm (S. Fogerty, in private communication) from the empirical extinction curves of McClure (2009) which present two composite extinction curves, one for $3 < A_V < 8$ and one for $A_V > 8$.

To select a final A_V for an object, we examine the SEDs which are extinction corrected with the derived A_V s from each intrinsic color choice. We make a judgment based on freedom from artifacts of the correction (e.g. artificial CO₂ ice features or spurious structure in the silicate

features) and good agreement with the photospheric spectrum of the star’s type, to find the most reasonable A_V . In spite of our best effort of judgment, we have some ($\sim 10\%$) objects which show modest or strong UV/optical excess in the extinction corrected SEDs. There are several possible explanations for the UV/optical excess, including contributions from background nebulosity, jets, over-correction of extinction, and/or less accurate photometry, if not all. The over-correction of reddening seems to be frequent in case the spectral type of an object is not known. We speculate that the following objects are over-corrected: OriA-31, 54, 65, 162, 207, 251, 255, and 297 due to the limit of spectral type information; and OriA-221 and 231 due to some other reason, since none of the various values of A_{Vs} are reasonable. We find frequently that photometry data from NOMAD show a sudden increment compared to other photometry, and the objects suffering this problem are OriA-30, 58, 66, 84, 97, 103, 127, 128, 183, 190, 192, 194, 206, and 222. They are usually located in nebulous regions. Another group for which we consider nebulosity and jets as possible contributors are OriA-3, 30, 37, 78, 81, 86, 90, 91, 122, 125, 217, 242, and 259. Among them, OriA-37, OriA-90, and OriA-91 are related with HH 505, HH 885, and HH 888, respectively. Even though we do not know the spectral type of OriA-207, it could be an edge-on disk because it shows up as an hourglass shape in the SDSS9 scattered light image. As can be seen from the preceding discussion, there is difficulty in measuring accurate extinction. We present final A_{Vs} and uncertainties along with the A_V method selected for each object: $I - J$, $J - H$, and $H - K$ in Table 4.

The estimation of extinction bears several sources of uncertainty: the uncertainties of photometry, intrinsic color, spectral type, and extinction curve. We do not account for all of those uncertainties because those uncertainties are not larger than the range of A_V values estimated through different choice of color excess described above. We indicate the range of A_{Vs} for each object with the finally selected A_V in Table 4. The range of A_{Vs} for most objects lies in few magnitudes: the average offset of the smallest from the adopted A_V is 1.65 for objects which have the lower offset is less than 3 magnitudes (77%); the average difference between the highest and the adopted A_V is 1.67 for objects which have the offset is less than 3 magnitudes (43%). Only 2% of our sample have the lower or upper offset greater than 10 magnitude from the adopted A_V .

The distributions of the visual extinctions according to the sub-regions of Orion A are shown in Figure 6. When taking only objects with known spectral types, the median A_V of L1641 ($A_V=2.34$) is higher than that of the Trapezium ($A_V=1.26$) or ONC ($A_V=1.25$). We performed Kolmogorov-Smirnov (K-S) tests on the distributions of A_V of pairs of sub-regions and list the results in Table 5. From the K-S test, where D is the maximum difference between the empirical distribution function of two groups and p indicates the probability that there is no significant difference between the distributions, we confirm that the difference of A_V distributions by sub-regions is real and significant. The differences are caused by the following mechanisms: (1) less extinction for the objects located in a cavity in the Trapezium and the ONC due to the strong UV field from OB stars in the Trapezium, which has blown out small dust grains (Hillenbrand 1997); (2) large extinction for the objects located inside of several local dark clouds in L1641. We verified

that the objects with the highest visual extinction values reside in denser clouds within this region. The trend of the A_V medians in the Trapezium, ONC, and L1641 imply that most of the extinction is local, within the star-forming region and not along the largest part of the line of sight between Orion and the Earth (observers).

3.3. Spectral Energy Distributions

We constructed SEDs of our sample with the broad band photometry that we assembled in Section 2.3 and SpeX and IRS spectra. We plot SEDs of 257 Class II objects observed in full IRS wavelength coverage from 5.2–37 μm in Figure 7. We only present the SEDs of 44 of 62 objects observed with partial IRS wavelength coverage of 5.2–14 μm in Figure 8, because there are 18 objects in the Trapezium for which IRS spectral data was saturated at some wavelengths and hence unusable.

There are ten spectra among 257 observed in full IRS wavelength coverage that we do not include our general analysis. We summarize these ten objects below.

- OriA-7, 88, 136, 148: They have incomplete spectra due to saturation.
- OriA-247, 261, 296: They vary substantially over time.
- OriA-216: We identify OriA-216 as a galaxy because the PAH features are located at redshifted wavelengths with $z=0.35$ (Figure 9). It is also classified as a galaxy by SDSS classification (Adelman-McCarthy & et al. 2011).
- OriA-208: The SED of it includes interesting information: the system is revealed as a binary from SpeX observation, and SDSS and UKIDSS photometry agree with our SpeX spectra of the fainter object. It was not possible to distinguish two sources from IRS because the separation is about 1~2 arcsec.
- OriA-95: it is not a galaxy, but it has very uncertain extinction correction.

We do not include these 10 objects for the analysis in the present work, except OriA-88 in the analysis related to TDs.

There are many interesting individual objects in our survey. For example, we speculate possible variable sources based on the flux density disagreement of IRS spectrum with the IRAC and WISE photometry. The possible variability candidates are OriA-6, 9, 60, 61, 117, 166, 189, 190, 197, 202, 210, 212, 231, 244, 247, 256, 258, 261, 276, 277, 289, 301, 304, 316, and 318. We also find several objects with possible outer disk truncation based on the steeply decreasing emission beyond 20 μm : OriA-15, 45, 98, 173, 180, and 225.

A detailed description and discussion of individual objects is deferred to later papers.

3.4. Stellar Luminosity and Stellar Mass

The photospheric emission indicated with long dash-dot line in each SED in Figure 7 and Figure 8 was derived from the intrinsic colors of Pecaut & Mamajek (2013) at temperature T_{eff} , scaled to match the de-reddened 2MASS J band photometry (see SEDs in Figures 7 and 8). From the scaling factor, which is a solid angle applied to the photosphere model to get the observed flux density at J band and the assumed distance to Orion A ($d=414$ pc), we estimate the stellar radius (R_*). We derived the stellar luminosity (L_*) of each object from T_{eff} and the stellar radius (R_*). The adopted T_{eff} and estimated L_* are listed in Table 6. We display the distribution of L_* of 291 objects from the samples in the ONC and L1641 in Figure 10. Performing a K-S test on the luminosity distributions of the ONC and L1641 regions, we conclude there is no significant difference in the distribution of the luminosity of both regions.

To infer the stellar mass (M_*), we plot the derived L_* and T_{eff} of our targets on evolutionary tracks. In this paper, we use the Siess PMS evolutionary tracks (Siess et al. 2000). The adopted M_* in Table 6 are the average M_* read from the tracks of various metallicities. We take the standard deviation of M_* s measured in various metallicity conditions as the uncertainty of M_* . Figure 11 shows the objects with known spectral types in an H-R diagram along with the solar-metallicity ($Z=0.02$) evolutionary tracks as an example. We compared M_* distribution for the Class II disks in ONC and L1641 in Figure 12. There is no significant difference in the mass distribution of the two regions.

Since L_* and M_* distributions between ONC and L1641 are not statistically very different, we will assume that any statistical differences between the two populations seen in further analysis with disk properties or star/disk accretion properties originate in disk properties, not in their stellar properties.

4. DISK PROPERTIES

4.1. Spectral Index

To deduce characteristics of disks, we measure the spectral indices defined as

$$n_{\lambda_1-\lambda_2} = \frac{\log(\lambda_2 F_{\lambda_2}) - \log(\lambda_1 F_{\lambda_1})}{\log(\lambda_2) - \log(\lambda_1)} , \quad (2)$$

where λ_1 and λ_2 are the anchor wavelengths. We use spectral indices to infer the radial and vertical distribution of dust. Spectral slopes between near-IR and mid-IR such as n_{K-25} , n_{5-12} , and n_{12-20} are the spectral indices commonly used for disk classification. We will discuss our usage of n_{K-25} , n_{5-12} , and n_{12-20} for disk classification in Section 4.3.

The indices most commonly used to infer the degree of dust settling (vertical structure) and inner/outer disk truncation (radial structure) are n_{K-6} , n_{6-13} , and n_{13-31} (e.g. McClure et al.

2010; Manoj et al. 2011; Furlan et al. 2011; Arnold et al. 2012). Using self-consistent disk models of T Tauri stars, D’Alessio et al. (2006) discussed the relation between the depletion (ϵ) of the small grains relative to the standard dust-to-gas mass ratio and the spatial distribution of the emergent flux, as well as the dependence of ϵ on other properties such as the radial structure and grains size distributions. The emitting regions, corresponding to fluxes emitted in certain wavelengths, change depending on dust grain sizes and degree of settling. For example, in a case of a model with ISM dust in the least settled disks with the largest depletion parameter ($\epsilon = 1$, i.e. no depletion of small grains in the upper disk layers), most (> 90 %) of the emergent flux at 6, 13, and 31 μm come from less than 0.3, 10, and 75 AU from the host star, respectively, while the most emitted fluxes at 6, 13, and 31 μm are from less than 0.3, 5, and 10 AU, in the case of the most settled disk ($\epsilon=0.001$, i.e. a factor of 1000 depletion of small grains in the upper disk layers) (D’Alessio et al. 2006, Fig. 9). The stellar temperature also affects the distance of the emitting regions from a host star. Stars with higher effective temperature will have a 6 μm flux disk-emitting region beyond 0.3 AU, while this region will be closer to the host star if the star is colder than the effective temperature (4000K) of a typical T Tauri star. Regardless of the host-star’s temperature or the degree of disk settling, the wavelengths of 6, 13, and 31 μm are between the silicate emission features around 10 and 20 μm . Therefore, the spectral indices between two adjacent wavelength regions of them (n_{6-13} and n_{13-31}) are considered continuum spectral indices that can probe different regions of disks. In addition, we make use of n_{K-6} in order to measure characteristics of the innermost parts of disks.

The anchor positions for measuring spectral indices have been selected to be useful in comparison of radial properties of disks from various previous studies (Furlan et al. 2006; McClure et al. 2010; Manoj et al. 2011; Arnold et al. 2012). At each anchor wavelength, we averaged flux values from a small wavelength region to derive a representative flux value; so, for the 5 μm flux (“5”) we used the wavelength region 5.2–5.54 μm ; for “6” we used 5.4–6.0 μm ; for “12” we used 12.7–13.1 μm ; for “13” we used 12.8–14.0 μm ; for “20” we used 19.7–19.95 μm ; for “25” we used 24.5–25.5 μm ; for “31” we used 30.3–31.0 μm . For “K” we adopted the 2MASS K_s (K_s band: 2.00–2.31 μm .)

Spectral indices measured with any combinations of two wavelengths, n_{K-6} , n_{6-13} , n_{13-31} , n_{5-12} , n_{12-20} , and n_{K-25} are listed in Table 7. We report n_{20-31} , which is used as an index of outer disk truncation/evaporation in Section 6, in Table 11. The uncertainties reported with these spectral indices in Table 7 and 11 are the propagated uncertainties from their spectra without including other uncertainties of determination of effective temperatures and extinction.

4.2. Parameters of the Degree of Dust Processing

Along with the continuum spectral indices, which are sensitive to the dust distribution within the disk, we can utilize some parameters that can be extracted from silicate features at 10, 20,

and/or $33 \mu\text{m}^1$ to acquire clues of how much small dust grains are processed.

A parameter commonly used for understanding the strength of absorption or emission features is the equivalent width. The equivalent width for the silicate emission features is a measure of optically thin emission per unit area of underlying optically thick continuum:

$$EW(\lambda) = \int_{\lambda_1}^{\lambda_2} \frac{F_\lambda - F_{\lambda,\text{cont}}}{F_{\lambda,\text{cont}}} d\lambda , \quad (3)$$

where $F_{\lambda,\text{cont}}$ is the continuum emission determined from a polynomial fit to certain wavelength regions where the silicate emission features do not exist.

In the limit of small silicate feature optical depth, the equivalent width is proportional to the optical depth itself, or similarly the column density of dust in the inner disk (Watson et al. 2009). We compute EW10 and EW20 for amorphous silicate emission features around $10 \mu\text{m}$ and $20 \mu\text{m}$. The wavelength ranges for integrating are $8\text{--}13 \mu\text{m}$ and $16\text{--}28 \mu\text{m}$ for $10 \mu\text{m}$ and $20 \mu\text{m}$ features, respectively. We list EW10 and EW20 in Table 8.

Another useful parameter is the integrated flux of the feature, $F(\lambda)$.

$$F(\lambda) = \int_{\lambda_1}^{\lambda_2} (F_\lambda - F_{\lambda,\text{cont}}) d\lambda , \quad (4)$$

$F(\lambda)$, the integrated flux after continuum subtraction, is a probe of the mass of dust lying in the uppermost surface of the disk, while $EW(\lambda)$ indicates the relative strength of the optically thin emission feature to the continuum emission from optically thick dust in the disk. We calculate F_{10} and F_{20} in the same wavelength limits used for the measurement of EW10 and EW20.

A parameter generally adopted as an index of the degree of dust processing is the ratio of the continuum-subtracted and normalized flux at $11.3 \mu\text{m}$ and $9.8 \mu\text{m}$. This index, $F_{11.3}/F_{9.8}$, has been used to probe the degree of grain growth and crystallinity in the inner (1–2 AU) parts of disks (Przygoda et al. 2003; van Boekel et al. 2005; Kessler-Silacci et al. 2006; Honda et al. 2006; Bouwman et al. 2008; Olofsson et al. 2009). When grains are still unprocessed and in their pristine state, amorphous silicate grains show a broad emission peak at $9.8 \mu\text{m}$. As small grains become crystallized, a strong feature at $11.2 \mu\text{m}$, due to forsterite, appears. Also, as grains grow, the broad amorphous silicate feature becomes flat-topped. Therefore, $F_{11.3}/F_{9.8}$ is also known as a shape index because the shape of the silicate feature at $10 \mu\text{m}$ gets broader and flatter as the degree of crystallinity and grain growth gets higher with the larger values of $F_{11.3}/F_{9.8}$. Interstellar grains show narrow silicate profiles indicative of submicron, amorphous grains; protoplanetary-disk grains in addition have profiles with narrow substructure owing to crystallization and widening long-wavelengths due to grain growth. Both forms of processing are captured in the $F_{11.3}/F_{9.8}$

¹We note that the crystalline olivine features at $33 \mu\text{m}$ is not reliable for most objects because there were many noisy pixels over this wavelength range. Therefore, we do not use EW33 for analysis in this work.

(“shape”) index. Previous studies of dust features in Taurus disks (Watson et al. 2009; Sargent et al. 2009) found that the change in shape is mostly due to crystallization.

The major contributor to the uncertainties of extracting information from the silicate emission features at 10 and 20 μm is how to determine the underlying continuum. Based on our previous experiences (e.g. Manoj et al. 2011; Arnold et al. 2012), the determination of continuum of 10 μm silicate feature is better than that of 20 μm feature. We estimate the uncertainties of properties measured with 10 μm silicate features by assuming the uncertainty of 10% in the underlying continuum. We assume an uncertainty of 20 % of the continuum for the measurement of EW20 and other properties measured from 20 μm silicate feature. We report the parameters related to dust processing and their uncertainties in Table 8.

4.3. Disk Classification

4.3.1. Classification of Disks Using Continuum Spectral Indices

One assessment of the evolutionary state of a young stellar object (YSO) comes from the slope of its SED (Lada 1987). Two wavelengths at near- and at mid-IR, typically K ($\sim 2 \mu\text{m}$) and 25 μm , have been used for YSO classification. n_{K-25} is used to define the SED classes: Class I if $n_{K-25} > 0.3$; Flat Spectrum if $-0.3 < n_{K-25} < 0.3$; Class II if $-1.6 < n_{K-25} < -0.3$; Class III for $n_{K-25} < -1.6$. However, as is well known, SED classification can also give a wrong impression of evolutionary state for objects viewed close to face-on or edge-on (Robitaille et al. 2006; Crapsi et al. 2008; McClure et al. 2010).

To minimize the extinction effect on evolutionary classification based on spectral indices, McClure et al. (2010) made good use of the “extinction-free” indices, n_{5-12} and n_{12-20} , which are independent of extinction because A_λ at the anchors are same in the McClure (2009) extinction curves, to classify the evolutionary stages of the YSOs in the Ophiuchus star-forming region (Oph). They calibrated their classification scheme with Class I, II, and III samples in Taurus (Furlan et al. 2006, 2008) and applied to Oph objects. It divides objects into photospheres ($n_{5-12} < -2.25$), disks ($-2.25 < n_{5-12} < -0.2$), and envelope ($n_{5-12} > -0.2$). The second extinction-free index, n_{12-20} , includes not only continuum but also the 20 μm silicate feature. This index is used to determine roughly how much the disk is cleared, i.e., to suggest candidate debris or transitional disks. These extinction-free indices have been used in the literature (e.g. Furlan et al. 2011; Manoj et al. 2011; Arnold et al. 2012) as an initial filter to classify evolutionary stage of objects in the format of n_{K-25} versus n_{5-12} and n_{12-20} versus n_{5-12} .

In Figure 13 and 14 we apply n_{K-25} , n_{5-12} , and n_{12-20} spectral indices of the objects in our Orion A sample to classify their evolutionary stages. We see that our sample is mostly placed into Class II (from n_{K-25}) and disks (from n_{5-12} and n_{12-20}) area in Figure 13 and Figure 14. Some objects, however, are located in the area for “transitional disks”, “FS”, or “envelopes”. We confirm

that all Orion A objects that fall into “transitional disks” region in Figure 14 are the transitional disks previously identified by Kim et al. (2013). Almost half of the objects in the “envelopes” area are also previously identified transitional disks, as indicated with open circles in Figure 14.

We notice that TDs that lie in the “envelopes” region due to their n_{5-12} values have $n_{12-20} \gtrsim 0$ for both ONC and L1641 (see Figure 14). The list of objects which are not identified as TDs but located in the “envelopes” area is as follows, from high to low n_{12-20} : OriA-123, 159, 190, 21, 86, and 305 in ONC; OriA-311, 289, 191, 266, 209, 231, 258, 272, and 312 in L1641. We examine their SEDs and do not find strong evidence for envelopes, such as silicate absorption at $10 \mu\text{m}$, CO₂ ice absorption at $15 \mu\text{m}$ or steeply increasing flux after $20 \mu\text{m}$. Instead, the common characteristics of their SEDs are that they show strong $10 \mu\text{m}$ and $20 \mu\text{m}$ silicate emission features with rather flatter and redder spectral index between $5 \mu\text{m}$ and $12 \mu\text{m}$ while having low/less excess over photosphere at near-IR wavelengths ($< 5 \mu\text{m}$). We investigate the possibility of introducing a strong $10 \mu\text{m}$ silicate feature by over-correcting of extinction. We find that most of them are not highly extincted except two objects, OriA-209 and OriA-231, which have A_V greater than 10. Therefore, the over-correction of extinction of deeply embedded protostars cannot be the major reason for the objects with $n_{5-12} \gtrsim -0.2$ in Orion sample. Even though these objects lie in the “envelopes” area in Figure 14, we do not classify them as “envelopes-dominant” objects.

In order to figure out the differences of classification and sample distribution among star-forming regions, we also plot Taurus and NGC 1333 objects studied in Furlan et al. (2011) and Arnold et al. (2012) in Figure 14. We chose Taurus and NGC 1333 because Taurus is a fiducial region in many studies and NGC 1333 is one of the youngest star-forming region. In the upper panel of Figure 14 we find that two TDs in Taurus are located in the “envelopes” area and that most of Taurus objects having large $n_{5-12} (>-0.2)$ have $n_{12-20} > 0$. We also notice that there are many objects distributed in $-2 < n_{12-20} < 2$ in NGC 1333 in the “envelopes” area. To better demonstrate how the Orion sample and Taurus/NGC 1333 samples in the “envelopes” region in Figure 14 are different, we plot n_{12-20} versus n_{K-25} for them in Figure 15. The objects located in the “envelopes” area in Figure 14 are indicated with colored symbols: magenta for ONC and L1641 and blue for Taurus and NGC 1333. We find that YSOs in our sample of Orion A falling in the “envelope” region as marked in magenta lie in “Class II” by n_{K-25} and “disks” by n_{12-20} , while most Taurus and NGC 1333 objects marked by blue squares are located in “Class I” or “FS” area in Figure 15.

The classification scheme by n_{5-12} versus n_{12-20} has worked well to reclassify as disks some disk-dominant objects that fall into Class I region according to n_{K-25} . Conversely, we would like to understand why so many YSOs in Orion A that lie in the “envelopes” are of the n_{5-12} index are classified as Class II based on n_{K-25} . Considering that the Orion sample was selected as exclusively disk candidates from IRAC/2MASS color-color diagrams from Megeath et al. (2012), the possible dominant reason of this different classification is because we have several TDs with a steep rise between 5 and $12 \mu\text{m}$ but more moderate changes between 12 and $20 \mu\text{m}$ than envelope sources. If an object is in an initial stage of inner disk dissipation, it would have little excess around $5 \mu\text{m}$,

but still a strong excess at longer wavelengths, so its 5–12 μm spectral index would be large and thus in the “envelopes” area, while its K–25 μm index would be more typical of Class II objects.

From the comparison of sample distributions and source classifications done in Figure 13, 14 and 15, we reaffirm that the disk classification schemes based on spectral indices (n_{K-25} , n_{5-12} and n_{12-20}) work well as a first classification filter and they are complementary to each other, but one needs to check the SEDs carefully to avoid ambiguous classifications.

4.3.2. Transitional Disks

Transitional disks (TDs) have radial gap(s) or central holes, so their SEDs are different from the SEDs of radially continuous full disks (FDs). Thus TDs are distributed in a separate region from the FDs on the spectral indices diagrams. We have described how spectral indices and EW10 can be used to find TD candidates in Kim et al. (2013). Here, we revisit the selection criteria for transitional disks that we described previously (Kim et al. 2013): $n_{K-6} \leq -2.1$; $n_{13-31} \geq 0.5$; $\text{EW10} \geq 4.3$. After updating spectral type information and adding 16 objects in Orion A Class II disk sources, we recalculate the selection criteria to check if any significant changes are needed for the thresholds of n_{K-6} , n_{13-31} , and EW10. We find that the lowest 12.5% (octile) of n_{K-6} and the highest 12.5% of EW10 for Class II disks in Ori A, Tau, Cha I, Ophiuchus, and NGC 1333 are very similar to the previous values. The highest 12.5% of n_{13-31} has somewhat noticeably changed from 0.5 to 0.57, but this change is still uncertain and does not affect much on the TDs already identified. Therefore, we keep the selection criteria used by Kim et al. (2013). We indicate how TDs are separated from the distribution of FDs in ONC and L1641 in Figure 16. We identify three more TDs from the 16 Class II disks added in our sample.

There are three subtypes of TDs depending on the disk’s radial structure inferred by the morphology of their SED and self-consistent disk modeling: CTD, PTD, and WTD. CTD is an acronym for “classical transitional disk” – a TD with a central hole. The characteristics of an SED of a CTD is no/negligible disk excess over 2–6 μm and a steep flux increment after 13 μm . A “pre-transitional disk” (PTD) shows a strong disk excess similar to optically thick disk emission in the near-IR, a dip, and redder emission after 13 μm , which is explained with a radial gap between the optically thick inner and outer disk (Espaillat et al. 2007). In case there is weak excess somewhat between that of CTD and PTD, the excess may be due to optically thin inner disk emission. We call these TDs as “weak-excess transitional disk” (WTD). Kim et al. (2013) defined Inner Disk Excess Fraction (IDEF) to classify three subtypes of TDs from their disk excess in 2–6 μm .

Among three newly identified TDs, OriA-306 and OriA-307 belong to the ONC, and they are subclassified as a PTD and a CTD, respectively. OriA-314 belongs to L1641 and is classified as a WTD. Thus, we have a total of 65 transitional disks: 34 in ONC and 31 in L1641.

4.4. Mass Accretion Rates

We observed 120 Class II disks with IRTF/SpeX in SXD mode from 0.8-2.4 μm . We utilize Pa γ (1.094 μm), Pa β (1.282 μm), and Br γ (2.166 μm) which are in the wavelength coverage of SpeX SXD spectra in order to measure mass accretion rates from the hydrogen recombination lines. We start with the de-reddened SpeX spectra with the A_V determined as described in Section 3.2. We obtain mass accretion rates of 113 objects among the 120 observed. The objects excluded from the determination of mass accretion rates are OriA-21, 45, 52, 88, 135, 170, and 266, which are mostly earlier spectral type objects with strong hydrogen absorption lines. We also analyze the reduced SpeX spectra of companions of nine objects, OriA-4, 26, 38, 47, 98, 173, 208, 280, and 290. Among them, six objects show emission of the hydrogen recombination lines, and three companions show absorption lines. We do not include the mass accretion rates of companions in the following analysis due to the lack of information about the companions' properties. In addition, we do not include the mass accretion rate of OriA-208 and OriA-247 in our analysis because they belong to the ten objects that have incomplete IRS spectra, are variable, and/or are a galaxy as described in Section 3.3. Therefore, we use mass accretion rates of 111 objects in ONC and L1641 for any analysis related to disk-stellar mass accretion properties in this work.

To get the mass accretion rates from three hydrogen recombination lines, we first fit each hydrogen recombination line with a gaussian function plus a local continuum to get the line luminosity: $L_{Pa\gamma}$, $L_{Pa\beta}$, and $L_{Br\gamma}$. Then we calculate the accretion luminosity, L_{acc} , from the line luminosity of each hydrogen recombination line. To do so, we adopt the empirical correlations between L_{acc} and L_{line} derived by Muzerolle et al. (1998) for Pa β and Br γ and Gatti et al. (2008) for Pa γ to convert to the line luminosity to the accretion luminosity as follows:

$$\log(L_{acc}/L_\odot) = 1.36 \times \log(L_{Pa\gamma}/L_\odot) + 4.1 \quad (5)$$

$$\log(L_{acc}/L_\odot) = 1.14 \times \log(L_{Pa\beta}/L_\odot) + 3.15 \quad (6)$$

$$\log(L_{acc}/L_\odot) = 1.26 \times \log(L_{Br\gamma}/L_\odot) + 4.43 \quad (7)$$

Finally, we obtain the disk-star mass accretion rate, \dot{M} , from the relation:

$$\dot{M} = \frac{L_{acc}R_\star}{GM_\star}, \quad (8)$$

where R_\star and M_\star are stellar radius and stellar mass which we calculated as described in Section 3.4, and L_{acc} is the accretion luminosity from Equation (5), (6), and (7).

The accretion rate estimates from three recombination lines in our spectra are generally within a factor of 2–3 of each other. We adopt the average \dot{M} and report it in Table 6. We regard the resulting average \dot{M} as an upper limit when fewer than three lines were observed with poor signal-to-noise ratio or when the fitting of three lines are not reliable due to low signal-to-noise. We adopt the average \dot{M} measured from two lines as a detection for some cases if two lines are prominent.

We find that the distributions of mass accretion rates of Class II objects in the ONC and L1641 are not very different when we include all possible \dot{M} in the distributions, either by visual inspection or by the K-S test (Figure 17). We compare \dot{M} distributions of two sub-groups, FDs and TDs, in Figure 18, and check that \dot{M} of TDs are decreased significantly compared to that of FDs. The median values of $\log \dot{M}$ of FDs are -7.81 for ONC and -7.99 for L1641. For TDs, they are -8.71 and -8.79 for ONC and L1641, respectively. We confirm that the difference of the median \dot{M} between FD and TDs in ONC and L1641 is almost a factor of 10, as seen in the Taurus-Aurigae association by Najita et al. (2007) and their extended study including Ophiuchus (Najita et al. 2015).

We compare the median values of \dot{M} between FDs and TDs in the narrower spectral type ranges, K–M, K type, M type, and M3 or later, to investigate any impact by the \dot{M} dependence on spectral types to the different mass accretion distribution between FDs and TDs because TDs are more weighted to the later types (K–M). The number of objects in the K–M group are 56 for FDs and 50 for TDs, which are comparable size of sample between two groups. The median \dot{M} of FDs and TDs for the K–M group are $1.03 \times 10^{-8} M_{\odot}/yr$ and $1.76 \times 10^{-9} M_{\odot}/yr$, respectively. When we take only K type objects, the median \dot{M} are $4.54 \times 10^{-8} M_{\odot}/yr$ for FDs with 23 objects and $4.77 \times 10^{-9} M_{\odot}/yr$ for TDs with 13 objects. We have 33 FDs and 37 TDs in the M type group, and the median \dot{M} is $3.51 \times 10^{-9} M_{\odot}/yr$ and $1.5 \times 10^{-9} M_{\odot}/yr$, respectively. For the M3 or later types with 11 objects of FDs and 18 objects of TDs, the median values are $1.93 \times 10^{-9} M_{\odot}/yr$ and $1.34 \times 10^{-9} M_{\odot}/yr$, respectively. We note that the median values of \dot{M} decreases from K through M/M3 or later types both in FDs and TDs. We find that the median \dot{M} of the K type objects for TDs are almost one magnitude lower than that for FDs. Even though the differences of the median \dot{M} between FDs and TDs for the M type and M3 or later groups are not as large as seen for the K type, the median values of TDs are lower than the median values of FDs in the corresponding sub-groups. Since the number of objects in the each sub-group divided by the spectral type ranges between TDs and FDs are not very different, we confirm that the displacement of the mass accretion rate distribution of TDs from that of FDs seen in Figure 18 are not the result of the intrinsic dependency on the spectral type of the mass accretion rates. The median \dot{M} of the sub-groups are summarized in Table 9.

5. COMPARISION TO DISKS IN TAURUS

In this section, we compare the distribution of spectral indices of the Orion A Class II samples to those of the Class II sample in Taurus. We first compare, in Section 5.1, the whole sample without classifying sources, whether their disk is radially continuous (FDs) or not (TDs). More detailed comparisons of samples of Orion A and Taurus broken down by radial structures (FDs/TDs) follow in Section 5.2.

Our goal is to provide the measured properties of disks in Orion A as well as to discern any differences with disks in Taurus. Therefore, results from an exhaustive study of the characteristics

of Orion A Class II disks and correlations between properties will be discussed in the next paper (Kim et al. 2016b, in preparation). Here, to measure the quantitative difference between the distributions of a given parameter among our sub-region (OriA, Trapezium, ONC, and L1641) and Taurus, we perform a K-S test and measure the median of the property for each group.

We consider a K-S difference D between two groups to be significant if p , the probability that D could result from two random selections from the same distribution, is less than 0.05. If p is less than 0.01, we take the deviation to be a highly significant. With small p , the value of D indicates a significant maximum difference between the cumulative distributions. In our data D varies all the way from nearly unity to about 0.1. The largest values indicate completely distinct, non-overlapping distributions; the smallest values indicate largely overlapping distributions with maximum differences consistent with Poisson statistics and the total numbers in our samples. We rank the significant differences as large ($D > 0.5$), medium ($0.25 \lesssim D \lesssim 0.5$), and small ($D < 0.25$). D and p for all pairs appear along with the histograms in Figure 19–24.

5.1. Index from 5–14 μm spectrum: Trapezium, ONC, L1641 and Taurus

As we described in Section 2, Class II objects in the Trapezium could only be observed with the SL module (5–14 μm). We show the distributions of n_{K-6} , n_{6-13} , EW10, and $F_{11.3}/F_{9.8}$, which are the properties taken from IRS SL spectra of objects in three sub-regions of Orion A and Taurus, in Figure 19, without separating objects by their radial structures.

The distributions of n_{K-6} from the disks in the three sub-regions of Orion A in the upper left panel of Figure 19 show that n_{K-6} of ONC and L1641 is biased toward higher values than Taurus, even though this difference is not statistically significant.

The upper right panel of Figure 19 shows that the distribution of n_{6-13} in ONC is shifted to higher values of n_{6-13} compared to Taurus. A K-S test result for ONC versus Taurus shows that this displacement is statistically highly significant. The n_{6-13} distribution of L1641 also tends to higher values than that of Taurus, but the displacement is not noticeably large.

The distributions of EW10 of the three sub-regions of Orion A in the lower left panel of Figure 19 are all statistically significantly different from that of Taurus: all three are skewed toward larger EW10. The $F_{11.3}/F_{9.8}$ distributions of Orion A disks in the lower right panel of Figure 19 show different distributions by subregion of Orion A. Comparing $F_{11.3}/F_{9.8}$ values of the Trapezium, the ONC, and L1641 to those of Taurus, the D values from K-S tests decrease and the p values increase from Trapezium through ONC to L1641 in the lower right panel. The $F_{11.3}/F_{9.8}$ distribution of ONC is concentrated around smaller values than that of Taurus. Considering the median age differences of ONC, L1641, and Taurus, we may infer that the $F_{11.3}/F_{9.8}$ distribution difference between ONC and Taurus, and the smaller — probably insignificant — difference between L1641 and Taurus, indicate increased processing of dust as time goes on.

On the other hand, despite lots of arguments in ages, the young stars in the Trapezium (i.e., the center of ONC) are probably somewhat younger (Getman et al. 2014; Megeath et al. 2016) than the rest of the ONC, L1641, and Taurus, but its $F_{11.3}/F_{9.8}$ distribution is broad and skewed toward higher values than that of Taurus. This large shape difference between Trapezium and Taurus, which goes in the direction of larger degrees of dust processing, is possibly a disk-evolutionary difference rather than a dust-evolutionary difference: less-processed material at somewhat larger radii, which is still warm enough to contribute significantly to the $10\ \mu\text{m}$ silicate feature, may have been selectively removed from the systems, by radiation from the Trapezium O/B type stars. We discuss the outer disk evolution in Trapezium in detail in Section 6. We also compare subdivisions of $F_{11.3}/F_{9.8}$ distribution separated by the disk radial structures in the following subsection.

5.2. Disk and Dust Processing Indicators from Full IRS Spectra: ONC, L1641 and Taurus

Now, we consider the properties of Class II samples in ONC and L1641 observed with full IRS spectrum, $5\text{--}37\ \mu\text{m}$. Here we look into how the distributions of disk and dust properties are different not only by the star-forming region among ONC, L1641, and Taurus but also by the radial structure of disks between TDs and FDs. We compare the distributions of n_{K-6} , n_{6-13} , n_{13-31} , EW10, and $F_{11.3}/F_{9.8}$. A caveat concerning the comparison of the grouped sub-samples in Orion A and Taurus is the small sample size of TDs in Taurus. The K-S test is powerful two-sample non-parametric test that is reliable even for small number of sample (<10 ; Wall & Jenkins (2003)). Therefore, we perform the K-S test for the sub-samples and discuss their similarities or differences based on the performance. The output from the statistical tests, median and D and p from K-S test, are listed in Table 10.

We find that the distributions of TDs in Orion A or the subsets by the regions, ONC and L1641, are not much different from the distributions of TDs in Taurus for the properties, n_{K-6} , n_{6-13} , EW10, $F_{11.3}/F_{9.8}$, and n_{13-31} , by checking through histograms in the lower panels of Figure 20 through Figure 24.

In the case of FDs, we notice that the properties of FDs in Orion A tend to have higher values than that in Taurus, in general, except n_{13-31} and $F_{11.3}/F_{9.8}$. Even though D is not large in both cases of OriA-Tau and L1641-Tau, D values are larger in the case of the ONC-Tau comparison of FDs than in the case of the L1641-Tau comparison, and p values indicate that the differences between ONC and Taurus are significant for n_{K-6} , n_{6-13} , and EW10.

The spectral index, n_{K-6} in Figure 20 and n_{6-13} in Figure 21, are measures of the optically thick disk continuum structure in the inner radius of a disk. EW10 in Figure 22 is related to the optically thin small dust grains. Therefore, we can infer that disks in the ONC are less processed and still have more flared disks and more small grains in vertically optically thin regions than disks in Taurus. The inner disks in L1641 seem to be more processed than disks in the ONC and less

processed than those in Taurus because their n_{K-6} , n_{6-13} , and EW10 are distributed somewhat in the middle of ONC and Taurus.

Among the properties compared here, EW10 of FDs between ONC and Taurus show the most significant and largest difference. EW10 measures amounts of small dust relative to the underlying dust continuum. From the higher EW10, in spite of higher n_{K-6} and n_{6-13} indicating the less continuum depletion in the ONC, we infer large amounts of small dust in optically thin regions in disks of ONC.

We look into the distribution of $F_{11.3}/F_{9.8}$ to learn more about dust properties in Figure 23. The results from the K-S test for $F_{11.3}/F_{9.8}$ do not support any significantly different distribution between disks in Orion A and disks in Taurus, at a first glance. However, we note the peak and median shift of $F_{11.3}/F_{9.8}$ of FDs: ONC has the smallest median; L1641 has a median larger than that of ONC, but it is smaller than Taurus. These median shifts in $F_{11.3}/F_{9.8}$ along the median ages of star-forming region may be a clue regarding dust evolution (e.g. growth/crystallization). When we include our analysis to include the star-forming regions, NGC 1333 and Chamaeleon I, we observe an interesting evolution of $F_{11.3}/F_{9.8}$ along the median age of star-forming regions: 0.5 (NGC 1333) 0.52 (ONC) 0.53 (L1641) 0.57 (Taurus) 0.59 (Chamaeleon I). However, the dust evolution is very complicated, and a detailed analysis to understand it is beyond the scope of this work.

In contrast to the comparison of the inner disk and grain processing indicators, the comparisons of the distribution of n_{13-31} of ONC, L1641, and Taurus do not show significant differences (Figure 24). This index is sensitive to the degree of sedimentation in the outer disk (e.g. Furlan et al. 2006); thus we find no difference in the settling of dust to the disk mid-plane among these three regions.

Combining our findings from the distributions of n_{K-6} , n_{6-13} , n_{13-31} , EW10, and $F_{11.3}/F_{9.8}$, we suggest that the inner disk evolves faster than the outer disk and dust grain processing (growth and/or crystallization) occurs faster with inner disk evolution while the outer disk is less processed and sedimented at 1-3 Myr old.

5.3. Median Spectra

Analysis with a median SED gives a general insight on how the protoplanetary disks in a star-forming region evolve. D'Alessio et al. (1999) applied a median T Tauri star SED to compare their disk models and observational data of T Tauri stars in Taurus. Their choice of a median SED was with K5–M2 stars in Kenyon & Hartmann (1995) because the majority of spectral types of the disk sample in Taurus lies in spectral types of K5–M2 and the selection of narrow spectral type ranges can reduce the large variation in fluxes by restricting the range of stellar effective temperatures (D'Alessio et al. 1999). In this vein, Furlan et al. (2006) generated a K5–M2 median spectrum in 5–36 μm range with the available IRS spectra of Class II disks in Taurus. After

assembling a more complete sample of disks in Taurus, Furlan et al. (2011) updated the K5–M2 median spectrum of Taurus disks. They were also able to generate median spectra of M3–M5 and M6–M9 with large number of samples. The analysis with the median IRS spectra of Class II disks observed in nearby star-forming regions is a broadly adopted method to evaluate generally the evolutionary state of disks by comparing median SEDs from region to region (Furlan et al. 2006, 2009, 2011; McClure et al. 2010; Manoj et al. 2011; Arnold et al. 2012). Especially the Taurus K5–M2 median has been widely used as a fiducial reference to examine the status of disk evolution in many other works (e.g. Fang et al. 2013).

Therefore, in order to figure out the general state of evolution of Class II disks in ONC and L1641, we generate the median spectra of disks in ONC and L1641, and compare them to the median spectrum of Class II disks in Taurus taken from Furlan et al. (2011). To generate median spectrum, we first select the spectra of disks that do not show evidence of time variability or evidence for a radial gap or central hole. We exclude the spectra without host-star spectral type information in the selection for a median. Then, we group the spectra in three spectral type ranges: A0–K4, K5–M2, and M3–M5(M7). We made the group of K5–M2 because it is a prevailing selection as explained in the previous paragraph. To compare with the median SED of M3–M5 of Taurus, we calculated a median SED of ONC and L1641 with objects having spectral type of M3 or later than M3. The spectral types of all objects used for the ONC median lie between M3 and M5. We include one M7.5 object to generate the L1641 median because the number of L1641 objects in the spectral type ranges (M3 or later) is small. The A0–K4 group has not been used previously with Taurus sample due to the broad range of spectral types and low fraction of objects belong to the group. Even though we hold the similar limitation to calculate A0–K4 median SEDs with Orion A sample, we created the group with A0–K4 objects to check the evolution situation of objects with spectral types earlier than K5 because we have frequently noticed diminishing fluxes in longer wavelength from objects with earlier spectral types in Orion A sample.

With three separated groups, we first normalized the *H*-band flux of each spectrum in each category to the median *H*-band flux of the corresponding group and then we calculate the median flux at individual wavelength, as described in D’Alessio et al. (1999), to minimize the effect of different stellar luminosity in a given group. The displayed median spectra in Figure 25 were normalized to the corresponding median *H*-band flux of Taurus disks in each panel for the comparison to the median spectrum of Taurus. In Figure 25, the Taurus median spectra of K5–M2 and M3–M5 are adopted from Furlan et al. (2011). The Taurus median of A0–K4 is what we calculated in the same manner applied for other median spectra in order to compare with the median spectrum of ONC and L1641.

In the top panels of Figure 25, the median of the A0–K4 group for the ONC and L1641 differ noticeably from the median spectrum of Taurus. The median spectrum of the A0–K4 group in ONC has slightly higher flux levels of disk emission than the A0–M4 median spectrum of Taurus over the wavelength range of SL coverage, but the ONC median spectrum shows steeply decreasing fluxes beyond 13 μm with prominent crystalline-silicate features. The median spectrum of the A0–K4

group in L1641 has high fluxes compared to the A0–K4 median of Taurus over the wavelengths of IRS SL spectral coverage, similarly to the case of ONC median with stronger excess at 5–13 μm , and the L1641 median spectrum also shows lower flux in LL coverage compared to that of Taurus. We also note that the flux level of the L1641 A0–K4 median is higher than the ONC A0–K4 median. There are several possible causes contributing to the steep SEDs beyond 13 μm : disk settling as grains grow and settle toward midplane; outer disk truncation by the gravitational effect of companions; ablation of disk atmosphere by the strong external radiation from nearby OB stars. The objects contributing to the A0–K4 ONC median are OriA-3, 21, 35, 36, 40, 45, 112, 117, 125, 131, 135, 141, 170, 173, and 205. For the A0–K4 L1641 median, the contributing objects are OriA-191, 196, 199, 201, 224, 225, 226, 235, 236, 262, 266, 269, 280, 284, and 295. Among them, OriA-45 and OriA-205 are reported as a double lined and a single lined spectroscopic binary, respectively. We also discussed that OriA-125 is a potential binary system from our SpeX observation as we discussed in Section 2. OriA-280 has a very close neighbor based on the SpeX observation, too. Even though there is still a lack of complete mutiplicity information for objects in Orion, we can speculate that it is not rare that the outer disk truncation happens around A0–K4 host stars due to the gravitational effect by neighbor sources in ONC and L1641. Again, a caveat of the A0–K4 median spectra comparison is that the spectral type range for A0–K4 median is very broad compared to the K5–M2 and M3–M5(M7) median spectra. However, the fractions of non-K type objects used for A0–K4 median for ONC and L1641 are 40% which is comparable to 37.5% of that for Taurus. Therefore, we consider that the samples for A0–K4 median spectra of ONC, L1641, and Taurus are still comparable, even though the median spectra do not represent the disk properties in a narrow spectral type range.

We compare the median spectra of the K5–M2 groups of ONC, L1641, and Taurus in the middle panels of Figure 25. In the case of ONC versus Taurus, the median spectrum from ONC disks has more excess over 5–35 μm , which indicates less evolution of inner disk and less depletion of small (micron-sized) grains than that of Taurus. We notice that fluxes of 50% of objects used for the K5–M2 ONC median are higher than the Taurus K5–M2 median by examining the quartiles indicated with the dotted lines in the panel. On the other hand, the K5–M2 median spectra of L1641 and Taurus are generally similar. Even though some details like grain properties may show somewhat different characteristics, the general degree of dust settling between Class II disks with K5–M2 spectral types in L1641 and Taurus appear to be similar. The quartiles indicated in the plot with the L1641 K5–M2 median support it.

The bottom row in Figure 25 contains the comparison of the M3–M5(M7) median spectra. Due to the small numbers in the group, we included the spectra of M3 and later than M3 to compare to the M3–M5 median of Taurus. In both L1641 and ONC, the M3–M5(M7) median spectra appear to have higher excess emission than Taurus. A possible explanation of this higher emission of disks around host-stars of M3 or later spectral type in Orion A is the younger ages of the systems with M3 or later spectral types in Orion A resulting in less time for disk evolution than the systems in Taurus. Alternatively, the M3–M5(M7) systems in Orion could have had larger initial disk masses

than systems with later spectral type in Taurus. We will discuss the M3–M5 median in a future paper, until such time as a complete survey of Orion A including faint objects is carried out.

In Figure 26 we compare 10 μm silicate features of the A0–K4, K5–M2, and M3–M5(M7) medians of our targets and Taurus to the pristine, ISM-like, silicate feature which is generated from LkCa 15 and GM Aur. LkCa 15 and GM Aur are protoplanetary disks, and they are transitional disks (Calvet et al. 2005) in Taurus and have a silicate features that are most similar to those of ISM dust grains (Watson et al. 2009; Sargent et al. 2009). In the figure we plot the continuum-subtracted and -normalized flux. From that, we can check how the silicate feature strength varies from median to median and how the feature shape differs from median to median. The profile of the 10 μm silicate feature of the K5–M2 median of the ONC is very close to the profile of the pristine silicate feature. However, the profile of L1641 for the K5–M2 median is broader than the width of the profile of the pristine silicate feature, and the height is also decreased compared to that of K5–M2 median of ONC. This indicates that grains grow, and there are smaller amounts of small dust grains compared to the ONC. The K5–M2 median profile shape of L1641 is similar to that of Taurus, even though detailed features and dust compositions might be different. For the M3 and later spectral types, we also see a somewhat similar pattern of profile changes in the case of K5–M2: the median profiles become broader from ONC to Taurus. However, we suspect a greater degree of dust processing in the M3–M5 median for ONC, because the M3–M5 profile of the ONC is neither as smooth nor as narrow as the pristine profile or the K5–M2 profile of the ONC. We notice also that the flatness of the median profile of M3 and later types is increased from ONC toward Taurus, which supports our finding of the evolution trend of $F_{11.3}/F_{9.8}$ as we discussed before. On the other hand, for the K4 and earlier spectral types, the continuum-subtracted and -normalized 10 micron silicate feature looks more evolved for ONC and L1641 than Taurus. As we have seen and discussed in the median comparison in Figure 25, the faster outer disk evolution by dynamical effects and photoevaporative effects in Orion environments, if they are dominant and effective, seem to affect the dust processing in the inner disk and disk surface area that gives rise to the 10 μm silicate emission feature and the 10 μm features to show evidence of more processed dust.

Shuping et al. (2006) discusses the significant degree of grain processing by the UV radiation field of θ^1 Ori C in 10 μm silicate feature of eight proplyds in the vicinity (< 30 arcsec) of θ^1 Ori C. We looked up the spectral types of the proplyds in (Shuping et al. 2006) and found that only four objects have known spectral type information. Three objects have spectral types of early K and one with M type. It looks like our experiments with K5–M2 and M3 later spectral types show the opposite results if we consider only the distance from θ^1 Ori C. However, there is an obstacle in comparing our results directly with their result. The objects in Shuping et al. (2006) are located in much harsher environments (< 0.1 pc from θ^1 Ori C) while our objects are located further than 0.7 pc from θ^1 Ori C. Even though it is difficult to make a clear comparison between our findings regarding silicate dust processing in the A0–K4 median spectra in ONC/L1641 and results from Shuping et al. (2006) due to the limited information, we speculate there are similar

causes of dust processing in the inner disk regions of the objects which shows the evidences of outer disk dissipation, i.e., the flux reduction at longer wavelengths suffered by proplyds due to outer disk erosion by the strong UV radiation. However, we are cautious with any further interpretation because the spectral type range in A0–K4 median is broad and the median cannot represent general characteristics of objects in a narrow range of spectral types.

6. ENVIRONMENTAL EFFECTS AND EVOLUTIONARY FEATURES OF THE OUTER DISKS

The Orion A star-forming region is a much richer environment than Taurus and Cha I, in which the stellar density is small throughout, and the UV radiation field is not much larger than the interstellar field. However, most stars form in denser clusters containing high mass stars (Lada et al. 1991; Carpenter 2000; Lada & Lada 2003; Evans et al. 2009; Koenig & Leisawitz 2014; Megeath et al. 2016), like Orion. Not only the high stellar density in Orion but also the strong ionizing radiation from OB associations affect the evolution of protoplanetary disks. The evidence of action of photoevaporative winds from the Trapezium cluster over the outer disks of protoplanetary disks within or near the Orion Nebula —“proplyds”— were observed by the *Hubble Space Telescope* (HST) (O’Dell & Wen 1994): comet-shaped ionized gas clouds surrounding each disk, and smaller-than-usual disk sizes measured directly from the disk silhouette. The outward truncation of proplyds in ONC has been detected at a submillimeter wavelength with Atacama Large Millimeter/submillimeter Array (ALMA) (Mann et al. 2014).

To test better this hypothesis of outer disk ablation by UV radiation from the Trapezium with IRS spectra, we construct a spectral index sensitive to the optically thick continuum of the outer disk ($r > 5$ AU from 5–37 μm coverage of IRS) and the optically thin small dust grains in the surface of the outer disk, $n_{20–31}$. The anchor points for 20 μm and 31 μm are same as indicated in the Section 4.2, 19.7–19.95 μm and 30.3–31 μm , respectively. The measured $n_{20–31}$ and the projected distances (d) of objects from θ^1 Ori C are listed in Table 11.

We present the variation of $n_{20–31}$ over finer scale of distance by plotting $n_{20–31}$ and the projected distance of each target from θ^1 Ori C in Figure 27. In the figure, we use three different symbols to break the objects into three sub-groups of spectral type ranges as defined in Section 5.3 for the median spectra discussion. This is to examine patterns that are dependent on properties of host stars, if any exist. At first glance, we notice that the objects of A0–K4 group have generally low $n_{20–31}$ while the objects of M3–M6 group are located in rather higher side of $n_{20–31}$. We measure the K5–M2 median and the median of all objects of $n_{20–31}$ of each sub-region to see the general pattern better with the scattered data points in Figure 27. From the medians and the distribution of scattered data points, we see that $n_{20–31}$ of FDs in the region B increases as the projected distance, d , increases. At greater distance ($d > 1.5$ pc), we do not see the steep variation pattern of $n_{20–31}$ as seen in the region B, through region C to L1641.

The distribution of n_{13-31} with the projected distance is shown in Figure 28. Even though the declining pattern of n_{13-31} closer to θ^1 Ori C is not as remarkable as shown for n_{20-31} , there is also a weak declining tendency for n_{13-31} in B and C. We also notice that some objects show significant drop of n_{13-31} in B region.

It seems that the effect of UV illumination by the Trapezium stars, if that is the dominant one, is largest within 1.5 pc (~ 730 arcsec) from θ^1 Ori C, based on the observed variation patterns of n_{20-31} and n_{13-31} . Combining the clues acquired from the observed variation pattern in the distribution of n_{20-31} and n_{13-31} along the projected distance, we suggest a possible solution to explain our observations. Considering that n_{20-31} is the index combining optically thin small grains and the optically thick continuum while n_{13-31} is more directly represents continuum variation, we infer that evaporation of small particles and gases on the surface of the outer disk may be dominant and faster than the outward truncation of the optically-thick disk itself. This may be consistent with outward truncation of the disks by the photoevaporative disk erosion and small dust removal as seen in stars closer (< 0.5 pc) to O type stars in NGC 2244 (Balog et al. 2007, 2008). The ablation of the outer disks are also seen in the disks closer to the central star (O9) in σ Ori cluster from the smaller infrared excess at 70 and 160 μm from PACS observation than disk bearing objects located far from the massive star (J. Hernández et al. 2014, personal communication).

We examine the parameters useful to infer the evolutionary status of inner disks ($r < 1$ AU), n_{K-6} , EW10, F_{10} , and $F_{11.3}/F_{9.8}$ via distance from θ^1 Ori C. We do not see any prominent dependence of the parameters to a target's separation from θ^1 Ori C. An interpretation is that UV radiation can affect the outer disks where the thermal velocities of the ionized heated gas exceeds the escape velocity from the central stars, but does not affect the inner disk much. On the other hand, as we have discussed in Section 5.2, if an object is located in much closer to the UV source, the inner disk can be influenced by the UV radiation. However, we do not make any detailed inference about the environmental effect on the inner disk evolution based on our observations of n_{K-6} , EW10, F_{10} , and $F_{11.3}/F_{9.8}$.

7. SUMMARY AND CONCLUSION

We present IRS/Spitzer observations of 319 Class II disks in Orion A. We also present SpeX spectra of 120 objects and report mass accretion rates measured from hydrogen recombination lines in SpeX spectra. We analyzed the distributions of stellar, disk, and dust properties of our objects. We compared their distributions separated by sub-regions in Orion A, and we also compared the properties of Orion A disks to those of disks in the Taurus star-forming region. We draw the following conclusions from the analysis done in this work:

1. The median visual extinction A_V is larger in L1641 than ONC and the Trapezium. It confirms the effect of strong UV radiation from OB stars in the Trapezium to blow out small dust grains near them.

2. We confirm that the \dot{M} distribution of TDs in ONC and L1641 is about a factor of 10 lower than that of FDs. The median \dot{M} of FDs in ONC and L1641 are $1.55 \times 10^{-8} M_{\odot}/yr$ and $1.01 \times 10^{-8} M_{\odot}/yr$, respectively. The median \dot{M} of TDs in ONC and L1641 are $1.95 \times 10^{-9} M_{\odot}/yr$ and $1.62 \times 10^{-9} M_{\odot}/yr$, respectively. When we compared \dot{M} for disks in ONC and that of L1641 separately, the distribution of \dot{M} in ONC is slightly skewed toward a higher value, but there is no statistically significant difference in \dot{M} between ONC and L1641 when the same disk groups (FD vs. FD; TD vs. TD) in two sub-regions are compared.

3. We have compared disk properties between FDs in Orion A sub-regions and FDs in Taurus. We found that n_{K-6} and n_{6-13} , which probe the inner regions of disks, tend to be statistically-significantly higher in the ONC compared with Tau. We also notice that the distribution of EW10 in ONC is statistically-significantly shifted from that of Taurus toward higher values and that in L1641 is distributed in between those of the ONC and Taurus. We also detected possible evolution of the degrees of grain growth and crystallization from $F_{11.3}/F_{9.8}$ in different star-forming regions following their median ages (NGC 1333, ONC, L1641, Tau, Cha I). By comparing the $10 \mu m$ silicate features of median spectra after subtracting continuum and normalization to the continuum, we confirmed that the ONC profile of $10 \mu m$ features are much smoother and narrower, similar to the profile of pristine silicate features, while the profile of L1641 indicates grain growth and crystallization, similar to Taurus. However, unlike the indicators of different properties of small dust grains, EW10 and $F_{11.3}/F_{9.8}$, we found no significant differences in the “sedimentation index” n_{13-31} among ONC, L1641, and Taurus. All of these findings support that the disk evolution occurs faster in the inner regions and the dust processing time scale is faster than the disk sedimentation time scale. Considering the median age of the ONC (<1 Myr), L1641 (~ 1 Myr), and Taurus (2 Myr), grain growth and crystallization are increased in the 1-2 Myr age range.

4. We have searched for trends between disk parameters and the strength of the UV illumination upon the disks. From the examination of median spectra in subsections of Orion A, we found the median spectra of the subsections of ONC are blue at long wavelengths beyond $20 \mu m$, which is consistent with outward truncation of the disks due to UV radiation field from the Trapezium, as in the case for the proplyds. We compared the distributions of spectral indices, equivalent widths, and integrated fluxes to the variation of the distance of objects from θ^1 Ori C. We observed a remarkable decline of n_{20-31} toward to the center of Trapezium. The distribution of n_{13-31} shows a similar declining pattern. These decreasing trends of n_{20-31} and n_{13-31} are dominantly observed within 1.5 pc from θ^1 Ori C. Considering the definitions and the implications of the parameters studied in this work, we suggest a depletion of optically thin surface material of outer disk ($r \gtrsim 1$ AU–10 AU).

The IRS survey of protoplanetary disks in Orion A presented in this work opens a new catalog of protoplanetary disks by offering disk properties measured from IRS spectra. We will discuss how the properties are interactively related each other in the next paper. Future observations of the objects in this work with instruments capable of greater angular resolution and sensitivity in multi-wavelength ranges from IR to submm/mm will enhance our understanding of the process of

disk evolution and planet formation.

This work is based on observations made with the Spitzer Space Telescope, which is operated by the Jet Propulsion Laboratory, California Institute of Technology under NASA contract 1407. Support for this work was provided by NASA through Contract Number 1257184 issued by JPL/Caltech, and Cornell subcontracts 31419-5714 to the University of Rochester. This publication makes use of data products from the Two Micron All Sky Survey, which is a joint project of the University of Massachusetts and the Infrared Processing and Analysis Center/California Institute of Technology, funded by the National Aeronautics and Space Administration and the National Science Foundation. This research has made use of the SIMBAD database, operated at CDS, Strasbourg, France. This research has made use of the VizieR catalogue access tool, CDS, Strasbourg, France. The original description of the VizieR service was published in A&AS 143, 23. This publication makes use of data products from the Wide-field Infrared Survey Explorer, which is a joint project of the University of California, Los Angeles, and the Jet Propulsion Laboratory/California Institute of Technology, funded by the National Aeronautics and Space Administration. Funding for SDSS-III has been provided by the Alfred P. Sloan Foundation, the Participating Institutions, the National Science Foundation, and the U.S. Department of Energy Office of Science. SDSS-III is managed by the Astrophysical Research Consortium for the Participating Institutions of the SDSS-III Collaboration including the University of Arizona, the Brazilian Participation Group, Brookhaven National Laboratory, University of Cambridge, Carnegie Mellon University, University of Florida, the French Participation Group, the German Participation Group, Harvard University, the Instituto de Astrofisica de Canarias, the Michigan State/Notre Dame/JINA Participation Group, Johns Hopkins University, Lawrence Berkeley National Laboratory, Max Planck Institute for Astrophysics, Max Planck Institute for Extraterrestrial Physics, New Mexico State University, New York University, Ohio State University, Pennsylvania State University, University of Portsmouth, Princeton University, the Spanish Participation Group, University of Tokyo, University of Utah, Vanderbilt University, University of Virginia, University of Washington, and Yale University. The UKIDSS project is defined in Lawrence et al (2007). UKIDSS uses the UKIRT Wide Field Camera (WFCAM; Casali et al, 2007). The photometric system is described in Hewett et al (2006), and the calibration is described in Hodgkin et al. (2009). The pipeline processing and science archive are described in Irwin et al (2009, in prep) and Hambly et al (2008). K.H.Kim was a visiting Astronomer at the Infrared Telescope Facility, which is operated by the University of Hawaii under contract NNH14CK55B with the National Aeronautics and Space Administration.

Facilities: Spitzer (IRS), IRTF (SpeX).

REFERENCES

- Adams, F. C., Lada, C. J., & Shu, F. H. 1988, ApJ, 326, 865
Adelman-McCarthy, J. K., & et al. 2011, VizieR Online Data Catalog, 2306, 0

- Allen, L., & Mosby, G. 2008, personal communication
- Allen, L. E. 1995, PhD thesis, School of Physics, University of New South Wales, Sydney, NSW 2052, Australia [EMAIL]lea@newt.phys.unsw.edu.au[EMAIL]
- Andre, P., Ward-Thompson, D., & Barsony, M. 1993, ApJ, 406, 122
- Andrews, S. M., Wilner, D. J., Espaillat, C., Hughes, A. M., Dullemond, C. P., McClure, M. K., Qi, C., & Brown, J. M. 2011, ApJ, 732, 42
- Arnold, L. A., Watson, D. M., Kim, K. H., Manoj, P., Remming, I., Sheehan, P., Adame, L., Forrest, W. J., Furlan, E., Mamajek, E., McClure, M., Espaillat, C., Ausfeld, K., & Rapson, V. A. 2012, ApJS, 201, 12
- Balog, Z., Muzerolle, J., Rieke, G. H., Su, K. Y. L., Young, E. T., & Megeath, S. T. 2007, ApJ, 660, 1532
- Balog, Z., Rieke, G. H., Muzerolle, J., Bally, J., Su, K. Y. L., Misselt, K., & Gáspár, A. 2008, ApJ, 688, 408
- Bertout, C., Siess, L., & Cabrit, S. 2007, A&A, 473, L21
- Bouwman, J., Henning, T., Hillenbrand, L. A., Meyer, M. R., Pascucci, I., Carpenter, J., Hines, D., Kim, J. S., Silverstone, M. D., Hollenbach, D., & Wolf, S. 2008, ApJ, 683, 479
- Calvet, N., D'Alessio, P., Watson, D. M., Franco-Hernández, R., Furlan, E., Green, J., Sutter, P. M., Forrest, W. J., Hartmann, L., Uchida, K. I., Keller, L. D., Sargent, B., Najita, J., Herter, T. L., Barry, D. J., & Hall, P. 2005, ApJ, 630, L185
- Caratti O Garatti, A., Garcia Lopez, R., Antoniucci, S., Nisini, B., Giannini, T., Eislöffel, J., Ray, T. P., Lorenzetti, D., & Cabrit, S. 2012, A&A, 538, A64
- Cardelli, J. A., Clayton, G. C., & Mathis, J. S. 1989, ApJ, 345, 245
- Carpenter, J. M. 2000, AJ, 120, 3139
- Casassus, S., van der Plas, G., M, S. P., Dent, W. R. F., Fomalont, E., Hagelberg, J., Hales, A., Jordán, A., Mawet, D., Ménard, F., Wootten, A., Wilner, D., Hughes, A. M., Schreiber, M. R., Girard, J. H., Ercolano, B., Canovas, H., Román, P. E., & Salinas, V. 2013, Nature, 493, 191
- Crapsi, A., van Dishoeck, E. F., Hogerheijde, M. R., Pontoppidan, K. M., & Dullemond, C. P. 2008, A&A, 486, 245
- Currie, T., Lada, C. J., Plavchan, P., Robitaille, T. P., Irwin, J., & Kenyon, S. J. 2009, ApJ, 698, 1
- Cushing, M. C., Rayner, J. T., & Vacca, W. D. 2005, ApJ, 623, 1115

- Cushing, M. C., Vacca, W. D., & Rayner, J. T. 2004, PASP, 116, 362
- Cutri, R. M., & et al. 2012, VizieR Online Data Catalog, 2311, 0
- da Rio, N., Robberto, M., Soderblom, D. R., Panagia, N., Hillenbrand, L. A., Palla, F., & Stassun, K. 2010, VizieR Online Data Catalog, 218, 30261
- Daemgen, S., Correia, S., & Petr-Gotzens, M. G. 2012, A&A, 540, A46
- D'Alessio, P., Calvet, N., Hartmann, L., Franco-Hernández, R., & Servín, H. 2006, ApJ, 638, 314
- D'Alessio, P., Calvet, N., Hartmann, L., Lizano, S., & Cantó, J. 1999, ApJ, 527, 893
- DENIS Consortium. 2005, VizieR Online Data Catalog, 2263
- Espaillat, C., Calvet, N., D'Alessio, P., Hernández, J., Qi, C., Hartmann, L., Furlan, E., & Watson, D. M. 2007, ApJ, 670, L135
- Espaillat, C., Ingleby, L., Hernández, J., Furlan, E., D'Alessio, P., Calvet, N., Andrews, S., Muze-rolle, J., Qi, C., & Wilner, D. 2012, ApJ, 747, 103
- Espaillat, C., Muzerolle, J., Najita, J., Andrews, S., Zhu, Z., Calvet, N., Kraus, S., Hashimoto, J., Kraus, A., & D'Alessio, P. 2014, ArXiv e-prints
- Evans, II, N. J., Dunham, M. M., Jørgensen, J. K., Enoch, M. L., Merín, B., van Dishoeck, E. F., Alcalá, J. M., Myers, P. C., Stapelfeldt, K. R., Huard, T. L., Allen, L. E., Harvey, P. M., van Kempen, T., Blake, G. A., Koerner, D. W., Mundy, L. G., Padgett, D. L., & Sargent, A. I. 2009, ApJS, 181, 321
- Fang, M., Kim, J. S., van Boekel, R., Sicilia-Aguilar, A., Henning, T., & Flaherty, K. 2013, ApJS, 207, 5
- Fang, M., van Boekel, R., Wang, W., Carmona, A., Sicilia-Aguilar, A., & Henning, T. 2009, A&A, 504, 461
- Fűrész, G., Hartmann, L. W., Megeath, S. T., Szentgyorgyi, A. H., & Hamden, E. T. 2008, ApJ, 676, 1109
- Furlan, E., Hartmann, L., Calvet, N., D'Alessio, P., Franco-Hernández, R., Forrest, W. J., Watson, D. M., Uchida, K. I., Sargent, B., Green, J. D., Keller, L. D., & Herter, T. L. 2006, ApJS, 165, 568
- Furlan, E., Luhman, K. L., Espaillat, C., D'Alessio, P., Adame, L., Manoj, P., Kim, K. H., Watson, D. M., Forrest, W. J., McClure, M. K., Calvet, N., Sargent, B. A., Green, J. D., & Fischer, W. J. 2011, ApJS, 195, 3
- Furlan, E., McClure, M., Calvet, N., Hartmann, L., D'Alessio, P., Forrest, W. J., Watson, D. M., Uchida, K. I., Sargent, B., Green, J. D., & Herter, T. L. 2008, ApJS, 176, 184

- Furlan, E., Watson, D. M., McClure, M. K., Manoj, P., Espaillat, C., D'Alessio, P., Calvet, N., Kim, K. H., Sargent, B. A., Forrest, W. J., & Hartmann, L. 2009, *ApJ*, 703, 1964
- Gâlfalk, M., & Olofsson, G. 2008, *A&A*, 489, 1409
- Gatti, T., Natta, A., Randich, S., Testi, L., & Sacco, G. 2008, *A&A*, 481, 423
- Getman, K. V., Feigelson, E. D., & Kuhn, M. A. 2014, *ApJ*, 787, 109
- Glebocki, R., & Gnacinski, P. 2005, *VizieR Online Data Catalog*, 3244, 0
- Grankin, K. N., Melnikov, S. Y., Bouvier, J., Herbst, W., & Shevchenko, V. S. 2007, *A&A*, 461, 183
- Greene, T. P., Wilking, B. A., Andre, P., Young, E. T., & Lada, C. J. 1994, *ApJ*, 434, 614
- Herbig, G. H., & Bell, K. R. 1988, *Third Catalog of Emission-Line Stars of the Orion Population : 3* : 1988
- Hernandez, J. 2008, personal communication
- Hernández, J., Calvet, N., Briceño, C., Hartmann, L., Vivas, A. K., Muzerolle, J., Downes, J., Allen, L., & Gutermuth, R. 2007, *ApJ*, 671, 1784
- Hernandez, J., & Tobin, J. 2009, personal communication
- Higdon, S. J. U., Devost, D., Higdon, J. L., Brandl, B. R., Houck, J. R., Hall, P., Barry, D., Charmandaris, V., Smith, J. D. T., Sloan, G. C., & Green, J. 2004, *PASP*, 116, 975
- Hillenbrand, L. A. 1997, *AJ*, 113, 1733
- Hillenbrand, L. A., & Carpenter, J. M. 2000, *ApJ*, 540, 236
- Hillenbrand, L. A., Hoffer, A. S., & Herczeg, G. J. 2013, *AJ*, 146, 85
- Honda, M., Kataza, H., Okamoto, Y. K., Yamashita, T., Min, M., Miyata, T., Sako, S., Fujiyoshi, T., Sakon, I., & Onaka, T. 2006, *ApJ*, 646, 1024
- Houk, N., & Swift, C. 2000, *VizieR Online Data Catalog*, 3214, 0
- Hsu, W.-H., Hartmann, L., Allen, L., Hernández, J., Megeath, S. T., Mosby, G., Tobin, J. J., & Espaillat, C. 2012, *ApJ*, 752, 59
- Hsu, W.-H., Hartmann, L., Allen, L., Hernández, J., Megeath, S. T., Tobin, J. J., & Ingleby, L. 2013, *ApJ*, 764, 114
- Kenyon, S. J., & Hartmann, L. 1995, *ApJS*, 101, 117

- Kessler-Silacci, J., Augereau, J.-C., Dullemond, C. P., Geers, V., Lahuis, F., Evans, II, N. J., van Dishoeck, E. F., Blake, G. A., Boogert, A. C. A., Brown, J., Jørgensen, J. K., Knez, C., & Pontoppidan, K. M. 2006, *ApJ*, 639, 275
- Kim, K. H., Watson, D. M., & Forrest, W. J. 2016, in preparation
- Kim, K. H., Watson, D. M., Manoj, P., Forrest, W. J., Najita, J., Furlan, E., Sargent, B., Espaillat, C., Muzerolle, J., Megeath, S. T., Calvet, N., Green, J. D., & Arnold, L. 2013, *ApJ*, 769, 149
- Koenig, X. P., & Leisawitz, D. T. 2014, *ApJ*, 791, 131
- Kukarkin, B. V., Kholopov, P. N., Pskovsky, Y. P., Efremov, Y. N., Kukarkina, N. P., Kurochkin, N. E., & Medvedeva, G. I. 1971, in General Catalogue of Variable Stars, 3rd ed. (1971), 0–+
- Lada, C. J. 1987, in IAU Symposium, Vol. 115, Star Forming Regions, ed. M. Peimbert & J. Jugaku, 1–17
- Lada, C. J., & Lada, E. A. 2003, *ARA&A*, 41, 57
- Lada, E. A., Depoy, D. L., Evans, II, N. J., & Gatley, I. 1991, *ApJ*, 371, 171
- Lebouteiller, V., Bernard-Salas, J., Sloan, G. C., & Barry, D. J. 2010, *PASP*, 122, 231
- Lubow, S. H., & D'Angelo, G. 2006, *ApJ*, 641, 526
- Mann, R. K., Di Francesco, J., Johnstone, D., Andrews, S. M., Williams, J. P., Bally, J., Ricci, L., Hughes, A. M., & Matthews, B. C. 2014, *ApJ*, 784, 82
- Manoj, P., Bhatt, H. C., Maheswar, G., & Muneer, S. 2006, *ApJ*, 653, 657
- Manoj, P., Kim, K. H., Furlan, E., McClure, M. K., Luhman, K. L., Watson, D. M., Espaillat, C., Calvet, N., Najita, J. R., D'Alessio, P., Adame, L., Sargent, B. A., Forrest, W. J., Bohac, C., Green, J. D., & Arnold, L. A. 2011, *ApJS*, 193, 11
- Mathis, J. S. 1990, *ARA&A*, 28, 37
- McClure, M. 2009, *ApJ*, 693, L81
- McClure, M. K., Furlan, E., Manoj, P., Luhman, K. L., Watson, D. M., Forrest, W. J., Espaillat, C., Calvet, N., D'Alessio, P., Sargent, B., Tobin, J. J., & Chiang, H.-F. 2010, *ApJS*, 188, 75
- Megeath, S. T., Fischer, W., Ali, B., Allen, L., Poteet, C., Watson, D., Wilson, T., & HOPS Team. 2010, in Bulletin of the American Astronomical Society, Vol. 42, American Astronomical Society Meeting Abstracts #215, #440.13

- Megeath, S. T., Gutermuth, R., Muzerolle, J., Kryukova, E., Flaherty, K., Hora, J. L., Allen, L. E., Hartmann, L., Myers, P. C., Pipher, J. L., Stauffer, J., Young, E. T., & Fazio, G. G. 2012, AJ, 144, 192
- Megeath, S. T., Gutermuth, R., Muzerolle, J., Kryukova, E., Hora, J. L., Allen, L. E., Flaherty, K., Hartmann, L., Myers, P. C., Pipher, J. L., Stauffer, J., Young, E. T., & Fazio, G. G. 2016, AJ, 151, 5
- Menten, K. M., Reid, M. J., Forbrich, J., & Brunthaler, A. 2007, A&A, 474, 515
- Meyer, M. R., Calvet, N., & Hillenbrand, L. A. 1997, AJ, 114, 288
- Muzerolle, J., Hartmann, L., & Calvet, N. 1998, AJ, 116, 2965
- Najita, J. R., Andrews, S. M., & Muzerolle, J. 2015, MNRAS, 450, 3559
- Najita, J. R., Strom, S. E., & Muzerolle, J. 2007, MNRAS, 378, 369
- Ochsenbein, F. 1980, Bulletin d'Information du Centre de Donnees Stellaires, 19, 74
- O'Dell, C. R., & Wen, Z. 1994, ApJ, 436, 194
- Olofsson, J., Augereau, J.-C., van Dishoeck, E. F., Merín, B., Lahuis, F., Kessler-Silacci, J., Dullemond, C. P., Oliveira, I., Blake, G. A., Boogert, A. C. A., Brown, J. M., Evans, II, N. J., Geers, V., Knez, C., Monin, J.-L., & Pontoppidan, K. 2009, A&A, 507, 327
- Olofsson, J., Benisty, M., Augereau, J.-C., Pinte, C., Ménard, F., Tatulli, E., Berger, J.-P., Malbet, F., Merín, B., van Dishoeck, E. F., Lacour, S., Pontoppidan, K. M., Monin, J.-L., Brown, J. M., & Blake, G. A. 2011, A&A, 528, L6
- Parenago, P. P. 1954, Trudy Gosudarstvennogo Astronomicheskogo Instituta, 25, 1
- Parihar, P., Messina, S., Distefano, E., Shantikumar, N. S., & Medhi, B. J. 2009a, MNRAS, 400, 603
- . 2009b, MNRAS, 400, 603
- Pecaut, M. J., & Mamajek, E. E. 2013, ApJS, 208, 9
- Poteet, C., Watson, D. M., Megeath, S. T., & Muzerolle, J. 2016, in preparation
- Prisinzano, L., Micela, G., Flaccomio, E., Stauffer, J. R., Megeath, T., Rebull, L., Robberto, M., Smith, K., Feigelson, E. D., Grosso, N., & Wolk, S. 2008, ApJ, 677, 401
- Przygodda, F., van Boekel, R., Åbrahmà, P., Melnikov, S. Y., Waters, L. B. F. M., & Leinert, C. 2003, A&A, 412, L43
- Rayner, J. T., Cushing, M. C., & Vacca, W. D. 2009, ApJS, 185, 289

- Rayner, J. T., Toomey, D. W., Onaka, P. M., Denault, A. J., Stahlberger, W. E., Vacca, W. D., Cushing, M. C., & Wang, S. 2003, PASP, 115, 362
- Rebull, L. M. 2001, AJ, 121, 1676
- Rebull, L. M., Hillenbrand, L. A., Strom, S. E., Duncan, D. K., Patten, B. M., Pavlovsky, C. M., Makidon, R., & Adams, M. T. 2000, AJ, 119, 3026
- Riaz, B., Gizis, J. E., & Harvin, J. 2006, AJ, 132, 866
- Robberto, M., Soderblom, D. R., Scandariato, G., Smith, K., Da Rio, N., Pagano, I., & Spezzi, L. 2010, AJ, 139, 950
- Robitaille, T. P., Whitney, B. A., Indebetouw, R., Wood, K., & Denzmore, P. 2006, ApJS, 167, 256
- Sargent, B. A., Forrest, W. J., Tayrien, C., McClure, M. K., Watson, D. M., Sloan, G. C., Li, A., Manoj, P., Bohac, C. J., Furlan, E., Kim, K. H., & Green, J. D. 2009, ApJS, 182, 477
- Shuping, R. Y., Kassis, M., Morris, M., Smith, N., & Bally, J. 2006, ApJ, 644, L71
- Siess, L., Dufour, E., & Forestini, M. 2000, A&A, 358, 593
- Skrutskie, M. F., Cutri, R. M., Stiening, R., Weinberg, M. D., Schneider, S., Carpenter, J. M., Beichman, C., Capps, R., Chester, T., Elias, J., Huchra, J., Liebert, J., Lonsdale, C., Monet, D. G., Price, S., Seitzer, P., Jarrett, T., Kirkpatrick, J. D., Gizis, J. E., Howard, E., Evans, T., Fowler, J., Fullmer, L., Hurt, R., Light, R., Kopan, E. L., Marsh, K. A., McCallon, H. L., Tam, R., Van Dyk, S., & Wheelock, S. 2006, AJ, 131, 1163
- Tayrien, C., & Forrest, W. J. 2016, in preparation
- Tobin, J. J., Hartmann, L., Furesz, G., Mateo, M., & Megeath, S. T. 2009, ApJ, 697, 1103
- . 2013, ApJ, 773, 81
- UKIDSS Consortium. 2012, VizieR Online Data Catalog, 2314, 0
- Vacca, W. D., Cushing, M. C., & Rayner, J. T. 2003, PASP, 115, 389
- van Boekel, R., Min, M., Waters, L. B. F. M., de Koter, A., Dominik, C., van den Ancker, M. E., & Bouwman, J. 2005, A&A, 437, 189
- Wall, J. V., & Jenkins, C. R. 2003, Practical Statistics for Astronomers, ed. R. Ellis, J. Huchra, S. Kahn, G. Rieke, & P. B. Stetson
- Watson, D. M., Kemper, F., Calvet, N., Keller, L. D., Furlan, E., Hartmann, L., Forrest, W. J., Chen, C. H., Uchida, K. I., Green, J. D., Sargent, B., Sloan, G. C., Herter, T. L., Brandl, B. R., Houck, J. R., Najita, J., D'Alessio, P., Myers, P. C., Barry, D. J., Hall, P., & Morris, P. W. 2004, ApJS, 154, 391

- Watson, D. M., Leisenring, J. M., Furlan, E., Bohac, C. J., Sargent, B., Forrest, W. J., Calvet, N., Hartmann, L., Nordhaus, J. T., Green, J. D., Kim, K. H., Sloan, G. C., Chen, C. H., Keller, L. D., d'Alessio, P., Najita, J., Uchida, K. I., & Houck, J. R. 2009, ApJS, 180, 84
- Wolff, S. C., Strom, S. E., & Hillenbrand, L. A. 2004, ApJ, 601, 979
- Wouterloot, J. G. A., & Brand, J. 1992, A&A, 265, 144
- Zacharias, N., Monet, D. G., Levine, S. E., Urban, S. E., Gaume, R., & Wycoff, G. L. 2005, VizieR Online Data Catalog, 1297, 0

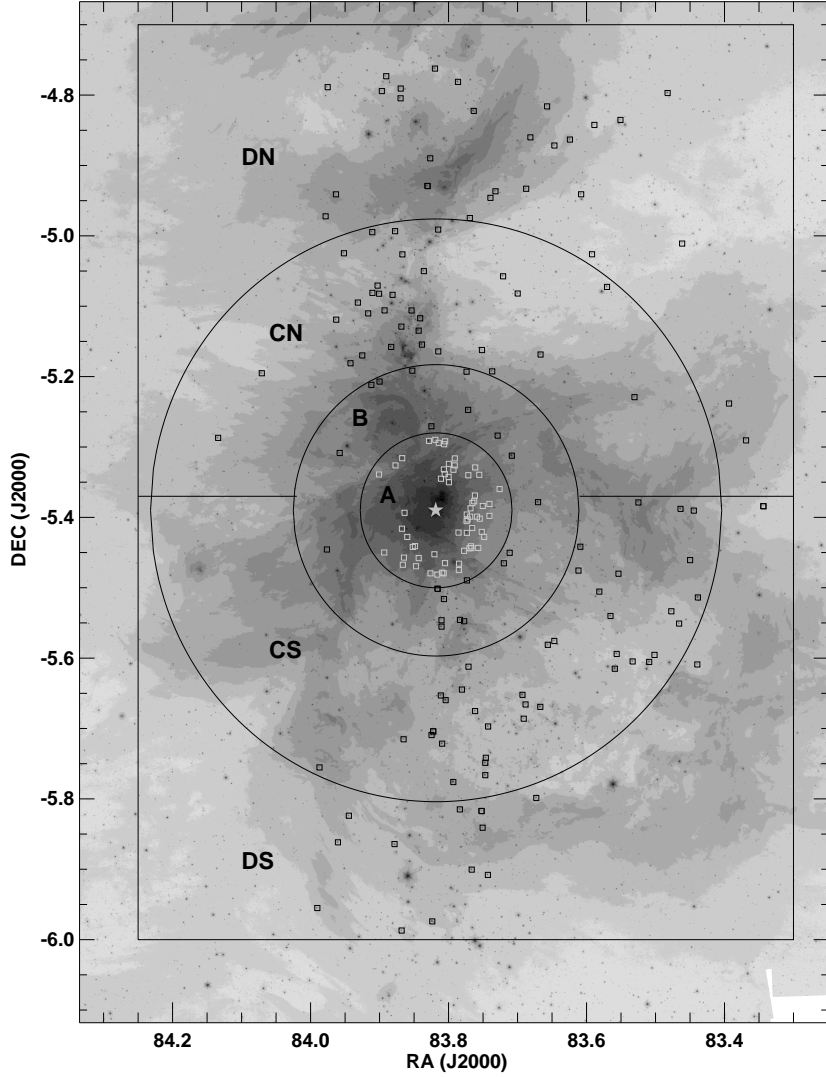


Fig. 1.— IRS targets in ONC plotted over the IRAC/Spitzer ch2 ($4.5 \mu\text{m}$) image. The squares indicate the Class II objects observed with IRS. The Black squares are for objects observed in the SLLL mode. The gray squares are for objects observed in the SL mode only. Sub-sections of ONC separated by the projected distance (d) from θ^1 Ori C (a five point yellow star) are indicated. The criteria of sub-sections: A: $d \leq 0.7 \text{ pc}$; B: $0.7 \text{ pc} < d \leq 1.5 \text{ pc}$; C: $1.5 \text{ pc} < d \leq 2.5 \text{ pc}$; D: $d > 2.5 \text{ pc}$ and $\text{DEC} > -6^\circ$. Sub-section B, C, and D are also separated by N and S from the DEC of θ^1 Ori C.

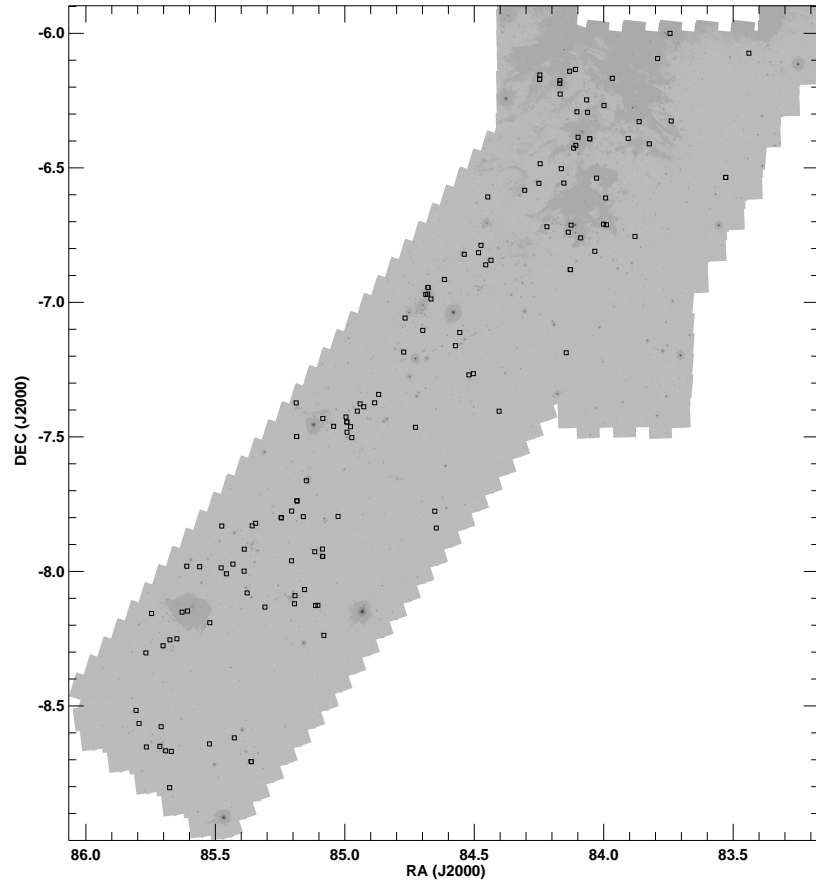


Fig. 2.— IRS targets in L1641 plotted over the IRAC/Spitzer ch2 ($4.5 \mu\text{m}$) image. The squares indicate the Class II objects observed with IRS.

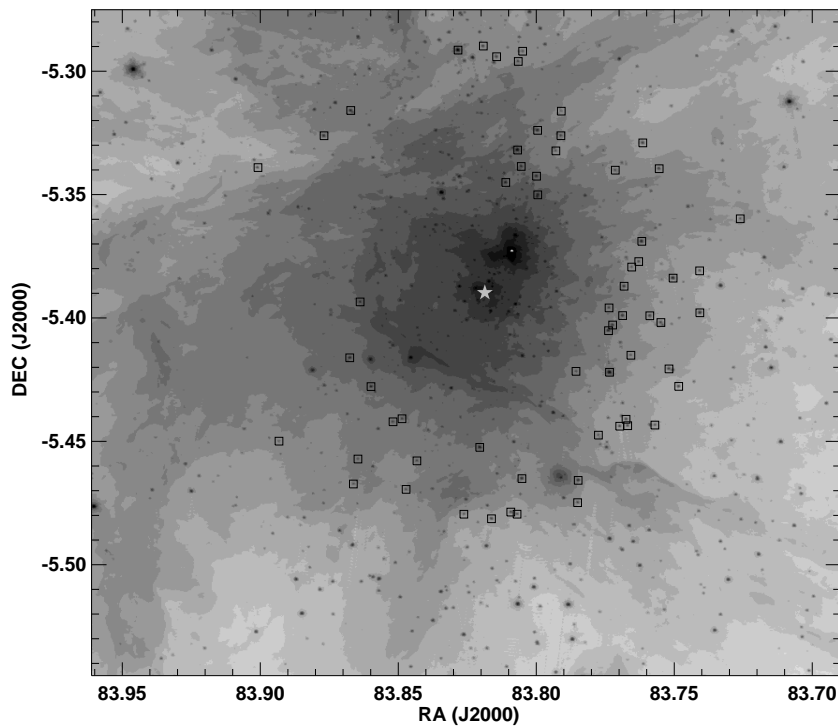


Fig. 3.— Close up of sub-section A (Trapezium region) in Fig 1. θ^1 Ori C is indicated with a five point star.

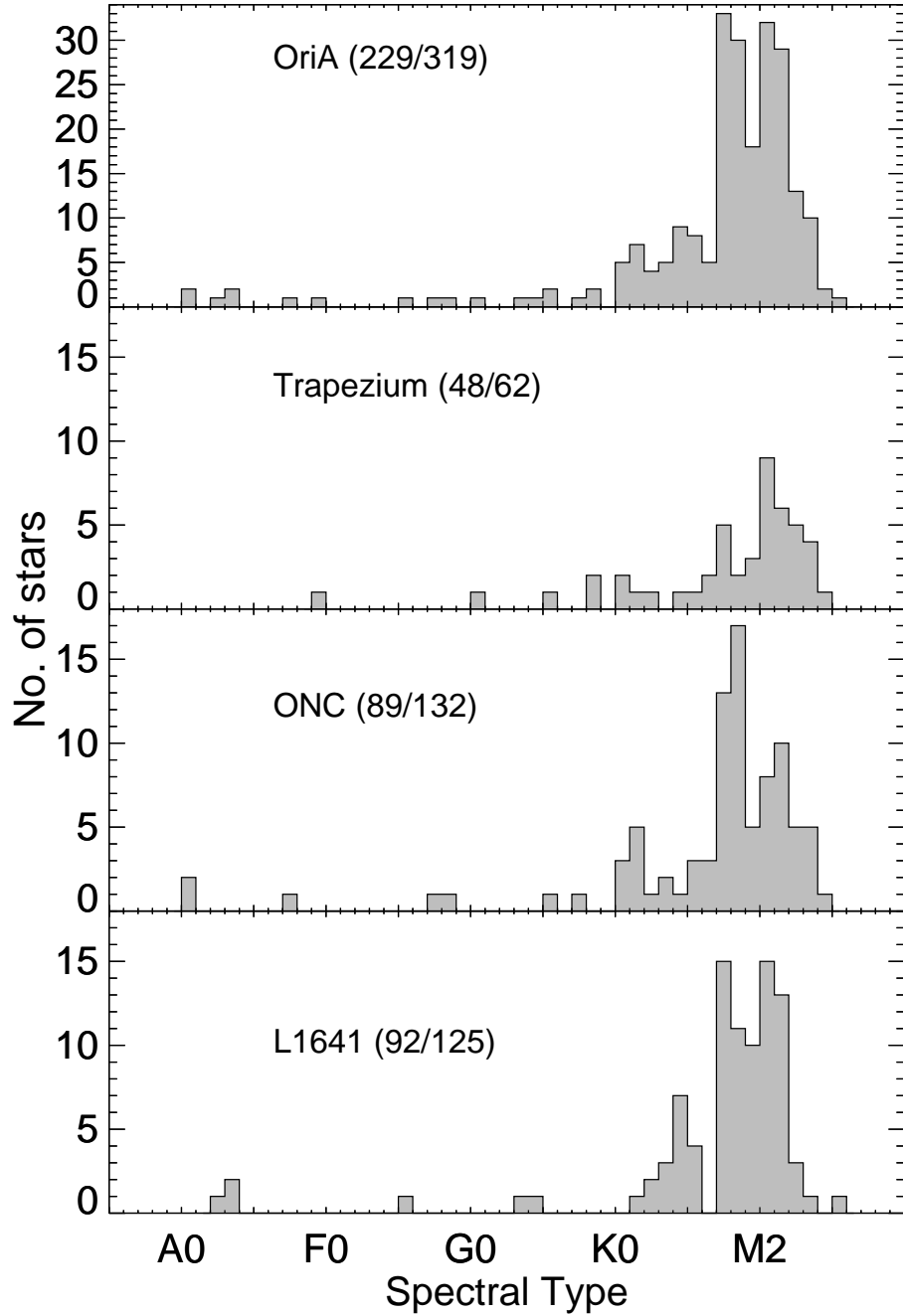


Fig. 4.— Spectral type distribution of Class II objects in Orion A that have available spectral types among those observed with IRS. (note: OriA-227 is classified as K7.9 and it is the only one we adopted as K8. We merged bin of K8 into the bin of M0 in order to plot the histogram in the same binning scheme in literature.)

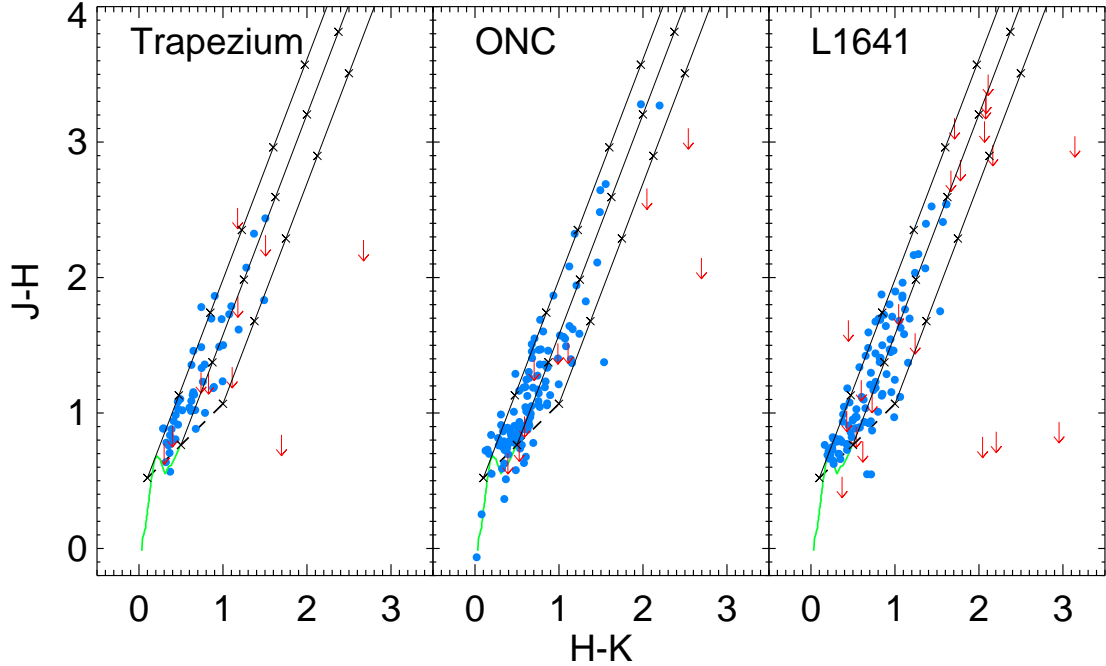


Fig. 5.— $J - H$ versus $H - K$ color-color diagram of Class II objets observed with IRS in the sub-regions of Orion A: Trapezium (the left panel), ONC (the middle panel), and L1641 (the right panel). J , H , and K photometry is from 2MASS. The CTTS locus is indicated with the dashed line. The colors of main-sequence giants and dwarf (Bessell & Brett 1998) are also plotted with green solid line. The solid lines started from the CTTS locus indicate the increasing extinction. The increments of A_V are denoted by crosses by the interval of $A_V=5$. The downward arrows are used for objects which their 2MASS photometry have any bad flags.

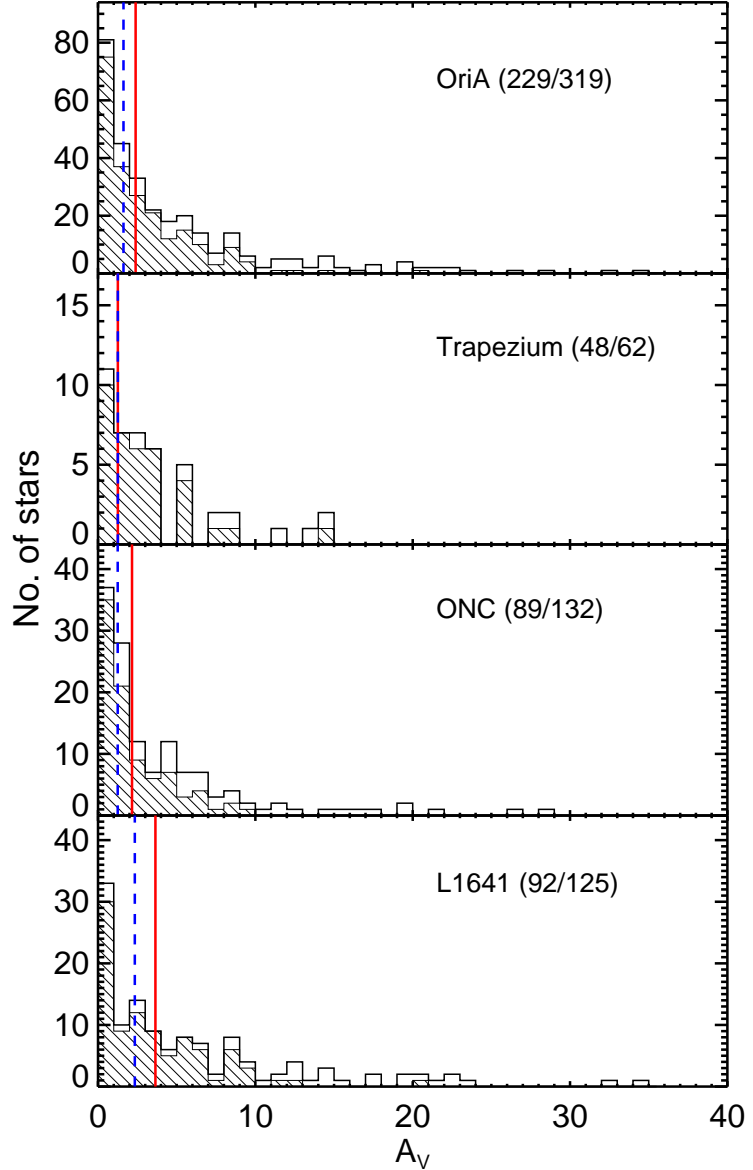


Fig. 6.— Distribution of visual extinction, A_V , for 319 Class II disks in Orion A observed with IRS. Hashed lines indicate the A_V distribution of the objects with known spectral type information. The solid vertical lines indicate the median A_V of all objects. The dashed lines are for the median A_V of the objects with available spectra types. The numbers in each pannels are for the number of objects with available spectral types and the number of objects without regard to the availability of spectral type.

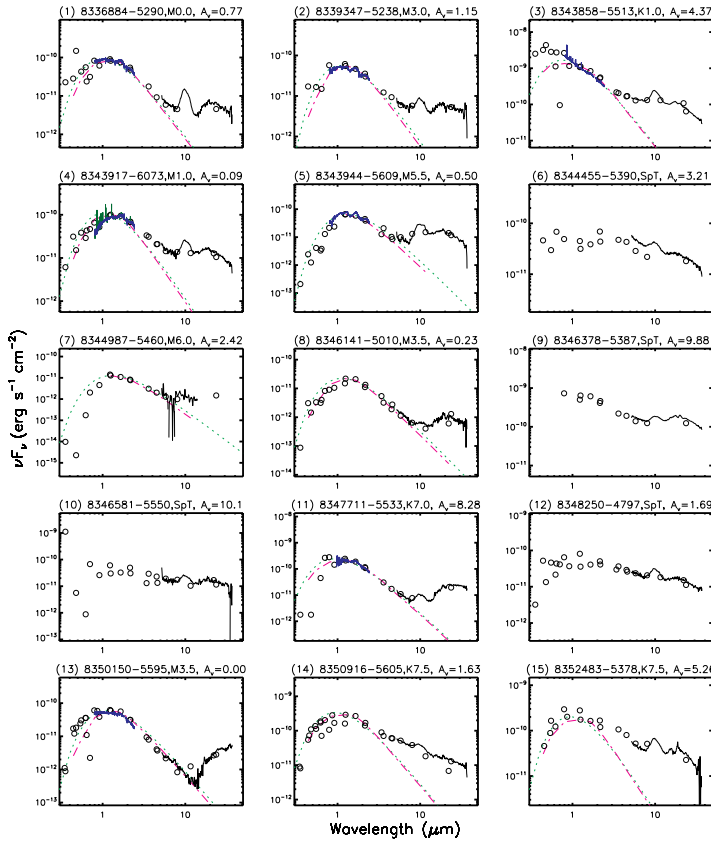


Fig. 7.— De-reddened SEDs of our samples in ONC and L1641, which were observed with IRS SL and LL modules. The SEDs are composed of the following components: IRS (solid line in the wavelength range of 5.2–35 (or 14) μm); SpeX (solid line in the wavelength range of 0.8–2.4 μm); photospheric models: a blackbody radiation of the host-star's effective temperature (short dashed line) and a photosphere derived from the intrinsic colors from Pecaut & Mamajek (2013) (long dash-dot line); photometric data (open circles): UBVRI from da Rio et al. (2010), SDSS, UKIDSS, BVR from NOMAD, DENIS IJH, 2MASS JHK, IRAC, MIPS (24 μm), and WISE.

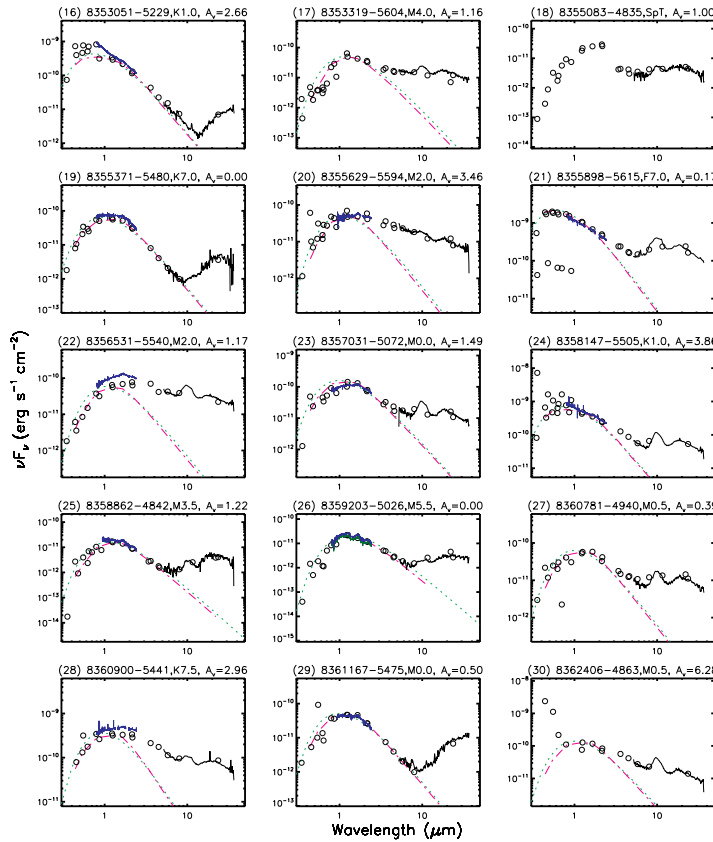


Fig. 7.— continued.

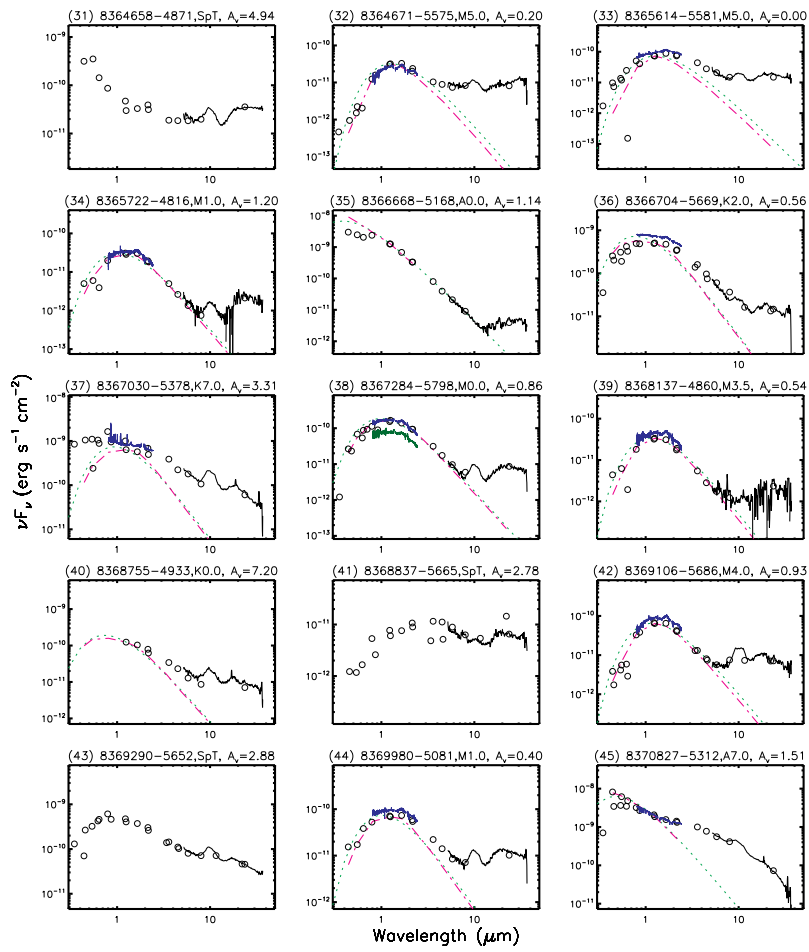


Fig. 7.— continued.

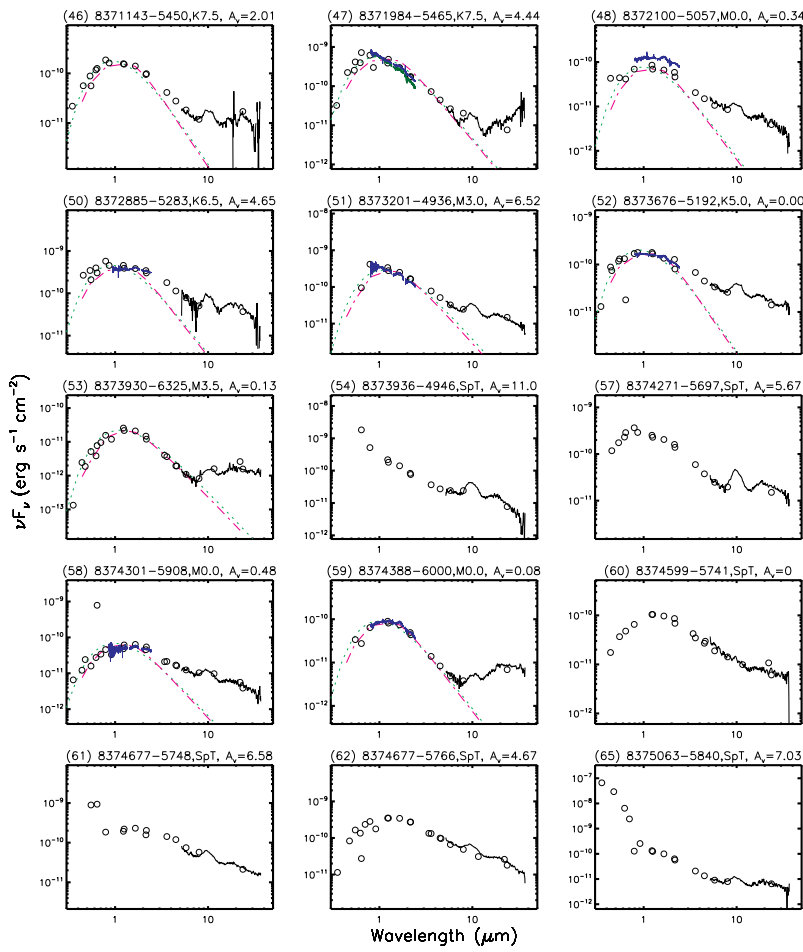


Fig. 7.— continued.

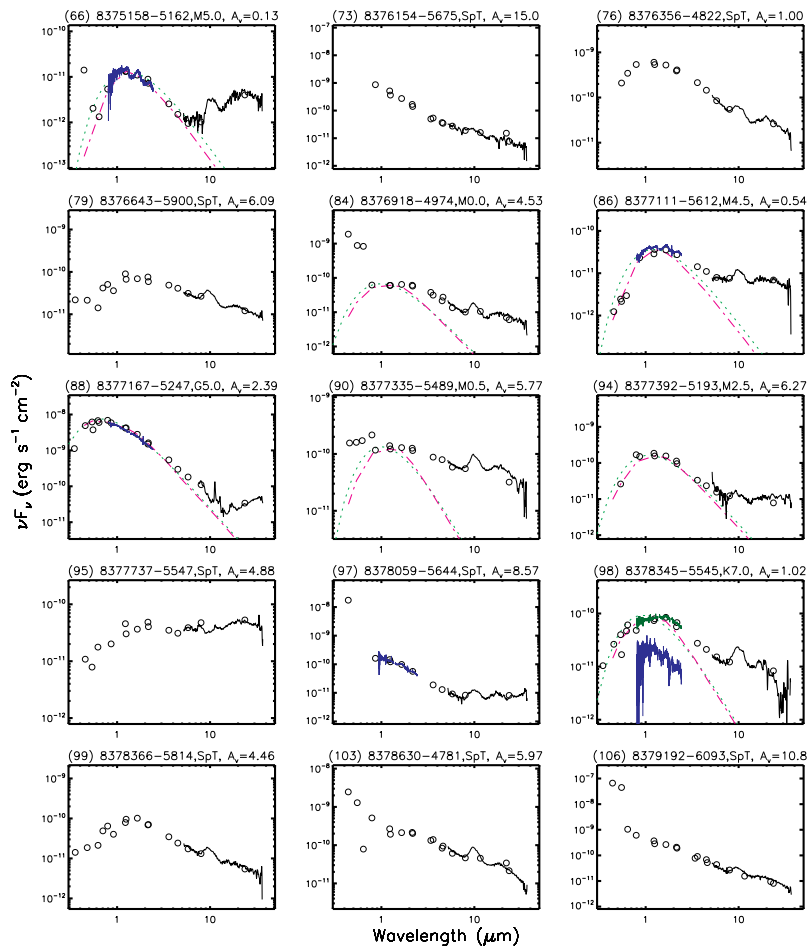


Fig. 7.— continued.

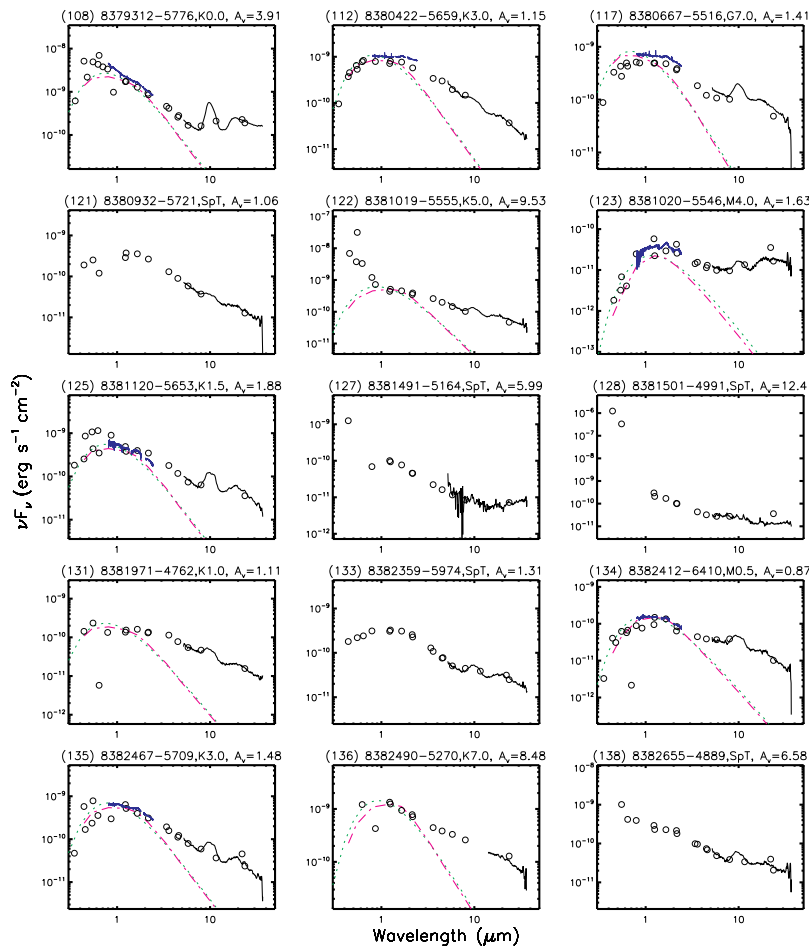


Fig. 7.— continued.

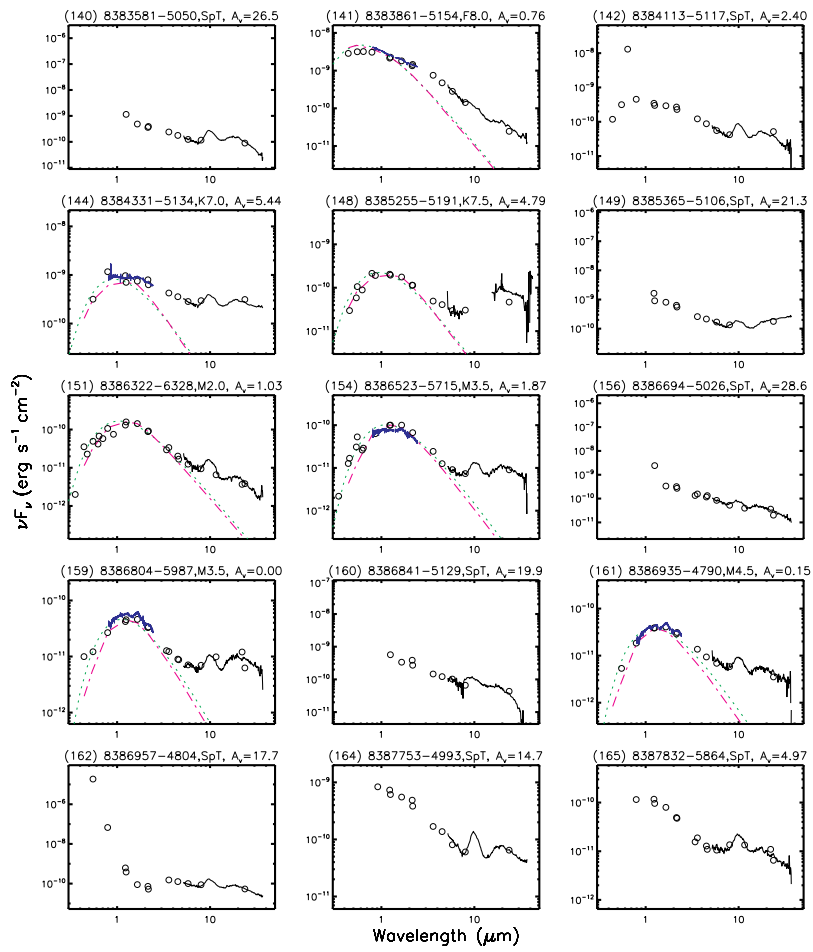


Fig. 7.— continued.

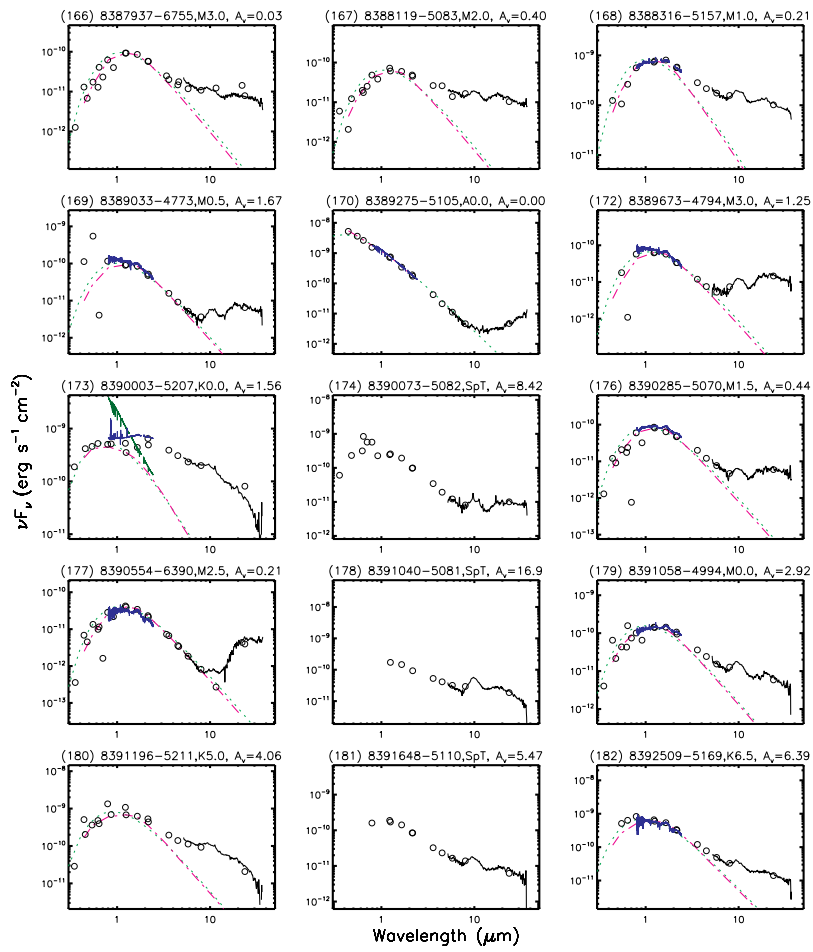


Fig. 7.— continued.

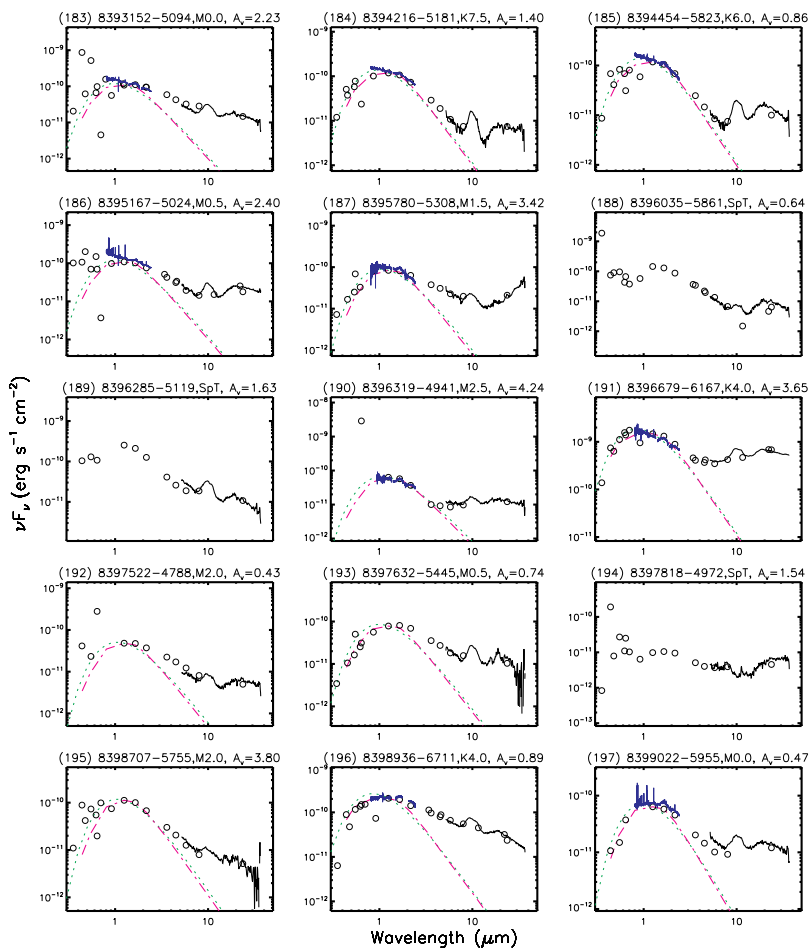


Fig. 7.— continued.

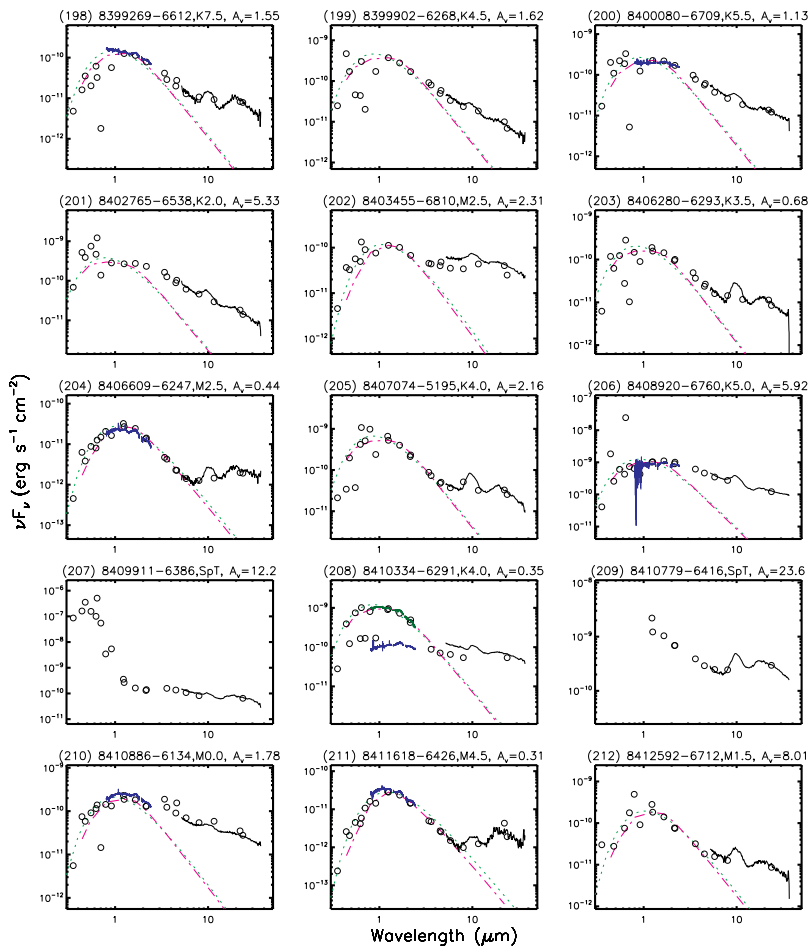


Fig. 7.— continued.

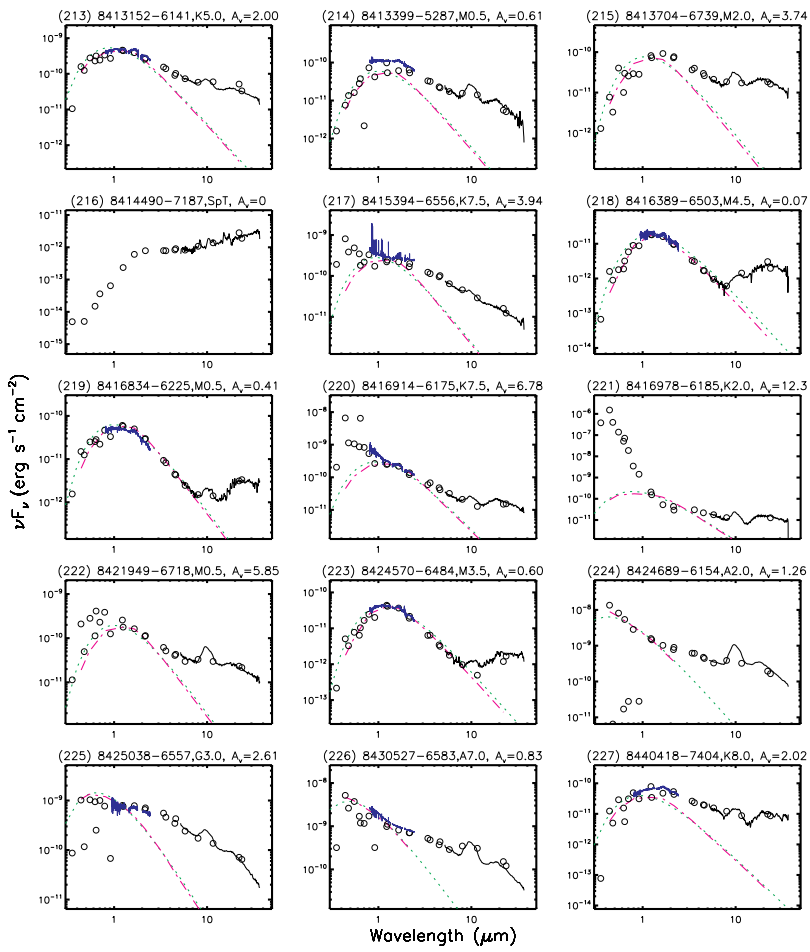


Fig. 7.— continued.

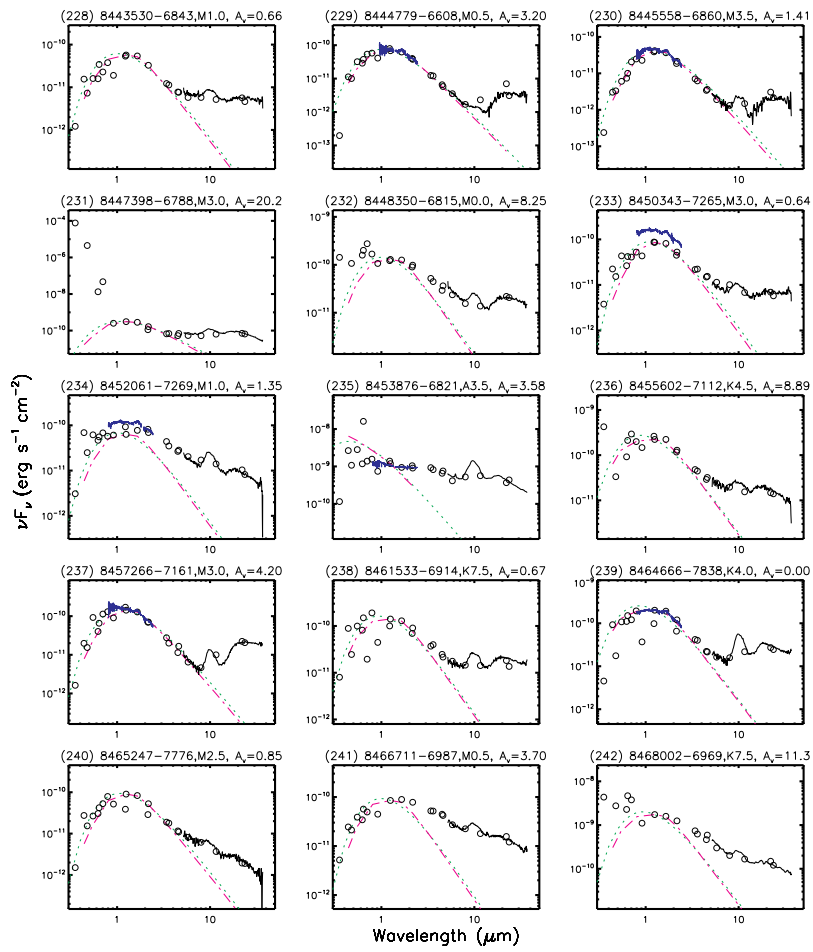


Fig. 7.— continued.

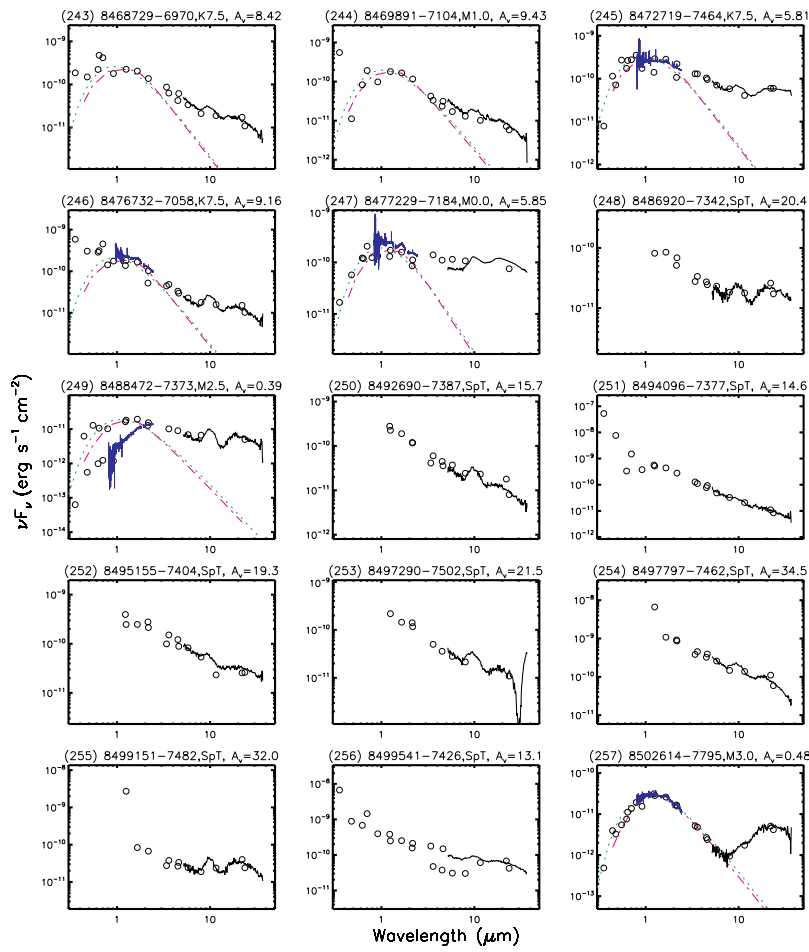


Fig. 7.— continued.

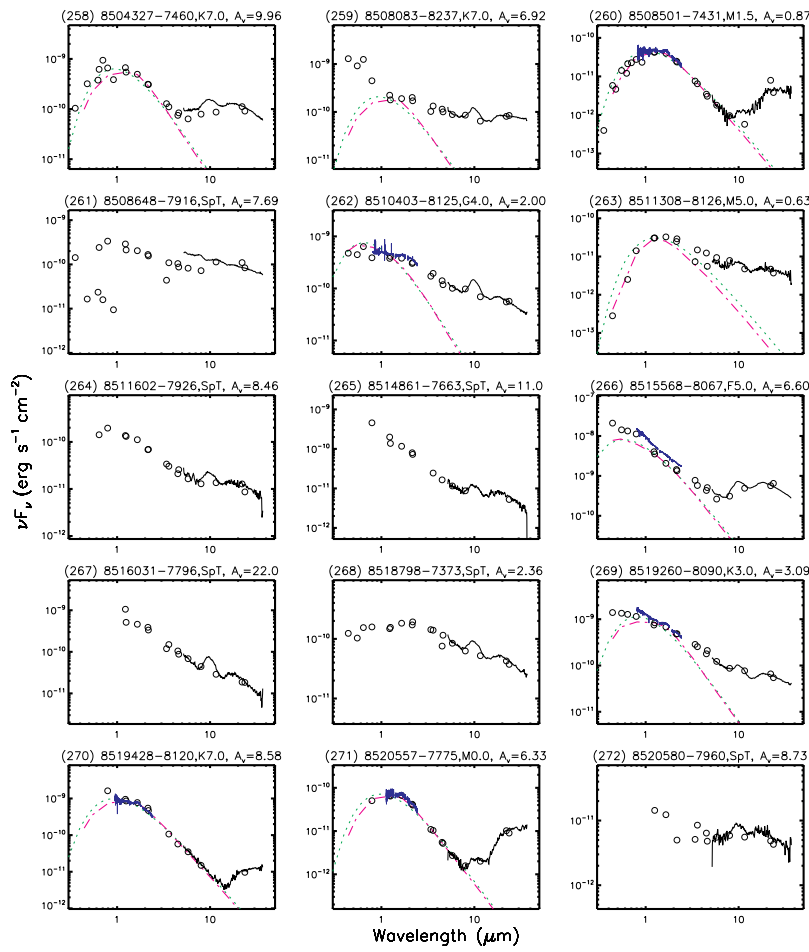


Fig. 7.— continued.

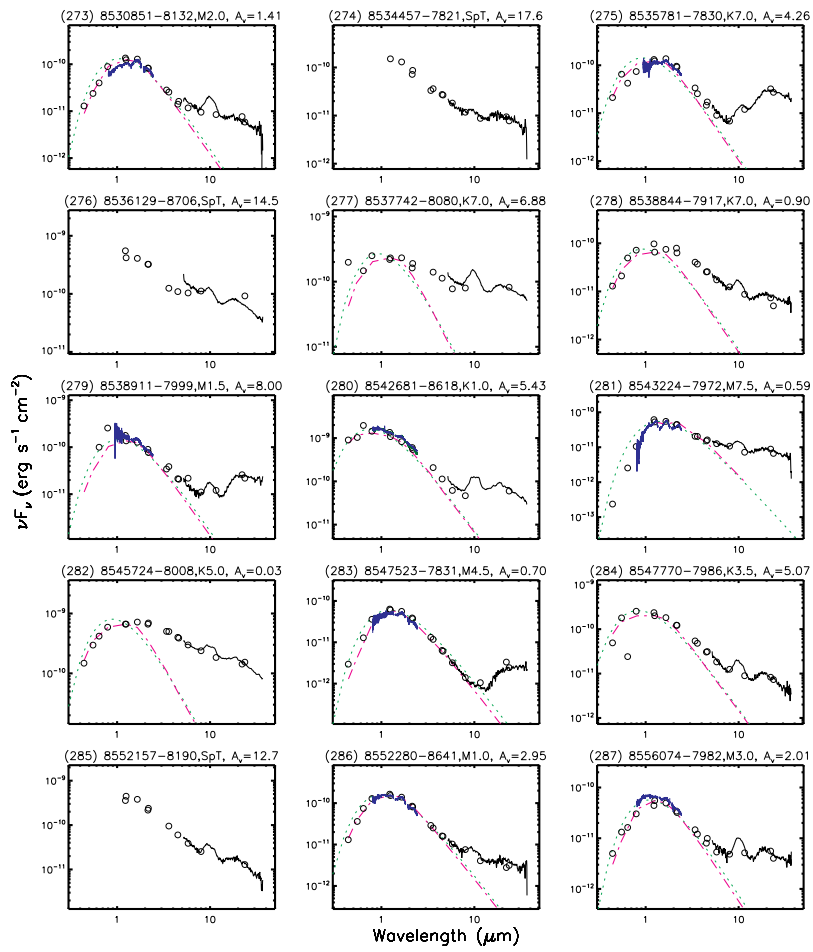


Fig. 7.— continued.

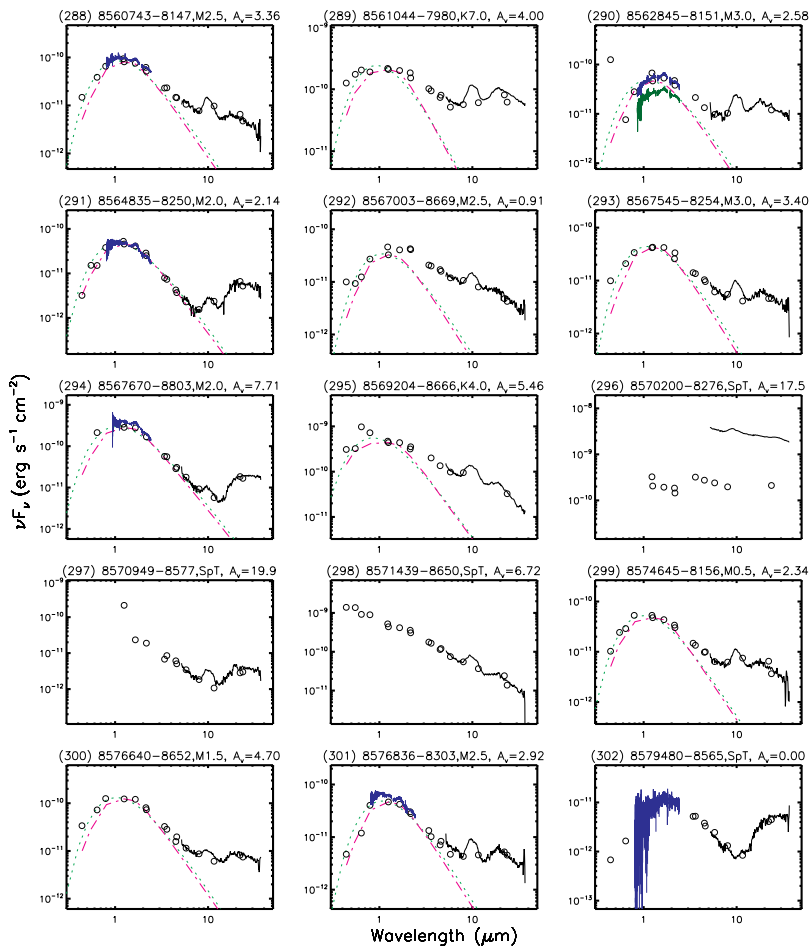


Fig. 7.— continued.

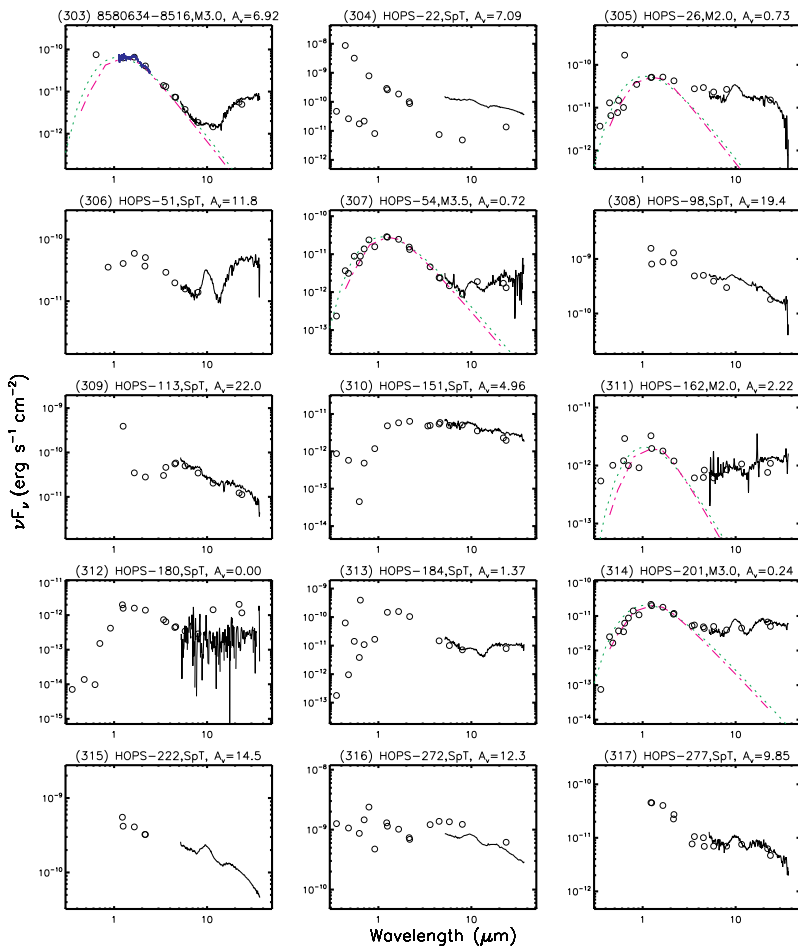


Fig. 7.— continued.

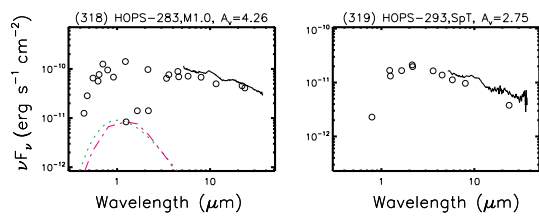


Fig. 7.— continued.

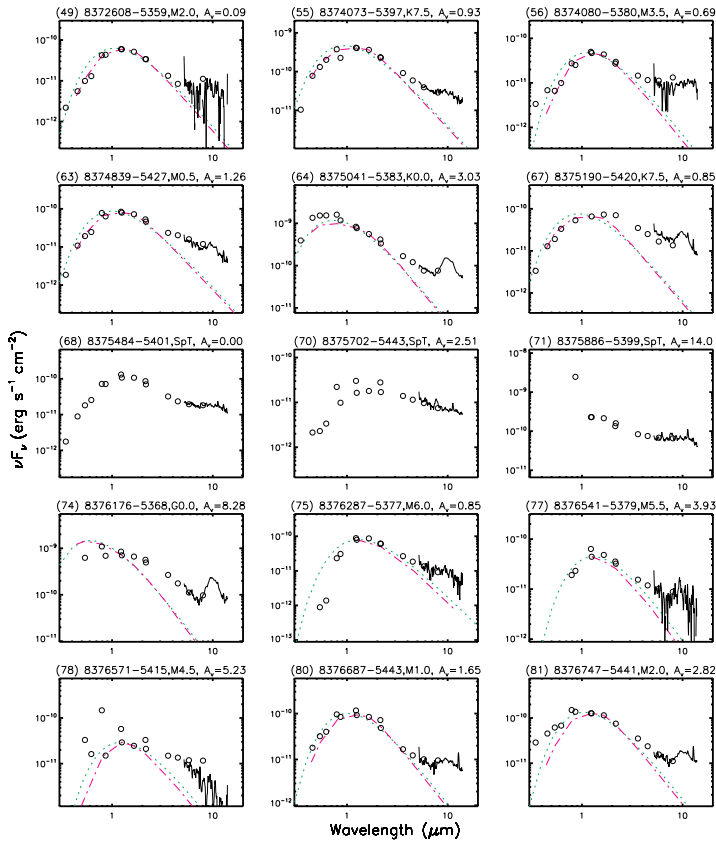


Fig. 8.— De-reddened SEDs of the reduced samples in Trapezium, which were observed with IRS SL module only. The meanings of symbols are same as in Figure 7.

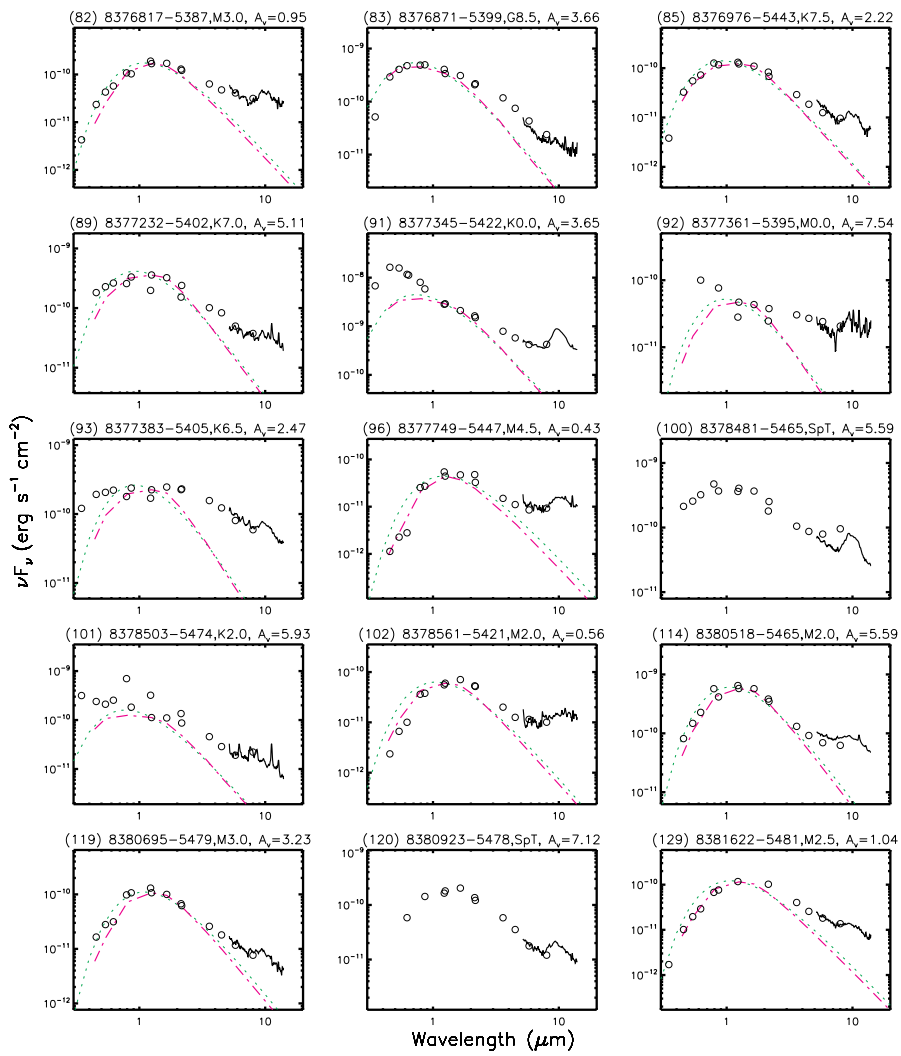


Fig. 8.— Continued.

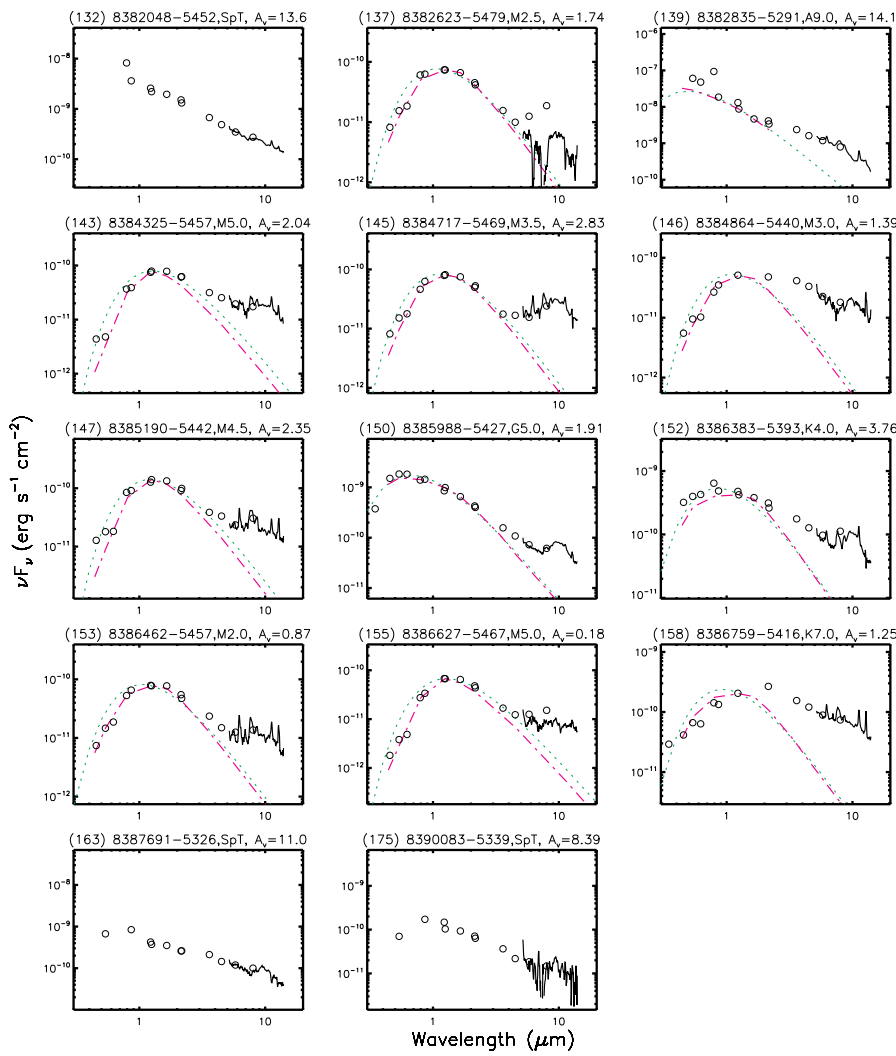


Fig. 8.— Continued.

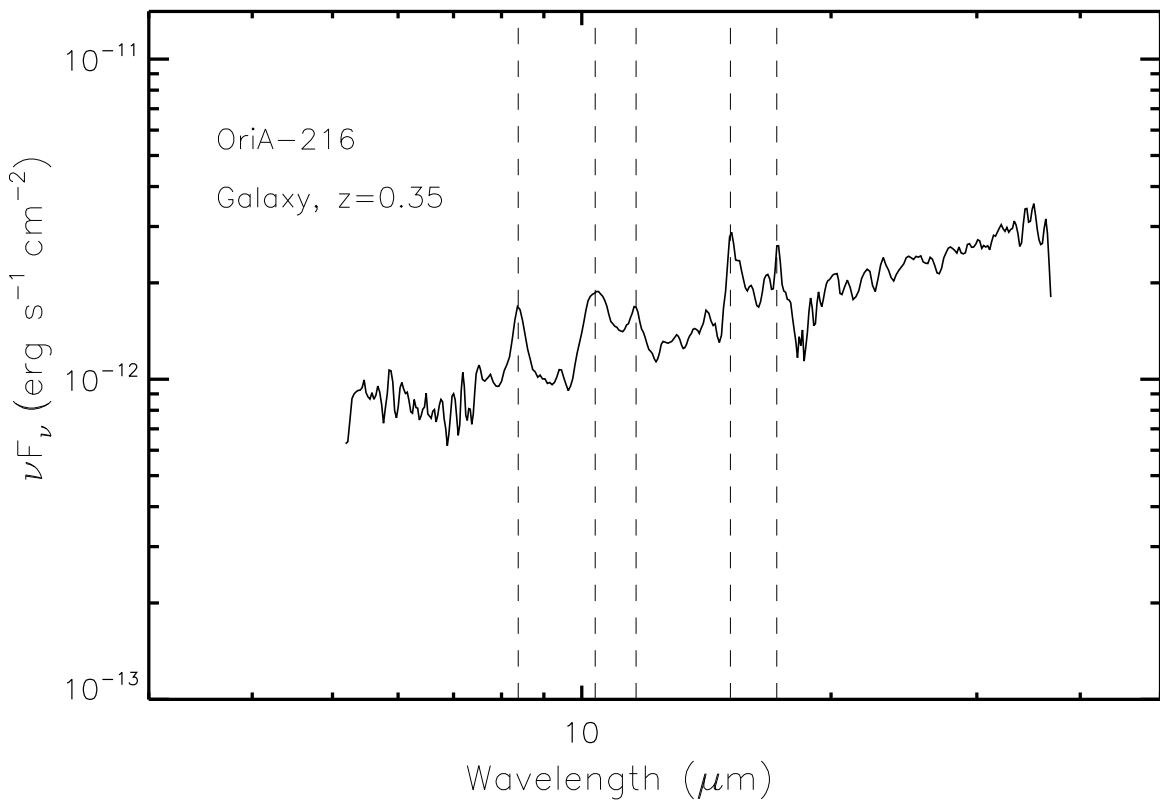


Fig. 9.— IRS spectrum of OriA-216 which is a background galaxy with redshift, $z=0.35$. The dashed lines indicate the PAHs features of 6.2, 7.7, 8.6, 11.2, and 12.7 μm at the redshifted wavelengths at 8.38, 10.38, 11.63, 15.12, and 17.2 μm , respectively.

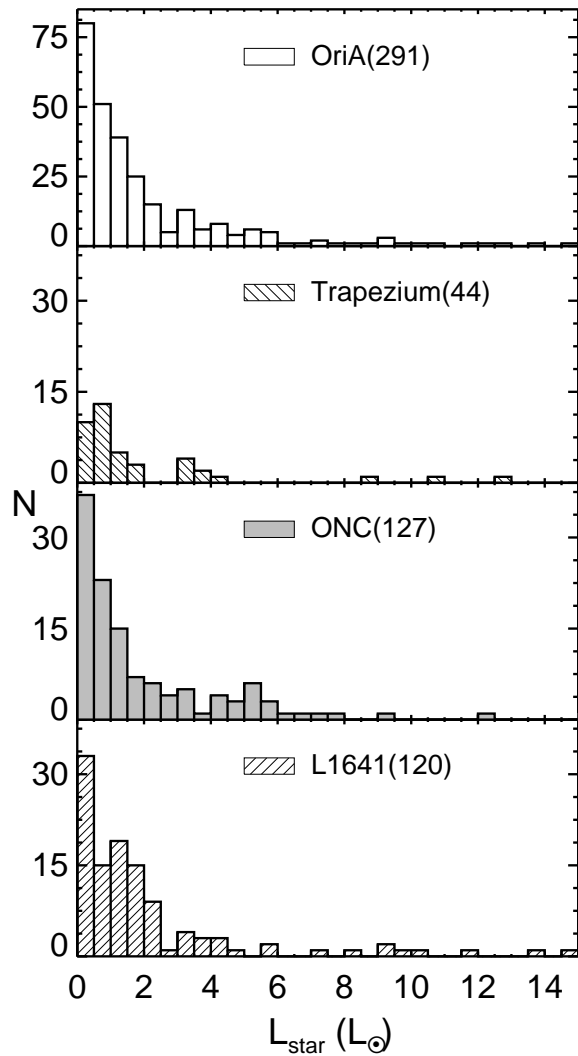


Fig. 10.— Distributions of L_{\star} of the objects in Orion A.

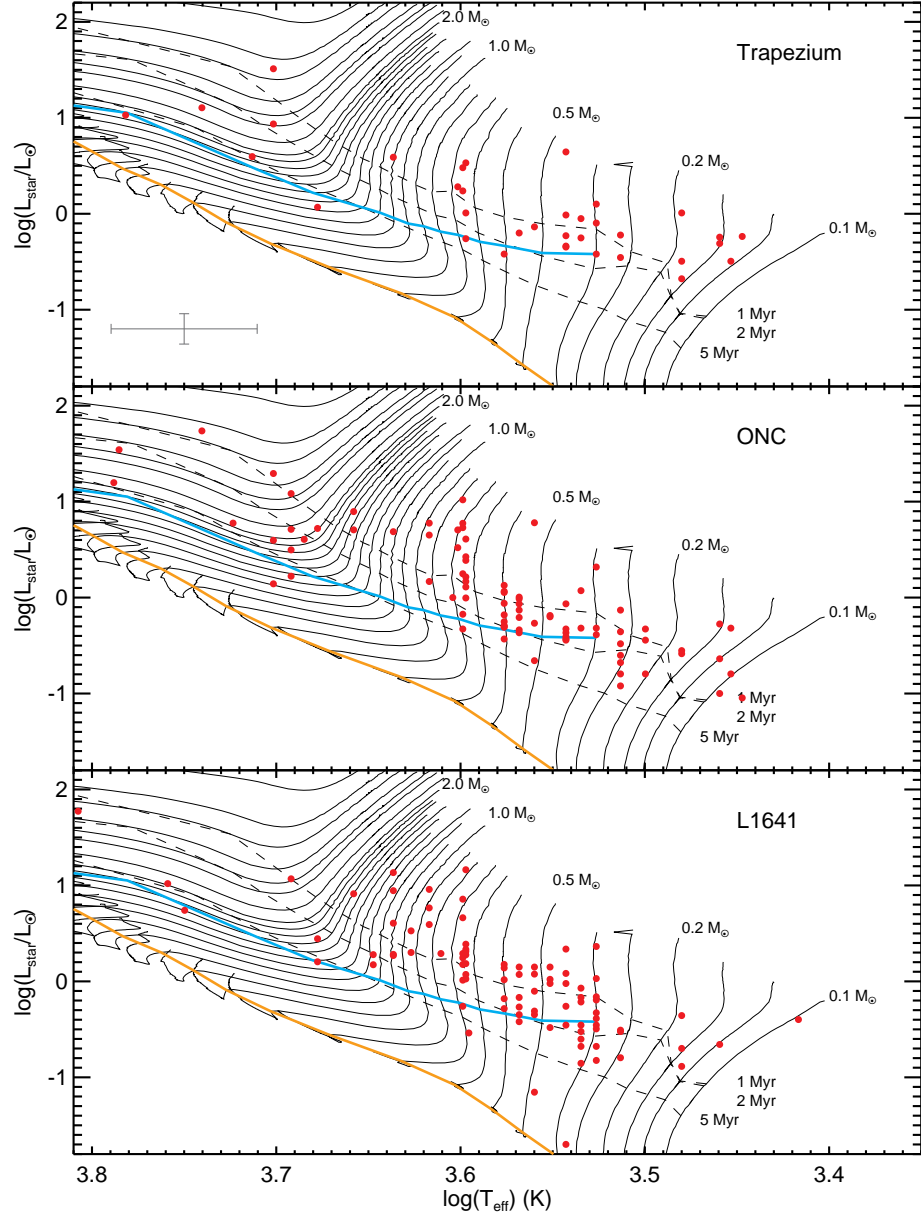


Fig. 11.— H-R diagrams for host stars of Class II objects in Orion A. Evolutionary tracks and isochrones are from Siess et al. (2000) ($Z=0.02$). Isochrone ages of systems of Class II objects in Orion A range from < 1 Myr to ~ 5 Myr. The average disk life time in Tau-Aur (Bertout et al. 2007) and the Zero Age Main Sequence (ZAMS) are also shown as cyan and orange solid lines, respectively, for reference. The cross on the left bottom of the top pannel represents a typical uncertainty in the spectral types of few (~ 3) subclasses. The represented uncertainty is calculated by assuming the uncertainty of T_{eff} is about 345 K, which is 0.16 in $\log(L_{\star}/L_{\odot})$ and 0.04 in $\log(T_{\text{eff}})$.

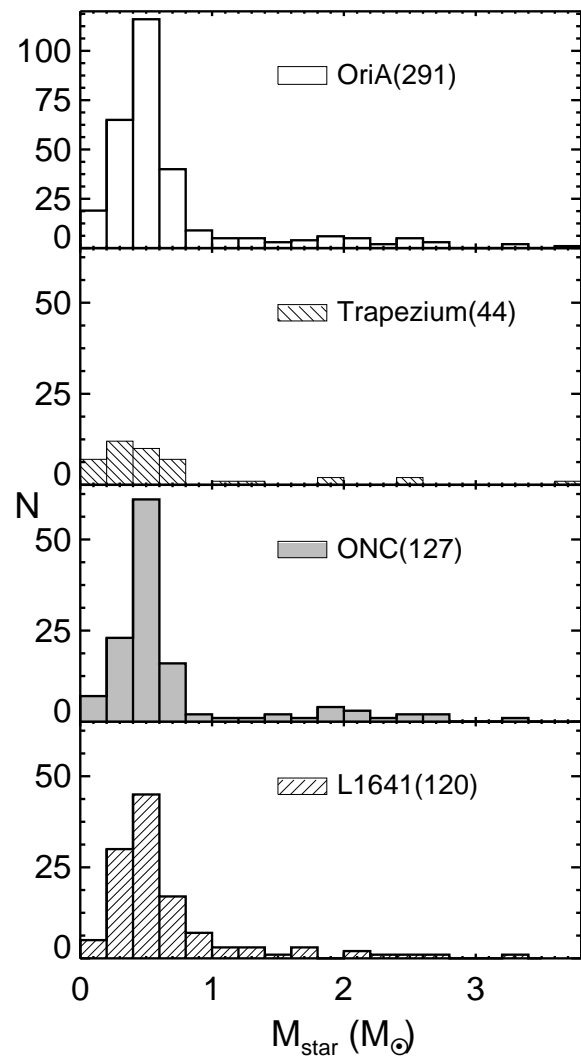


Fig. 12.— Distributions of M_{\star} of the objects in Orion A.

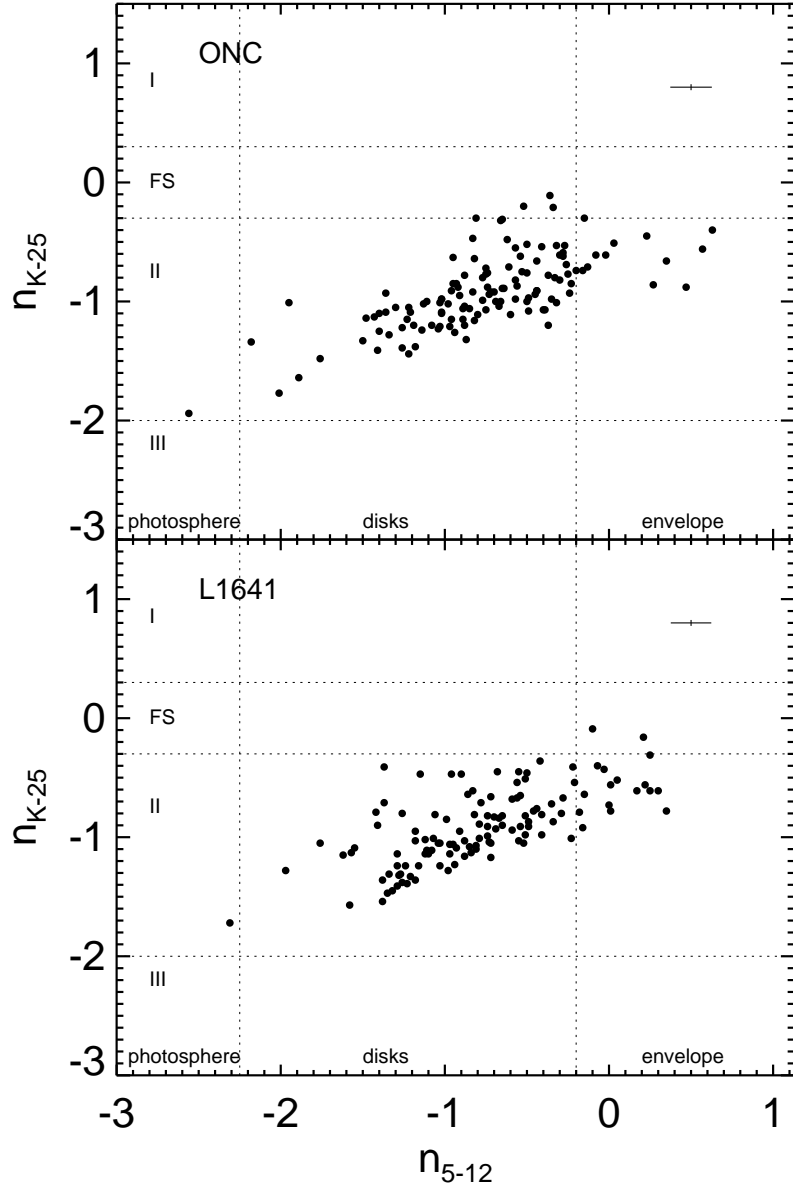


Fig. 13.— Comparison of the observed spectral indices and disk classification by n_{5-12} versus n_{K-25} for ONC (top) and L1641 (bottom). The horizontal dotted lines divide the regions occupied by Class I, Flat spectrum (FS), Class II, and Class III objects by the n_{K-25} criteria. The vertical dotted lines split the regions into photosphere, disks, and envelope by n_{5-12} . The typical errors are indicated on the top-right corner of each panel.

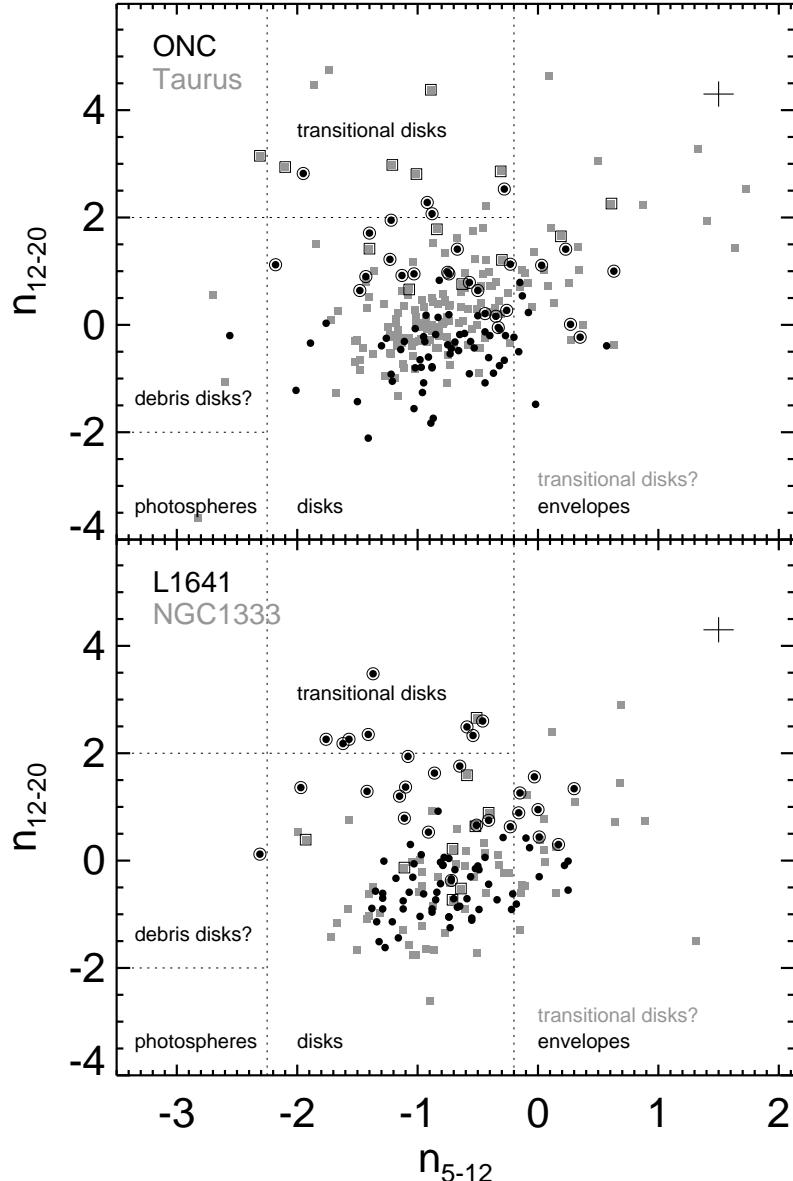


Fig. 14.— Comparison of the observed spectral indices and disk classification by n_{5-12} versus n_{12-20} . The vertical dotted lines indicate general division of envelopes, disks, and photospheric objects. Envelopes usually lie at $n_{5-12} \geq -0.2$, disks at $-2.25 \leq n_{5-12} < -0.2$, and photospheres at $n_{5-12} \leq -2.25$. Transitional disks occupy the region of disks in n_{5-12} , but have $n_{12-20} > 2$; a few can also be found at $0 \leq n_{12-20} < 2$ and $n_{5-12} \geq -0.2$. Debris disks have n_{5-12} values of photospheres, but n_{12-20} in the disk range. The upper panel is for objects in ONC (black circles) and for objects in Taurus (Furlan et al. (2011): gray squares) for comparison. The lower panel is for objects in L1641 (black circles) and for objects in NGC 1333 (Arnold et al. (2012): gray squares) for comparison. TDs classified in Kim et al. (2013) are indicated with larger open circles encompassing the filled circles for ONC and L1641 and larger open squares encompassing the filled squares for Taurus and NGC 1333. The typical errors are indicated on the top-right corner of each panel.

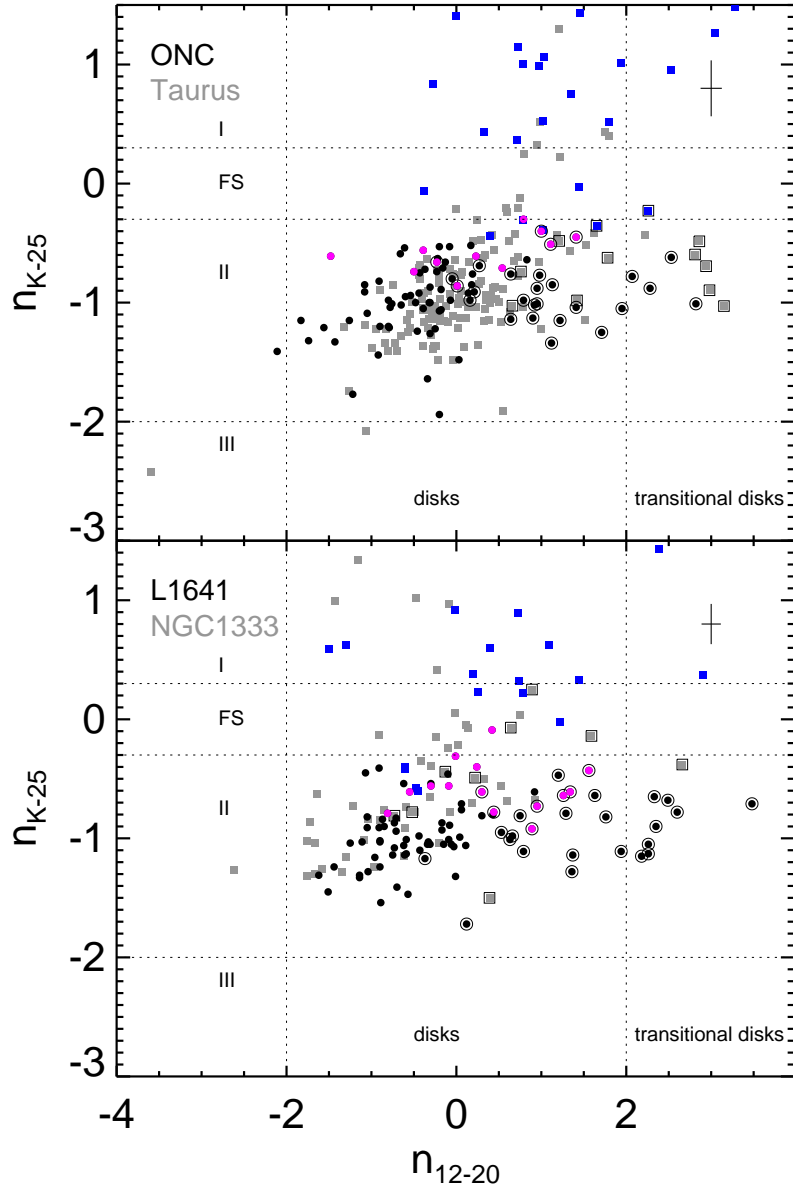


Fig. 15.— Comparison of the observed spectral indices and disk classification by n_{12-20} versus n_{K-25} . TDs classified in Kim et al. (2013) are indicated with larger open circles encompassing the filled circles for ONC and L1641 and larger open squares encompassing the filled squares for Taurus and NGC 1333. The colored symbols (magenta: ONC and L1641; blue: Taurus and NGC 1333) indicate the objects with $n_{5-12} > -0.2$, which are in the “envelopes” area in Figure 14. The typical errors are indicated on the top-right corner of each panel.

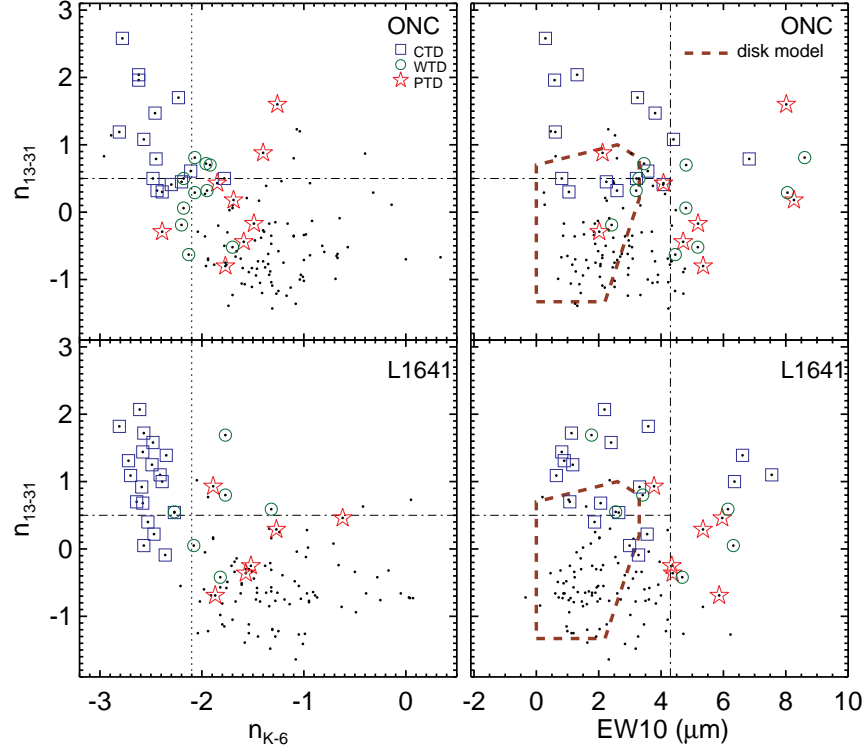


Fig. 16.— Classification of transitional disks in Orion A, and selection by n_{13-31} vs. n_{K-6} (left panels) and n_{13-31} vs. $EW10$ (right panels). In the right panels, the polygon with thick dashed brown line indicates the coverage area by a typical accretion disk model (D'Alessio et al. 2006). The upper panels are for the TD selection in ONC, and the lower panels are for the TD selection in L1641. The dash-dotted lines indicate the upper octile; the dotted lines indicate the lower octile. The blue squares indicate the candidates of CTDs. The green circles are for WTDs, and the red stars indicate PTDs. The definition of CTD, WTD, and PTD are in the section 4.3.2.

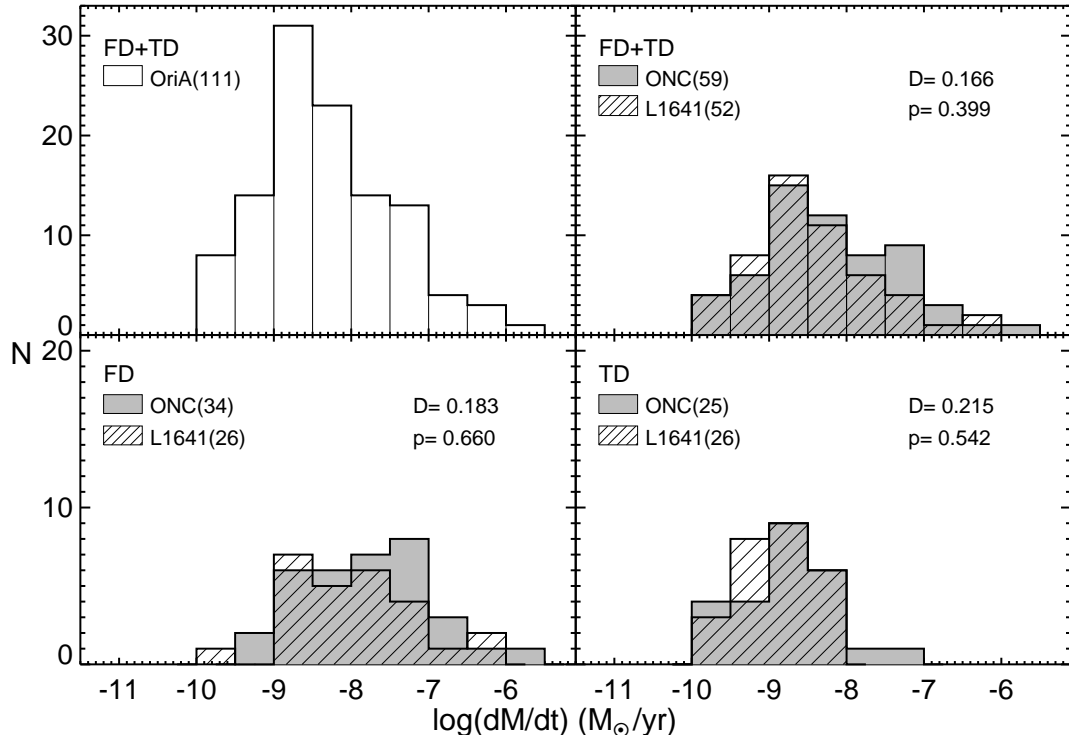


Fig. 17.— Distribution of \dot{M} . All of objects with available \dot{M} in Orion A is in the upper left panel. The upper right panel shows the distributions of \dot{M} of objects in ONC and L1641. The lower left panel is for the comparison of \dot{M} distribution of FDs in the ONC and L1641. The \dot{M} distribution of TDs in ONC and L1641 is in the lower right panel. The distribution of \dot{M} is slightly skewed toward to the higher value for ONC, but there is no statistically significant difference in \dot{M} between ONC and L1641 when the same disk group in two regions is compared. The K-S test results (D and p) are marked in each panel.

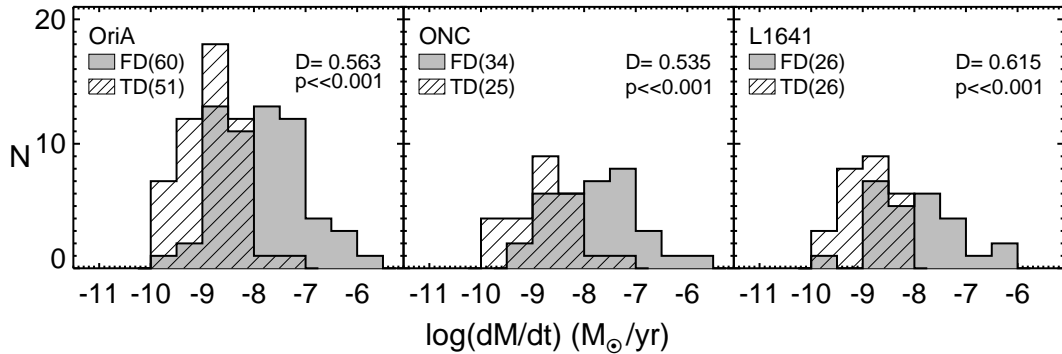


Fig. 18.— \dot{M} distributions between two groups, FD and TD, are compared in different regions: Orion A (left), ONC (middle), and L1641 (right). Distributions of \dot{M} are strongly significantly different between FD and TD in all three comparisons cases. The K-S test result of each comparison is shown in each panel.

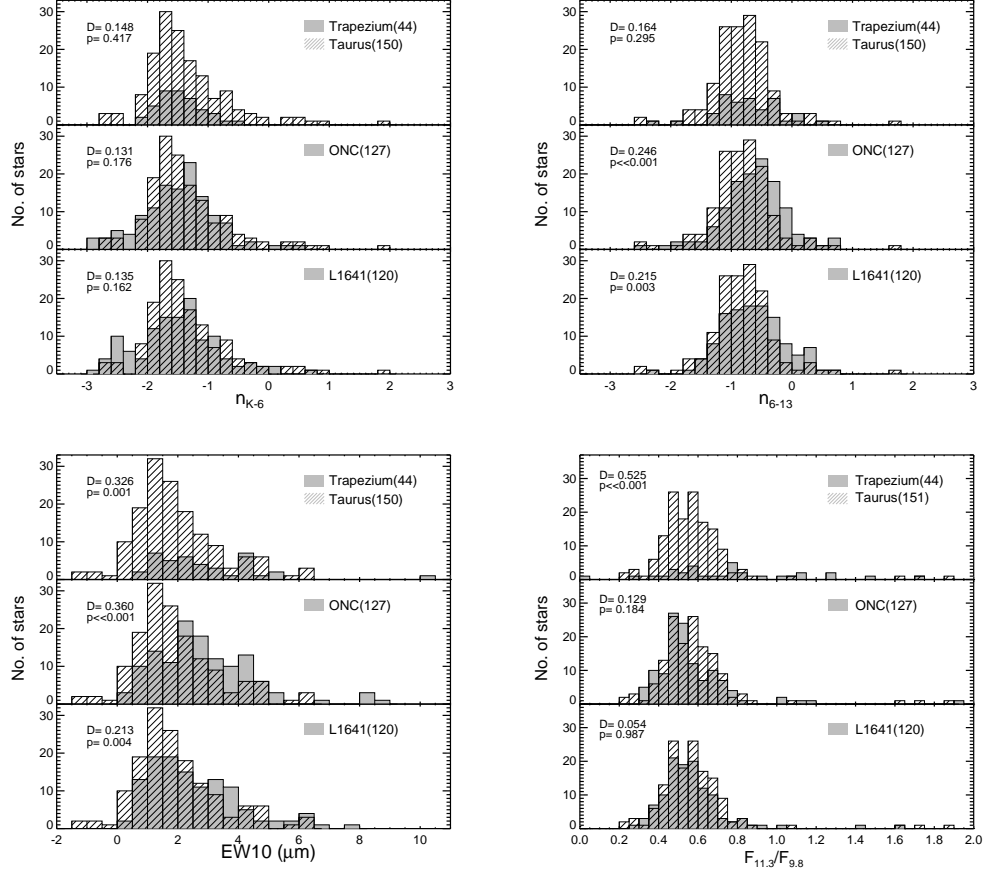


Fig. 19.— Histogram comparision of disk and dust properties measured from SL spectra. We include disks having n_{K-6} (upper left), n_{6-13} (upper right), EW10 (lower left), and $F_{11.3}/F_{9.8}$ (lower right) without separating the samples by their radial structures, FDs or TDs. We compare the distribution of each properties in this figure in three sub-regions of Orion A (Trapezium, ONC, and L1641) to that of Taurus. The K-S test result of each comparison is shown in each panel.

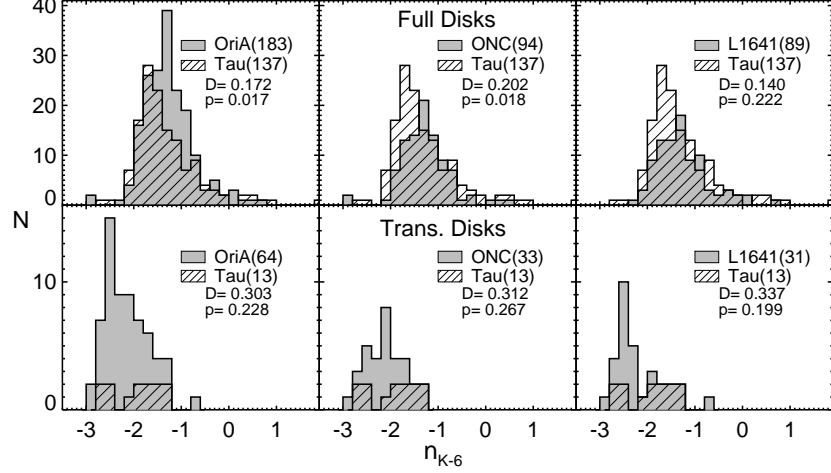


Fig. 20.— Comparison of n_{K-6} between Orion A (solid) and Taurus (hatched). The objects in the sample are separated by their radial strucuture, FDs or TDs (upper panels or lower panels), and by the sub-regions, OriA, ONC, or L1641 (left, middle, or right panels). The K-S test result of each comparison is shown in each panel.

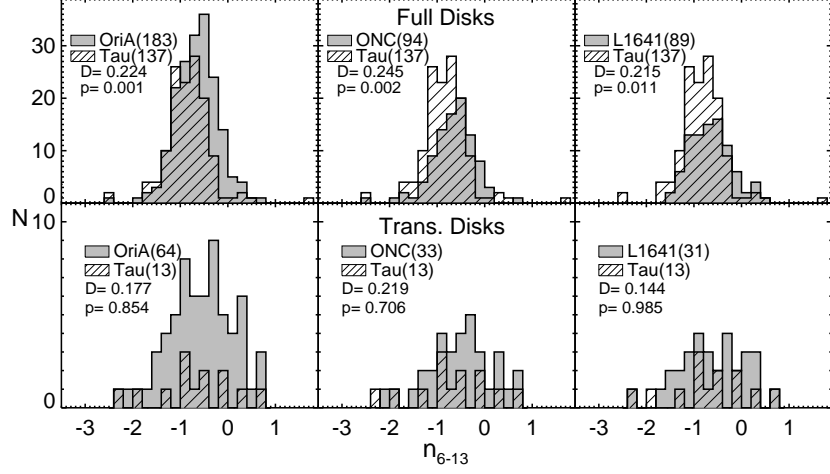


Fig. 21.— Comparison of n_{6-13} between Orion A (solid) and Taurus (hatched). The objects in the sample are separated by their radial strucuture, FDs or TDs (upper panels or lower panels), and by the sub-regions, OriA, ONC, or L1641 (left, middle, or right panels). The K-S test result of each comparison is shown in each panel.

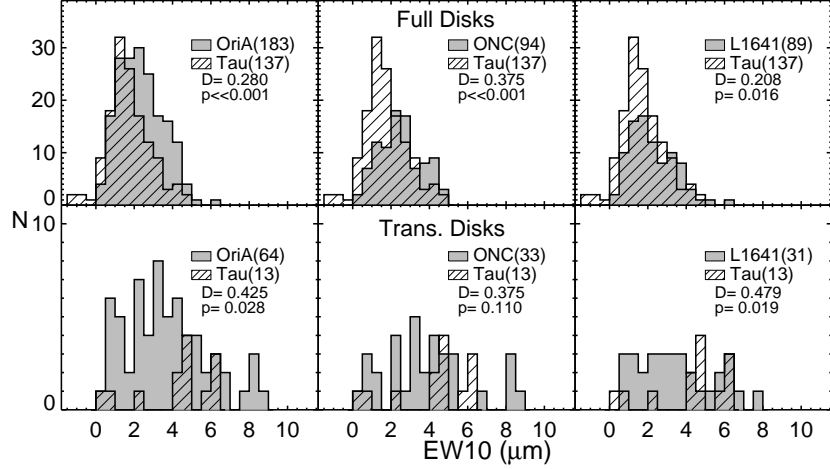


Fig. 22.— Comparison of $EW10$ between Orion A (solid) and Taurus (hatched). The objects in the sample are separated by their radial strucuture, FDs or TDs (upper panels or lower panels), and by the sub-regions, OriA, ONC, or L1641 (left, middle, or right panels). The K-S test result of each comparison is shown in each panel.

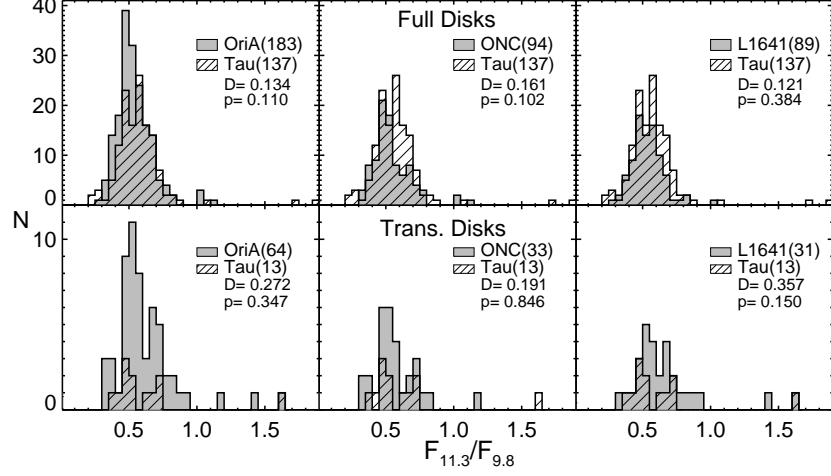


Fig. 23.— Comparison of $F_{11.3}/F_{9.8}$ between Orion A (solid) and Taurus (hatched). The objects in the sample are separated by their radial strucutre, FDs or TDs (upper panels or lower panels), and by the sub-regions, OriA, ONC, or L1641 (left, middle, or right panels). The K-S test result of each comparison is shown in each panel.

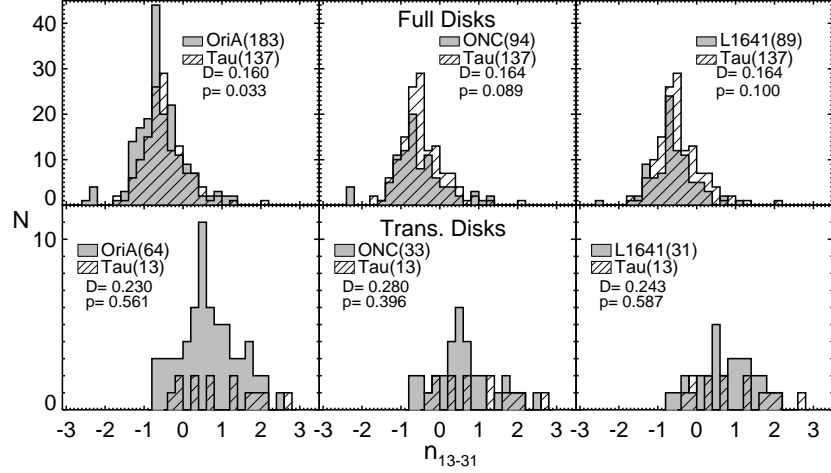


Fig. 24.— Comparison of n_{13-31} between Orion A (solid) and Taurus (hatched). The objects in the sample are separated by their radial strucuture, FDs or TDs (upper panels or lower panels), and by the sub-regions, OriA, ONC, or L1641 (left, middle, or right panels). The K-S test result of each comparison is shown in each panel.

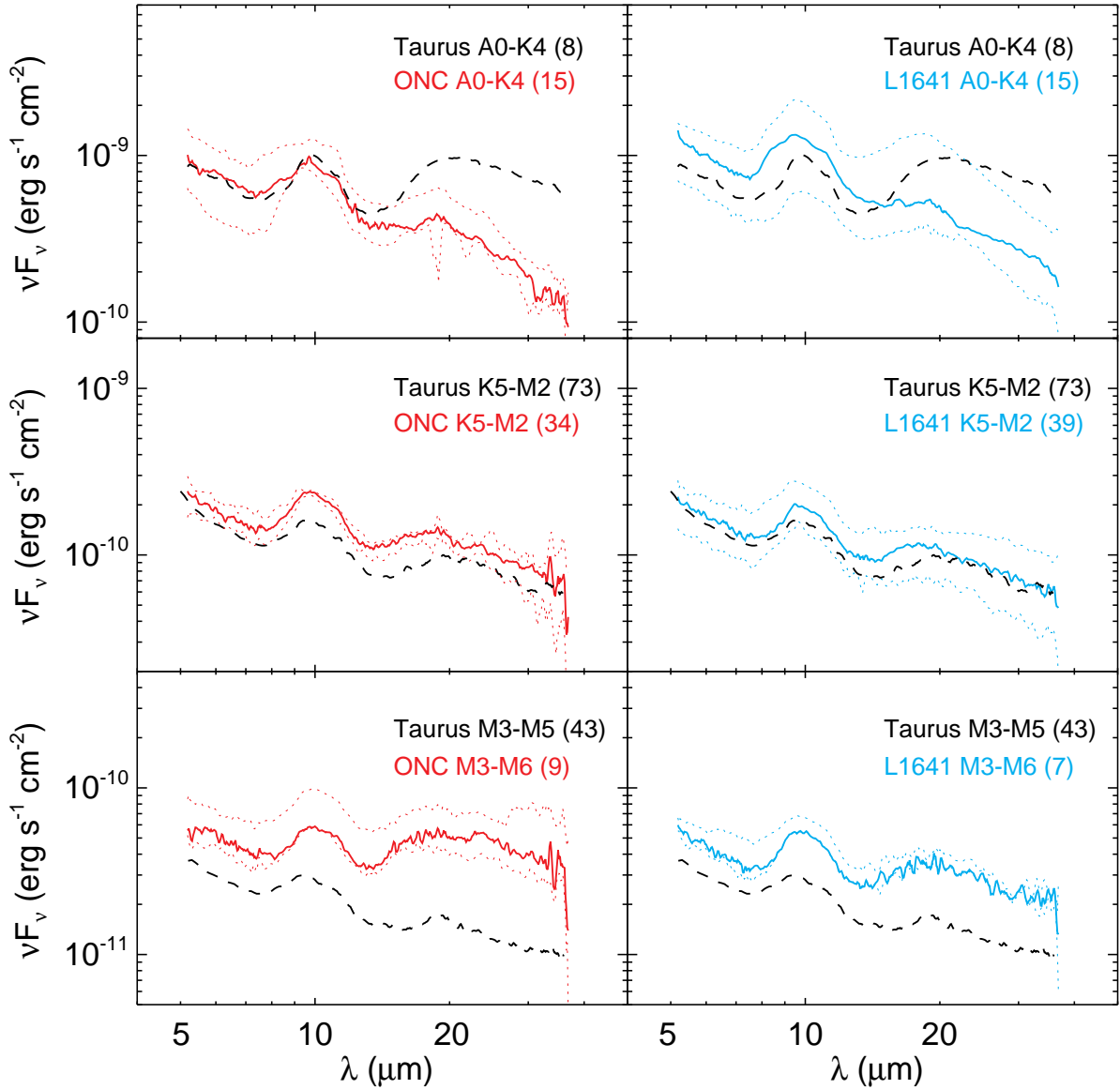


Fig. 25.— The median spectra of FDs in Orion A, separated by sub-regions and spectral type ranges. They are compared to Taurus median spectra. The number of objects used to generate a median spectrum is indicated next to the sign of spectral type range in each panel. The solid lines are the ONC median (left panels) and the L1641 median (right panels), and the dotted lines in each panel indicate upper and lower quartiles. The dashed lines are for the Taurus median indicated in each panel. The ONC median spectra and L1641 median spectra are normalized to the 2MASS H band median flux of the Taurus median spectra in each spectral range.

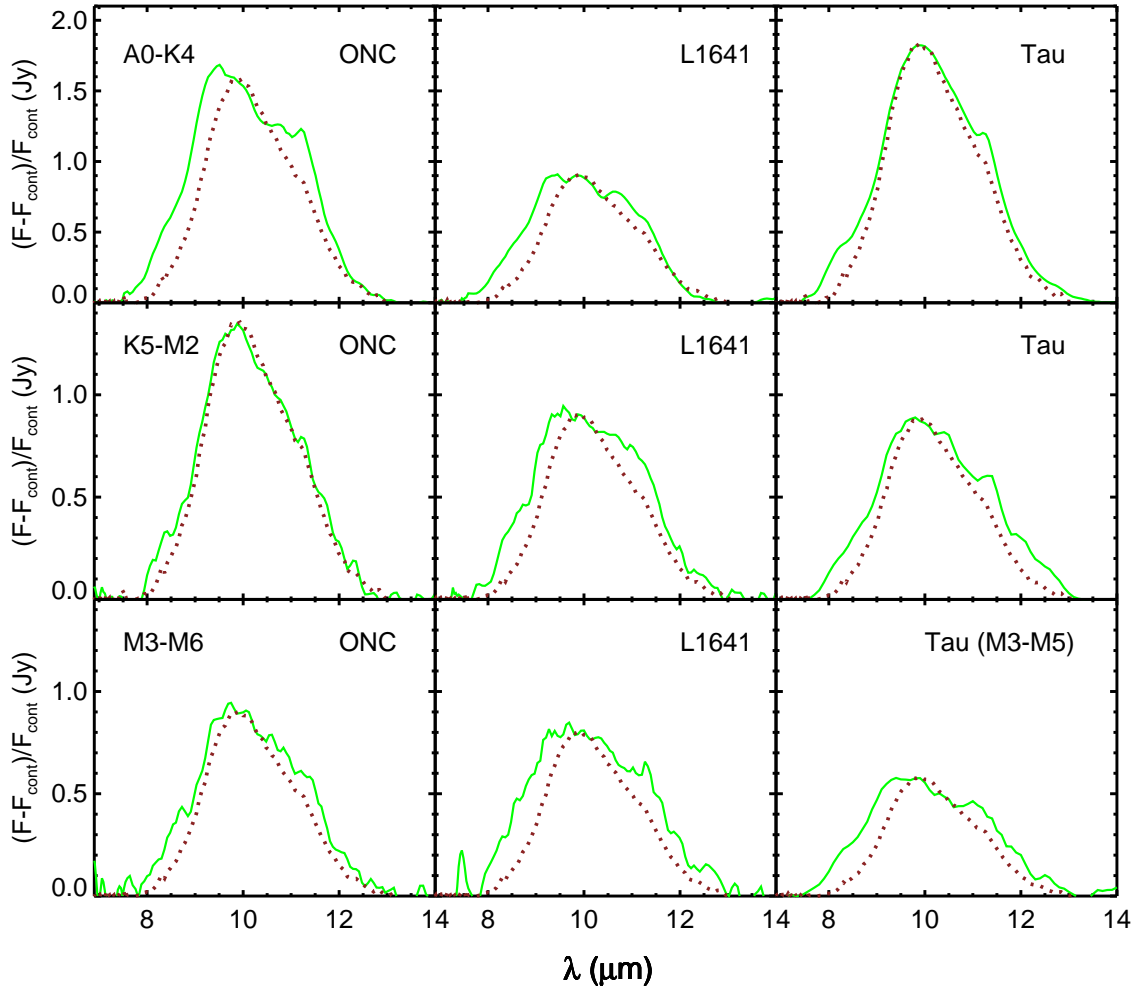


Fig. 26.— Comparison of continuum-subtracted and -normalized $10 \mu\text{m}$ silicate feature of median spectra (solid lines) to the pristine silicate feature (dotted lines). The pristine silicate profile is derived by averaging ISM-like reference spectra of LkCa 15 and GM Aur (Watson et al. 2009; Sargent et al. 2009) after subtracting continuum and dividing it with continuum. The pristine silicate profile are scaled to match to each median silicate profile at $9.8 \mu\text{m}$.

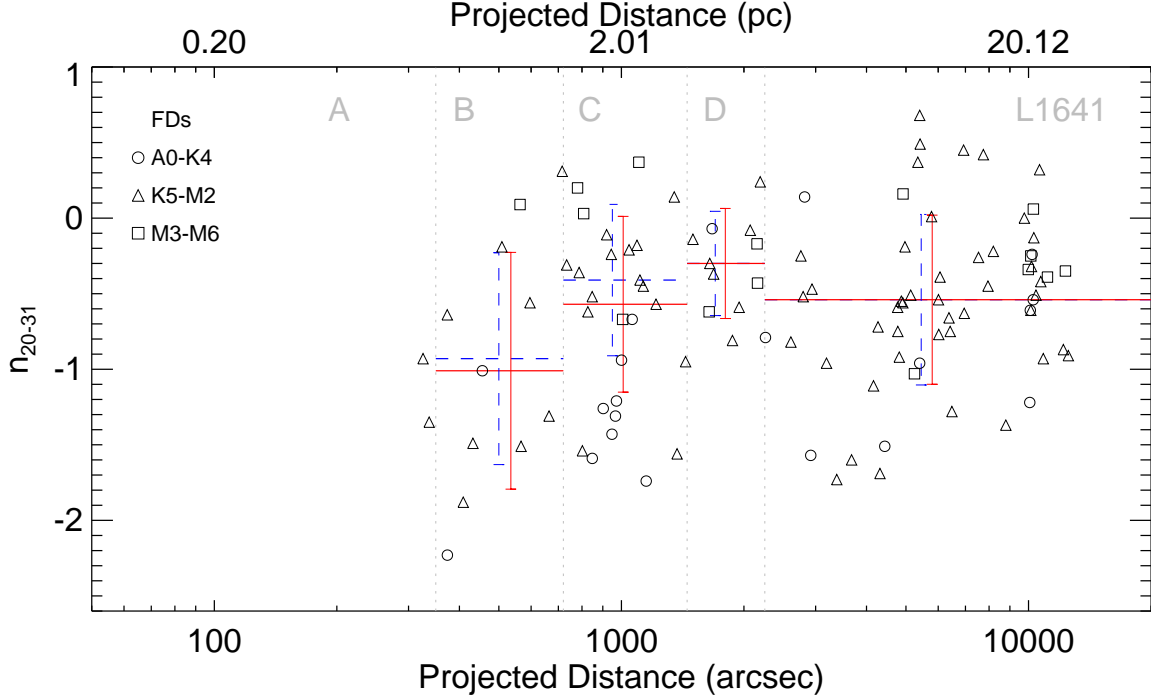


Fig. 27.— Variation of n_{20-31} with projected distance from θ^1 Ori C. The empty symbols indicate the spectral type ranges to which a object belongs: circle for A0–K4; triangle for K5–M2; square for M3–M6. The dashed horizontal lines indicate the n_{20-31} median of objects in K5–M2 group in each sub-section, which is indicated in Figure 1 and Figure 2. The solid horizontal lines indicate the median of all objects from A to M type in each sub-section. The error bars on the medians are taken from the standard deviation of n_{20-31} in each sub-section.

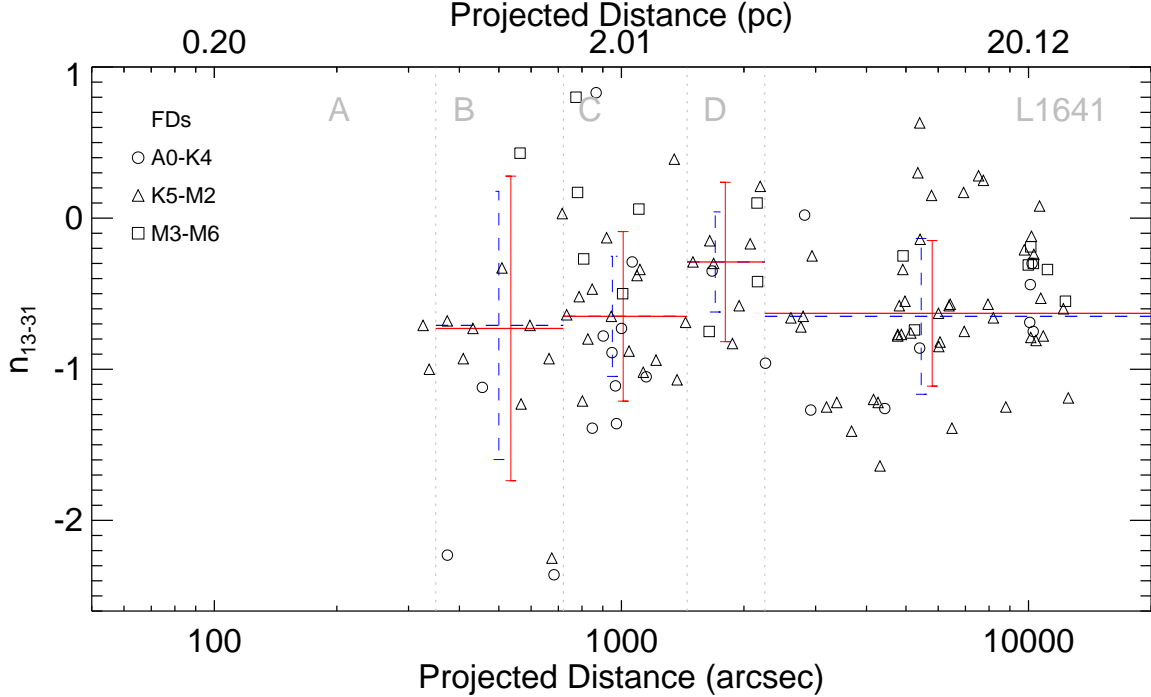


Fig. 28.— Variation of n_{13-31} with projected distance from θ^1 Ori C. The meanings of symbols are same as in Figure 27. The dashed horizontal lines indicate the n_{13-31} median of objects in K5–M2 group in each sub-section, which is indicated in Figure 1 and Figure 2. The solid horizontal lines indicate the median of all objects from A to M type in each sub-section. The error bars on the medians are taken from the standard deviation of n_{13-31} in each sub-section.

Table 1. Observation and Reduction Log of IRS Spectra

Num. (1)	IRS name (2)	RA (J2000) (3)	DEC (J2000) (4)	AORID (5)	IRS Camp. (6)	Date observed (7)	modules (8)	region (9)	reduction (10)
1	8336884-5290	5 33 28.52	-5 17 26.16	18804224	39	2007 Mar 12	SLLL	ONC	AdOpt
2	8330347-5238	5 33 34.43	-5 14 17.70	18843904	39	2007 Mar 12	SLLL	ONC	AdOpt
3	8343858-5513	5 33 45.26	-5 30 49.75	18825472	39	2007 Mar 12	SLLL	ONC	AdOpt
4	8343917-6073	5 33 45.40	-6 04 25.86	18848000	39	2007 Mar 09	SLLL	Li641	man
5	8343944-5609	5 33 45.47	-5 36 32.54	18833152	39	2007 Mar 12	SLLL	ONC	opse/AdOpt ^a
6	8344455-5390	5 33 46.69	-5 23 25.44	18802944	39	2007 Mar 24	SLLL	ONC	opse
7	8344987-5460	5 33 47.97	-5 27 38.56	18780672	44	2007 Oct 05	SLLL	ONC	man
8	8346141-5010	5 33 50.74	-5 00 39.46	18781952	39	2007 Mar 22	SLLL	ONC	AdOpt
9	8346378-5387	5 33 51.31	-5 23 16.62	18849536	39	2007 Mar 12	SLLL	ONC	man/AdOpt ^b
10	8346581-5550	5 33 51.79	-5 33 03.35	18830848	39	2007 Mar 12	SLLL	ONC	man
11	8347711-5533	5 33 54.51	-5 32 00.42	18844416	39	2007 Mar 12	SLLL	ONC	AdOpt
12	8348250-4797	5 33 55.80	-4 47 49.34	18832896	39	2007 Mar 24	SLLL	ONC	man
13	8350150-5595	5 34 00.36	-5 35 43.51	18778880	39	2007 Mar 12	SLLL	ONC	man
14	8350916-5605	5 34 02.20	-5 36 19.48	18811648	39	2007 Mar 12	SLLL	ONC	AdOpt
15	8352483-5378	5 34 05.96	-5 22 43.72	188117280	39	2007 Mar 12	SLLL	ONC	AdOpt
16	8353051-5229	5 34 07.32	-5 13 45.12	18801048	39	2007 Mar 22	SLLL	ONC	AdOpt
17	83553319-5604	5 34 07.97	-5 36 17.06	18838272	39	2007 Mar 09	SLLL	ONC	opse
18	83550833-4835	5 34 12.20	-4 50 07.12	18810624	39	2007 Mar 24	SLLL	ONC	AdOpt
19	83553371-5480	5 34 12.89	-5 28 48.29	18779904	44	2007 Oct 05	SLLL	ONC	Adopt/opse ^c
20	8355629-5594	5 34 13.51	-5 35 38.58	18840320	39	2007 Mar 12	SLLL	ONC	man
21	83558398-5615	5 34 14.16	-5 36 54.14	18832640	39	2007 Mar 12	SLLL	ONC	Adopt/man ^d
22	8356531-5540	5 34 15.67	-5 32 24.43	18820608	39	2007 Mar 12	SLLL	ONC	AdOpt
23	8357031-5072	5 34 16.87	-5 04 21.14	18836736	39	2007 Mar 22	SLLL	ONC	man
24	8358147-5505	5 34 19.55	-5 30 19.84	18812928	39	2007 Mar 24	SLLL	ONC	AdOpt
25	8358862-4842	5 34 21.27	-4 50 32.68	18776576	44	2007 Oct 11	SLLL	ONC	AdOpt
26	8359203-5026	5 34 22.09	-5 01 34.21	18776320	39	2007 Mar 22	SLLL	ONC	AdOpt
27	8360781-4940	5 34 25.87	-4 56 27.35	18830592	39	2007 Mar 22	SLLL	ONC	AdOpt
28	8360900-5441	5 34 26.16	-5 26 30.26	18837760	39	2007 Mar 24	SLLL	ONC	AdOpt
29	8361167-5475	5 34 26.80	-5 28 32.09	18778624	44	2007 Oct 05	SLLL	ONC	AdOpt
30	8362406-4863	5 34 29.77	-4 51 47.56	18809600	39	2007 Mar 24	SLLL	ONC	AdOpt
31	8364658-4871	5 34 35.18	-4 52 17.90	18836992	39	2007 Mar 24	SLLL	ONC	AdOpt
32	8364671-5575	5 34 35.21	-5 34 32.23	18823424	39	2007 Mar 27	SLLL	ONC	AdOpt
33	8365614-5581	5 34 37.47	-5 34 51.78	18840064	39	2007 Mar 27	SLLL	ONC	AdOpt
34	8365722-4816	5 34 37.73	-4 48 57.85	18781440	44	2007 Oct 11	SLLL	ONC	man

Table 1—Continued

Num. (1)	IRS name (2)	RA (J2000) (3)	DEC (J2000) (4)	AORID (5)	IRS Camp. (6)	Date observed (7)	modules (8)	region (9)	reduction (10)
35	8366668-51.68	5 34 40.00	-5 10 07.00	18815488	39	2007 Mar 22	SLLL	ONC	AdOpt
36	8366704-5669	5 34 40.09	-5 40 09.30	18844160	39	2007 Mar 12	SLLL	ONC	man
37	8367030-53.78	5 34 40.87	-5 22 42.28	18812160	39	2007 Mar 27	SLLL	ONC	AdOpt
38	8367284-57.98	5 34 41.48	-5 47 55.46	18838528	39	2007 Mar 24	SLLL	ONC	AdOpt
39	8368137-48.60	5 34 43.53	-4 51 36.25	18778368	44	2007 Oct 05	SLLL	ONC	AdOpt
40	8368755-49.33	5 34 45.01	-4 55 59.20	18809088	39	2007 Mar 24	SLLL	ONC	AdOpt
41	8368837-50.65	5 34 45.21	-5 39 57.02	18838784	39	2007 Mar 12	SLLL	ONC	man
42	8369106-56.86	5 34 45.85	-5 41 09.78	18840832	39	2007 Mar 12	SLLL	ONC	AdOpt
43	8369290-56.52	5 34 46.30	-5 39 07.74	18841600	39	2007 Mar 27	SLLL	ONC	man
44	8369980-50.81	5 34 47.95	-5 40 54.88	18817792	39	2007 Mar 22	SLLL	ONC	AdOpt
45	8370827-53.12	5 34 49.98	-5 18 44.50	18852352	39	2007 Mar 22	SLLL	ONC	man/opse e
46	8371143-54.50	5 34 50.74	-5 27 01.12	18810112	39	2007 Mar 27	SLLL	ONC	AdOpt
47	8371984-54.65	5 34 52.76	-5 27 54.90	18843648	39	2007 Mar 09	SLLL	ONC	AdOpt
48	8372100-50.57	5 34 53.04	-5 03 27.00	18803968	39	2007 Mar 22	SLLL	ONC	AdOpt
49	8372608-53.59	5 34 54.26	-5 21 35.28	18782464	39	2007 Mar 12	SL	Trapezium	AdOpt
50	8372885-52.83	5 34 54.92	-5 17 01.86	18847744	39	2007 Mar 22	SLLL	ONC	AdOpt
51	8373201-49.36	5 34 55.68	-4 56 12.12	18806016	39	2007 Mar 27	SLLL	ONC	AdOpt
52	8373676-51.92	5 34 56.82	-5 11 33.11	18828032	36	2006 Nov 10	SLLL	ONC	AdOpt
53	8373930-63.25	5 34 57.43	-6 19 33.02	18781696	39	2007 Mar 09	SLLL	L1641	man
54	8373936-49.46	5 34 57.45	-4 56 45.64	18808064	39	2007 Mar 26	SLLL	ONC	AdOpt
55	8374073-53.97	5 34 57.78	-5 23 52.44	18782720	39	2007 Mar 12	SL	Trapezium	AdOpt
56	8374080-53.80	5 34 57.79	-5 22 51.24	18782976	39	2007 Mar 22	SL	Trapezium	AdOpt/man m
57	8374271-56.97	5 34 58.25	-5 41 49.74	18842368	39	2007 Mar 12	SLLL	ONC	man
58	8374301-59.08	5 34 58.32	-5 54 28.84	18808320	39	2007 Mar 12	SLLL	ONC	AdOpt
59	8374388-60.00	5 34 58.53	-6 00 00.43	18820864	44	2007 Oct 05	SLLL	L1641	man
60	8374599-57.41	5 34 59.04	-5 44 29.80	18813952	39	2007 Mar 12	SLLL	ONC	AdOpt
61	8374677-57.48	5 34 59.22	-5 44 55.32	18806272	39	2007 Mar 12	SLLL	ONC	man/opse e
62	8374677-57.66	5 34 59.22	-5 45 58.72	18810880	39	2007 Mar 12	SLLL	ONC	opse
63	8374839-54.27	5 34 59.61	-5 25 39.83	18783232	39	2007 Mar 24	SL	Trapezium	AdOpt
64	8375041-53.83	5 35 00.10	-5 23 01.86	18783488	39	2007 Mar 22	SL	Trapezium	man
65	8375063-5840	5 35 00.15	-5 50 27.38	18839040	39	2007 Mar 12	SLLL	ONC	AdOpt
66	8375158-51.62	5 35 00.38	-5 09 43.99	18779648	44	2007 Oct 05	SLLL	ONC	AdOpt
67	8375190-54.20	5 35 00.46	-5 25 14.30	18783744	39	2007 Mar 24	SL	Trapezium	AdOpt
68	8375484-54.01	5 35 00.16	-5 24 06.66	18784000	39	2007 Mar 24	SL	Trapezium	AdOpt

Table 1—Continued

Num. (1)	IRS name (2)	RA (J2000) (3)	DEC (J2000) (4)	AORID (5)	IRS Camp. (6)	Date observed (7)	modules (8)	region (9)	reduction (10)
69	8375546-5339	5 35 01.31	-5 20 22.24	18784256	39	2007 Mar 22	SL	Trapezium	failed
70	8375702-5443	5 35 01.68	-5 26 36.24	18784512	39	2007 Mar 24	SL	Trapezium	AdOpt
71	8375886-5399	5 35 02.13	-5 23 56.76	18784768	39	2007 Mar 21	SL	Trapezium	AdOpt
72	8376139-5329	5 35 02.73	-5 19 44.54	18785024	39	2007 Mar 22	SL	Trapezium	failed
73	8376154-5675	5 35 02.77	-5 40 30.86	18834944	40	2007 Apr 18	SLLL	ONC	AdOpt
74	8376176-5368	5 35 02.82	-5 22 08.18	18785280	39	2007 Mar 22	SL	Trapezium	AdOpt
75	8376287-5377	5 35 03.09	-5 22 37.70	18785536	39	2007 Mar 22	SL	Trapezium	AdOpt
76	8376336-4822	5 35 03.25	-4 49 21.00	18803456	39	2007 Mar 24	SLLL	ONC	AdOpt
77	8376541-5379	5 35 03.70	-5 22 45.77	18785792	39	2007 Mar 22	SL	Trapezium	AdOpt
78	8376571-5415	5 35 03.77	-5 24 54.40	18786048	39	2007 Mar 24	SL	Trapezium	AdOpt
79	8376643-5900	5 35 03.94	-5 54 01.84	18812416	39	2007 Mar 12	SLLL	ONC	AdOpt
80	8376687-5443	5 35 04.05	-5 26 37.18	18786304	39	2007 Mar 24	SL	Trapezium	AdOpt
81	8376747-5441	5 35 04.19	-5 26 27.82	18786560	39	2007 Mar 24	SL	Trapezium	AdOpt
82	8376817-5387	5 35 04.36	-5 23 13.70	18786816	39	2007 Mar 22	SL	Trapezium	AdOpt
83	8376871-5399	5 35 04.49	-5 23 56.51	18787072	39	2007 Mar 24	SL	Trapezium	AdOpt
84	8376918-4974	5 35 04.60	-4 58 28.92	18805760	39	2007 Mar 26	SLLL	ONC	AdOpt
85	8376976-5443	5 35 04.74	-5 26 37.93	18787328	39	2007 Mar 24	SL	Trapezium	AdOpt
86	8377111-5612	5 35 05.07	-5 36 43.78	18851328	40	2007 Apr 18	SLLL	ONC	AdOpt
87	8377137-5340	5 35 05.13	-5 20 24.40	18787584	39	2007 Mar 22	SL	Trapezium	failed
88	8377167-5247	5 35 05.20	-5 14 50.28	18802176	39	2007 Mar 24	SLLL	ONC	AdOpt
89	8377232-5402	5 35 05.36	-5 24 10.30	18787840	39	2007 Mar 22	SL	Trapezium	AdOpt
90	8377335-5489	5 35 05.60	-5 29 22.31	18828544	39	2007 Mar 25	SLLL	ONC	AdOpt
91	8377345-5422	5 35 05.63	-5 25 19.24	18788096	39	2007 Mar 22	SL	Trapezium	AdOpt/man m
92	8377361-5395	5 35 05.67	-5 23 45.31	18788352	39	2007 Mar 22	SL	Trapezium	AdOpt
93	8377383-5405	5 35 05.72	-5 24 18.54	18788608	39	2007 Mar 24	SL	Trapezium	AdOpt
94	8377392-5193	5 35 05.74	-5 11 34.94	18831872	39	2007 Mar 22	SLLL	ONC	AdOpt
95	8377737-5547	5 35 06.57	-5 32 51.40	18814976	39	2007 Mar 27	SLLL	ONC	AdOpt
96	8377749-5447	5 35 06.60	-5 26 50.96	18788864	39	2007 Mar 24	SL	Trapezium	AdOpt
97	8377803-5644	5 35 07.34	-5 38 40.96	18816512	39	2007 Mar 27	SLLL	ONC	AdOpt
98	83778345-5545	5 35 08.03	-5 32 44.34	18846464	39	2007 Mar 27	SLLL	ONC	AdOpt
99	83778366-5814	5 35 08.08	-5 48 53.78	18839296	39	2007 Mar 12	SL	Trapezium	AdOpt
100	83778481-5465	5 35 08.35	-5 27 56.95	18789120	39	2007 Mar 24	SL	Trapezium	AdOpt
101	83778503-5474	5 35 08.41	-5 28 29.42	18789376	39	2007 Mar 24	SL	Trapezium	AdOpt
102	83778561-5421	5 35 08.55	-5 25 17.90	18789632	39	2007 Mar 24	SL	Trapezium	AdOpt

Table 1—Continued

Num. (1)	IRS name (2)	RA (J2000) (3)	DEC (J2000) (4)	AORID (5)	IRS Camp. (6)	Date observed (7)	modules (8)	region (9)	reduction (10)
103	8378630-4781	5 35 08.71	-4 46 52.46	18833920	39	2007 Mar 24	SLLL	ONC	man
104	8379094-5316	5 35 09.83	-5 18 58.28	18789888	39	2007 Mar 24	SL	Trapezium	failed
105	8379108-5326	5 35 09.86	-5 19 34.07	18790144	39	2007 Mar 22	SLLL	Trapezium	failed
106	8379192-6093	5 35 10.06	-6 05 36.42	18844672	39	2007 Mar 09	SLLL	L1641	man
107	8379289-5332	5 35 10.29	-5 19 56.24	18790400	39	2007 Mar 22	SL	Trapezium	failed
108	8379312-5776	5 35 10.35	-5 46 33.82	18850560	39	2007 Mar 12	SLLL	ONC	man
109	8379445-5350	5 35 11.87	-5 21 00.36	18790656	39	2007 Mar 22	SL	Trapezium	failed
110	8379950-5323	5 35 11.88	-5 19 26.29	18790912	39	2007 Mar 22	SL	Trapezium	failed
111	8379990-5342	5 35 11.98	-5 20 33.14	18791168	39	2007 Mar 22	SL	Trapezium	failed
112	8380422-5659	5 35 13.01	-5 39 34.99	18824960	40	2007 Apr 18	SLLL	ONC	AdOpt
113	8380493-5291	5 35 13.18	-5 17 30.84	18791424	39	2007 Mar 22	SL	Trapezium	failed
114	8380518-5465	5 35 13.24	-5 27 54.36	18791680	39	2007 Mar 24	SL	AdOpt	AdOpt
115	8380544-5338	5 35 13.31	-5 20 18.92	18791936	39	2007 Mar 22	SL	Trapezium	failed
116	8380651-5296	5 35 13.56	-5 17 45.74	18792192	39	2007 Mar 22	SL	Trapezium	failed
117	8380667-5516	5 35 13.60	-5 30 57.67	18819840	40	2007 Apr 18	SLLL	ONC	AdOpt
118	8380675-5331	5 35 13.62	-5 19 55.02	18792448	39	2007 Mar 22	SL	Trapezium	failed
119	8380695-5479	5 35 13.67	-5 28 46.27	18792704	39	2007 Mar 24	SL	AdOpt	AdOpt
120	8380923-5478	5 35 14.22	-5 28 43.21	18792960	39	2007 Mar 22	SL	Trapezium	failed
121	8380932-5721	5 35 14.24	-5 43 17.58	18845440	39	2007 Mar 12	SLLL	ONC	AdOpt
122	8381019-5555	5 35 14.45	-5 33 18.94	18851840	39	2007 Mar 27	SLLL	ONC	AdOpt
123	8381020-5546	5 35 14.45	-5 32 46.36	18809856	39	2007 Mar 27	SLLL	ONC	AdOpt
124	8381104-5345	5 35 14.65	-5 20 42.29	18793216	39	2007 Mar 22	SL	Trapezium	failed
125	8381120-5653	5 35 14.69	-5 39 10.94	18832128	39	2007 Mar 22	SLLL	ONC	AdOpt
126	8381436-5294	5 35 15.45	-5 17 38.80	18793472	39	2007 Mar 22	SL	Trapezium	failed
127	8381491-5164	5 35 15.58	-5 09 51.26	18834688	39	2007 Mar 22	SLLL	ONC	AdOpt
128	8381501-4991	5 35 15.60	-4 59 27.96	18799360	39	2007 Mar 26	SLLL	ONC	AdOpt
129	8381622-5481	5 35 15.89	-5 28 52.93	18793728	39	2007 Mar 09	SL	Trapezium	AdOpt
130	8381919-5289	5 35 16.61	-5 17 23.28	18793984	39	2007 Mar 22	SL	Trapezium	failed
131	8381971-4762	5 35 16.73	-4 45 44.50	18852096	39	2007 Mar 24	SLLL	ONC	man
132	8382048-5452	5 35 16.92	-5 27 08.78	18794240	39	2007 Mar 24	SL	Trapezium	AdOpt
133	8382359-5974	5 35 17.66	-5 58 26.76	18799616	40	2007 Apr 18	SLLL	ONC	AdOpt
134	8382412-6410	5 35 17.79	-6 24 38.34	18845952	39	2007 Mar 09	SLLL	L1641	man
135	8382467-5709	5 35 17.92	-5 42 33.48	18802988	39	2007 Mar 12	SLLL	ONC	AdOpt
136	8382490-5270	5 35 17.98	-5 16 13.91	18827776	39	2007 Mar 24	SLLL	ONC	AdOpt

Table 1—Continued

Num. (1)	IRS name (2)	RA (J2000) (3)	DEC (J2000) (4)	AORID (5)	IRS Camp. (6)	Date observed (7)	modules (8)	region (9)	reduction (10)
137	8382623-5479	5 35 18.30	-5 28 46.34	18794496	39	2007 Mar 12	SL	Trapezium	AdOpt
138	8382635-4889	5 35 18.37	-4 53 23.46	18849024	39	2007 Mar 26	SLLL	ONC	AdOpt
139	8382835-5291	5 35 18.80	-5 17 29.18	18794752	36	2006 Nov 11	SL	Trapezium	AdOpt
140	8383581-5050	5 35 20.59	-5 03 00.58	18851072	39	2007 Mar 25	SLLL	ONC	AdOpt
141	8383861-5154	5 35 21.27	-5 09 16.20	18803712	39	2007 Mar 25	SLLL	ONC	AdOpt
142	8384113-5117	5 35 21.87	-5 07 01.74	18842112	39	2007 Mar 25	SLLL	ONC	AdOpt
143	8384325-5457	5 35 22.38	-5 27 28.48	18795008	39	2007 Mar 24	SL	Trapezium	AdOpt
144	8384331-5134	5 35 22.39	-5 08 04.99	18824704	39	2007 Mar 25	SLLL	ONC	man/AdOpt ^b
145	8384717-5469	5 35 23.32	-5 28 10.09	18795264	39	2007 Mar 24	SL	Trapezium	AdOpt
146	8384864-5440	5 35 23.67	-5 26 27.06	18795520	39	2007 Mar 24	SL	Trapezium	AdOpt
147	8385190-5442	5 35 24.46	-5 26 31.45	18795776	39	2007 Mar 09	SL	Trapezium	AdOpt
148	8385255-5191	5 35 24.61	-5 11 29.80	18813696	39	2007 Mar 25	SLLL	ONC	man
149	8385365-5106	5 35 24.88	-5 06 21.60	18798592	39	2007 Mar 25	SLLL	ONC	AdOpt
150	8385988-5427	5 35 26.37	-5 25 40.12	18796032	39	2007 Mar 22	SL	Trapezium	AdOpt
151	8386322-6328	5 35 27.17	-6 19 41.88	18802432	39	2007 Mar 09	SLLL	L1641	man
152	8386383-5393	5 35 27.32	-5 23 36.56	18796288	39	2007 Mar 22	SL	Trapezium	AdOpt
153	8386462-5457	5 35 27.51	-5 27 25.81	18796544	39	2007 Mar 24	SL	Trapezium	AdOpt
154	8386523-5715	5 35 27.66	-5 42 55.08	18801664	39	2007 Mar 12	SLLL	ONC	AdOpt
155	8386627-5467	5 35 27.90	-5 28 02.24	18796800	39	2007 Mar 24	SL	Trapezium	AdOpt
156	8386694-5026	5 35 28.07	-5 01 34.82	18835456	39	2007 Mar 26	SLLL	ONC	opse
157	8386722-5315	5 35 28.13	-5 18 57.28	18797056	39	2007 Mar 22	SL	Trapezium	failed
158	8386739-5416	5 35 28.22	-5 24 58.10	18797312	39	2007 Mar 22	SL	Trapezium	AdOpt
159	8386804-5987	5 35 28.33	-5 59 13.38	18841088	40	2007 Apr 18	SLLL	ONC	AdOpt
160	8386841-5129	5 35 28.42	-5 07 44.44	18808576	39	2007 Mar 25	SLLL	ONC	AdOpt
161	8386935-4790	5 35 28.64	-4 47 26.59	18823680	39	2007 Mar 24	SLLL	ONC	AdOpt
162	8386937-4804	5 35 28.70	-4 48 16.31	18828288	39	2007 Mar 24	SLLL	ONC	man
163	8387691-5326	5 35 30.46	-5 19 34.10	18797568	36	2006 Nov 11	SL	Trapezium	AdOpt
164	8387753-4993	5 35 30.61	-4 59 36.02	18835200	39	2007 Mar 26	SLLL	ONC	opse/AdOpt ^f
165	8387832-5864	5 35 30.80	-5 51 51.19	18821632	40	2007 Apr 18	SLLL	ONC	AdOpt
166	8387937-6755	5 35 31.05	-6 45 18.18	18840576	39	2007 Mar 09	SLLL	L1641	AdOpt
167	8388119-5083	5 35 31.49	-5 05 01.75	18829216	39	2007 Mar 25	SLLL	ONC	AdOpt
168	8388316-5157	5 35 31.96	-5 09 28.08	18807552	39	2007 Mar 25	SLLL	ONC	AdOpt
169	8389033-4773	5 35 33.68	-4 46 23.52	18775040	39	2007 Mar 24	SLLL	ONC	AdOpt
170	8389275-5105	5 35 34.26	-5 06 21.38	18839552	39	2007 Mar 27	SLLL	ONC	AdOpt

Table 1—Continued

Num. (1)	IRS name (2)	RA (J2000) (3)	DEC (J2000) (4)	AORID (5)	IRS Camp. (6)	Date observed (7)	modules (8)	region (9)	reduction (10)
171	8389323-5449	5 35 34.38	-5 26 59.75	18797824	36	2006 Nov 10	SL	Trapezium	failed
172	8389673-4794	5 35 35.22	-4 47 39.52	18810368	39	2007 Mar 24	SLLL	ONC	man
173	8390003-5207	5 35 36.01	-5 12 25.27	18820096	39	2007 Mar 25	SLLL	ONC	AdOpt
174	8390073-5082	5 35 36.18	-5 04 56.03	18826752	39	2007 Mar 26	SLLL	ONC	AdOpt
175	8390083-5339	5 35 36.20	-5 20 20.58	18798080	39	2007 Mar 22	SL	Trapezium	AdOpt
176	8390285-5070	5 35 36.68	-5 04 14.56	18815744	39	2007 Mar 26	SLLL	ONC	AdOpt
177	8390554-6390	5 35 37.33	-6 23 26.23	18780928	39	2007 Mar 12	SLLL	L1641	AdOpt
178	8391040-5081	5 35 38.50	-5 04 51.67	18819584	39	2007 Mar 26	SLLL	ONC	AdOpt
179	8391058-4994	5 35 38.54	-4 59 41.10	18846976	39	2007 Mar 26	SLLL	ONC	AdOpt
180	8391196-5211	5 35 38.87	-5 12 42.16	18816000	39	2007 Mar 25	SLLL	ONC	AdOpt/opse ^c
181	8391648-5110	5 35 39.96	-5 06 36.72	18800640	39	2007 Mar 27	SLLL	ONC	AdOpt
182	8392509-5169	5 35 42.02	-5 10 11.68	18819328	39	2007 Mar 27	SLLL	ONC	AdOpt
183	8393152-5094	5 35 43.56	-5 05 41.35	18825728	39	2007 Mar 27	SLLL	ONC	AdOpt
184	8394216-5181	5 35 46.12	-5 10 51.71	18825984	39	2007 Mar 27	SLLL	ONC	AdOpt
185	8394454-5823	5 35 46.69	-5 49 26.08	18818048	39	2007 Mar 25	SLLL	ONC	AdOpt
186	8395167-5024	5 35 48.40	-5 01 28.96	18816256	39	2007 Mar 27	SLLL	ONC	AdOpt
187	8395780-5308	5 35 49.87	-5 18 30.64	18813184	36	2006 Nov 11	SLLL	ONC	AdOpt
188	8396035-5861	5 35 50.48	-5 51 42.26	18838016	44	2007 Oct 05	SLLL	ONC	AdOpt
189	8396285-5119	5 35 51.08	-5 07 08.83	18821120	39	2007 Mar 27	SLLL	ONC	AdOpt
190	8396319-4941	5 35 51.17	-4 56 27.71	18826240	39	2007 Mar 26	SLLL	ONC	AdOpt
191	8396679-6167	5 35 52.03	-6 10 01.56	18800128	39	2007 Mar 09	SLLL	L1641	man
192	8397522-4788	5 35 54.05	-4 47 19.50	18847232	39	2007 Mar 24	SLLL	ONC	AdOpt
193	8397632-5445	5 35 54.32	-5 26 44.30	18837504	39	2007 Mar 27	SLLL	ONC	AdOpt
194	8397818-4972	5 35 54.76	-4 58 20.06	18834432	39	2007 Mar 26	SLLL	ONC	AdOpt
195	8398707-5755	5 35 56.90	-5 45 19.08	18801920	39	2007 Mar 25	SLLL	ONC	AdOpt/opse ^g
196	8398936-6711	5 35 57.45	-6 42 41.90	18837248	39	2007 Mar 09	SLLL	L1641	AdOpt
197	8399022-5955	5 35 57.65	-5 57 18.36	18799872	40	2007 Apr 18	SLLL	ONC	opse/AdOpt ^f
198	8399269-6612	5 35 58.25	-6 36 43.20	18798336	39	2007 Mar 12	SLLL	L1641	man
199	8399902-6268	5 35 59.76	-6 16 06.64	18813440	39	2007 Mar 12	SLLL	L1641	man
200	8400080-6709	5 36 00.19	-6 42 33.98	18836480	39	2007 Mar 09	SLLL	L1641	opse
201	8402765-6538	5 36 06.64	-6 32 17.16	18800384	39	2007 Mar 12	SLLL	L1641	man
202	8403455-6810	5 36 08.29	-6 48 36.36	18799104	39	2007 Mar 09	SLLL	L1641	man
203	8406280-6293	5 36 15.07	-6 17 36.78	18845696	39	2007 Mar 12	SLLL	L1641	AdOpt
204	8406609-6247	5 36 15.86	-6 14 50.60	18777088	39	2007 Mar 12	SLLL	L1641	AdOpt

Table 1—Continued

Num. (1)	IRS name (2)	RA (J2000) (3)	DEC (J2000) (4)	AORID (5)	IRS Camp. (6)	Date observed (7)	modules (8)	region (9)	reduction (10)
205	8407074-5195	5 36 16.98	-5 11 42.72	18801152	39	2007 Mar 25	SLLL	ONC	AdOpt
206	8408920-6760	5 36 21.41	-6 45 36.90	18842880	39	2007 Mar 12	SLLL	L1641	AdOpt
207	8409911-6386	5 36 23.79	-6 23 11.08	18811904	39	2007 Mar 12	SLLL	L1641	AdOpt
208	8410334-6291	5 36 24.80	-6 17 30.48	18806784	39	2007 Mar 09	SLLL	L1641	man
209	8410779-6416	5 36 25.87	-6 24 58.82	18835712	39	2007 Mar 12	SLLL	L1641	AdOpt
210	8410886-6134	5 36 26.13	-6 08 03.84	18803200	39	2007 Mar 11	SLLL	L1641	man
211	8411618-6426	5 36 27.88	-6 25 35.90	18780160	39	2007 Mar 12	SLLL	L1641	man
212	8412592-6712	5 36 30.22	-6 42 46.19	18830080	39	2007 Mar 12	SLLL	L1641	man/AdOpt ^b
213	8413152-6141	5 36 31.56	-6 08 27.82	18849792	39	2007 Mar 09	SLLL	L1641	man
214	8413399-5287	5 36 32.16	-5 17 13.42	18850816	39	2007 Mar 27	SLLL	ONC	opse
215	8413704-6739	5 36 32.89	-6 44 20.94	18842624	39	2007 Mar 12	SLLL	L1641	opse
216	8414490-7187	5 36 34.78	-7 11 13.70	18778112	39	2007 Mar 09	SLLL	L1641	man
217	8415394-6556	5 36 36.95	-6 33 23.87	18829312	39	2007 Mar 12	SLLL	L1641	AdOpt
218	8416389-6503	5 36 39.33	-6 30 11.27	18781184	39	2007 Mar 12	SLLL	L1641	man
219	8416834-6225	5 36 40.40	-6 13 33.35	18775808	39	2007 Mar 09	SLLL	L1641	man
220	8416914-6175	5 36 40.59	-6 10 33.42	18849280	39	2007 Mar 09	SLLL	L1641	AdOpt/ECO ^h
221	8416978-6185	5 36 40.75	-6 11 08.16	18804992	39	2007 Mar 11	SLLL	L1641	AdOpt
222	8421949-6718	5 36 52.68	-6 43 08.18	18839808	40	2007 Apr 18	SLLL	L1641	AdOpt
223	8424570-6484	5 36 58.97	-6 29 04.85	18780416	39	2007 Mar 12	SLLL	L1641	AdOpt
224	8424689-6154	5 36 59.25	-6 09 16.60	18814720	39	2007 Mar 11	SLLL	L1641	man
225	8425038-6557	5 37 00.09	-6 33 27.40	18815232	39	2007 Mar 12	SLLL	L1641	man
226	8430527-6583	5 37 13.26	-6 35 00.38	18835968	39	2007 Mar 09	SLLL	L1641	AdOpt
227	8440418-7404	5 37 37.00	-7 24 16.60	18814464	39	2007 Mar 09	SLLL	L1641	AdOpt/ECO ⁱ
228	8445530-6843	5 37 44.47	-6 50 36.64	18812672	40	2007 Apr 16	SLLL	L1641	man
229	8444779-6608	5 37 47.47	-6 36 29.63	18776064	39	2007 Mar 12	SLLL	L1641	AdOpt
230	8445558-6860	5 37 49.34	-6 51 37.26	18777600	44	2007 Oct 06	SLLL	L1641	AdOpt
231	8447398-6788	5 37 53.76	-6 47 17.20	18809344	39	2007 Mar 09	SLLL	L1641	opse/AdOpt ^f
232	8448350-6815	5 37 56.04	-6 48 55.15	18822144	39	2007 Mar 09	SLLL	L1641	opse/AdOpt/man ^j
233	8450343-7265	5 38 00.82	-7 15 54.04	18807808	39	2007 Mar 09	SLLL	L1641	opse/man ^k
234	8452061-7269	5 38 04.95	-7 16 10.56	18805504	39	2007 Mar 09	SLLL	L1641	opse/man ^k
235	8453876-6821	5 38 09.30	-6 49 16.46	18834176	39	2007 Mar 09	SLLL	L1641	man
236	8455602-7112	5 38 13.44	-7 06 43.42	18850048	39	2007 Mar 09	SLLL	L1641	man
237	8457266-7161	5 38 17.44	-7 09 39.74	18831360	39	2007 Mar 09	SLLL	L1641	man
238	8461533-6914	5 38 27.68	-6 54 53.68	18818304	39	2007 Mar 09	SLLL	L1641	man

Table 1—Continued

Num. (1)	IRS name (2)	RA (J2000) (3)	DEC (J2000) (4)	AORID (5)	IRS Camp. (6)	Date observed (7)	modules (8)	region (9)	reduction (10)
239	8464666-7838	5 38 35.20	-7 50 19.72	18817536	39	2007 Mar 09	SLLL	L1641	man
240	8465247-7776	5 38 36.59	-7 46 34.39	18821888	40	2007 Apr 16	SLLL	L1641	man
241	8466711-6987	5 38 40.11	-6 59 14.75	18827520	39	2007 Mar 09	SLLL	L1641	AdOpt
242	8468002-6969	5 38 43.20	-6 58 08.98	18851584	39	2007 Mar 09	SLLL	L1641	AdOpt
243	8468729-6970	5 38 44.95	-6 58 14.59	18823936	39	2007 Mar 09	SLLL	L1641	AdOpt
244	8469891-7104	5 38 47.74	-7 06 14.94	18841856	39	2007 Mar 09	SLLL	L1641	man
245	8472719-7464	5 38 54.53	-7 27 51.91	18822656	39	2007 Mar 09	SLLL	L1641	man
246	8476732-7058	5 39 04.16	-7 03 29.92	18811392	39	2007 Mar 12	SLLL	L1641	AdOpt
247	8477229-7184	5 39 05.35	-7 11 05.32	18816768	39	2007 Mar 09	SLLL	L1641	man
248	8486920-7342	5 39 28.61	-7 20 31.34	18831616	39	2007 Mar 09	SLLL	L1641	man
249	8488472-7373	5 39 32.33	-7 22 24.42	18844928	39	2007 Mar 09	SLLL	L1641	AdOpt
250	8492690-7387	5 39 42.46	-7 23 16.48	18818816	40	2007 Apr 16	SLLL	L1641	man
251	8494096-7377	5 39 45.83	-7 22 37.20	18798848	40	2007 Apr 16	SLLL	L1641	opse/man k
252	8495155-7404	5 39 48.37	-7 24 14.90	18833664	40	2007 Apr 16	SLLL	L1641	man
253	8497290-7502	5 39 53.50	-7 30 09.43	18823168	39	2007 Mar 12	SLLL	L1641	AdOpt/opse g
254	8497797-7462	5 39 54.71	-7 27 44.10	18843136	39	2007 Mar 09	SLLL	L1641	opse/man k
255	8499151-7482	5 39 57.96	-7 28 57.54	18846208	39	2007 Mar 09	SLLL	L1641	AdOpt
256	8499541-7426	5 39 58.90	-7 25 33.71	18826496	39	2007 Mar 09	SLLL	L1641	opse/man k
257	8502614-7795	5 40 06.27	-7 47 44.59	18779136	44	2007 Oct 07	SLLL	L1641	man
258	8504327-7460	5 40 10.38	-7 27 38.16	18804736	39	2007 Mar 09	SLLL	L1641	man
259	8508083-8237	5 40 19.40	-8 14 16.26	18848768	36	2006 Nov 10	SLLL	L1641	man
260	8508501-7431	5 40 20.40	-7 25 54.16	18779392	44	2007 Oct 07	SLLL	L1641	man
261	8508648-7916	5 40 20.76	-7 55 00.23	18829824	36	2006 Nov 14	SLLL	L1641	man
262	8510403-8125	5 40 24.97	-8 07 33.28	18818560	36	2006 Nov 13	SLLL	L1641	man
263	8511308-8126	5 40 27.14	-8 07 36.48	18807040	36	2006 Nov 10	SLLL	L1641	opse/man k
264	8511602-7926	5 40 27.84	-7 22 25.07	18848256	39	2007 Mar 12	SLLL	L1641	opse/man k
265	8514861-7663	5 40 35.67	-7 39 46.94	18832384	39	2007 Mar 12	SLLL	L1641	man
266	8515568-8067	5 40 37.36	-8 04 02.78	18836224	36	2006 Nov 10	SLLL	L1641	man
267	8516031-7796	5 40 38.47	-7 47 47.15	18827264	39	2007 Mar 12	SLLL	L1641	AdOpt/man d
268	8518798-7373	5 40 45.12	-7 22 25.07	18829056	39	2007 Mar 12	SLLL	L1641	man
269	8519260-8090	5 40 46.22	-8 05 24.40	18808832	36	2006 Nov 10	SLLL	L1641	man
270	8519428-8120	5 40 46.63	-8 07 12.79	18821376	36	2006 Nov 10	SLLL	L1641	man
271	8520557-7775	5 40 49.34	-7 46 32.56	18777856	44	2007 Oct 07	SLLL	L1641	man
272	8520580-7960	5 40 49.39	-7 57 38.16	18804480	36	2006 Nov 14	SLLL	L1641	man

Table 1—Continued

Num. (1)	IRS name (2)	RA (J2000) (3)	DEC (J2000) (4)	AORID (5)	IRS Camp. (6)	Date observed (7)	modules (8)	region (9)	reduction (10)
273	8530851-8132	5 41 14.04	-8 07 57.40	18814208	36	2006 Nov 10	SLLL	L1641	opse
274	8534457-7821	5 41 22.70	-7 49 16.10	18833408	36	2006 Nov 14	SLLL	L1641	AdOpt
275	8535781-7830	5 41 25.87	-7 49 50.88	18806528	36	2006 Nov 13	SLLL	L1641	man
276	8536129-8706	5 41 26.71	-8 42 24.48	18807296	36	2006 Nov 09	SLLL	L1641	man
277	8537742-8080	5 41 30.58	-8 04 48.14	18831104	36	2006 Nov 10	SLLL	L1641	man
278	8538844-7917	5 41 33.23	-7 55 02.35	18822400	36	2006 Nov 14	SLLL	L1641	AdOpt
279	8538911-7999	5 41 33.39	-7 59 56.47	18820352	36	2006 Nov 13	SLLL	L1641	man
280	8542681-8618	5 41 42.43	-8 37 07.14	18846720	36	2006 Nov 09	SLLL	L1641	man
281	8543224-7972	5 41 43.74	-7 58 22.26	18847488	36	2006 Nov 13	SLLL	L1641	opse/man ^k
282	8545724-8008	5 41 49.74	-8 00 32.08	18819072	36	2006 Nov 13	SLLL	L1641	man
283	8547523-7831	5 41 54.06	-7 49 53.22	18777344	36	2006 Nov 13	SLLL	L1641	man
284	8547770-7986	5 41 54.65	-7 59 12.52	18817024	36	2006 Nov 13	SLLL	L1641	opse
285	8552157-8190	5 42 05.18	-8 11 26.59	18824192	36	2006 Nov 15	SLLL	L1641	opse
286	8552280-8641	5 42 05.47	-8 38 28.32	18800896	36	2006 Nov 12	SLLL	L1641	man
287	8556074-7982	5 42 14.58	-7 58 57.79	18824448	36	2006 Nov 13	SLLL	L1641	man
288	8560743-8147	5 42 25.78	-8 08 50.03	18827008	39	2007 Mar 12	SLLL	L1641	AdOpt
289	8561044-7980	5 42 26.51	-7 58 50.63	18829568	36	2006 Nov 13	SLLL	L1641	man
290	8562845-8151	5 42 30.83	-8 09 05.47	18822912	36	2006 Nov 13	SLLL	L1641	AdOpt
291	8564835-8250	5 42 35.60	-8 15 01.84	18775296	44	2007 Oct 07	SLLL	L1641	man
292	8567003-8669	5 42 40.81	-8 40 08.58	18841344	36	2006 Nov 09	SLLL	L1641	opse/man ^k
293	8567545-8254	5 42 42.11	-8 15 15.30	18843392	36	2006 Nov 13	SLLL	L1641	AdOpt
294	8567670-8803	5 42 42.41	-8 48 13.79	18830336	36	2006 Nov 09	SLLL	L1641	man
295	8569204-8666	5 42 46.09	-8 40 00.66	18848512	36	2006 Nov 09	SLLL	L1641	man
296	8570200-8276	5 42 48.48	-8 16 34.72	18811136	39	2007 Mar 12	SLLL	L1641	man
297	8570949-8577	5 42 50.28	-8 34 38.10	18782208	36	2006 Nov 09	SLLL	L1641	man
298	8571439-8650	5 42 51.45	-8 39 01.98	18845184	36	2006 Nov 09	SLLL	L1641	man
299	8574645-8156	5 42 59.15	-8 09 23.76	18805248	36	2006 Nov 14	SLLL	L1641	AdOpt/man ^l
300	8576640-8652	5 43 03.94	-8 39 09.47	18828800	36	2006 Nov 15	SLLL	L1641	opse/man ^k
301	8576836-8303	5 43 04.41	-8 18 11.02	18850304	36	2006 Nov 15	SLLL	L1641	man
302	8579480-8565	5 43 10.75	-8 33 55.22	18775552	36	2006 Nov 09	SLLL	L1641	man
303	8580634-8516	5 43 13.52	-8 31 00.05	18776832	39	2007 Mar 12	SLLL	L1641	man
304	8373220-5817	5 35 00.53	-5 49 01.96	20832000	39	2007 Mar 24	SLLL	ONC	man ⁿ
305	8382228-5704	5 35 17.34	-5 42 14.50	20954624	39	2007 Mar 27	SLLL	ONC	man ⁿ
306	8381598-5501	5 35 15.83	-5 30 05.50	20863488	39	2007 Mar 27	SLLL	ONC	AdOpt ⁿ

Table 1—Continued

Num. (1)	IRS name (2)	RA (J2000) (3)	DEC (J2000) (4)	AORID (5)	IRS Camp. (6)	Date observed (7)	modules (8)	region (9)	reduction (10)
307	8334366-5384	5 33 22.48	-5 23 02.87	20865024	39	2007 Mar 22	SLLL	ONC	man ⁿ
308	8383054-4929	5 35 19.32	-4 55 44.94	20823040	39	2007 Mar 27	SLLL	ONC	man ⁿ
309	8499216-7444	5 39 58.13	-7 26 41.22	20844544	40	2007 Apr 16	SLLL	L1641	AdOpt ⁿ
310	8467876-6944	5 38 42.88	-6 56 40.76	20954368	40	2007 Apr 16	SLLL	L1641	man ⁿ
311	8412906-6878	5 36 30.97	-6 52 40.94	20836864	40	2007 Apr 18	SLLL	L1641	man ⁿ
312	8424745-6171	5 36 59.39	-6 10 15.60	26117376	56	2008 Nov 16	SLLL	L1641	AdOpt ^o
313	8405394-6391	5 36 12.95	-6 23 30.62	20819712	39	2007 Mar 21	SLLL	L1641	man ⁿ
314	8352892-6535	5 34 06.94	-6 32 07.98	20846848	39	2007 Mar 17	SLLL	L1641	man ⁿ
315	8536117-8706	5 41 26.68	-8 42 24.52	20840448	39	2007 Mar 15	SLLL	L1641	man ⁿ
316	8508553-7944	5 40 20.53	-7 56 39.62	20830720	40	2007 Apr 17	SLLL	L1641	man ⁿ
317	85118494-7737	5 40 44.36	-7 44 16.69	20953088	40	2007 Apr 16	SLLL	L1641	man ⁿ
318	85118616-7498	5 40 44.67	-7 29 54.47	20845568	39	2007 Mar 15	SLLL	L1641	man ⁿ
319	8524538-7800	5 40 58.89	-7 48 02.05	26103552	56	2008 Nov 15	SLLL	L1641	man ^o

Note. — Column (1) Num.: Numbers in this column are from the number sequence of 303 Class II objects observed in the IRS program ID 30706 and additional 16 Class II objects candidates identified from *Herschel* Orion Protostar Survey. We use these numbers to identify objects conveniently. This number sequence will be used consistently in other future papers dealing with the objects in this work.

Column (2) IRS name: IRS name indicated as in the column are used to identify objects often in other works. The IRS names come from the position of each object.

Column (10) reduction: It indicates the methods of source extraction to get the SEDs in Figure 7 and Figure 8. ECO: an automated tapered column extraction in SMART with off-nod or off-order sky subtraction; man: a manual tapered column extraction in SMART with a constant or linear sky subtraction; AdOpt: an optimal source extraction using an empirical point response function (PRF) in SMART; opse: an optimal source extraction using an analytical PRF.

^aSL & LL1: opse; LL2: AdOpt

^bSL: man; LL: AdOpt

^cSL: AdOpt; LL:opse

^dSL & LL1: AdOpt; LL2:man

^eSL & LL2: man; LL1: opse

^fSL: opse; LL:AdOpt

^gSL & LL2: AdOpt; LL1:opse

^hSL & LL2: AdOpt; LL1: ECO

ⁱSL: AdOpt; LL:ECO

^jSL: opse; LL2: AdOpt; LL1: man

^kSL: opse; LL:man

^lSL & LL2: AdOpt; LL1:man

^mSL2: AdOpt; SL1:man

ⁿThe IRS program ID 30859

^oThe IRS program ID 50374

Table 2. Identifications of the Objects

Num.	IRS name	2MASS name	other names selected
1	8336884-5290	05332852-0517262	V719 Ori, [FHM2008] F22-ap40, Parenago 1190
2	8339347-5238	05333443-0514177	[FHM2008] S1-ap78
3	8343858-5513	05334525-0530498	WZ Ori, [FHM2008] S3-ap68, HBC 106, Parenago 1260
4	8343917-6073	05334537-0604253	V1006 Ori, HBC 108, Parenago 1267
5	8343944-5609	05334545-0536323	V726 Ori, [FHM2008] S1-ap42
6	8344455-5390	05334668-0523256	V1897 Ori, [FHM2008] S2-ap3
7	8344987-5460	05334797-0527385	[FHM2008] S2-ap6
8	8346141-5010	05335074-0500394	V1902 Ori, [FHM2008] F11-ap39
9	8346378-5387	05335131-0523164	V1903 Ori, [FHM2008] S2-ap5
10	8346581-5550	05335179-0533035	V1905 Ori
11	8347111-5533	05335450-0532003	[FHM2008] S3-ap64
12	8348250-4797	05335580-0447497	SU Ori, [FHM2008] S2-ap66, HBC 110, Parenago 1301
13	8350150-5595	05340034-0535434	Parenago 1327
14	8350916-5605	05340217-0536195	II Ori, [FHM2008] S3-ap58, Parenago 1333
15	8352483-5378	05340595-0522435	V1922 Ori, [FHM2008] S2-ap8
16	8353051-5229	05340731-0513454	WX Ori, HBC 111, Parenago 1352
17	8353319-5604	05340797-0536170	V396 Ori, [FHM2008] S1-ap33
18	8355083-4835	05341221-0450072	BT Ori, Parenago 1373
19	8355371-5480	05341289-0528482	Parenago 1382
20	8355629-5594	05341351-0535386	V1935 Ori
21	8355898-5615	05341416-0536542	[FHM2008] S3-ap41, HBC 442, Parenago 1394
22	8356531-5540	05341566-0532241	WY Ori, [FHM2008] S2-ap238, Parenago 1396
23	8357031-5072	05341687-0504210	BU Ori, [FHM2008] F22-ap62, Parenago 1403
24	8358147-5505	05341954-0530198	WZ Ori, [FHM2008] S3-ap65, Parenago 1424
25	8358862-4842	05342125-0450326	[FHM2008] S2-ap63
26	8359203-5026	05342207-0501342	[FHM2008] F22-ap69
27	8360781-4940	05342587-0456274	IP Ori, [FHM2008] S2-ap64, Parenago 1452
28	8360900-5441	05342616-0526304	V1956 Ori, [FHM2008] S2-ap239
29	8361167-5475	05342679-0528321	Parenago 1465
30	8362406-4863	05342978-0451477	V1970 Ori, [FHM2008] S2-ap72
31	8364658-4871	05343516-0452179	V1987 Ori
32	8364671-5575	05343519-0534322	V1988 Ori, [FHM2008] S1-ap32, [FHM2008] F22-ap234
33	8365614-5581	05343746-0534519	IV Ori, [FHM2008] S3-ap52, Parenago 1527
34	8365722-4816	05343772-0448577	...
35	8366668-5168	05343999-0510070	Parenago 1539

Table 2—Continued

Num.	IRS name	2MASS name	other names selected
36	8366704-5669	05344007-0540094	V398 Ori, [FHM2008] S3-ap40, Parenago 1553
37	8367030-5378	05344086-0522423	IX Ori, [FHM2008] S2-ap234, HBC 118, Parenago 1552
38	8367284-5798	05344146-0547561	V764 Ori, Parenago 1571
39	8368137-4860	05344351-0451364	[FHM2008] F11-ap50
40	8368755-4933	05344500-0455593	[FHM2008] S2-ap76, Parenago 1574
41	8368837-5665	05344521-0539571	V2021 Ori
42	8369106-5686	05344587-0541097	V1447 Ori, [FHM2008] F21-ap30
43	8369290-5652	05344629-0539077	V474 Ori, [FHM2008] S3-ap34, Parenago 1601
44	8369890-5081	05344794-0504550	V550 Ori, [FHM2008] F22-ap80, Parenago 1599
45	8370827-5312	05344998-0518447	V2056 Ori, [FHM2008] S1-ap67, Parenago 1623
46	8371143-5450	05345073-0527010	[FHM2008] S1-ap37
47	8371184-5465	05345275-0527545	NA;V551 Ori, NA, [FHM2008] S3-ap92
48	8372100-5057	05345304-0503271	YZ Ori, [FHM2008] S1-ap101, HBC 120, Parenago 1648
49	8372608-5359	05345424-0521353	...
50	8372885-5283	05345494-04517017	V2073 Ori, [FHM2008] S1-ap80
51	8373201-4936	05345566-0456117	V2079 Ori, [FHM2008] S2-ap71
52	8373676-5192	05345681-0511330	KN Ori, [FHM2008] S3-ap118, HBC 123, Parenago 1665
53	8373830-6325	05345744-0619331	...
54	8373836-4946	05345745-0456454	[FHM2008] S1-ap115
55	8374073-5397	05345776-0523522	...
56	8374080-5380	05345778-0522511	V402 Ori, [FHM2008] S3-ap109,
57	8374271-5697	05345825-0541498	V2091 Ori
58	8374301-5908	05345833-0554288	BX Ori, [FHM2008] S3-ap7, Parenago 1688
59	8374388-6000	05345852-0600004	...
60	8374599-5741	05345908-0544303	KT Ori, [FHM2008] S3-ap12, Parenago 1687
61	8374677-5748	05345923-0544553	V1712 Ori
62	8374677-5766	05345923-0545588	V2097 Ori
63	8374839-5427	05345962-0525399	V1477 Ori, [FHM2008] S3-ap106, Parenago 1686
64	8375041-5383	05350011-0523019	KR Ori, [FHM2008] S2-ap222, HBC 125, Parenago 1684
65	8375063-5840	05350015-0550274	...
66	8375158-5162	05350039-0509441	[FHM2008] S2-ap7
67	8375190-5420	05350046-0525143	V2102 Ori
68	8375484-5401	05350117-0524067	[FHM2008] S2-ap211, Parenago 1694
69	8375546-5339	05350133-0520221	V2109 Ori, [FHM2008] S1-ap55
70	8375702-5443	05350167-0526363	V2114 Ori

Table 2—Continued

Num.	IRS name	2MASS name	other names selected
71	8375886-5399	05350213-0523569	V2121 Ori
72	8376139-5329	05350274-0519444	V2123 Ori
73	8376154-5675	05350278-0540310	...
74	8376176-5368	05350284-0522082	V2125 Ori
75	8376287-5377	05350309-0522378	V404 Ori, [FHM2008] S3-ap114
76	8376356-4822	05350326-0449209	V1718 Ori, [FHM2008] S2-ap83, Parenago 1701; Parenago 1702
77	8376541-5379	05350370-0522457	...
78	8376571-5415	05350378-0524543	V375 Ori, Parenago 1713
79	8376643-5900	05350395-0554019	V2135 Ori, [FHM2008] S3-ap8
80	8376687-5443	05350406-0526371	V1482 Ori, [FHM2008] F22-ap222
81	8376747-5441	05350419-0526278	V1322 Ori
82	8376817-5387	05350437-0523338	V1274 Ori
83	8376871-5399	05350450-0523565	V2140 Ori, Parenago 1737
84	8376918-4974	05350460-0458289	V554 Ori, Parenago 1723
85	8376976-5443	05350475-0526380	V2143 Ori, [FHM2008] S1-ap27
86	8377111-5612	05350506-0536438	V2148 Ori, [FHM2008] S1-ap19
87	8377137-5340	05350513-0520244	V479 Ori
88	8377167-5247	05350519-0514503	V2149 Ori, [FHM2008] S1-ap95, Parenago 1736
89	8377232-5402	05350537-0524105	V2150 Ori, [FHM2008] S1-ap36
90	8377335-5489	05350561-0529223	V407 Ori
91	8377345-5422	05350563-0525195	LL Ori, [FHM2008] S1-ap25, HBC 126, Parenago 1746
92	8377361-5395	05350567-0523452	V2156 Ori
93	8377383-5405	05350572-0524184	V480 Ori
94	8377392-5193	05350572-0511350	V2157 Ori, [FHM2008] S1-ap107
95	8377737-5547	05350656-0532515	V2168 Ori
96	8377749-5447	05350660-0526509	...
97	8378059-5644	05350732-0538409	V2172 Ori
98	8378345-5545	05350801-0532442	LN Ori, [FHM2008] S3-ap69, HBC 128, Parenago 1766
99	8378366-5814	05350807-0548539	V2179 Ori
100	8378481-5465	05350834-0527569	V2182 Ori
101	8378503-5474	05350838-0528293	V1397 Ori
102	8378561-5421	05350853-0525179	V2184 Ori
103	8378630-4781	05350869-0446523	V555 Ori, Parenago 1753
104	8379094-5316	05350982-0518583	V2192 Ori
105	8379108-5326	05350985-0519339	...

Table 2—Continued

Num.	IRS name	2MASS name	other names selected
106	8379192-6093	05351004-0605364	V2195 Ori
107	8379289-5332	05351029-0519563	[FHM2008] F21-ap127
108	8379312-5776	05351033-0546335	AA Ori, [FHM2008] S1-ap1, Parenago 1787
109	8379495-5350	05351188-0521032	V2220 Ori
110	837950-5323	05351188-0519261	...
111	8379930-5342	05351197-0520331	V2221 Ori
112	8380422-5659	05351299-0539348	LX Ori, [FHM2008] S1-ap14, HBC 133, Parenago 1828
113	8380493-5291	05351317-0511307	V2233 Ori
114	8380518-5465	05351324-0527541	V2237 Ori
115	8380544-5338	05351330-0520189	V2238 Ori
116	8380651-5296	05351356-0517457	V2244 Ori
117	8380667-5516	05351360-0530575	V488 Ori, HBC 134, Parenago 1827
118	8380675-5331	05351362-0519548	...
119	838095-5479	05351365-0528462	v1495 Ori
120	8380923-5478	05351419-0528434	V2256 Ori
121	8380932-5721	05351423-0513175	AB Ori, [FHM2008] S3-ap231, HBC 135, Parenago 1848
122	8381019-5555	05351444-0533190	V2660 Ori
123	8381020-5546	05351444-0532464	V1498 Ori
124	8381104-5345	05351465-0520424	...
125	8381120-5653	05351467-0539108	MO Ori, Parenago 1876
126	8381436-5294	05351545-0517383	V2271 Ori
127	8381491-5164	05351556-0509512	[FHM2008] S1-ap122
128	8381501-4991	05351559-0459278	V2273 Ori
129	8381622-5481	...	V2277 Ori
130	8381919-5289	05351661-0517234	V2291 Ori
131	8381971-4762	05351673-0445444	TT Ori, HBC 136, Parenago 1856
132	8382048-5452	05351691-0527087	V2296 Ori
133	8382359-5974	05351767-0553265	V1812 Ori, HBC 138, Parenago 1931
134	8382412-6410	05351780-0624384	V794 Ori
135	8382467-5709	05351790-0542340	V2318 Ori, Parenago 1929
136	8382490-5270	05351799-0516136	...
137	8382623-5479	05351829-0523461	...
138	8382655-4889	05351838-0453234	V2329 Ori
139	8382835-5291	05351880-0517291	V2338 Ori, [FHM2008] S1-ap104
140	8383581-5050	05352061-0503008	V2369 Ori

Table 2—Continued

Num.	IRS name	2MASS name	other names selected
141	8383861-5154	05352125-0509161	MX Ori, [FHM2008] S3-ap124, HBC 462, Parenago 1953
142	8384113-5117	05352187-0507018	V415 Ori, [FHM2008] S2-ap157, Parenago 1952
143	8384325-5457	05352237-0527283	V1340 Ori
144	8384331-5134	05352240-0508051	V492 Ori, [FHM2008] S2-ap165
145	8384717-5469	05352331-0528100	V1530 Ori
146	8384864-5440	...	V2411 Ori
147	8385190-5442	05352445-0526314	V1283 Ori
148	8385255-5191	05352459-0511296	V2427 Ori
149	8385365-5106	05352486-0506216	...
150	8385988-5427	05352634-0525401	AK Ori, [FHM2008] S1-ap233, HBC 468, Parenago 2032
151	8386322-6328	05352716-0619420	V799 Ori
152	8386383-5393	05352730-0523366	V2463 Ori
153	8386462-5457	05352749-0527259	V1287 Ori, [FHM2008] F21-ap240
154	8386523-5715	05352765-0542551	V2468 Ori, Parenago 2059
155	8386627-5467	05352788-0528020	V1542 Ori
156	8386694-5026	05352805-0501349	V2470 Ori
157	8386722-5315	05352812-0518572	...
158	8386759-5416	...	V420 Ori, Parenago 2046
159	8386804-5987	05352831-0559132	V1546 Ori, [FHM2008] F31-ap113
160	8386841-5129	05352849-0507465	...
161	8386935-4790	05352864-0447265	V1547 Ori, [FHM2008] F11-ap13, Parenago 2041
162	8386957-4804	05352868-0448163	V418 Ori, Parenago 2042
163	8387691-5326	05353046-0519340	V2489 Ori
164	8387753-4993	05353060-0459360	V2493 Ori
165	8387832-5864	05353080-0551509	...
166	8387937-6755	05353105-0645181	TW Ori, HBC 145, Parenago 2105
167	8388119-5083	05353149-0505016	V422 Ori, [FHM2008] F21-ap146, Parenago 2072
168	8388316-5157	05353195-0509279	V360 Ori, [FHM2008] S2-ap163, HBC 144, Parenago 2084
169	8389033-4773	05353369-0446237	V2528 Ori, Parenago 2092
170	8389275-5105	05353428-0506212	HD 37060, Parenago 2102
171	8389323-5449	05353437-0526596	[FHM2008] F22-ap173
172	8389673-4794	05353522-0447396	V2544 Ori, [FHM2008] F11-ap153
173	8390003-5207	05353601-0512253	NY Ori, [FHM2008] S1-ap148, HBC 148, Parenago 2119
174	8390073-5082	05353620-0504559	V2549 Ori
175	8390083-5339	05353621-0520204	V2550 Ori

Table 2—Continued

Num.	IRS name	2MASS name	other names selected
176	8390285-5070	05353668-0504145	V424 Ori, [FHM2008] S2-ap135, Parenago 2116
177	8390554-6390	05353733-0623263	...
178	8391040-5081	05353851-0504515	...
179	8391058-4994	05353852-0459411	V1572 Ori, [FHM2008] S2-ap113
180	8391196-5211	05353885-0512419	V426 Ori, [FHM2008] S1-ap143, Parenago 2144
181	8391648-5110	05353995-0506368	V1578 Ori, [FHM2008] S2-ap143
182	8392509-5169	05354201-0510115	V2573 Ori, [FHM2008] S1-ap147
183	8393152-5094	05354355-0505414	AO Ori, [FHM2008] S2-ap145, Parenago 2171
184	8394216-5181	05354612-0510517	V808 Ori, [FHM2008] F22-ap120
185	839454-5823	05354669-0549262	CF Ori, [FHM2008] F31-ap126, Parenago 2218
186	8395167-5024	05354838-0501287	CE Ori, [FHM2008] S2-ap136, HBC 152, Parenago 2203
187	8395780-5308	05354987-0518308	V2605 Ori, [FHM2008] S2-ap187
188	8396635-5861	05355047-0551422	OU Ori, [FHM2008] S3-ap224, Parenago 2254
189	8396285-5119	05355109-0507088	V575 Ori, [FHM2008] S2-ap156, Parenago 2243
190	8396319-4941	05355118-0456276	V2610 Ori, [FHM2008] S2-ap122
191	8396679-6167	05355202-0610016	V1296 Ori
192	8397322-4788	05355405-0447193	AS Ori, [FHM2008] S2-ap114, Parenago 2255
193	8397632-5445	05355433-0326444	OW Ori, [FHM2008] S1-ap215, Parenago 2269
194	8397818-4972	05355476-0458200	V2620 Ori, [FHM2008] S2-ap129, Parenago 2262
195	8398707-5755	05355690-0545191	V1589 Ori, [FHM2008] S1-ap239
196	8398836-6711	05355745-0642418	V577 Ori, HBC 158, Parenago 2299
197	8399022-5955	05355765-0557183	AU Ori, [FHM2008] S3-ap226, HBC 157, Parenago 2285
198	8399269-6612	05355825-0636431	OY Ori, Parenago 2297
199	8399902-6268	05355975-0616065	V1178 Ori, Parenago 2307
200	8400080-6709	05360017-0642339	AV Ori, HBC 159, HBC 481, Parenago 2312
201	8402765-6538	05360665-0632171	V823 Ori
202	8403455-6810	05360828-0648363	AY Ori, Parenago 2350
203	8406280-6293	05361506-0617369	BB Ori, Parenago 2369
204	8406609-6247	05361584-0614507	V1076 Ori, [FHM2008] F31-ap197
205	8407074-5195	05361698-0511427	AZ Ori, [FHM2008] S1-ap165, HBC 162, Parenago 2368
206	8408920-6760	05362140-0645366	V2669 Ori, HBC 483
207	8409911-6386	053622378-0623113	V2674 Ori
208	8410334-6291	05362499-0617324	PR Ori, Parenago 2388
209	8410779-6416	05362586-0624587	...
210	8410886-6134	05362611-0608038	V2679 Ori

Table 2—Continued

Num.	IRS name	2MASS name	other names selected
211	8411618-64226	05362788-0625360	[FHM2008] F31-ap209
212	8412552-6712	05363023-0642460	V2687 Ori
213	8413152-61441	05363158-0608271	V1183 Ori, Parenago 2409
214	8413389-5287	05363213-0517135	V367 Ori, [FHM2008] S2-ap161, Parenago 2403
215	8413704-6739	05363288-0644208	...
216	8414490-7187	05363476-0711133	...
217	8415394-6556	05363692-0633241	V585 Ori
218	8416389-6503	05363933-0630111	[FHM2008] F31-ap207
219	8416834-6225	05364039-06113334	[FHM2008] F31-ap190
220	8416914-6175	05364058-0610332	V2702 Ori
221	8416978-6185	05364075-0611082	V2703 Ori
222	8421949-6718	05365269-0643083	V2713 Ori
223	8424570-6484	05365897-0629049	V2720 Ori
224	8424689-6154	05365925-0609164	V586 Ori, HD 37258, HBC 485, Parenago 2473
225	8425038-6557	0537010-0633273	BE Ori, HBC 168, Parenago 2479
226	8430527-6583	05371326-0635005	BF Ori, HBC 169, Parenago 2510
227	8440418-7404	05373700-0724167	V875 Ori
228	8443530-6843	05374448-0650366	V589 Ori
229	8444779-6608	05374746-0636298	...
230	8445558-6860	05374934-0651373	...
231	8447398-6788	05375376-0647170	...
232	8448350-6815	05375602-0648549	...
233	8450343-7265	05380082-0715541	V593 Ori
234	8452061-7269	05380496-0716107	V878 Ori, Parenago 2588
235	8453876-6821	05380931-0649166	V1187 Ori, Parenago 2649
236	8455602-7112	05381345-0706433	...
237	8457266-7161	05381743-0709395	...
238	8461533-6914	05382767-0654537	V594 Ori, Parenago 2682
239	8464666-7338	05383519-0750197	HBC 174
240	8465247-7776	05383660-0746344	...
241	8466711-6987	05384011-0659148	...
242	8468002-6969	05384322-0658089	...
243	8468729-6970	05384495-0658146	...
244	8469891-7104	05384773-0706148	...
245	8472719-7464	05385451-0727520	...

Table 2—Continued

Num.	IRS name	2MASS name	other names selected
246	8476732-7058	05390415-0703299	...
247	8477229-7184	05390536-0711052	...
248	8486920-7342	05392860-0720314	...
249	8488472-7373	05393231-0722241	V892 Ori
250	8492690-7387	05394244-0723165	...
251	8494096-7377	05394582-0722373	...
252	8495155-7404	05394838-0724147	...
253	8497290-7502	05395350-0730095	...
254	8497797-7462	05395474-0727443	...
255	8499151-7482	05395796-0728576	...
256	8499541-7426	05395891-0725335	...
257	8502614-7795	05400626-0747445	...
258	8504327-7460	05401036-0727384	...
259	8508083-8237	05401940-0814163	...
260	8508501-7431	05402040-0725540	...
261	8508648-7916	05402073-0755000	...
262	8510403-8125	05402496-0807332	V1304 Ori, HBC 179
263	8511308-8126	05402714-0807365	...
264	8511602-7926	05402783-0753365	...
265	8514861-7663	05403566-0739468	...
266	8515568-8067	05403736-0804030	V1791 Ori
267	8516031-7796	05403847-0747470	...
268	8518798-7373	05404511-0722250	V902 Ori
269	8519260-8090	05404622-0805243	UU Ori, CoKu DL Ori/G4, HBC 495
270	8519428-8120	05404661-0807128	CoKu DL Ori/G3, HBC 497 ^a
271	8520557-7775	05404931-0746327	...
272	8520580-7960	05404939-0757379	...
273	8530851-8132	05411403-0807573	...
274	8534457-7821	05412269-0749160	...
275	8535781-7830	05412586-0749506	...
276	8536129-8706	05412670-0842245	...
277	8537742-8080	05413058-0804482	...
278	8538844-7917	05413322-075022	...
279	853891-7999	05413358-0759562	...
280	8542681-8618	05414245-0837075	...

Table 2—Continued

Num.	IRS name	2MASS name	other names selected
281	8543224-7972	05414373-0758223	...
282	8545724-8008	05414973-0800322	V1305 Ori, HBC 182
283	8547523-7831	05415405-0749534	...
284	8547770-7986	05415466-0759124	...
285	8552157-8190	05420517-0811266	...
286	8552280-8641	05420547-0838284	...
287	8556074-7982	05421459-0755579	...
288	8560743-8147	05422578-0808501	...
289	8561044-7980	05422649-0755508	...
290	8562845-8151	05423081-0809055	...
291	8564835-8250	05423560-0815020	...
292	8567003-8669	05424081-0840086	...
293	8567545-8254	05424210-0815152	...
294	8567670-8803	05424242-0848140	...
295	8569204-8666	05424609-0840007	...
296	8570200-8276	05424848-0816347	V2775 Ori
297	8570949-8577	05425027-0834378	...
298	8571439-8650	05425142-0839020	...
299	8574645-8156	05425913-0809236	...
300	8576640-8652	05430392-0839094	...
301	8576836-8303	05430440-0818105	...
302	8579480-8565
303	8580634-8516	05431353-0831004	...
304	8375220-5817	05350054-0548591	HOPS-22 ^b
305	8382228-5704	05351734-0542145	HOPS-26, V411 Ori, Parenago 1917
306	8381598-5501	...	HOPS-51, V2275 Ori ^c
307	8334366-5384	05332249-0523031	HOPS-54, V1662 Ori
308	8383054-4929	05351932-0455450	HOPS-98, V2348 Ori
309	8499216-7444	05395811-0726412	HOPS-113
310	8467876-6944	05384288-0656406	HOPS-151
311	8412906-6878	05363096-0652410	HOPS-162
312	8424745-6171	05365939-0610157	HOPS-180
313	8405394-6391	05340695-0632079	HOPS-184 ^b
314	8352892-6535	05340695-0632079	HOPS-201, V1925 Ori
315	8536117-8706	05412670-0842245	HOPS-222

Table 2—Continued

Num.	IRS name	2MASS name	other names selected
316	8508553-7944	05402054-0756398	HOPS-272
317	8518494-7737	05404438-0744166	HOPS-277
318	8518616-7498	05404438-0744166	HOPS-283, IRAS 05333-0731
319	8524538-7800	05405889-0748030	HOPS-293

Note. — The sources of selected objects names: Parenago (1954) for Parenago XXX; Fűrész et al. (2008) for [FHM2008]XXX-XXXX; V* indicate the General Catalogue of Variable Stars (GCVS) (Kukarkin et al. 1971); HBC XXX indicate Herbig+Bell Catalog (Herbig & Bell 1988); HOPS-XXX indicate the identification of these sources in *Herschel* Orion Protostar Survey (HOPS, Megeath et al. 2010).

^aThe coordinate of HBC 497 (DL Ori/G3) does not exactly matched to the IRS coordinate of OriA-270.

^bA 2MASS source is 2-3 arcsec away from the target.

^cJHK photometry is from Robberto et al. (2010)

Table 3. Observation log of SpeX spectra

Num. (1)	Obs. Date (UT) (2)	Slit Width (") (3)	Total Int. Time (sec) (4)	PA (°) (5)	note (6)
1	2011 Nov 06	0.5	480
2	2011 Feb 28	0.8	480	-10.73	...
3	2011 Nov 07	0.8	120
4	2011 Feb 28	0.8	320	-30	b
5	2011 Feb 28	0.8	400	-10.73	...
11	2010 Feb 18	0.8	480
13	2010 Feb 17	0.8	480
16	2010 Feb 18	0.8	240
19	2010 Feb 17	0.8	720
20	2011 Nov 07	0.8	720
21	2011 Feb 26	0.8	960	60.12	...
22	2011 Nov 10	0.8	400	...	c
23	2011 Nov 07	0.8	240
24	2011 Feb 27	0.8	240
25	2010 Feb 16	0.5	480
26	2011 Nov 10	0.8	480	-27	b
28	2011 Nov 07	0.8	200
29	2010 Feb 18	0.8	480
32	2011 Feb 26	0.8	960
33	2011 Nov 06	0.5	480
34	2010 Feb 16	0.3	2520
36	2011 Nov 10	0.8	240
37	2011 Feb 27	0.8	240	62.31	...
38a	2010 Feb 18	0.8	240	...	a
38b	2010 Feb 18	0.8	240	...	a
39	2011 Nov 06	0.5	480
42	2011 Nov 06	0.5	720
44	2010 Feb 16	0.5	240
45	2011 Feb 26	0.8	120
47	2011 Nov 07	0.8	480	...	b
48	2011 Nov 07	0.8	480
50	2011 Nov 07	0.8	480
51	2011 Feb 28	0.8	400	53.01	...

Table 3—Continued

Num.	Obs. Date (UT)	Slit Width (")	Total Int. (sec)	Time (o)	PA (o)	note
(1)	(2)	(3)	(4)	(5)	(6)	
52	2011 Feb 26	0.8	480	
58	2011 Nov 07	0.8	480	
59	2010 Feb 17	0.8	480	
66	2010 Feb 16	0.5	960	
86	2011 Feb 28	0.8	480	-10.73	...	
88	2011 Feb 26	0.8	120	
97	2011 Feb 26	0.8	960	
98	2011 Nov 07	0.8	240	-55	b	
108	2010 Feb 16	0.5	240	
112	2011 Nov 07	0.8	120	
117	2011 Nov 07	0.8	480	
123	2010 Feb 18	0.8	720	
125	2011 Feb 27	0.8	240	62.31	c	
134	2011 Nov 07	0.8	480	
135	2011 Feb 27	0.8	480	62.31	...	
141	2011 Feb 27	0.8	120	
144	2011 Nov 10	0.8	480	
154	2011 Feb 28	0.8	320	53.01	c	
159	2011 Nov 07	0.8	480	
161	2011 Feb 28	0.8	480	-10.73	...	
168	2011 Feb 26	0.8	480	63.33	...	
169	2010 Feb 17	0.8	480	
170	2011 Feb 27	0.8	120	
172	2010 Feb 17	0.8	480	
173a	2011 Feb 28	0.8	120	45	a	
173b	2011 Feb 28	0.8	120	45	a	
176	2011 Nov 10	0.8	240	
177	2010 Feb 16	0.5	240	
179	2011 Nov 10	0.8	400	
182	2011 Feb 28	0.8	240	60.97	...	
183	2011 Feb 28	0.8	200	60.97	...	
184	2011 Nov 10	0.8	400	
185	2010 Feb 16	0.5	240	

Table 3—Continued

Num.	Obs. Date (UT)	Slit Width (")	Total Int. (sec)	Time (\circ)	PA (\circ)	note
(1)	(2)	(3)	(4)	(5)	(6)	
186	2010 Feb 16	0.5	240	
187	2011 Nov 07	0.8	240	
190	2011 Nov 10	0.8	720	
191	2011 Feb 27	0.8	80	62.31	...	
196	2011 Feb 28	0.8	240	60.97	...	
197	2011 Nov 10	0.8	240	
198	2011 Feb 28	0.8	240	60.97	...	
200	2011 Nov 07	0.8	200	
204	2011 Feb 28	0.8	960	-10.73	...	
206	2011 Feb 27	0.8	240	62.31	...	
208a	2011 Nov 10	0.8	120	...	a	
208b	2011 Nov 10	0.8	120	...	a	
210	2011 Feb 28	0.8	200	60.97	...	
211	2011 Nov 10	0.8	240	
213	2011 Feb 28	0.8	240	60.97	c	
214	2011 Feb 26	0.8	480	
217	2011 Nov 06	0.5	400	
218	2010 Feb 16	0.5	480	
219	2010 Feb 17	0.8	480	
220	2011 Feb 28	0.8	240	60.97	...	
223	2011 Feb 26	0.8	960	
225	2011 Feb 26	0.8	720	65.64	...	
226	2011 Feb 28	0.8	120	
227	2011 Feb 28	0.8	360	-10.73	...	
229	2010 Feb 16	0.5	240	
230	2010 Feb 18	0.8	720	
233	2011 Feb 26	0.8	480	...	c	
234	2011 Feb 28	0.8	400	60.97	...	
235	2011 Nov 07	0.8	240	
237	2010 Feb 17	0.8	480	
239	2010 Feb 18	0.8	240	
245	2011 Feb 28	0.8	200	60.97	...	
246	2011 Nov 06	0.5	480	

Table 3—Continued

Num.	Obs. Date (UT)	Slit Width (")	Total Int. (sec)	Time ($^{\circ}$)	PA ($^{\circ}$)	note
(1)	(2)	(3)	(4)	(5)	(6)	
247	2011 Nov 07	0.8	480	
249	2011 Feb 26	0.8	1440	90	...	
257	2010 Feb 17	0.8	480	
260	2010 Feb 17	0.8	240	
262	2011 Nov 06	0.5	200	
266	2011 Nov 06	0.5	120	
269	2011 Feb 27	0.8	120	62.31	...	
270	2010 Feb 18	0.8	240	
271	2010 Feb 18	0.8	960	
273	2011 Feb 28	0.8	400	53.01	...	
275	2010 Feb 17	0.8	240	
279	2010 Feb 17	0.8	960	
280	2011 Nov 10	0.8	360	-42	b	
281	2011 Feb 28	0.8	400	-10.73	...	
283	2010 Feb 17	0.8	240	
286	2011 Feb 28	0.8	400	53.01	...	
287	2011 Nov 10	0.8	240	
288	2011 Nov 10	0.8	200	
290a	2011 Feb 28	0.8	480	-20	a	
290b	2011 Feb 28	0.8	480	-20	a	
291	2010 Feb 17	0.8	480	
294	2010 Feb 18	0.8	240	
301	2011 Feb 28	0.8	480	-10.73	...	
302	2010 Feb 18	0.8	240	
303	2010 Feb 18	0.8	960	

Note. — Column (1): Num. The numbers are assigned in Table 1. When an object was revealed having a nearby companion and it was observed separately from the target object with SpeX, we add "a" and "b" next to the Num. Column (5): PA. The slit's positional angle for observation of a target. Column (6): Note for observation of binary systems: "a" indicates for the system which its primary and secondary were observed separately; "b" indicates for the system

which its primary and secondary were observed simultaneously and extracted their spectra separately; "c" indicates for the system which is suspected to have a secondary, but the spectrum of each component were not resolved, and the spectrum is the composite spectrum of a primary and a secondary.

Table 4. Spectral Type and Extinction

Num. (1)	IRS name (2)	Spectral types (3)	Spectral type adopted (4)	EW(H_{α}) (5)	EW(L_i) (6)	A_V (7)	A_V method (8)
1	8336884-5290	M0.0(8) M3.0(8)	M0.0	-22.5	0.5	$0.77^{+1.02}_{-0.39}$	J-H
2	8339347-5238	K1(3)	M3.0	-12.5	0.4	$1.15^{+1.52}_{-0.52}$	J-H
3	8343858-5513	M1.5(1); M1.0(24) M5.5(3); M5.5(8)	K1.0	$4.37^{+2.50}_{-3.05}$	J-H
4	8343917-6073	M1.0	M1.0	-101.0	0.2	$0.09^{+2.70}_{-0.09}$	CTTS J-H
5	8343944-5609	M5.5	M5.5	-33.3	0.3	$0.50^{+0.24}_{-0.29}$	L-J
6	8344455-5390	$3.21^{+0.26}_{-0.29}$	CTTS J-H
7	8344987-5460	M6(3)	M6.0	$2.42^{+1.07}_{-1.09}$	J-H
8	8346141-5010	M2(3); M3.5(8)	M3.5	-8.6	0.3	$0.23^{+1.47}_{-0.99}$	L-J
9	8346378-5387	$9.88^{+4.85}_{-4.85}$	CTTS J-H
10	8346581-5550	$10.10^{+7.48}_{-7.48}$	CTTS J-H
11	834711-5533	K7.0(SpeX)	K7.0	$8.28^{+3.70}_{-3.70}$	J-H
12	8348250-4797	$1.69^{+3.18}_{-3.18}$	CTTS J-H
13	8350150-5555	M3.5(3)	M3.5	$0.00^{+0.59}_{-0.59}$	L-J
14	8350916-5605	K7.5(8); K7(11)	K7.5	-5.5	0.4	$1.63^{+1.00}_{-1.00}$	L-J
15	8352483-5378	K7.5(8)	K7.5	-28.3	0.5	$5.26^{+3.10}_{-2.30}$	CTTS J-H
16	8353051-5229	K1.0(SpeX)	K1.0	$2.66^{+1.18}_{-2.39}$	J-H
17	8353319-5604	M4.0(8); M3.5(9)	M4.0	-116.2	0.2	$1.16^{+2.67}_{-2.67}$	J-H
18	8355083-4835	$1.00^{+7.67}_{-7.67}$	CTTS J-H
19	8355371-5480	K7.0(H)(2)	K7.0	$0.00^{+1.84}_{-0.00}$	L-J
20	8355629-5594	M1.9(9)	M2.0	$3.46^{+4.70}_{-3.21}$	CTTS J-H
21	8355898-5615	F6(5); F7.0(8); F8(12)	F7.0	$0.17^{+3.29}_{-0.17}$	L-J
22	8356531-5540	M2.0(8); K8e(3)	M2.0	-52.9	0.3	$1.17^{+5.90}_{-0.90}$	L-J
23	8357031-5072	K7(3); M0.0(8)	M0.0	-3.8	0.5	$1.49^{+1.22}_{-0.22}$	J-H
24	8358147-5505	K5(H)(2); K1e(3)	K1.0	$3.86^{+2.79}_{-2.79}$	J-H
25	8358862-4842	M3.0(7); M3.5(8)	M3.5	-15.0	0.4	$1.22^{+2.66}_{-0.54}$	J-H
26	8359203-5026	M5.5(8)	M5.5	-16.7	0.3	$0.00^{+0.49}_{-0.00}$	L-J
27	8360781-4940	M0.5(8)	M0.5	-81.1	0.2	$0.39^{+2.46}_{-0.90}$	L-J
28	8360900-5441	K2-K3e(2); K7.5(8); K2.5e(11)	K7.5	48.6	0.0	$2.96^{+5.55}_{-1.28}$	CTTS J-H
29	8361167-5475	M0.0(SpeX)	M0.0	$0.50^{+3.01}_{-0.50}$	L-J
30	8362406-4863	M0.5(8); K7(11)	M0.5	-36.2	0.4	$6.28^{+2.81}_{-3.45}$	J-H
31	8364658-4871	$4.94^{+6.75}_{-3.47}$	CTTS J-H
32	8364671-5575	M4(2); M5.0(8)	M5.0	-101.0	0.2	$0.20^{+3.17}_{-0.00}$	L-J
33	8365614-5581	K2-K5e(2); M5.0(8); K3.5(11)	M5.0	$0.00^{+5.80}_{-0.90}$	L-J
34	8365722-4816	M1.0(SpeX)	M1.0	$1.20^{+1.88}_{-0.38}$	L-J

Table 4—Continued

Num. (1)	IRS name (2)	Spectral types (3)	Spectral type adopted (4)	EW(H_{α}) (5)	EW(Li) (6)	A_V (7)	A_V method (8)
35	8366668-5168	B8, A0(2); B8(5); A0(11) K2(5); K0e(11)	A0.0	1.14 ^{+2.17} _{-1.14}	I-J
36	8366704-5669	K1e, G-Ke, K7.3(2); K7(5); G-e(11) M0(3)	K2.0	0.56 ^{+3.94} _{-3.94}	I-J
37	8367030-5378	M3.5(8)	K7.0	3.31 ^{+5.63} _{-2.47}	J-H
38	8367284-5798	K0(3)	M0.0	0.86 ^{+2.64} _{-0.86}	I-J
39	8368137-4860	K0(3)	M3.5	-18.8	0.5	0.54 ^{+0.89} _{-0.33}	I-J
40	8368755-4933	...	K0.0	7.20 ^{+4.87} _{-3.39}	CTTS J-H
41	8368837-5665	2.78 ^{+6.86} _{-0.71}	CTTS H-K
42	8369106-5686	M3.5(3); M4.0(8); M3.0e(9)	M4.0	-19.5	0.4	0.93 ^{+2.59} _{-0.55}	I-J
43	8369290-5652	2.88 ^{+2.35} _{-1.99}	CTTS J-H
44	8369980-5081	K7(3); M1.0(8)	M1.0	-40.0	0.5	0.40 ^{+2.93} _{-0.00}	I-J
45	8370827-5312	A3, A2, A2V _p , A5V, A6-7V, Am(2); A3, A2(5); A7.0(8) M0e(2); K7.5(8); M0(13)	A7.0	1.51 ^{+7.23} _{-0.51}	I-J
46	8371143-5450	K7.5(8)	K7.5	-44.1	0.5	2.01 ^{+2.45} _{-0.31}	CTTS J-H
47	8371984-5465	K5(2); M0.0(8); G-e(11)	K7.5	-7.8	0.6	4.44 ^{+0.00} _{-4.44}	H-K
48	8372100-5057	M2(2)	M0.0	0.34 ^{+2.20} _{-0.00}	I-J
49	8372608-5359	K4-K6e(2); K6.5(8); K4.7;e(15)	M2.0	0.09 ^{+0.11} _{-0.09}	I-J
50	8372885-5283	M3.0(8)	K6.5	-36.1	0.6	4.65 ^{+4.29} _{-2.46}	CTTS J-H
51	8373201-4936	K5, K6(2); K5(11) M3.5(1); M3.5(24)	M3.0	-5.0	0.5	6.52 ^{+2.92} _{-3.63}	J-H
52	8373676-5192	...	K5.0	0.00 ^{+0.24} _{-0.00}	I-J
53	8373930-6325	...	M3.5	-9.8	0.4	0.13 ^{+2.62} _{-0.13}	I-J
54	8373936-4946	11.00 ^{+3.76} _{-6.17}	CTTS J-H
55	8374073-5397	K8(2)	K7.5	0.93 ^{+0.82} _{-0.32}	J-H
56	8374080-5380	M3(2); M3.5(8)	M3.5	-39.7	0.3	0.69 ^{+1.17} _{-0.32}	I-J
57	8374271-5697	5.67 ^{+3.16} _{-3.20}	CTTS J-H
58	8374301-5908	M0.0(8)	M0.0	-46.1	0.1	0.48 ^{+5.07} _{-0.36}	CTTS J-H
59	8374338-6000	K5(3); M2.5(8); M0.1(24)	M0.0	-77.7	0.4	0.08 ^{+0.40} _{-0.08}	J-H
60	8374599-5741	0.00 ^{+2.45} _{-0.00}	CTTS J-H
61	8374677-5748	...	K0.0	6.58 ^{+5.66} _{-2.77}	CTTS J-H
62	8374677-5766	4.67 ^{+4.11} _{-1.77}	CTTS J-H
63	8374839-5427	M2(2); M0.5(8)	M0.5	-13.6	0.5	1.26 ^{+0.80} _{-0.68}	J-H
64	8375041-5333	K0-K2e, K0e, K6(2)	3.03 ^{+1.35} _{-1.96}	J-H
65	8375063-5840	7.03 ^{+2.35} _{-2.95}	CTTS J-H
66	8375158-5162	M5.5(2); M5.0(8)	M5.0	-10.3	0.4	0.13 ^{+0.34} _{-0.13}	I-J
67	8375190-5420	K6e(2); K7.5(8)	K7.5	-23.3	0.6	0.85 ^{+7.05} _{-0.02}	CTTS H-K
68	8375484-5401	0.00 ^{+2.04} _{-0.00}	CTTS J-H

Table 4—Continued

Num. (1)	IRS name (2)	Spectral types (3)	Spectral type adopted (4)	EW(H_{α}) (5)	EW(Li) (6)	A_V (7)	A_V method (8)
70	8375702-5443	2.51 ^{+6.62} _{-0.73}	CTTS J-H
71	8375886-5399	14.00 ^{+7.40} _{-2.04}	CTTS J-H
73	8376154-5675	15.00 ^{+5.97} _{-5.97}	CTTS J-H
74	8376176-5368	G;(H)(2)	G0.0	8.28 ^{+9.97} _{-2.53}	CTTS H-K
75	8376287-5377	M6(2)	M6.0	0.85 ^{+3.58} _{-0.06}	I-J
76	8376356-4822	1.00 ^{+3.80} _{-0.06}	CTTS J-H
77	8376541-5379	M5.5e (2)	M5.5	3.93 ^{+5.13} _{-0.55}	H-K
78	8376571-5415	M4.3(9)	M4.5	5.23 ^{+4.20} _{-1.20}	J-H
79	8376643-5900	6.09 ^{+5.23} _{-1.54}	CTTS J-H
80	8376687-5443	M2(2); M1.0(8)	M1.0	-19.3	0.5	1.65 ^{+1.54} _{-1.04}	J-H
81	8376747-5441	M2e(2)	M2.0	2.82 ^{+1.26} _{-2.03}	J-H
82	8376817-5387	M0.5-M2e, M1.2, M3, K4-M0(2)	M3.0	0.95 ^{+2.01} _{-0.00}	I-J
83	8376871-5399	K2, M0, M4(2); G8.5(8)	G8.5	-19.9	0.5	3.66 ^{+4.91} _{-1.15}	CTTS J-H
84	8376918-4974	M0.0(8)	M0.0	-26.9	0.3	4.53 ^{+5.87} _{-1.15}	CTTS J-H
85	8376976-5443	M0.5(2); K7.5(8)	K7.5	-15.2	0.5	2.22 ^{+1.00} _{-2.02}	J-H
86	8377111-5612	M4.5(2); M4.5(8)	M4.5	-16.4	0.2	0.54 ^{+2.60} _{-0.00}	CTTS J-H
88	8377167-5247	F8, G (2); F8, G2(5); G0+F7 (16)	G5.0	2.39 ^{+1.07} _{-1.39}	J-H
89	8377232-5402	M0(2); K7.0(8)	K7.0	-88.1	0.2	5.11 ^{+3.40} _{-1.70}	J-H
90	8377335-5489	M0.5(2)	M0.5	5.77 ^{+5.69} _{-3.39}	CTTS J-H
91	8377345-5422	K0, K0-K3e, A0V+K1V, A0V, K4eIV, K3 (2); K0, K2(5)	K0.0	3.65 ^{+3.35} _{-3.49}	J-H
92	8377361-5395	<M0e(2)	M0.0	7.54 ^{+3.50} _{-1.79}	J-H
93	8377383-5405	K2-K7e(2); K6.5(8)	K6.5	-237.6	0.2	2.47 ^{+6.79} _{-1.31}	CTTS J-H
94	8377392-5193	M2.5(8)	M2.5	-27.2	0.0	6.27 ^{+4.04} _{-2.87}	H-K
95	8377737-5547	4.88 ^{+8.94} _{-6.00}	CTTS J-H
96	8377749-5447	M4.5e(2)	M4.5	0.43 ^{+3.27} _{-0.43}	CTTS J-H
97	8378059-5644	8.57 ^{+3.10} _{-3.02}	CTTS J-H
98	8378345-5545	K7.0(8); M0(13)	K7.0	-37.6	0.5	1.02 ^{+4.32} _{-0.00}	CTTS J-H
99	8378366-5814	4.46 ^{+4.79} _{-2.44}	I-J
100	8378481-5465	5.59 ^{+3.24} _{-3.02}	CTTS J-H
101	8378503-5474	K2(2)	K2.0	5.93 ^{+5.71} _{-3.56}	CTTS J-H
102	8378561-5421	M2(2)	M2.0	0.56 ^{+3.63} _{-0.00}	I-J
103	8378630-4781	5.97 ^{+6.78} _{-3.94}	CTTS J-H
106	8379192-6093	10.80 ^{+5.92} _{-5.68}	CTTS J-H
108	8379312-5776	K4(14), K0.0(7); K _e (17)	K0.0	3.91 ^{+2.68} _{-2.89}	J-H

Table 4—Continued

Num. (1)	IRS name (2)	Spectral types (3)	Spectral type adopted (4)	EW(H_{α}) (5)	EW(Li) (6)	A_V (7)	A_V method (8)
112	8380422-5659	K3(5)	K3.0	1.15 $^{+3.86}_{-0.00}$	CTTS J-H
114	8380518-5465	M2.0(11)	M2.0	...	5.59 $^{+3.60}_{-0.00}$	H-K	
117	8380667-5516	K5e, F8-G0III-IV(2); G7e(13)	G7.0	...	1.41 $^{+6.51}_{-0.46}$	I-J	
119	8380695-5479	M2.8(9)	M3.0	...	3.23 $^{+1.93}_{-0.41}$	H-K	
120	8380923-5478	7.12 $^{+6.65}_{-2.20}$	H-K	
121	8380932-5721	1.06 $^{+3.13}_{-0.00}$	CTTS J-H	
122	8381019-5555	K5, K4-M0(2)	K5.0	...	9.53 $^{+5.69}_{-5.78}$	J-H	
123	8381020-5546	M4(13)	M4.0	...	1.63 $^{+6.01}_{-0.00}$	I-J	
125	8381120-5653	K0-K3(P)(2)	K1.5	...	1.88 $^{+6.34}_{-0.00}$	CTTS J-H	
127	8381491-5164	5.99 $^{+2.20}_{-0.00}$	CTTS J-H	
128	8381501-4991	12.40 $^{+4.86}_{-3.96}$	CTTS J-H	
129	8381622-5481	M2.5(11)	M2.5	...	1.04 $^{+3.10}_{-0.00}$	I-J	
131	8381971-4762	K1e(14)	K1.0	...	1.11 $^{+5.81}_{-0.00}$	I-J	
132	8382048-5452	13.60 $^{+6.48}_{-7.76}$	CTTS J-H	
133	8382339-5974	1.31 $^{+2.97}_{-0.92}$	CTTS J-H	
134	8382412-6410	M0.5(1); M2(4); M1(10); M0.5(24)	M0.5	-12.1	0.6	0.87 $^{+1.02}_{-0.96}$	J-H
135	8382467-5709	K3(5)	K3.0	1.48 $^{+4.48}_{-1.48}$	H-K
136	8382490-5270	K7+M1.5(16)	K7.0	...	8.48 $^{+3.79}_{-2.99}$	J-H	
137	8382623-5479	M2.5(9)	M2.5	...	1.74 $^{+6.78}_{-0.97}$	J-H	
138	8382655-4889	6.58 $^{+4.75}_{-3.45}$	CTTS J-H	
139	8382835-5291	A8-F0(2)	A9.0	-2.2	0.0	14.10 $^{+6.35}_{-7.92}$	J-H
140	8383581-5050	26.50 $^{+4.63}_{-8.04}$	CTTS H-K	
141	8383861-5154	G1, G0, F9IV, K2Ve, F8-G0III-IV, G0III (2); G1, G0(5); F8.0(8)	F8.0	...	0.76 $^{+5.83}_{-0.76}$	I-J	
142	8384113-5117	2.40 $^{+3.80}_{-1.84}$	CTTS J-H	
143	8384325-5457	M4.5e (2); M5.0(8)	M5.0	-119.3	0.3	2.04 $^{+3.46}_{-5.07}$	CTTS J-H
144	8384331-5134	K7.0(8)	K7.0	-28.5	0.6	5.44 $^{+5.21}_{-2.67}$	CTTS J-H
145	8384717-5469	M3.5(2)	M3.5	...	2.83 $^{+1.82}_{-0.92}$	CTTS J-H	
146	8384864-5440	M3.0(11)	M3.0	...	1.39 $^{+0.00}_{-0.00}$	I-J	
147	8385190-5442	M4-M4.5e, M5.3, M4(2)	M4.5	...	2.35 $^{+2.66}_{-1.48}$	CTTS J-H	
148	8385255-5191	K6e(2); K7.5(8)	K7.5	-76.2	0.2	4.79 $^{+2.14}_{-2.10}$	J-H
149	8385365-5106	21.30 $^{+9.91}_{-4.98}$	CTTS J-H	
150	8385988-5427	G5, G0III, G-K, K1, M3(2)	G5.0	...	1.91 $^{+1.58}_{-1.58}$	J-H	
151	8386322-6228	M2.0(1); M2.5(4); M1.5(10); M2.1(24)	M2.0	-6.5	0.4	1.03 $^{+0.64}_{-0.63}$	J-H
152	8386383-5393	K4(2)	K4.0	...	3.76 $^{+2.51}_{-2.09}$	CTTS J-H	

Table 4—Continued

Num. (1)	IRS name (2)	Spectral types (3)	Spectral type adopted (4)	EW(H_{α}) (5)	EW(Li) (6)	A_V (7)	A_V method (8)
153	8386462-5457	M3, M3.2(2); M2.0(8)	M2.0	-2.0	0.5	$0.87^{+2.45}_{-0.27}$	H-K
154	8386523-5715	M3.6(9)	M3.5	$1.87^{+2.43}_{-0.98}$	J-H
155	8386627-5467	M5(2)	M5.0	$0.18^{+2.06}_{-0.06}$	I-J
156	8386694-5026	$28.60^{+4.03}_{-1.99}$	CTTS H-K
158	8386759-5416	K7.0(11)	K7.0	$1.25^{+0.06}_{-0.06}$	I-J
159	8386804-5987	M3.5(8)	M3.5	-30.8	0.3	$0.00^{+2.19}_{-0.00}$	I-J
160	8386841-5129	$19.90^{+4.06}_{-5.09}$	CTTS H-K
161	8386935-4790	K1(3); M4.5(8)	M4.5	-108.2	0.4	$0.15^{+2.93}_{-0.05}$	I-J
162	8386957-4804	$17.70^{+0.05}_{-17.70}$	H-K
163	8387691-5326	$11.00^{+6.16}_{-1.12}$	CTTS J-H
164	8387753-4993	$14.70^{+7.23}_{-2.89}$	CTTS J-H
165	8387832-5864	$4.97^{+1.88}_{-2.23}$	CTTS J-H
166	8387937-6755	M3(4); M3.1(0); M2.9(24)	M3.0	-95.0	0.3	$0.03^{+1.01}_{-0.01}$	I-J
167	8388119-5083	M2.0(8)	M2.0	-143.1	0.2	$0.40^{+3.14}_{-0.00}$	I-J
168	8388316-5157	K3, K6, K4-M0eIV(2); K4(5); M0.5+M1.5(16)	M1.0	$0.21^{+2.52}_{-0.00}$	I-J
169	8389033-4773	K4(3); M0.5(8)	M0.5	-66.5	0.4	$1.67^{+1.18}_{-1.50}$	J-H
170	8389275-5105	A0(5)	A0.0	$0.00^{+0.16}_{-0.00}$	J-H
172	8389673-4794	M1.0(7); M3.0(8)	M3.0	$1.25^{+1.27}_{-1.09}$	J-H
173	8390003-5207	G6-K2e (2)	K0.0	-6.2	0.5	$1.56^{+10.02}_{-0.00}$	I-J
174	8390073-5082	$8.42^{+2.16}_{-5.24}$	CTTS J-H
175	8390083-5339	$8.39^{+4.34}_{-1.33}$	CTTS J-H
176	8390285-5070	M1.5(8)	M1.5	-32.1	0.5	$0.44^{+3.06}_{-0.44}$	I-J
177	8390554-6390	M2.5(1); M2.4(24)	M2.5	-53.8	...	$0.21^{+0.20}_{-0.00}$	I-J
178	8391040-5081	$16.90^{+7.45}_{-7.46}$	CTTS J-H
179	8391058-4994	M0.0(8)	M0.0	-43.6	0.3	$2.92^{+2.72}_{-0.97}$	J-H
180	8391196-5211	K2 (2); K5.0(8)	K5.0	-5.2	0.5	$4.06^{+2.77}_{-2.16}$	CTTS J-H
181	8391648-5110	$5.47^{+2.06}_{-2.86}$	CTTS J-H
182	8392509-5169	K6-K8 (2); K6.5(8)	K6.5	-8.1	0.2	$6.39^{+2.86}_{-3.16}$	J-H
183	8393152-5094	M0.0(8)	M0.0	-27.9	0.3	$2.23^{+3.06}_{-1.68}$	CTTS J-H
184	8394216-5181	K7e (2); K7.5(8)	K7.5	-34.9	0.5	$1.40^{+2.18}_{-0.11}$	J-H
185	8394454-5823	K6.0(7)	K6.0	$0.86^{+1.42}_{-0.00}$	J-H
186	8395167-5024	M0.5(8); K5e(14)	M0.5	-89.3	0.1	$2.40^{+2.89}_{-0.90}$	CTTS J-H
187	8395780-5308	M1.5(8)	M1.5	-60.5	0.0	$3.42^{+3.56}_{-0.00}$	CTTS J-H
188	8396035-5861	$0.64^{+1.66}_{-0.00}$	CTTS J-H

Table 4—Continued

Num. (1)	IRS name (2)	Spectral types (3)	Spectral type adopted (4)	EW(H_{α}) (5)	EW(Li) (6)	A_V (7)	A_V method (8)
189	8396285-5119	...	M2.5(8)	1.63 ^{+0.49} 4.24 ^{+1.90}	CTTS J-H
190	8396319-4941	K4.0(1)	K4.0	3.65 ^{+0.97} 0.00	J-H
191	8396679-6167	M2.0(8)	M2.0	-94.1	0.5	0.43 ^{+0.63} 0.00	CTTS J-H
192	8397522-4788	M0.5e (2); M0.5(8)	M0.5	-30.0	0.5	0.74 ^{+0.03} 0.00	CTTS J-H
193	8397632-5445	1.54 ^{+0.97} 0.00	CTTS J-H
194	8397818-4972	M2(3)	M2.0	3.80 ^{+1.17} 0.32	CTTS J-H
195	8398707-5755	K7.5(1); M0(4); K4(10); K4.0(24)	K4.0	-27.9	0.6	0.89 ^{+0.32} 0.00	CTTS J-H
196	8398936-6711	K7.5(1); M0(8); M0e(3); K7, M0 (14)	M0.0	-106.0	0.3	0.47 ^{+3.90} 0.00	J-H
197	8399022-5055	K6.5(1); M0(4); M0(10); K7.6(24)	K7.5	-13.1	0.4	1.55 ^{+2.16} 0.10	J-H
198	8399269-6612	K6.5(1); M0(4); K4.5(10); K7(18); K4.5(24)	K4.5	-4.0	0.4	1.62 ^{+0.72} 1.62	J-H
199	8399902-6268	M2.5(1); M0(4); K5(10); K5.4(24)	K5.5	-42.2	1.2	1.13 ^{+4.04} 0.00	CTTS J-H
200	8400080-6709	K5.5(1); K5(4); K5(10); K5.4(24)	K2.0	-22.0	0.5	5.33 ^{+5.98} 0.00	CTTS J-H
201	8402765-6538	K6.5(1); K5(4); K5(10); K2.0(24)	M2.5	-38.8	0.4	2.31 ^{+1.14} 0.00	J-H
202	8403455-6810	M0.5(1); M2(4); M0.5(10); M2.5(24)	K3.5	-5.0	0.6	0.68 ^{+2.78} 0.00	CTTS J-H
203	8406280-6293	K5(4); K3(10); K3.3(24)	M2.5	-63.3	0.5	0.44 ^{+0.44} 0.00	J-H
204	8406609-6247	M2.5(4); M2.5(8); M2.5(10); M2.6(24)	K4.0	2.16 ^{+0.00} 0.00	H-K
205	8407074-5195	K6(19); K4IV-Ve(2)	K5.0	-17.0	0.5	5.92 ^{+6.49} 1.51	CTTS J-H
206	8408920-6760	K5.0(1); Cs(11); K5.1(24)	12.20 ^{+5.56} 9.41	J-H
207	8409911-6386	...	K4.0	0.35 ^{+0.32} 0.00	I-J
208	8410334-6291	K4e (11)	23.60 ^{+10.16} 6.95	CTTS H-K
209	8410779-6416	...	M0.0	-18.0	0.6	1.78 ^{+2.52} 0.14	I-J
210	8410886-6134	M1.5(1); M0.0(24)	M4.5	-15.6	0.3	0.31 ^{+0.31} 0.37	J-H
211	8411618-6426	M3.5(1); M3.5(8); M3(10); M4.3(24)	M1.5	-31.7	0.3	8.01 ^{+1.45} 4.65	CTTS J-H
212	8412592-6712	M1.5(1); M2(4); M1.5(10); M1.3(24)	K5.0	-31.5	0.4	2.00 ^{+2.64} 0.38	J-H
213	8413152-6141	K7.5(1); K5.0(24)	M0.5	0.61 ^{+0.39} 0.00	I-J
214	8413399-5287	M0.5(8); K8e (3)	M2.0	-93.9	...	3.74 ^{+5.93} 0.00	I-J
215	8413704-6739	M2.0(1); M2(4); M1.0(10); M2.0(24)	K7.0(1); K8(4); K8(10); K7.5(24)
216	8414490-7187	...	M4.5(1); M4.5(8); M4.5(24)	K7.5	-153.0	3.94 ^{+6.24} 2.49	J-H
217	8415394-6556	M0.5(7); M0.5(8); M0.7(24)	M4.5	-14.1	...	0.07 ^{+0.89} 0.97	I-J
218	8416389-6503	M0.0(1); K7.7(24)	M0.5	-8.2	0.6	0.41 ^{+0.35} 0.35	I-J
219	8416834-6225	K7.5(1); K2.1(24)	K7.5	-19.2	0.3	6.78 ^{+4.27} 4.27	CTTS J-H
220	8416914-6175	K2.0	-45.9	0.3	12.30 ^{+0.02} -12.62	H-K	
221	8416978-6185	M0.5(1); M0.4(24)	M0.5	-4.1	0.5	5.85 ^{+2.62} -3.36	J-H
222	8421949-6718

Table 4—Continued

Num. (1)	IRS name (2)	Spectral types (3)	Spectral type adopted (4)	Spectral type (5)	EW(H_{α}) (6)	EW($L\lambda$) (6)	A_V (7)	A_V method (8)
223	8424570-6484	M3.0(7); M3.7(24)	M3.5	-10.1	0.4	0.60 ^{+1.17} _{-0.60}	I-J	
224	8424689-6154	A0.0 (12); A2/3 (20); A2V (21)	A2.0	1.26 ^{+1.48} _{-1.28}	I-J	
225	8425038-6557	K5.0(1); K0(14); G3.0(24)	G3.0	-18.6	0.5	2.61 ^{+1.45}	I-J	
226	8430527-6583	A3.5(1); A5II-II ^{ev} (14); A6.9(24)	A7.0	-5.2	...	0.83 ^{+0.56}	I-J	
227	8440418-7404	M0.0(1); K7.9(24)	K8.0	-10.3	0.5	2.02 ^{+0.83}	I-J	
228	8443530-6843	M0.5(1); M0e(22); M1.0(24)	M1.0	-104.0	0.4	0.66 ^{+0.00}	I-J	
229	8444779-6608	>M0.0(7); M0.3(24)	M0.5	-3.1	0.6	3.20 ^{+1.44}	J-H	
230	8445558-6860	M0(SpEx); M3.5(24)	M3.5	-13.1	0.5	1.41 ^{+1.05}	J-H	
231	8447398-6788	M3.0(7)	M3.0	20.20 ^{+9.12}	J-H	
232	8448350-6815	M0.0(1)	M0.0	8.25 ^{+4.39}	CTTS J-H	
233	8450343-7265	M1.5(1); K7(22); M3.2(24)	M3.0	-126.0	0.4	0.64 ^{+1.24}	I-J	
234	8452061-7269	M0.5(1); M1.0(24)	M1.0	-7.1	0.5	1.35 ^{+5.65}	I-J	
235	8453876-6821	A3.5(1); A5e(23)	A3.5	3.58 ^{+9.18}	I-J	
236	8455602-7112	M1.0(1); K4.5(10); K4.5(24)	K4.5	-5.4	...	8.89 ^{+5.73}	H-K	
237	8457266-7161	M1.5(7); M2.9(24)	M3.0	-11.0	0.4	4.20 ^{+1.97}	J-H	
238	8461533-6914	K6.0(1); K7.5(24)	K7.5	-21.1	0.6	0.67 ^{+2.44}	CTTS J-H	
239	8464666-7838	M1.0(1); K5e(14); K4.2(24)	K4.0	-25.5	0.6	0.00 ^{+1.51}	I-J	
240	8465247-7776	M1.5(1); M2.3(24)	M2.5	-12.6	0.5	0.85 ^{+0.99}	J-H	
241	8466711-6987	K6.0(1); M0.5(24)	M0.5	-162.0	...	3.70 ^{+5.45}	CTTS J-H	
242	8468902-6969	K7.5(10)	K7.5	-88.3	...	11.30 ^{+5.04}	J-H	
243	8468729-6970	M1.0(10); K7.3(24)	K7.5	-77.0	0.5	8.42 ^{+3.77}	J-H	
244	8468911-7104	M1.5(1); M1.0(10); M1.0(24)	M1.0	-76.8	...	9.43 ^{+1.21}	J-H	
245	8472719-7464	M2.0(1); K7.4(24)	K7.5	-159.0	0.3	5.81 ^{+1.10}	CTTS J-H	
246	8476732-7058	K7.5(1)	K7.5	-66.8	...	9.16 ^{+4.66}	J-H	
247	8477229-7184	M3.0(1); M0.2(24)	M0.0	-63.6	0.4	5.85 ^{+2.62}	J-H	
248	8486920-7342	20.40 ^{+1.34}	CTTS H-K	
249	8488472-7373	M2.5(SpEx)	M2.5	0.39 ^{+3.61}	CTTS J-H	
250	8492690-7387	15.70 ^{+6.72}	CTTS J-H	
251	8494096-7377	14.60 ^{+6.33}	CTTS J-H	
252	8495155-7404	19.30 ^{+10.44}	CTTS H-K	
253	8497290-7502	21.50 ^{+6.21}	CTTS H-K	
254	8497797-7462	34.50 ^{+4.69}	CTTS H-K	
255	8499151-7482	32.00 ^{+4.68}	CTTS H-K	
256	8499541-7426	13.10 ^{+7.98}	CTTS J-H	

Table 4—Continued

Num. (1)	IRS name (2)	Spectral types (3)	Spectral type adopted (4)	Spectral type (5)	EW(H_{α}) (6)	EW($L\delta$) (7)	A_V (8)	A_V method
257	8502614-7795	M3.0(1); M3.1(24)	M3.0	-263.0	0.3	0.48 ^{+1.35} _{-0.46}	I-J	
258	8504327-7460	K7.0(1)	K7.0	9.96 ^{+3.99} _{-3.99}	J-H	
259	8505083-8237	K7e(4); K7.0(10); K7.0(24)	K7.0	0.0	...	6.92 ^{+6.23} _{-4.23}	CTTS J-H	
260	8508501-7431	M2.0(1); M1.3(24)	M1.5	-24.9	0.5	0.87 ^{+1.87} _{-0.56}	I-J	
261	8508648-7916	7.69 ^{+4.90} _{-3.57}	CTTS J-H	
262	8510403-8125	K0e(4); K0(10); G4.1(24)	G4.0	-46.9	0.3	2.00 ^{+6.06} _{-1.40}	I-J	
263	8511308-8126	M3e(4); M3(10); M5.0(24)	M5.0	-57.2	0.4	0.63 ^{+4.39} _{-0.45}	CTTS J-H	
264	8511602-7926	8.46 ^{+3.68} _{-4.29}	CTTS J-H	
265	8514861-7663	11.00 ^{+4.29} _{-6.11}	CTTS J-H	
266	8515568-8067	F0-G0e(4); F(10); F5.0(24)	F5.0	0.0	...	6.60 ^{+3.01} _{-5.76}	J-H	
267	8516031-7796	22.00 ^{+10.21} _{-4.67}	CTTS H-K	
268	8518798-7373	2.36 ^{+8.18} _{-1.42}	CTTS J-H	
269	8519260-8090	K4.0(1); K1e(4); K1(10); K3.0(24)	K3.0	-18.3	0.5	3.09 ^{+3.27} _{-1.94}	J-H	
270	8519428-8120	K7(4); K7(10); K7.0(24)	K7.0	0.0	...	8.58 ^{+3.83} _{-4.53}	J-H	
271	8520557-7775	M2.0(SpeX); M0.2(24)	M0.0	-67.9	...	6.33 ^{+4.33} _{-2.09}	H-K	
272	8520580-7960	8.74 ^{+3.89} _{-8.74}	J-H	
273	8530851-8132	M2(1); M2(4); M2(10); M2.1(24)	M2.0	-7.2	0.4	1.41 ^{+2.58} _{-0.33}	J-H	
274	8534457-7821	17.60 ^{+7.90} _{-4.14}	CTTS H-K	
275	8535781-7830	<M5.0(7); K7.0(24)	K7.0	-6.9	0.5	4.26 ^{+4.62} _{-0.71}	J-H	
276	8536129-8706	14.50 ^{+8.11} _{-1.54}	CTTS J-H	
277	8537742-8080	K7e(4); K7(10); K7.0(24)	K7.0	-40.0	...	6.88 ^{+4.84} _{-3.10}	CTTS J-H	
278	8538844-7917	M2(11); K7.0(24)	K7.0	-18.7	0.4	0.90 ^{+6.22} _{-0.90}	I-J	
279	8538911-7999	M1.5(10); M1.5(24)	M1.5	-69.8	...	8.00 ^{+3.80} _{-3.80}	H-K	
280	8542681-8618	K7.0(1); K1.0(24)	K1.0	-26.7	0.4	5.43 ^{+2.67} _{-3.96}	J-H	
281	8543224-7972	M5.5(10); M7.4(24)	M7.5	-247.0	...	0.59 ^{+2.31} _{-2.31}	I-J	
282	8545724-8008	K5(4); K5(10); K5.0(24)	K5.0	-18.0	...	0.03 ^{+7.29} _{-0.03}	I-J	
283	8547523-7831	M2.0(7); M4.5(24)	M4.5	-14.5	...	0.70 ^{+1.66} _{-0.54}	J-H	
284	8547770-7986	K8(4); K3.5(10); K3.5(24)	K3.5	-6.6	0.6	5.07 ^{+3.34} _{-2.05}	J-H	
285	8552157-8190	12.70 ^{+5.54} _{-3.33}	CTTS J-H	
286	8552280-8641	M3.0(1); M1.0(24)	M1.0	-10.0	0.8	2.95 ^{+1.71} _{-1.35}	J-H	
287	8556074-7982	M3.5(10); M2.8(24)	M3.0	-34.5	0.4	2.01 ^{+0.89} _{-0.77}	J-H	
288	8560743-8147	M2.5(10); M2.0(24)	M2.5	-115.0	...	3.36 ^{+1.93} _{-1.26}	J-H	
289	8561044-7980	K6.0(10); K7.2(24)	K7.0	-130.0	0.3	4.00 ^{+3.74} _{-1.50}	CTTS J-H	
290	8562845-8151	M2.5(1); M2.8(24)	M3.0	-46.1	...	2.58 ^{+4.21} _{-1.93}	I-J	

Table 4—Continued

Num. (1)	IRS name (2)	Spectral types (3)	Spectral type adopted (4)	EW(H_{α}) (5)	EW(Li) (6)	A_V (7)	A_V method (8)
291	856435-8250	M2.5(1); M1.8(24)	M2.0	-40.0	0.5	$2.14^{+1.17}_{-0.80}$	J-H
292	8567003-8669	M1.0(1); M2.4(24)	M2.5	-105.0	0.3	$0.91^{+0.96}_{-0.90}$	I-J
293	8567345-8254	M3.0(1); M1(4); M1.0(10); M3.0(24)	M3.0	-155.0	0.3	$3.40^{+3.95}_{-1.93}$	CTTS J-H
294	8567670-8803	M2.5(SpeX); M2.0(24)	M2.0	-2.9	...	$7.71^{+1.93}_{-2.35}$	H-K
295	8569204-8666	K4.0(24)	K4.0	-3.1	0.4	$5.46^{+2.35}_{-2.99}$	CTTS J-H
296	8570200-8276	$17.50^{+8.92}_{-3.00}$	CTTS J-H
297	8570949-8577	$19.90^{+4.61}_{-1.90}$	CTTS H-K
298	8571439-8650	-47.0	...	$6.72^{+4.28}_{-3.99}$	CTTS J-H
299	8574645-8156	M1.0(1); M1(4); M1.0(10); M0.5(24)	M0.5	-65.8	0.4	$2.34^{+2.96}_{-3.99}$	J-H
300	8576640-8652	M1.4(24)	M1.5	-11.1	0.7	$4.70^{+3.24}_{-1.45}$	H-K
301	8576836-8303	M3.5(1); M2.5(24)	M2.5	-4.3	0.4	$2.92^{+1.31}_{-0.14}$	J-H
302	8579480-8565	M(SpeX)	M
303	8580634-8516	M3.0(7)	M3.0	$6.92^{+4.90}_{-2.94}$	H-K
304	HOPS-22	$7.09^{+5.94}_{-1.03}$	CTTS J-H
305	HOPS-26	M2.0(9)	M2.0	$0.73^{+2.21}_{-0.00}$	CTTS J-H
306	HOPS-51	$11.80^{+11.97}_{-0.00}$	J-H
307	HOPS-54	M3.5(3)	M3.5	$0.72^{+1.68}_{-0.72}$	J-H
308	HOPS-98	$19.40^{+11.70}_{-1.03}$	CTTS J-H
309	HOPS-113	$22.00^{+14.69}_{-1.90}$	CTTS H-K
310	HOPS-151	$4.96^{+8.82}_{-0.00}$	CTTS J-H
311	HOPS-162	M2.0(10)	M2.0	$2.25^{+1.34}_{-0.93}$	J-H
312	HOPS-180	$0.00^{+5.45}_{-0.00}$	CTTS J-H
313	HOPS-184	$1.37^{+3.49}_{-1.37}$	CTTS J-H
314	HOPS-201	M3.0(25)	M3.0	$0.24^{+0.37}_{-0.00}$	I-J
315	HOPS-222	$14.50^{+8.11}_{-5.54}$	CTTS J-H
316	HOPS-272	$12.30^{+6.02}_{-6.66}$	CTTS J-H
317	HOPS-277	$9.85^{+4.91}_{-5.72}$	CTTS J-H
318	HOPS-283	M1.0(25)	M1.0	$4.26^{+5.22}_{-1.26}$	J-H
319	HOPS-293	$2.75^{+9.91}_{-0.00}$	CTTS J-H

Note. — The methods or literature reference for spectral type determination is indicated with parentheses, and the meaning of the numbers in parentheses is listed as follows: (1) Allen & Mosby (2008), private communication; spectral types are measured from HECTOSPEC spectra (2) Hillenbrand (1997) (3) Rebull et al. (2000) (4) Allen (1995) (5) Wolff et al. (2004) (6) Hillenbrand & Carpenter (2000) (7) Hernandez (2008), private communication; spectral types measured

from MDM spectroscopic data (8) Hernandez & Tobin (2009), private communication; spectral types are measured from HECTOSPEC spectra or FAST spectra (9) da Rio et al. (2010) (10) Fang et al. (2009) (11) Parihar et al. (2009a) (12) Manoj et al. (2006) (13) Parihar et al. (2009b) (14) Herbig & Bell (1988) (15) Glebocki & Gnacinski (2005) (16) Daemgen et al. (2012) (17) Frankin et al. (2007) (18) Riaz et al. (2006) (19) Rebull (2001) (20) Houk & Swift (2000) (21) Ochsenbein (1980) (22) Wouterloot & Brand (1992) (23) Caratti O Garatti et al. (2012) (24) Hsu et al. (2012) (25) Fang et al. (2013) (SpeX) Spectral typing with SpeX spectra in this work

Note. — The unit of column (5) and (6) is Å. EW(H_{α}) and EW(L_{λ}) values are from Hernandez (2008); Hernandez & Tobin (2009); Hsu et al. (2012). Column (7) is the adopted A_V and the range of A_V values calculated by several methods described in the text. Column (8) A_V method: the method used to derive the adopted A_V in the column (7).

Table 5: K-S test for the visual extinction distribution

Regions compared	All objects		available spectral types	
	D	p	D	p
Trapezium. vs. ONC	0.30	$\ll 0.001$	0.25	0.03
Trapezium. vs. L1641	0.30	$\ll 0.001$	0.25	0.03
ONC vs. L1641	0.19	0.02	0.21	0.04

D is the maximum deviation between the cumulative distribution of two groups. *p* indicates the probability that there is no significant difference between the distributions

Table 6. Basic Stellar Properties and Mass Accretion Rate

Num.	IRS name	T_{eff} (K)	L_\star (L_\odot)	M_\star (M_\odot)	\dot{M} (10^{-9}) (M_\odot/yr)
1	8336884-5290	3770	0.66	0.49 ± 0.07	0.63 ± 0.11
2	8339347-5238	3360	0.41	0.29 ± 0.06	1.19 ± 0.96
3	8343858-5513	4920	12.12	2.67 ± 0.30	235.57 ± 133.24
4	8343917-6073	3630	0.79	0.40 ± 0.06	2.91 ± 0.45
5	8343944-5609	2840	0.48	0.15 ± 0.03	< 9.79
6	8344455-5390	3770	0.25	0.50 ± 0.09	...
7	8344987-5460	2800	0.09	0.09 ± 0.03	...
8	8346141-5010	3260	0.16	0.24 ± 0.06	...
9	8346378-5387	3770	5.17	0.51 ± 0.08	...
10	8346581-5550	3770	0.24	0.50 ± 0.09	...
11	8347711-5533	3970	1.77	0.62 ± 0.09	< 4.77
12	8348250-4797	3770	0.29	0.50 ± 0.09	...
13	8350150-5595	3260	0.44	0.25 ± 0.04	0.47 ± 0.18
14	8350916-5605	3955	2.44	0.61 ± 0.09	...
15	8352483-5378	3955	1.47	0.61 ± 0.08	...
16	8353051-5229	4920	3.14	1.82 ± 0.10	2.90 ± 0.66
17	8353319-5604	3160	0.36	0.23 ± 0.05	...
18	8355083-4835	3770	0.18	0.50 ± 0.09	...
19	8355371-5480	3970	0.47	0.67 ± 0.08	1.84 ± 0.62
20	8355629-5594	3490	0.36	0.34 ± 0.07	5.00 ± 1.52
21	8355898-5615	6140	15.76	2.13 ± 0.12	...
22	8356531-5540	3490	0.43	0.35 ± 0.06	15.54 ± 9.60
23	8357031-5072	3770	1.16	0.48 ± 0.07	< 0.77
24	8358147-5505	4920	5.14	2.06 ± 0.15	68.36 ± 15.59
25	8358862-4842	3260	0.12	0.24 ± 0.07	< 0.30
26	8359203-5026	2840	0.16	0.11 ± 0.04	1.90 ± 0.34
27	8360781-4940	3700	0.46	0.45 ± 0.08	...
28	8360900-5441	3955	2.66	0.61 ± 0.09	203.07 ± 22.13
29	8361167-5475	3770	0.37	0.50 ± 0.08	1.28 ± 0.11
30	8362406-4863	3700	1.01	0.44 ± 0.06	...
31	8364658-4871	3770	0.24	0.50 ± 0.09	...
32	8364671-5575	2880	0.23	0.13 ± 0.06	3.51 ± 1.79
33	8365614-5581	2880	0.53	0.16 ± 0.03	24.07 ± 8.21
34	8365722-4816	3630	0.22	0.41 ± 0.08	< 0.10
35	8366668-5168	9700	49.99	2.53 ± 0.13	...
36	8366704-5669	4760	5.25	1.94 ± 0.23	14.32 ± 4.09
37	8367030-5378	3970	5.35	0.66 ± 0.10	1375.03 ± 571.74
38	8367284-5798	3770	1.34	0.48 ± 0.06	1.93 ± 1.08
39	8368137-4860	3260	0.25	0.25 ± 0.05	0.78 ± 0.80
40	8368755-4933	5030	1.39	1.35 ± 0.05	...
41	8368837-5665	3770	0.05	0.47 ± 0.07	...
42	8369106-5686	3160	0.47	0.22 ± 0.04	2.34 ± 1.12
43	8369290-5652	3770	3.26	0.49 ± 0.07	...
44	8369980-5081	3630	0.54	0.41 ± 0.07	4.53 ± 1.68
45	8370827-5312	7800	45.87	2.51 ± 0.06	...

Table 6—Continued

Num.	IRS name	T_{eff} (K)	L_\star (L_\odot)	M_\star (M_\odot)	\dot{M} (10^{-9}) (M_\odot/yr)
46	8371143-5450	3955	1.29	0.62 ± 0.08	...
47	8371984-5465	3955	4.07	0.63 ± 0.09	< 0.29
48	8372100-5057	3770	0.56	0.49 ± 0.08	8.78 ± 1.15
49	8372608-5359	3490	0.45	0.34 ± 0.06	...
50	8372885-5283	3995	3.31	0.66 ± 0.09	45.41 ± 12.77
51	8373201-4936	3360	2.08	0.29 ± 0.03	< 16.15
52	8373676-5192	4140	1.47	0.78 ± 0.10	...
53	8373930-6325	3260	0.16	0.24 ± 0.06	...
54	8373936-4946	3770	1.46	0.48 ± 0.06	...
55	8374073-5397	3955	3.39	0.62 ± 0.09	...
56	8374080-5380	3260	0.35	0.25 ± 0.05	...
57	8374271-5697	3770	1.84	0.48 ± 0.06	...
58	8374301-5908	3770	0.50	0.49 ± 0.08	2.46 ± 1.31
59	8374388-6000	3770	0.66	0.49 ± 0.07	3.12 ± 0.41
60	8374599-5741	3770	0.84	0.48 ± 0.07	...
61	8374677-5748	3770	1.77	0.48 ± 0.06	...
62	8374677-5766	3770	2.81	0.48 ± 0.07	...
63	8374839-5427	3700	0.63	0.45 ± 0.07	...
64	8375041-5383	5030	8.62	2.51 ± 0.14	...
65	8375063-5840	3770	1.00	0.48 ± 0.07	...
66	8375158-5162	2880	0.10	0.10 ± 0.04	< 0.19
67	8375190-5420	3955	0.55	0.64 ± 0.09	...
68	8375484-5401	3770	0.87	0.48 ± 0.07	...
70	8375702-5443	3770	0.13	0.50 ± 0.09	...
71	8375886-5399	3770	1.84	0.48 ± 0.07	...
73	8376154-5675	3770	2.92	0.48 ± 0.07	...
74	8376176-5368	6050	10.67	1.87 ± 0.03	...
75	8376287-5377	2800	0.58	0.14 ± 0.03	...
76	8376356-4822	3770	4.32	0.50 ± 0.07	...
77	8376541-5379	2840	0.32	0.13 ± 0.06	...
78	8376571-5415	3020	0.21	0.17 ± 0.05	...
79	8376643-5900	3770	0.54	0.49 ± 0.08	...
80	8376687-5443	3630	0.73	0.40 ± 0.07	...
81	8376747-5441	3490	0.97	0.34 ± 0.04	...
82	8376817-5387	3360	1.26	0.28 ± 0.04	...
83	8376871-5399	5165	3.94	1.88 ± 0.05	...
84	8376918-4974	3770	0.49	0.49 ± 0.08	...
85	8376976-5443	3955	1.02	0.62 ± 0.08	...
86	8377111-5612	3020	0.26	0.18 ± 0.05	1.77 ± 1.32
88	8377167-5247	5500	54.56	3.75 ± 0.07	...
89	8377232-5402	3970	3.02	0.63 ± 0.09	...
90	8377335-5489	3700	0.97	0.44 ± 0.07	...
91	8377345-5422	5030	32.44	3.70 ± 0.22	...
92	8377361-5395	3770	0.38	0.50 ± 0.08	...
93	8377383-5405	3995	1.91	0.64 ± 0.09	...

Table 6—Continued

Num.	IRS name	T_{eff} (K)	L_\star (L_\odot)	M_\star (M_\odot)	\dot{M} (10^{-9}) (M_\odot/yr)
94	8377392-5193	3425	1.18	0.31 ± 0.04	...
95	8377737-5547	3770	0.24	0.50 ± 0.09	...
96	8377749-5447	3020	0.32	0.18 ± 0.04	...
97	8378059-5644	3770	0.98	0.48 ± 0.07	33.15 ± 6.97
98	8378345-5545	3970	0.67	0.65 ± 0.08	0.35 ± 0.04
99	8378366-5814	3770	0.77	0.49 ± 0.07	...
100	8378481-5465	3770	3.27	0.49 ± 0.07	...
101	8378503-5474	4760	1.17	1.33 ± 0.06	...
102	8378561-5421	3490	0.46	0.35 ± 0.06	...
103	8378630-4781	3770	1.55	0.48 ± 0.07	...
106	8379192-6093	3770	2.29	0.48 ± 0.06	...
108	8379312-5776	5030	19.62	3.24 ± 0.23	26.66 ± 15.33
112	8380422-5659	4550	7.87	1.63 ± 0.24	60.55 ± 18.05
114	8380518-5465	3490	4.41	0.35 ± 0.04	...
117	8380667-5516	5290	5.97	2.07 ± 0.05	41.90 ± 1.45
119	8380695-5479	3360	0.80	0.29 ± 0.04	...
120	8380923-5478	3770	1.46	0.48 ± 0.06	...
121	8380932-5721	3770	3.01	0.49 ± 0.07	...
122	8381019-5555	4140	4.48	0.82 ± 0.11	...
123	8381020-5546	3160	0.16	0.21 ± 0.06	< 0.39
125	8381120-5653	4840	4.04	1.92 ± 0.15	6.22 ± 3.38
127	8381491-5164	3770	0.75	0.49 ± 0.07	...
128	8381501-4991	3770	1.68	0.48 ± 0.06	...
129	8381622-5481	3425	0.89	0.32 ± 0.05	...
131	8381971-4762	4920	1.67	1.47 ± 0.05	...
132	8382048-5452	3770	17.71	0.64 ± 0.14	...
133	8382359-5974	3770	2.64	0.48 ± 0.07	...
134	8382412-6410	3700	1.18	0.44 ± 0.06	2.66 ± 0.11
135	8382467-5709	4550	5.08	1.49 ± 0.20	...
136	8382490-5270	3970	10.44	0.75 ± 0.12	...
137	8382623-5479	3425	0.56	0.32 ± 0.05	...
138	8382655-4889	3770	1.85	0.48 ± 0.06	...
139	8382835-5291	7440	194.88	4.45 ± 0.19	...
140	8383581-5050	3770	9.24	0.56 ± 0.09	...
141	8383861-5154	6100	34.74	2.77 ± 0.05	< 5.55
142	8384113-5117	3770	2.41	0.48 ± 0.06	...
143	8384325-5457	2880	0.57	0.16 ± 0.03	...
144	8384331-5134	3970	5.94	0.68 ± 0.10	310.33 ± 129.45
145	8384717-5469	3260	0.60	0.26 ± 0.04	...
146	8384864-5440	3360	0.38	0.29 ± 0.06	...
147	8385190-5442	3020	1.02	0.19 ± 0.02	...
148	8385255-5191	3955	1.64	0.61 ± 0.08	...
149	8385365-5106	3770	7.28	0.54 ± 0.08	...
150	8385988-5427	5500	12.73	2.41 ± 0.03	...
151	8386322-6328	3490	1.21	0.34 ± 0.04	...

Table 6—Continued

Num.	IRS name	T_{eff} (K)	L_\star (L_\odot)	M_\star (M_\odot)	\dot{M} (10^{-9}) (M_\odot/yr)
152	8386383-5393	4330	3.88	1.06 ± 0.14	...
153	8386462-5457	3490	0.59	0.35 ± 0.05	...
154	8386523-5715	3260	0.74	0.25 ± 0.04	4.28 ± 2.77
155	8386627-5467	2880	0.49	0.15 ± 0.03	...
156	8386694-5026	3770	19.46	0.66 ± 0.14	...
158	8386759-5416	3970	1.73	0.62 ± 0.09	...
159	8386804-5987	3260	0.33	0.26 ± 0.05	1.48 ± 0.55
160	8386841-5129	3770	4.58	0.50 ± 0.07	...
161	8386935-4790	3020	0.28	0.18 ± 0.05	1.93 ± 1.22
162	8386957-4804	3770	3.09	0.49 ± 0.07	...
163	8387691-5326	3770	3.00	0.48 ± 0.07	...
164	8387753-4993	3770	4.93	0.51 ± 0.08	...
165	8387832-5864	3770	0.77	0.49 ± 0.07	...
166	8387937-6755	3360	0.69	0.29 ± 0.04	...
167	8388119-5083	3490	0.47	0.35 ± 0.06	...
168	8388316-5157	3630	6.02	0.43 ± 0.07	435.57 ± 31.03
169	8389033-4773	3700	0.74	0.45 ± 0.07	2.95 ± 1.69
170	8389275-5105	9700	29.78	2.31 ± 0.09	...
172	8389673-4794	3360	0.48	0.29 ± 0.05	< 1.08
173	8390003-5207	5030	3.95	1.94 ± 0.09	81.33 ± 11.09
174	8390073-5082	3770	2.07	0.47 ± 0.07	...
175	8390083-5339	3770	0.84	0.48 ± 0.07	...
176	8390285-5070	3560	0.63	0.37 ± 0.06	3.09 ± 0.55
177	8390554-6390	3425	0.30	0.32 ± 0.06	< 1.50
178	8391040-5081	3770	1.38	0.48 ± 0.06	...
179	8391058-4994	3770	1.13	0.48 ± 0.07	30.18 ± 1.89
180	8391196-5211	4140	5.97	0.85 ± 0.13	...
181	8391648-5110	3770	1.38	0.48 ± 0.07	...
182	8392509-5169	3995	5.07	0.68 ± 0.10	49.02 ± 30.68
183	8393152-5094	3770	0.87	0.48 ± 0.07	10.36 ± 2.85
184	8394216-5181	3955	0.99	0.62 ± 0.08	6.19 ± 0.82
185	8394454-5823	4020	1.00	0.68 ± 0.08	5.83 ± 3.94
186	8395167-5024	3700	0.86	0.44 ± 0.06	91.53 ± 23.57
187	8395780-5308	3560	0.65	0.37 ± 0.06	10.39 ± 4.58
188	8396035-5861	3770	1.17	0.48 ± 0.07	...
189	8396285-5119	3770	2.04	0.48 ± 0.07	...
190	8396319-4941	3425	0.48	0.32 ± 0.06	5.45 ± 0.44
191	8396679-6167	4330	13.60	1.35 ± 0.22	383.77 ± 79.73
192	8397522-4788	3490	0.37	0.35 ± 0.06	...
193	8397632-5445	3700	0.62	0.45 ± 0.07	...
194	8397818-4972	3770	0.08	0.49 ± 0.08	...
195	8398707-5755	3490	0.86	0.34 ± 0.05	...
196	8398936-6711	4330	1.91	1.01 ± 0.10	6.70 ± 3.94
197	8399022-5955	3770	0.51	0.50 ± 0.08	33.37 ± 2.90
198	8399269-6612	3955	1.06	0.62 ± 0.08	4.88 ± 1.50

Table 6—Continued

Num.	IRS name	T_{eff} (K)	L_\star (L_\odot)	M_\star (M_\odot)	\dot{M} (10^{-9}) (M_\odot/yr)
199	8399902-6268	4235	3.36	0.91 ± 0.12	...
200	8400080-6709	4080	1.95	0.72 ± 0.09	30.57 ± 5.17
201	8402765-6538	4760	2.78	1.70 ± 0.13	...
202	8403455-6810	3425	0.85	0.31 ± 0.04	...
203	8406280-6293	4440	1.49	1.20 ± 0.12	...
204	8406609-6247	3425	0.21	0.31 ± 0.07	1.66 ± 0.92
205	8407074-5195	4330	4.86	1.09 ± 0.15	...
206	8408920-6760	4140	9.09	0.92 ± 0.15	< 35.03
207	8409911-6386	3770	2.15	0.48 ± 0.07	...
208	8410334-6291	4330	8.82	1.20 ± 0.18	14.05 ± 3.12
209	8410779-6416	3770	9.84	0.57 ± 0.08	...
210	8410886-6134	3770	1.50	0.48 ± 0.06	< 1.71
211	8411618-6426	3020	0.20	0.17 ± 0.05	0.80 ± 0.76
212	8412592-6712	3560	1.41	0.37 ± 0.05	...
213	8413152-6141	4140	3.91	0.81 ± 0.11	10.32 ± 5.65
214	8413399-5287	3700	0.43	0.46 ± 0.08	2.41 ± 0.14
215	8413704-6739	3490	0.55	0.34 ± 0.06	...
216	8414490-7187	3770
217	8415394-6556	3955	2.05	0.61 ± 0.08	446.37 ± 139.47
218	8416389-6503	3020	0.13	0.14 ± 0.07	< 0.94
219	8416834-6225	3700	0.45	0.45 ± 0.08	< 0.24
220	8416914-6175	3955	2.15	0.64 ± 0.10	8.53 ± 8.38
221	8416978-6185	4760	1.60	1.47 ± 0.07	...
222	8421949-6718	3700	1.41	0.44 ± 0.06	...
223	8424570-6484	3260	0.30	0.28 ± 0.09	0.59 ± 0.04
224	8424689-6154	8840	47.31	2.41 ± 0.09	...
225	8425038-6557	5740	10.44	2.04 ± 0.03	12.88 ± 6.10
226	8430527-6583	7800	27.41	2.15 ± 0.07	71.49 ± 36.51
227	8440418-7404	3940	0.29	0.66 ± 0.09	0.18 ± 0.09
228	8443530-6843	3630	0.45	0.41 ± 0.07	...
229	8444779-6608	3700	0.54	0.45 ± 0.07	2.18 ± 1.60
230	8445558-6860	3260	0.31	0.26 ± 0.05	0.49 ± 0.18
231	8447398-6788	3360	2.31	0.29 ± 0.03	...
232	8448350-6815	3770	1.04	0.48 ± 0.07	...
233	8450343-7265	3360	0.64	0.29 ± 0.04	8.26 ± 1.50
234	8452061-7269	3630	0.49	0.41 ± 0.07	2.66 ± 1.69
235	8453876-6821	8410	34.38	2.26 ± 0.10	12.50 ± 4.34
236	8455602-7112	4235	2.00	0.90 ± 0.11	...
237	8457266-7161	3360	1.07	0.29 ± 0.04	< 3.35
238	8461533-6914	3955	1.18	0.62 ± 0.08	...
239	8464666-7838	4330	1.86	1.03 ± 0.12	3.00 ± 1.26
240	8465247-7776	3425	0.68	0.32 ± 0.05	...
241	8466711-6987	3700	0.68	0.48 ± 0.03	...
242	8468002-6969	3955	14.57	0.87 ± 0.07	...
243	8468729-6970	3955	1.89	0.66 ± 0.03	...

Table 6—Continued

Num.	IRS name	T_{eff} (K)	L_\star (L_\odot)	M_\star (M_\odot)	\dot{M} (10^{-9}) (M_\odot/yr)
244	8469891-7104	3630	1.41	0.43 ± 0.02	...
245	8472719-7464	3955	2.44	0.66 ± 0.04	204.50 ± 26.83
246	8476732-7058	3955	1.53	0.66 ± 0.03	65.34 ± 36.21
247	8477229-7184	3770	1.38	0.52 ± 0.03	101.10 ± 7.39
248	8486920-7342	3770	0.66	0.53 ± 0.04	...
249	8488472-7373	3425	0.14	0.35 ± 0.04	0.12 ± 0.07
250	8492690-7387	3770	1.81	0.52 ± 0.03	...
251	8494096-7377	3770	4.17	0.54 ± 0.04	...
252	8495155-7404	3770	1.99	0.52 ± 0.03	...
253	8497290-7502	3770	1.75	0.52 ± 0.03	...
254	8497797-7462	3770	53.61	0.93 ± 0.20	...
255	8499151-7482	3770	21.85	0.75 ± 0.06	...
256	8499541-7426	3770	2.00	0.52 ± 0.03	...
257	8502614-7795	3360	0.21	0.33 ± 0.03	1.68 ± 1.02
258	8504327-7460	3970	4.60	0.71 ± 0.04	...
259	8508083-8237	3970	1.50	0.67 ± 0.03	...
260	8508501-7431	3560	0.33	0.42 ± 0.04	2.13 ± 1.09
261	8508648-7916	3770	1.71	0.54 ± 0.04	...
262	8510403-8125	5620	5.50	1.71 ± 0.02	73.39 ± 11.43
263	8511308-8126	2880	0.22	0.13 ± 0.06	...
264	8511602-7926	3770	1.05	0.48 ± 0.07	...
265	8514861-7663	3770	1.11	0.48 ± 0.07	...
266	8515568-8067	6420	59.31	3.20 ± 0.08	...
267	8516031-7796	3770	4.13	0.49 ± 0.06	...
268	8518798-7373	3770	1.26	0.48 ± 0.07	...
269	8519260-8090	4550	8.18	1.63 ± 0.23	13.77 ± 15.24
270	8519428-8120	3970	7.19	0.69 ± 0.10	< 6.51
271	8520557-7775	3770	0.52	0.49 ± 0.08	< 0.28
272	8520580-7960	3770	0.12	0.50 ± 0.09	...
273	8530851-8132	3490	0.95	0.34 ± 0.05	< 3.04
274	8534457-7821	3770	1.22	0.48 ± 0.07	...
275	8535781-7830	3970	1.03	0.63 ± 0.08	< 1.10
276	8536129-8706	3770	3.37	0.49 ± 0.07	...
277	8537742-8080	3970	1.95	0.62 ± 0.08	...
278	8538844-7917	3970	0.55	0.62 ± 0.08	...
279	8538911-7999	3560	1.05	0.37 ± 0.05	< 0.82
280	8542681-8618	4920	11.71	2.66 ± 0.26	6.34 ± 3.62
281	8543224-7972	2610	0.40	0.10 ± 0.03	6.02 ± 7.94
282	8545724-8008	4140	5.83	0.85 ± 0.13	...
283	8547523-7831	3020	0.44	0.19 ± 0.04	1.63 ± 1.06
284	8547770-7986	4440	1.90	1.20 ± 0.14	...
285	8552157-8190	3770	3.60	0.49 ± 0.07	...
286	8552280-8641	3630	1.19	0.42 ± 0.03	< 1.83
287	8556074-7982	3360	0.41	0.29 ± 0.05	1.80 ± 1.35
288	8560743-8147	3425	0.61	0.32 ± 0.05	15.68 ± 2.33

Table 6—Continued

Num.	IRS name	T_{eff} (K)	L_\star (L_\odot)	M_\star (M_\odot)	\dot{M} (10^{-9}) (M_\odot/yr)
289	8561044-7980	3970	1.76	0.62 ± 0.09	...
290	8562845-8151	3360	0.35	0.29 ± 0.06	4.77 ± 2.64
291	8564835-8250	3490	0.35	0.35 ± 0.06	0.89 ± 0.64
292	8567003-8669	3425	0.25	0.32 ± 0.06	...
293	8567545-8254	3360	0.32	0.29 ± 0.06	...
294	8567670-8803	3490	2.17	0.34 ± 0.05	< 5.16
295	8569204-8666	4330	4.04	1.06 ± 0.14	...
296	8570200-8276	3770	1.65	0.48 ± 0.07	...
297	8570949-8577	3770	1.72	0.48 ± 0.07	...
298	8571439-8650	3770	3.54	0.48 ± 0.06	...
299	8574645-8156	3700	0.38	0.45 ± 0.08	...
300	8576640-8652	3560	0.95	0.37 ± 0.05	...
301	8576836-8303	3425	0.35	0.32 ± 0.06	0.63 ± 0.19
302	8579480-8565	3770	0.07	0.50 ± 0.09	0.73 ± 0.41
303	8580634-8516	3360	0.47	0.29 ± 0.05	9.66 ± 4.35
304	HOPS-22	3770	2.09	0.48 ± 0.07	...
305	HOPS-26	3490	0.39	0.34 ± 0.06	...
306	HOPS-51	3770	0.33	0.50 ± 0.09	...
307	HOPS-54	3260	0.21	0.25 ± 0.06	...
308	HOPS-98	3770	6.51	0.53 ± 0.08	...
309	HOPS-113	3770	3.14	0.48 ± 0.07	...
310	HOPS-151	3770	0.04	0.46 ± 0.06	...
311	HOPS-162	3490	0.02	0.29 ± 0.07	...
312	HOPS-180	3770	0.01	0.41 ± 0.05	...
313	HOPS-184	3770	1.19	0.48 ± 0.07	...
314	HOPS-201	3360	0.15	0.28 ± 0.07	...
315	HOPS-222	3770	3.37	0.49 ± 0.07	...
316	HOPS-272	3770	9.19	0.56 ± 0.10	...
317	HOPS-277	3770	0.36	0.49 ± 0.08	...
318	HOPS-283	3630	1.13	0.40 ± 0.06	...
319	HOPS-293	3770	0.11	0.50 ± 0.09	...
companions observed by SpeX					
4	8343917-6073			80.37 ± 18.77	
26	8359203-5026			1.16 ± 0.70	
38	8367284-5798			< 0.46	
47	8371984-5465			9.30 ± 3.28	
98	8378345-5545			< 5.2	
173	8390003-5207			...	
208	8410334-6291			...	
280	8542681-8618			...	
290	8562845-8151			2.24 ± 0.51	

Table 7. Spectral Indices

Num.	module	n_{K-6}	$\sigma_{n_{K-6}}$	n_{6-13}	$\sigma_{n_{6-13}}$	n_{13-31}	$\sigma_{n_{13-31}}$	n_{5-12}	$\sigma_{n_{5-12}}$	n_{12-20}	$\sigma_{n_{12-20}}$	n_{K-25}	$\sigma_{n_{K-25}}$
1	SLLL	-2.07	0.10	-0.89	0.13	0.29	0.23	-1.03	0.10	0.95	0.15	-1.01	0.04
2	SLLL	-1.70	0.08	-0.53	0.11	0.06	0.16	-0.65	0.13	-0.18	0.18	-0.89	0.03
3	SLLL	-1.51	0.03	-0.27	0.03	-1.11	0.06	-0.32	0.04	-0.76	0.04	-1.01	0.01
4	SLLL	-1.62	0.11	-0.13	0.13	-0.66	0.06	-0.49	0.07	-0.17	0.24	-0.87	0.02
5	SLLL	-1.77	0.16	0.71	0.20	-0.80	0.11	0.35	0.10	-0.23	0.09	-0.66	0.04
6	SLLL	0.00	0.05	-0.68	0.07	-0.70	0.11	-0.83	0.06	-0.80	0.07	-0.47	0.02
7	SLLL
8	SLLL	-2.39	0.07	-1.15	0.11	0.30	0.16	-1.40	0.08	1.71	0.37	-1.25	0.04
9	SLLL	-1.10	0.03	-0.17	0.03	-0.36	0.06	-0.30	0.03	0.07	0.03	-0.61	0.01
10	SLLL	-0.65	0.15	-0.31	0.18	-0.09	0.09	-0.62	0.45	-0.02	0.36	-0.48	0.02
11	SLLL	-2.46	0.08	-0.62	0.11	1.47	0.09	-0.88	0.15	2.07	0.17	-0.78	0.02
12	SLLL	-0.67	0.10	-0.43	0.12	-0.62	0.11	-0.54	0.10	-0.60	0.16	-0.62	0.01
13	SLLL	-2.78	0.07	-1.96	0.41	2.58	0.43	-1.95	0.45	2.82	0.91	-1.01	0.03
14	SLLL	-1.33	0.04	-1.02	0.07	-0.88	0.11	-1.03	0.07	-1.56	0.17	-1.21	0.02
15	SLLL	-1.03	0.05	-0.43	0.06	-0.93	0.19	-0.53	0.05	-0.43	0.12	-0.75	0.02
16	SLLL	-2.62	0.09	-2.19	0.27	1.96	0.26	-2.18	0.23	1.12	0.47	-1.34	0.01
17	SLLL	-0.82	0.08	-0.18	0.11	-0.50	0.17	-0.27	0.09	-0.20	0.11	-0.53	0.02
18	SLLL	-2.39	0.18	0.45	0.22	-0.29	0.26	0.47	0.49	-0.07	0.19	-0.88	0.04
19	SLLL	-2.81	0.14	-0.52	0.19	1.19	0.37	-0.92	0.11	2.28	0.27	-0.88	0.04
20	SLLL	-0.68	0.08	-0.80	0.11	-0.65	0.15	-0.95	0.15	-1.08	0.17	-0.85	0.04
21	SLLL	-1.40	0.05	0.60	0.05	-0.73	0.04	0.57	0.04	-0.39	0.08	-0.56	0.02
22	SLLL	-0.57	0.05	-0.32	0.05	-0.52	0.09	-0.41	0.07	-0.61	0.06	-0.54	0.02
23	SLLL	-1.70	0.15	-0.30	0.18	-0.52	0.11	-0.44	0.42	0.21	0.09	-0.91	0.02
24	SLLL	-1.59	0.07	-0.14	0.07	-0.44	0.10	-0.33	0.04	-0.05	0.07	-0.80	0.01
25	SLLL	-1.92	0.32	0.39	0.70	0.25	0.23	0.33	1.41	0.56	-0.45	0.06	0.02
26	SLLL	-2.20	0.17	0.21	0.19	0.45	0.13	-0.26	0.04	0.27	0.24	-0.69	0.05
27	SLLL	-1.75	0.15	0.03	0.18	-0.30	0.15	-0.20	0.19	-0.23	0.19	-0.74	0.02
28	SLLL	-0.98	0.05	-0.60	0.06	-0.33	0.06	-0.75	0.07	-0.37	0.09	-0.72	0.01
29	SLLL	-2.62	0.11	-0.27	0.18	2.04	0.18	-0.28	0.16	2.53	0.24	-0.62	0.02
30	SLLL	-1.25	0.06	-0.64	0.08	-0.58	0.10	-0.73	0.11	-0.54	0.11	-0.94	0.02
31	SLLL	-0.40	0.11	-0.44	0.12	0.87	0.05	-0.36	0.11	1.14	0.06	-0.11	0.01
32	SLLL	-1.10	0.09	-0.40	0.13	0.80	0.16	-0.50	0.11	0.17	0.32	-0.52	0.02
33	SLLL	-1.44	0.07	-0.64	0.09	0.17	0.07	-0.74	0.10	0.19	0.14	-0.76	0.02
34	SLLL	-2.57	0.16	-0.96	0.27	1.08	0.31	-1.22	0.24	1.95	1.27	-1.05	0.05
35	SLLL	-2.96	0.11	-2.54	0.38	0.83	0.38	-2.56	0.16	-0.20	0.91	-1.94	0.04

Table 7—Continued

Num.	module	n_{K-6}	$\sigma_{n_{K-6}}$	n_{6-13}	$\sigma_{n_{6-13}}$	n_{13-31}	$\sigma_{n_{13-31}}$	n_{5-12}	$\sigma_{n_{5-12}}$	n_{12-20}	$\sigma_{n_{12-20}}$	n_{K-25}	$\sigma_{n_{K-25}}$
36	SLLL	-2.04	0.13	-1.62	0.18	-0.29	0.16	-1.76	0.08	0.03	0.13	-1.48	0.02
37	SLLL	-1.04	0.06	-0.96	0.09	-1.00	0.14	-0.98	0.09	-0.65	0.15	-1.02	0.02
38	SLLL	-2.45	0.07	-1.08	0.11	0.79	0.18	-1.23	0.13	1.22	0.15	-1.15	0.02
39	SLLL	-2.48	0.26	-0.67	0.51	0.50	0.70	-0.67	0.47	1.41	1.24	-1.04	0.11
40	SLLL	-1.32	0.13	-0.74	0.16	-0.35	0.11	-0.91	0.09	-0.60	0.21	-0.95	0.02
41	SLLL	-0.32	0.08	-0.58	0.10	0.29	0.14	-0.81	0.14	0.68	0.17	-0.30	0.02
42	SLLL	-2.13	0.10	0.39	0.12	-0.63	0.20	0.27	0.14	0.01	0.31	-0.86	0.04
43	SLLL	-1.20	0.05	-0.49	0.06	-0.75	0.06	-0.64	0.06	-0.79	0.05	-0.89	0.01
44	SLLL	-1.85	0.10	-0.44	0.14	0.43	0.11	-0.75	0.06	0.98	0.21	-0.77	0.02
45	SLLL	-0.92	0.06	-1.35	0.09	-2.23	0.08	-1.41	0.04	-2.11	0.09	-1.41	0.01
46	SLLL	-1.94	0.08	-0.58	0.14	-0.71	0.68	-0.66	0.12	-0.48	0.19	-1.00	0.05
47	SLLL	-2.23	0.09	-1.48	0.25	1.70	0.24	-1.48	0.21	0.64	0.55	-1.14	0.07
48	SLLL	-1.47	0.08	-0.84	0.11	-0.94	0.35	-0.96	0.10	-1.26	0.13	-1.15	0.05
49	SL	-1.67	0.33	-1.52	2.09
50	SLLL	-1.45	0.13	-0.82	0.25	-0.73	0.43	-1.02	0.28	-0.07	0.23	-0.98	0.03
51	SLLL	-1.77	0.11	-0.75	0.14	-0.75	0.12	-0.97	0.09	-0.79	0.19	-1.21	0.01
52	SLLL	-0.94	0.07	-0.52	0.09	-0.64	0.08	-0.57	0.10	-0.91	0.18	-0.82	0.03
53	SLLL	-2.57	0.11	0.07	0.14	0.05	0.13	-0.23	0.14	0.63	0.18	-1.01	0.01
54	SLLL	-1.31	0.09	-0.47	0.12	-1.43	0.35	-0.49	0.24	-0.87	0.26	-1.08	0.02
55	SL	-1.89	0.07	-0.94	0.29	-1.03	0.18
56	SL	-1.29	0.20	0.04	0.38	-0.10	0.87
57	SLLL	-1.84	0.07	-0.43	0.09	-0.20	0.12	-0.49	0.09	-0.15	0.11	-0.97	0.02
58	SLLL	-1.60	0.10	-0.86	0.14	-0.83	0.20	-0.88	0.12	-0.80	0.32	-1.20	0.04
59	SLLL	-2.27	0.09	-0.18	0.13	0.54	0.10	-0.41	0.13	0.75	0.21	-0.81	0.02
60	SLLL	-1.10	0.07	-1.36	0.12	-0.35	0.21	-1.36	0.16	-0.89	0.20	-1.09	0.03
61	SLLL	-1.35	0.07	-0.73	0.09	-0.77	0.12	-0.89	0.05	-1.00	0.04	-1.06	0.03
62	SLLL	-1.41	0.05	-0.97	0.07	-1.20	0.14	-1.04	0.06	-1.05	0.10	-1.23	0.02
63	SL	-1.32	0.07	-1.21	0.33	-0.85	0.33
64	SL	-1.49	0.06	-0.45	0.10	-0.57	0.08
65	SLLL	-1.97	0.08	-0.52	0.10	-0.36	0.23	-0.60	0.11	-0.52	0.31	-1.11	0.06
66	SLLL	-1.96	0.18	0.61	0.25	0.72	0.20	0.63	0.37	1.00	0.40	-0.40	0.03
67	SL	-1.16	0.10	-1.11	0.34	-0.85	0.41
68	SL	-1.40	0.09	-0.38	0.23	-0.30	0.18
70	SL	-0.56	0.09	-0.71	0.15	-1.34	0.20
71	SL	-1.05	0.10	-0.25	0.21	-0.13	0.20

Table 7—Continued

Num.	module	n_{K-6}	$\sigma_{n_{K-6}}$	n_{6-13}	$\sigma_{n_{6-13}}$	n_{13-31}	$\sigma_{n_{13-31}}$	n_{5-12}	$\sigma_{n_{5-12}}$	n_{12-20}	$\sigma_{n_{12-20}}$	n_{K-25}	$\sigma_{n_{K-25}}$
73	SLLL	-1.76	0.09	-1.11	0.15	-0.78	0.36	-1.18	0.10	-1.32	0.47	-1.38	0.02
74	SL	-1.60	0.13	-0.37	0.26	-0.58	0.21
75	SL	-1.73	0.21	-1.07	0.90	-1.26	0.44
76	SLLL	-1.67	0.06	-1.29	0.09	-0.66	0.11	-1.34	0.08	-0.16	0.14	-1.28	0.02
77	SL	-1.41	0.26	-2.26	3.90	-0.54	0.89
78	SL	-0.99	0.18	-3.85	5.00	-5.09	1.46
79	SLLL	-0.80	0.06	-0.74	0.08	-0.59	0.10	-0.77	0.07	-0.72	0.08	-0.80	0.01
80	SL	-1.86	0.14	-0.23	0.42	0.20	0.39
81	SL	-1.81	0.15	-0.14	0.33	0.29	0.40
82	SL	-1.17	0.08	-0.61	0.23	-0.73	0.21
83	SL	-2.02	0.06	-1.12	0.29	-1.53	0.29
84	SLLL	-1.39	0.07	-0.95	0.10	-0.29	0.21	-1.11	0.09	-0.31	0.08	-1.00	0.04
85	SL	-1.52	0.08	-1.29	0.21	-2.28	0.27
86	SLLL	-1.40	0.06	-0.26	0.09	-0.27	0.18	-0.16	0.13	-0.50	0.13	-0.74	0.03
88	SLLL	0.72	0.49	-1.94	0.75	-0.37	0.02	...
89	SL	-1.80	0.08	-0.72	0.28	-0.36	0.28
90	SLLL	-0.67	0.05	-0.22	0.06	-0.68	0.14	-0.28	0.06	-0.66	0.09	-0.59	0.01
91	SL	-1.33	0.03	-0.28	0.08	-0.30	0.11
92	SL	-0.75	0.13	0.01	0.45	0.12	0.38
93	SL	-0.98	0.03	-1.02	0.08	-1.38	0.13
94	SLLL	-1.73	0.20	-1.00	0.29	0.03	0.26	-1.30	0.29	-0.39	0.36	-1.05	0.03
95	SLLL	-0.14	0.04	0.01	0.05	0.11	0.07	0.09	0.07	0.11	0.11	-0.09	0.01
96	SL	-1.23	0.10	0.05	0.24	0.17	0.27
97	SLLL	-1.97	0.10	-0.40	0.14	0.27	0.13	-0.45	0.23	-0.39	0.20	-0.94	0.02
98	SLLL	-1.70	0.07	-0.36	0.09	-1.23	0.38	-0.37	0.10	-0.90	0.19	-1.20	0.06
99	SLLL	-1.38	0.05	-1.05	0.09	-0.82	0.26	-1.08	0.11	-1.16	0.19	-1.20	0.03
100	SL	-1.56	0.05	-0.86	0.08	-0.95	0.07
101	SL	-1.63	0.10	-1.05	0.32	-0.65	0.33
102	SL	-1.78	0.19	0.41	0.35	-0.17	0.59
103	SLLL	-1.17	0.08	-0.89	0.10	-1.24	0.11	-1.02	0.07	-0.99	0.05	-1.10	0.01
106	SLLL	-1.80	0.10	-0.97	0.16	-1.12	0.16	-1.18	0.12	-1.28	0.15	-1.36	0.02
108	SLLL	-1.69	0.06	-0.32	0.06	0.18	0.02	-0.50	0.04	0.64	0.06	-0.76	0.01
112	SLLL	-1.08	0.08	-1.42	0.08	-1.36	0.08	-1.50	0.06	-1.43	0.08	-1.33	0.02
114	SL	-1.46	0.05	-0.64	0.09	-0.63	0.09
117	SLLL	-1.13	0.04	-0.35	0.04	-1.12	0.13	-0.44	0.06	-1.08	0.07	-0.91	0.02

Table 7—Continued

Num.	module	n_{K-6}	$\sigma_{n_{K-6}}$	n_{6-13}	$\sigma_{n_{6-13}}$	n_{13-31}	$\sigma_{n_{13-31}}$	n_{5-12}	$\sigma_{n_{5-12}}$	n_{12-20}	$\sigma_{n_{12-20}}$	n_{K-25}	$\sigma_{n_{K-25}}$
119	SL	-1.71	0.10	-1.29	0.18	-1.32	0.24
120	SL	-1.99	0.09	-0.76	0.16	-0.77	0.15
121	SLLL	-1.61	0.06	-1.20	0.08	-1.06	0.12	-1.26	0.05	-1.24	0.13	-1.39	0.01
122	SLLL	-1.00	0.04	-0.90	0.05	-0.71	0.07	-1.02	0.06	-0.80	0.06	-0.98	0.01
123	SLLL	-0.94	0.05	-0.08	0.08	0.43	0.13	-0.15	0.11	0.79	0.31	-0.30	0.01
125	SLLL	-1.54	0.06	-0.71	0.07	-0.89	0.07	-0.85	0.03	-0.18	0.07	-1.06	0.02
127	SLLL	-1.22	0.35	-1.21	0.52	0.46	0.35	-1.36	0.42	-1.37	0.54	-0.93	0.03
128	SLLL	-1.34	0.11	-0.71	0.21	-0.17	0.20	-0.50	0.18	-1.69	0.32	-1.00	0.02
129	SL	-1.18	0.15	-1.20	0.17
131	SLLL	-1.01	0.07	-1.07	0.09	-0.96	0.07	-1.21	0.06	-1.05	0.10	-1.09	0.01
132	SL	-1.45	0.05	-0.98	0.10	-0.94	0.11
133	SLLL	-1.66	0.08	-0.61	0.09	-0.58	0.08	-0.75	0.05	-0.45	0.09	-1.07	0.01
134	SLLL	-1.01	0.07	-0.59	0.10	-1.41	0.10	-0.55	0.10	-1.11	0.28	-1.03	0.02
135	SLLL	-1.43	0.05	-1.18	0.06	-1.05	0.10	-1.26	0.08	-0.25	0.12	-1.22	0.02
136	SLLL
137	SL	-2.09	0.16	-1.11	0.49	-1.00	0.35
138	SLLL	-1.35	0.06	-0.61	0.07	-0.62	0.10	-0.77	0.08	-0.55	0.08	-0.99	0.02
139	SL	-1.10	0.03	-1.99	0.21	-1.79	0.16
140	SLLL	-1.25	0.07	-0.07	0.07	-1.17	0.11	-0.25	0.11	-0.11	0.06	-0.77	0.02
141	SLLL	-1.74	0.09	-1.97	0.13	-1.39	0.12	-2.01	0.08	-1.22	0.14	-1.77	0.01
142	SLLL	-1.46	0.12	-0.58	0.14	-0.84	0.23	-0.70	0.08	-0.10	0.05	-0.92	0.02
143	SL	-1.43	0.08	-0.53	0.25	-0.53	0.38
144	SLLL	-0.92	0.06	-0.17	0.06	-0.13	0.03	-0.32	0.02	-0.08	0.05	-0.53	0.02
145	SL	-1.23	0.11	-0.21	0.23	-0.14	0.48
146	SL	-0.75	0.48	-0.25	0.57
147	SL	-1.63	0.11	-0.42	0.47	0.15	0.39
148	SLLL
149	SLLL	-1.40	0.05	-0.40	0.06	0.88	0.03	-0.57	0.07	0.53	0.09	-0.55	0.01
150	SL	-1.91	0.08	-0.76	0.20	-0.61	0.24
151	SLLL	-1.94	0.16	-1.23	0.19	-1.22	0.20	-1.35	0.12	-0.57	0.14	-1.47	0.02
152	SL	-1.29	0.07	-0.86	0.30	-1.08	0.66
153	SL	-1.64	0.19	-0.50	0.60	0.31	0.55
154	SLLL	-2.20	0.08	-0.16	0.10	-0.19	0.14	-0.35	0.12	0.16	0.16	-0.98	0.02
155	SL	-1.79	0.19	-0.23	0.30	-0.28	0.35
156	SLLL	-1.31	0.08	-0.76	0.13	-1.09	0.20	-1.02	0.10	-0.67	0.18	-1.09	0.02

Table 7—Continued

Num.	module	n_{K-6}	$\sigma_{n_{K-6}}$	n_{6-13}	$\sigma_{n_{6-13}}$	n_{13-31}	$\sigma_{n_{13-31}}$	n_{5-12}	$\sigma_{n_{5-12}}$	n_{12-20}	$\sigma_{n_{12-20}}$	n_{K-25}	$\sigma_{n_{K-25}}$
158	SL	-0.82	0.50	-0.29	0.48
159	SLLL	-1.70	0.07	-0.16	0.10	0.17	-0.13	0.09	0.54	0.20	-0.71	0.02	0.02
160	SLLL	-1.10	0.16	-0.51	0.20	-2.34	0.46	-0.39	0.21	-1.38	0.11	-1.07	0.02
161	SLLL	-1.48	0.09	-0.67	0.16	-0.42	0.30	-0.69	0.16	-0.32	0.24	-1.00	0.03
162	SLLL	0.52	0.05	-0.39	0.07	-1.04	0.08	-0.52	0.09	-0.41	0.10	-0.20	0.01
163	SL	-0.90	0.05	-1.16	0.17	-1.19	0.13
164	SLLL	-1.49	0.06	-0.79	0.10	-0.17	0.10	-0.96	0.05	0.38	0.04	-0.91	0.01
165	SLLL	-1.51	0.12	-0.15	0.13	-0.83	0.16	-0.24	0.10	-0.72	0.18	-0.93	0.01
166	SLLL	-1.38	0.05	-0.90	0.08	-0.25	0.14	-1.07	0.07	-0.59	0.27	-1.01	0.02
167	SLLL	-1.00	0.06	-0.54	0.09	-0.34	0.12	-0.61	0.10	-0.16	0.14	-0.71	0.02
168	SLLL	-1.32	0.05	-0.46	0.07	-0.47	0.05	-0.56	0.08	-0.31	0.09	-0.87	0.01
169	SLLL	-2.44	0.14	-0.32	0.17	0.32	0.18	-0.57	0.14	0.79	0.15	-0.98	0.03
170	SLLL	-2.89	0.10	-1.66	0.21	1.14	0.20	-1.89	0.15	-0.34	0.49	-1.64	0.04
172	SLLL	-1.78	0.17	0.14	0.21	0.50	0.13	0.03	0.20	1.11	0.16	-0.51	0.03
173	SLLL	-0.80	0.06	-0.86	0.10	-2.36	0.36	-0.89	0.06	-1.83	0.14	-1.15	0.02
174	SLLL	-2.30	0.14	-0.85	0.18	0.41	0.11	-0.80	0.14	0.84	0.22	-1.11	0.02
175	SL	-1.54	0.28	-0.86	1.14	-0.70	0.48
176	SLLL	-1.95	0.06	-0.87	0.12	0.32	0.24	-1.13	0.14	0.92	0.37	-1.02	0.02
177	SLLL	-2.61	0.06	-1.02	0.12	2.07	0.13	-1.37	0.08	3.48	0.40	-0.71	0.03
178	SLLL	-1.32	0.07	-0.14	0.09	-1.04	0.15	-0.30	0.11	-0.53	0.28	-0.82	0.02
179	SLLL	-1.94	0.07	-0.87	0.09	-0.69	0.28	-0.94	0.13	-0.31	0.20	-1.26	0.03
180	SLLL	-1.33	0.03	-0.85	0.07	-2.25	0.34	-0.87	0.07	-1.74	0.14	-1.32	0.03
181	SLLL	-1.78	0.05	-0.78	0.09	-0.50	0.30	-0.82	0.14	-0.57	0.29	-1.16	0.04
182	SLLL	-1.96	0.05	-1.16	0.09	-0.80	0.19	-1.22	0.05	-0.92	0.15	-1.44	0.02
183	SLLL	-1.42	0.07	-0.59	0.08	-0.38	0.08	-0.72	0.05	-0.44	0.20	-0.92	0.01
184	SLLL	-2.07	0.09	-1.38	0.26	0.81	0.28	-1.43	0.27	0.90	0.57	-1.13	0.04
185	SLLL	-2.18	0.10	-0.03	0.12	0.06	0.12	-0.23	0.11	1.13	0.14	-0.85	0.02
186	SLLL	-1.37	0.10	-0.52	0.12	0.39	0.08	-0.82	0.12	0.83	0.07	-0.64	0.01
187	SLLL	-1.07	0.04	-0.90	0.09	1.23	0.09	-0.95	0.09	-0.22	0.10	-0.63	0.03
188	SLLL	-2.18	0.10	-1.23	0.13	0.50	0.14	-1.40	0.11	1.73	0.23	-1.10	0.02
189	SLLL	-1.62	0.06	-1.04	0.09	-0.69	0.15	-0.23	0.11	-0.19	0.06	-1.20	0.02
190	SLLL	-1.28	0.08	0.00	0.11	-0.15	0.12	-0.08	0.07	0.23	0.09	-0.61	0.02
191	SLLL	-0.96	0.03	0.37	0.03	0.02	0.02	0.25	0.02	-0.01	0.03	-0.31	0.01
192	SLLL	-1.56	0.05	-0.85	0.11	0.21	0.15	-0.83	0.12	0.14	0.41	-0.92	0.02
193	SLLL	-1.34	0.05	-0.75	0.09	-0.93	0.02	-0.93	0.09	0.18	0.21	-0.85	0.04

Table 7—Continued

Num.	module	n_{K-6}	$\sigma_{n_{K-6}}$	n_{6-13}	$\sigma_{n_{6-13}}$	n_{13-31}	$\sigma_{n_{13-31}}$	n_{5-12}	$\sigma_{n_{5-12}}$	n_{12-20}	$\sigma_{n_{12-20}}$	n_{K-25}	$\sigma_{n_{K-25}}$
194	SLLL	-1.04	0.17	-0.55	0.21	1.20	0.15	-0.65	0.21	1.08	0.58	-0.31	0.02
195	SLLL	-1.58	0.08	-1.05	0.11	-1.07	0.74	-1.14	0.08	-0.46	0.23	-1.24	0.05
196	SLLL	-0.95	0.05	-0.63	0.06	-0.77	0.07	-0.70	0.04	-0.71	0.09	-0.83	0.01
197	SLLL	-1.16	0.09	-0.30	0.11	-0.17	0.16	-0.44	0.07	-0.13	0.05	-0.66	0.02
198	SLLL	-1.82	0.14	-1.06	0.18	-0.42	0.19	-1.11	0.18	0.79	0.10	-1.11	0.03
199	SLLL	-1.54	0.07	-1.32	0.10	-1.25	0.15	-1.32	0.06	-1.51	0.15	-1.45	0.01
200	SLLL	-1.43	0.09	-1.20	0.11	-0.78	0.12	-1.29	0.07	-0.90	0.17	-1.24	0.02
201	SLLL	-1.31	0.07	-1.23	0.08	-1.20	0.09	-1.34	0.06	-1.14	0.07	-1.31	0.01
202	SLLL	-0.25	0.05	-0.14	0.07	-0.76	0.08	-0.22	0.03	-0.91	0.05	-0.41	0.01
203	SLLL	-1.87	0.08	-0.65	0.14	-0.69	0.15	-0.72	0.10	-0.37	0.17	-1.17	0.02
204	SLLL	-2.47	0.12	0.07	0.14	0.22	0.24	-0.16	0.10	0.89	0.09	-0.92	0.02
205	SLLL	-1.88	0.04	-0.32	0.06	-0.78	0.08	-0.40	0.05	-0.20	0.11	-1.07	0.02
206	SLLL	-1.05	0.06	-1.05	0.07	-0.55	0.04	-1.12	0.04	-0.90	0.07	-1.02	0.01
207	SLLL	-0.17	0.05	-0.80	0.05	-0.32	0.09	-0.90	0.04	-0.21	0.07	-0.47	0.02
208	SLLL	-1.61	0.03	-0.49	0.04	-0.51	0.04	-0.57	0.03	-0.71	0.05	-1.00	0.01
209	SLLL	-1.21	0.07	0.21	0.07	-0.39	0.05	0.05	0.03	-0.10	0.06	-0.52	0.01
210	SLLL	-0.87	0.06	-0.64	0.07	-0.72	0.05	-0.74	0.04	-1.05	0.06	-0.82	0.01
211	SLLL	-2.36	0.10	-0.28	0.13	-0.09	0.36	-0.51	0.13	0.66	0.65	-0.98	0.05
212	SLLL	-1.46	0.10	-0.86	0.12	-0.58	0.17	-1.03	0.05	-0.06	0.10	-1.05	0.02
213	SLLL	-1.46	0.06	-0.75	0.06	-0.65	0.03	-0.95	0.05	-0.62	0.03	-1.06	0.01
214	SLLL	-1.27	0.07	-0.73	0.09	-1.21	0.38	-0.88	0.10	-0.78	0.23	-1.04	0.03
215	SLLL	-1.51	0.06	-0.20	0.09	-0.34	0.10	-0.44	0.10	0.06	0.10	-0.76	0.02
216	SLLL	0.05	0.21	0.54	0.20	0.73	0.14	0.50	0.30	0.30	0.07	0.30	0.05
217	SLLL	-1.25	0.05	-1.22	0.06	-1.22	0.13	-1.27	0.05	-1.62	0.06	-1.31	0.03
218	SLLL	-2.53	0.10	0.30	0.13	0.40	0.12	0.00	0.14	0.95	0.23	-0.73	0.04
219	SLLL	-2.59	0.10	-0.95	0.14	0.92	0.16	-1.08	0.10	1.94	0.38	-1.11	0.03
220	SLLL	-1.71	0.08	-0.78	0.11	-0.25	0.09	-0.97	0.08	0.11	0.20	-1.06	0.02
221	SLLL	-0.62	0.07	-1.04	0.12	0.46	0.14	-1.15	0.11	1.20	0.30	-0.47	0.03
222	SLLL	-1.28	0.06	-0.36	0.07	-0.77	0.12	-0.49	0.07	-0.91	0.08	-0.91	0.02
223	SLLL	-2.58	0.08	-0.83	0.18	0.68	0.22	-1.10	0.12	1.37	0.25	-1.14	0.03
224	SLLL	-1.05	0.05	-0.09	0.04	-1.27	0.06	-0.18	0.03	-0.81	0.07	-0.79	0.02
225	SLLL	-1.08	0.05	-1.06	0.06	-1.64	0.11	-1.16	0.04	-1.44	0.08	-1.24	0.02
226	SLLL	-0.99	0.06	-0.83	0.07	-1.26	0.06	-0.88	0.05	-0.90	0.10	-1.03	0.02
227	SLLL	-1.27	0.06	-1.23	0.13	0.29	0.19	-1.42	0.14	1.29	0.26	-0.79	0.03
228	SLLL	-1.66	0.12	-0.32	0.14	-0.14	0.12	-0.34	0.12	-0.73	0.08	-0.87	0.02

Table 7—Continued

Num.	module	n_{K-6}	$\sigma_{n_{K-6}}$	n_{6-13}	$\sigma_{n_{6-13}}$	n_{13-31}	$\sigma_{n_{13-31}}$	n_{5-12}	$\sigma_{n_{5-12}}$	n_{12-20}	$\sigma_{n_{12-20}}$	n_{K-25}	$\sigma_{n_{K-25}}$
229	SLLL	-2.49	0.07	-1.46	0.11	1.25	0.18	-1.62	0.11	2.18	0.36	-1.15	0.03
230	SLLL	-2.41	0.13	-1.29	0.23	1.10	0.23	-1.57	0.15	2.26	0.16	-1.13	0.05
231	SLLL	-1.03	0.07	0.14	0.09	-0.74	0.10	0.01	0.05	-0.30	0.05	-0.56	0.01
232	SLLL	-1.34	0.10	-0.94	0.12	0.30	0.07	-1.06	0.08	0.30	0.14	-0.81	0.02
233	SLLL	-1.89	0.10	-0.59	0.13	0.17	0.10	-0.79	0.09	-0.09	0.13	-1.01	0.03
234	SLLL	-1.47	0.07	-0.68	0.10	-0.75	0.12	-0.85	0.11	-0.73	0.10	-1.08	0.01
235	SLLL	-0.63	0.05	-0.08	0.05	-0.86	0.04	-0.21	0.03	-0.62	0.07	-0.54	0.01
236	SLLL	-1.82	0.09	-0.47	0.12	-0.57	0.10	-0.72	0.12	-0.34	0.20	-1.05	0.01
237	SLLL	-2.35	0.16	-0.34	0.19	1.39	0.07	-0.54	0.15	2.33	0.07	-0.65	0.01
238	SLLL	-1.89	0.14	-0.17	0.17	0.15	0.08	-0.29	0.15	0.43	0.14	-0.80	0.01
239	SLLL	-2.08	0.15	0.17	0.17	0.05	0.06	0.01	0.14	0.44	0.11	-0.78	0.01
240	SLLL	-2.04	0.17	-1.11	0.27	-1.25	0.32	-1.38	0.27	-0.89	0.31	-1.54	0.07
241	SLLL	-1.14	0.07	-0.53	0.11	-0.82	0.15	-0.74	0.06	-1.05	0.18	-0.91	0.02
242	SLLL	-1.32	0.06	-1.13	0.07	-0.63	0.06	-1.29	0.05	-0.61	0.07	-1.14	0.01
243	SLLL	-1.34	0.09	-1.01	0.12	-0.85	0.14	-1.12	0.10	-0.75	0.17	-1.14	0.03
244	SLLL	-1.58	0.10	-0.92	0.18	-1.39	0.18	-1.21	0.08	-1.14	0.15	-1.33	0.04
245	SLLL	-1.24	0.06	-0.64	0.07	0.25	0.04	-0.78	0.05	0.06	0.05	-0.71	0.01
246	SLLL	-1.76	0.06	-0.64	0.09	-0.58	0.14	-0.81	0.09	-0.43	0.25	-1.10	0.03
247	SLLL	-0.50	0.04	0.37	0.04	-0.34	0.03	0.23	0.03	-0.25	0.02	-0.20	0.01
248	SLLL	-1.32	0.13	-0.53	0.18	0.16	0.12	-0.28	0.25	0.55	0.13	-0.67	0.02
249	SLLL	-0.97	0.13	-0.87	0.18	0.28	0.24	-0.83	0.19	0.92	0.44	-0.61	0.03
250	SLLL	-1.54	0.10	-0.88	0.17	-1.12	0.21	-0.94	0.16	-0.70	0.17	-1.23	0.04
251	SLLL	-1.78	0.04	-1.48	0.12	-1.15	0.18	-1.58	0.15	-0.87	0.18	-1.57	0.04
252	SLLL	-1.09	0.07	-1.03	0.10	-0.48	0.11	-1.18	0.09	-0.73	0.16	-0.95	0.02
253	SLLL	-1.42	0.10	-0.97	0.13	-2.50	0.50	-0.97	0.13	-0.86	0.43	-1.14	0.06
254	SLLL	-1.28	0.07	-1.13	0.09	-1.30	0.09	-1.24	0.07	-0.77	0.17	-1.24	0.02
255	SLLL	-1.07	0.19	-0.34	0.19	-0.04	0.20	-0.51	0.11	0.74	0.28	-0.51	0.04
256	SLLL	-0.97	0.07	-0.31	0.08	-0.66	0.06	-0.35	0.07	-0.92	0.05	-0.72	0.01
257	SLLL	-2.64	0.23	0.67	0.27	0.70	0.18	0.30	0.31	1.34	0.11	-0.61	0.02
258	SLLL	-1.32	0.05	0.29	0.05	-0.57	0.05	0.25	0.04	-0.55	0.04	-0.61	0.01
259	SLLL	-0.71	0.07	-0.38	0.08	0.08	0.02	-0.50	0.04	-0.10	0.04	-0.46	0.01
260	SLLL	-2.72	0.16	-0.40	0.24	1.31	0.20	-0.65	0.23	1.76	0.23	-0.82	0.01
261	SLLL	0.03	0.05	-0.45	0.06	-0.72	0.05	-0.51	0.04	-1.31	0.09	-0.43	0.01
262	SLLL	-1.19	0.04	-0.50	0.04	-0.75	0.05	-0.65	0.04	-0.85	0.04	-0.90	0.01
263	SLLL	-1.57	0.12	-0.56	0.15	-0.30	0.10	-0.59	0.14	-0.71	0.49	-0.94	0.01

Table 7—Continued

Num.	module	n_{K-6}	$\sigma_{n_{K-6}}$	n_{6-13}	$\sigma_{n_{6-13}}$	n_{13-31}	$\sigma_{n_{13-31}}$	n_{5-12}	$\sigma_{n_{5-12}}$	n_{12-20}	$\sigma_{n_{12-20}}$	n_{K-25}	$\sigma_{n_{K-25}}$
264	SLLLL	-1.37	0.07	-0.49	0.08	-0.65	0.22	-0.54	0.08	-0.19	0.34	-0.91	0.03
265	SLLLL	-2.02	0.10	-0.56	0.13	-0.78	0.28	-1.03	0.13	-0.38	0.32	-1.24	0.04
266	SLLLL	-1.49	0.06	0.48	0.04	-0.44	0.04	0.22	0.06	-0.09	0.03	-0.56	0.02
267	SLLLL	-1.70	0.08	-1.19	0.12	-1.05	0.12	-1.26	0.11	-0.75	0.18	-1.38	0.04
268	SLLLL	-0.89	0.05	-0.67	0.05	-0.69	0.05	-0.82	0.06	-0.63	0.03	-0.81	0.01
269	SLLLL	-1.54	0.05	-0.90	0.06	-0.30	0.04	-1.04	0.05	-0.31	0.06	-1.05	0.01
270	SLLLL	-2.70	0.06	-2.40	0.20	1.09	0.20	-2.31	0.14	0.12	0.27	-1.72	0.03
271	SLLLL	-2.81	0.11	-0.32	0.14	1.82	0.09	-0.59	0.13	2.49	0.24	-0.68	0.02
272	SLLLL	0.04	0.18	0.20	0.19	-0.73	0.25	0.21	0.18	-0.76	0.31	-0.16	0.05
273	SLLLL	-1.80	0.08	-0.82	0.10	-0.81	0.24	-0.98	0.05	-1.04	0.36	-1.28	0.04
274	SLLLL	-1.75	0.08	-0.80	0.11	-0.49	0.14	-0.93	0.11	-0.25	0.13	-1.09	0.04
275	SLLLL	-2.27	0.12	0.21	0.15	0.55	0.10	-0.15	0.11	1.26	0.06	-0.64	0.01
276	SLLLL	-0.91	0.05	-0.85	0.05	-0.64	0.05	-0.99	0.06	-0.47	0.05	-0.85	0.01
277	SLLLL	-0.66	0.05	-0.45	0.05	-0.24	0.03	-0.56	0.04	-0.30	0.04	-0.54	0.01
278	SLLLL	-1.33	0.08	-1.12	0.10	-0.21	0.14	-1.18	0.11	-0.33	0.20	-1.03	0.02
279	SLLLL	-1.77	0.10	-0.53	0.12	0.80	0.09	-0.86	0.10	1.63	0.09	-0.64	0.02
280	SLLLL	-1.98	0.08	-0.28	0.08	-0.60	0.04	-0.52	0.05	-0.15	0.06	-1.05	0.02
281	SLLLL	-1.32	0.05	-0.67	0.09	-0.31	0.12	-0.79	0.07	-0.08	0.33	-0.89	0.02
282	SLLLL	-0.95	0.03	-0.55	0.03	-0.79	0.04	-0.67	0.05	-0.87	0.06	-0.84	0.01
283	SLLLL	-2.58	0.10	-1.73	0.17	1.44	0.16	-1.97	0.12	1.36	0.20	-1.28	0.03
284	SLLLL	-1.91	0.08	-1.17	0.11	-0.69	0.29	-1.28	0.09	-0.01	0.14	-1.32	0.01
285	SLLLL	-1.82	0.07	-1.18	0.16	-0.98	0.22	-1.23	0.09	-0.74	0.20	-1.39	0.04
286	SLLLL	-2.21	0.12	-1.10	0.17	-0.55	0.24	-1.29	0.11	-0.70	0.45	-1.41	0.03
287	SLLLL	-1.68	0.11	-0.55	0.14	-0.19	0.13	-0.74	0.09	0.04	0.23	-0.99	0.03
288	SLLLL	-1.61	0.08	-0.88	0.11	-0.53	0.21	-0.84	0.11	-0.59	0.37	-1.13	0.03
289	SLLLL	-0.98	0.05	0.12	0.05	-0.12	0.05	-0.07	0.05	0.24	0.05	-0.40	0.02
290	SLLLL	-1.52	0.13	0.29	0.15	-0.25	0.13	0.17	0.34	0.30	0.13	-0.61	0.02
291	SLLLL	-2.39	0.12	-0.42	0.17	1.00	0.20	-0.46	0.20	2.60	0.20	-0.78	0.04
292	SLLLL	-1.31	0.06	-0.55	0.09	-1.19	0.17	-0.73	0.09	-1.25	0.20	-1.04	0.02
293	SLLLL	-1.68	0.06	-0.53	0.09	-0.34	0.28	-0.69	0.10	-0.17	0.16	-0.93	0.03
294	SLLLL	-2.48	0.09	-1.44	0.14	1.58	0.11	-1.76	0.09	2.26	0.17	-1.05	0.01
295	SLLLL	-1.33	0.07	-0.73	0.09	-1.48	0.07	-0.88	0.07	-0.96	0.10	-1.16	0.02
296	SLLLL	3.22	0.03	-0.25	0.03	-0.36	0.03	-0.34	0.02	-1.02	0.02	0.98	0.01
297	SLLLL	-1.89	0.13	-0.97	0.16	0.93	0.16	-1.26	0.11	2.02	0.26	-0.80	0.04
298	SLLLL	-1.45	0.07	-1.28	0.10	-1.30	0.14	-1.38	0.07	-1.03	0.18	-1.36	0.02

Table 7—Continued

Num.	module	n_{K-6}	$\sigma_{n_{K-6}}$	n_{6-13}	$\sigma_{n_{6-13}}$	n_{13-31}	$\sigma_{n_{13-31}}$	n_{5-12}	$\sigma_{n_{5-12}}$	n_{12-20}	$\sigma_{n_{12-20}}$	n_{K-25}	$\sigma_{n_{K-25}}$
299	SLLL	-1.67	0.10	-0.21	0.13	-0.78	0.18	-0.41	0.10	-0.44	0.13	-0.98	0.02
300	SLLL	-1.97	0.11	-0.69	0.14	-0.05	0.11	-0.81	0.05	-0.03	0.16	-1.07	0.03
301	SLLL	-1.57	0.09	-0.70	0.13	-0.36	0.13	-0.91	0.14	0.53	0.28	-0.95	0.04
302	SLLL	-1.77	0.07	-0.62	0.20	1.69	0.24	-0.96	0.09	2.74	0.20	-0.47	0.04
303	SLLL	-2.57	0.17	-0.98	0.22	1.72	0.13	-1.41	0.08	2.35	0.17	-0.90	0.02
304	SLLL	0.34	0.06	-0.60	0.08	-0.67	0.05	-0.66	0.03	-1.01	0.04	-0.32	0.01
305	SLLL	-1.00	0.08	0.05	0.10	-1.02	0.15	-0.02	0.29	-1.48	0.55	-0.61	0.02
306	SLLL	-1.26	0.09	-0.47	0.18	1.60	0.25	-0.34	0.17	2.17	0.21	-0.21	0.01
307	SLLL	-2.11	0.11	-0.56	0.17	0.61	0.54	-0.74	0.07	0.95	0.19	-0.88	0.07
308	SLLL	-0.69	0.03	-0.33	0.05	-0.99	0.06	-0.37	0.05	-1.43	0.07	-0.78	0.01
309	SLLL	0.65	0.15	-1.23	0.16	-0.84	0.16	-1.37	0.08	-0.58	0.21	-0.41	0.04
310	SLLL	-0.28	0.19	-0.37	0.23	-0.42	0.12	-0.68	0.15	-0.96	0.32	-0.45	0.03
311	SLLL	-0.42	0.60	-0.27	0.81	0.63	0.47	-0.10	1.36	0.42	0.18	-0.09	0.04
312	SLLL	-1.94	1.29	-0.76	2.74	0.77	2.83	0.35	1.62	-1.99	4.76	-0.78	0.25
313	SLLL	-2.05	0.12	-1.45	0.16	1.02	0.14	-1.55	0.13	1.47	0.23	-1.09	0.02
314	SLLL	-1.32	0.18	-0.13	0.22	0.59	0.12	-0.03	0.33	1.56	0.18	-0.43	0.03
315	SLLL	-0.49	0.04	-0.52	0.06	-0.94	0.06	-0.56	0.04	-1.05	0.03	-0.67	0.01
316	SLLL	0.07	0.03	-0.36	0.03	-0.73	0.04	-0.42	0.02	-0.93	0.05	-0.36	0.01
317	SLLL	-1.26	0.13	-0.35	0.15	-0.65	0.19	-0.51	0.17	-0.29	0.31	-0.82	0.02
318	SLLL	-0.05	0.04	-0.51	0.05	-0.66	0.05	-0.55	0.06	-1.07	0.07	-0.45	0.01
319	SLLL	-0.39	0.06	-0.63	0.07	-0.66	0.17	-0.72	0.04	-1.32	0.21	-0.66	0.02

Note. — The wavelength interval for each anchor is as follows: The K band is at 2.17 μm ; 5 represent for wavelengths of 5.2–5.54 μm ; 6 for 5.4–6.0 μm ; 12 for 12.7–13.1 μm ; 13 for 12.8–14.0 μm ; 20 for 19.7–19.95 μm ; 25 for 24.5–25.5 μm ; 31 for 30.3–31.0 μm .

Table 8. Grain Properties

Num.	mod	EW10 (μm)	$\sigma_{\text{EW}10}$ (μm)	EW20 (μm)	$\sigma_{\text{EW}20}$ ($10^{-12}\text{erg/s/cm}^2$)	F10 ($10^{-12}\text{erg/s/cm}^2$)	$\sigma_{\text{F}10}$ ($10^{-12}\text{erg/s/cm}^2$)	F20 ($10^{-12}\text{erg/s/cm}^2$)	$\sigma_{\text{F}20}$ ($10^{-12}\text{erg/s/cm}^2$)	$F_{11.3}/F_{9.8}$	$\sigma_{F11.3}/F_{9.8}$	TD/FD
1	SLLL	8.054	0.157	3.243	0.326	2.698	0.022	0.759	0.068	0.45	0.01	TD
2	SLLL	2.781	0.088	2.392	0.305	1.127	0.023	0.553	0.054	0.53	0.02	FD
3	SLLL	2.509	0.085	2.464	0.305	29.600	0.634	9.833	0.833	0.41	0.02	FD
4	SLLL	2.595	0.086	2.533	0.309	3.219	0.075	1.470	0.145	0.44	0.02	FD
5	SLLL	5.348	0.12	2.515	0.308	5.381	0.061	1.491	0.147	0.51	0.02	TD
6	SLLL	1.247	0.069	1.485	0.288	3.608	0.161	1.449	0.247	0.49	0.04	FD
7	SLLL	TD
8	SLLL	1.045	0.067	3.142	0.323	0.049	0.003	0.119	0.012	0.54	0.05	TD
9	SLLL	1.23	0.069	1.205	0.281	15.890	0.726	9.294	1.827	0.55	0.05	FD
10	SLLL	2.338	0.082	2.514	0.311	3.035	0.078	1.637	0.174	0.54	0.03	FD
11	SLLL	3.809	0.1	4.104	0.339	1.736	0.028	2.983	0.209	0.49	0.02	TD
12	SLLL	2.739	0.087	1.76	0.294	4.220	0.092	1.178	0.166	0.52	0.02	FD
13	SLLL	0.291	0.059	4.723	0.359	-0.009	0.009	0.423	0.041	-1.23	0.28	TD
14	SLLL	1.264	0.069	0.522	0.269	3.397	0.151	0.357	0.186	0.59	0.05	FD
15	SLLL	2.942	0.089	2.033	0.297	9.263	0.175	3.033	0.357	0.45	0.02	FD
16	SLLL	0.585	0.062	3.271	0.328	0.111	0.029	0.631	0.062	21.30	39.95	TD
17	SLLL	2.224	0.081	2.653	0.31	2.916	0.077	1.653	0.155	0.52	0.03	FD
18	SLLL	2.017	0.079	2.467	0.31	0.596	0.019	0.467	0.056	0.33	0.02	TD
19	SLLL	0.608	0.062	5.529	0.381	0.050	0.010	0.697	0.079	1.19	0.18	TD
20	SLLL	0.997	0.066	1.647	0.289	1.365	0.083	0.753	0.116	0.77	0.07	FD
21	SLLL	3.807	0.099	2.421	0.305	68.760	0.972	22.100	2.087	0.59	0.02	FD
22	SLLL	3.068	0.091	1.547	0.287	9.249	0.168	2.089	0.308	0.54	0.02	FD
23	SLLL	5.178	0.118	4.337	0.343	5.852	0.075	2.437	0.140	0.47	0.02	TD
24	SLLL	4.708	0.112	2.786	0.313	19.510	0.232	6.684	0.567	0.39	0.02	TD
25	SLLL	4.803	0.114	5.329	0.373	0.509	0.011	0.794	0.058	0.56	0.02	TD
26	SLLL	2.245	0.081	2.984	0.321	0.271	0.011	0.334	0.036	0.83	0.04	TD
27	SLLL	3.378	0.095	3.427	0.327	2.544	0.050	1.409	0.109	0.47	0.02	FD
28	SLLL	1.528	0.072	1.752	0.294	10.870	0.392	6.091	0.823	0.71	0.05	FD
29	SLLL	1.307	0.07	2.654	0.314	0.128	0.009	0.705	0.089	4.40	0.55	TD
30	SLLL	3.708	0.1	2.725	0.311	6.213	0.094	1.729	0.153	0.41	0.02	FD
31	SLLL	3.047	0.091	1.88	0.295	4.781	0.091	2.481	0.336	0.53	0.02	FD
32	SLLL	2.584	0.085	0.859	0.277	1.519	0.036	0.343	0.120	0.58	0.03	FD
33	SLLL	2.258	0.081	3.896	0.339	2.467	0.064	2.518	0.169	0.61	0.03	FD
34	SLLL	4.398	0.107	3.931	0.369	0.270	0.014	0.273	0.076	0.72	0.02	TD
35	SLLL	0.618	0.062	3.67	0.347	0.208	0.036	0.525	0.067	2.05	0.76	FD
36	SLLL	1.846	0.076	5.002	0.36	2.855	0.127	2.794	0.147	0.66	0.04	FD
37	SLLL	3.572	0.097	3.335	0.324	33.210	0.520	10.540	0.772	0.61	0.02	FD
38	SLLL	6.827	0.139	4.664	0.354	1.870	0.019	1.278	0.090	0.48	0.01	TD
39	SLLL	0.814	0.067	4.415	0.403	0.403	0.017	0.249	0.066	-13.71	3.25	TD
40	SLLL	3.076	0.091	4.067	0.338	3.221	0.076	1.648	0.110	0.48	0.02	FD
41	SLLL	0.243	0.057	3.197	0.322	0.104	0.029	0.798	0.073	0.36	0.18	FD
42	SLLL	4.456	0.108	3.474	0.327	2.726	0.038	1.187	0.099	0.66	0.02	TD
43	SLLL	1.896	0.077	1.912	0.295	11.900	0.343	4.354	0.520	0.47	0.03	FD
44	SLLL	4.076	0.104	3.474	0.326	2.115	0.034	1.626	0.121	0.51	0.02	TD
45	SLLL	1.425	0.071	0.789	0.272	40.490	1.555	4.314	1.200	0.66	0.05	FD
46	SLLL	2.595	0.085	8.681	0.481	2.423	0.062	2.952	0.415	0.74	0.03	FD
47	SLLL	3.245	0.094	4.771	0.348	2.831	0.047	1.701	0.127	0.66	0.03	TD
48	SLLL	1.496	0.072	4.047	0.347	1.106	0.044	0.708	0.063	0.72	0.05	FD
49	SL	-12.961	0.122	...	4.237	0.232	0.77	0.01	TD
50	SLLL	4.339	0.108	3.872	0.338	15.400	0.313	7.070	0.489	0.43	0.02	FD

Table 8—Continued

Num.	mod	EW10 (μm)	σ_{EW10} (μm)	EW20 (μm)	σ_{EW20} (μm)	F10 ($10^{-12}\text{ erg/s/cm}^2$)	σ_{F10} ($10^{-12}\text{ erg/s/cm}^2$)	F20 ($10^{-12}\text{ erg/s/cm}^2$)	σ_{F20} ($10^{-12}\text{ erg/s/cm}^2$)	$F_{11.3}/F_{9.8}$	$\sigma_{F_{11.3}/F_{9.8}}$	TD/FD
51	SLLL	2.567	0.084	2.459	0.307	4.563	0.104	1.557	0.152	0.49	0.03	FD
52	SLLL	2.118	0.079	1.498	0.286	4.771	0.128	1.350	0.205	0.70	0.03	FD
53	SLLL	2.991	0.09	3.501	0.33	0.237	0.010	0.209	0.018	0.58	0.03	TD
54	SLLL	4.235	0.106	2.69	0.308	7.292	0.095	1.521	0.126	0.46	0.02	FD
55	SL	2.04	0.078	3.827	0.231	0.94	0.05	...
56	SL	4.477	0.107	2.112	0.076	0.65	0.02	...
57	SLLL	4.345	0.107	2.444	0.304	7.419	0.099	2.171	0.223	0.42	0.02	FD
58	SLLL	1.666	0.074	3.078	0.324	1.246	0.043	0.629	0.063	0.59	0.04	FD
59	SLLL	2.643	0.086	1.139	0.283	0.746	0.023	0.399	0.094	0.65	0.03	TD
60	SLLL	0.859	0.064	2.007	0.301	0.871	0.066	0.622	0.088	0.51	0.05	FD
61	SLLL	2.059	0.079	1.685	0.29	7.159	0.195	1.960	0.283	0.48	0.03	FD
62	SLLL	1.423	0.071	2.033	0.3	6.168	0.233	2.134	0.258	0.51	0.04	FD
63	SL	2.173	0.08	1.330	0.065	0.25	0.03	...
64	SL	5.484	0.121	28.170	0.302	0.56	0.02	...
65	SLLL	2.845	0.088	2.619	0.313	1.678	0.035	0.734	0.093	0.48	0.03	FD
66	SLLL	3.453	0.098	7.42	0.428	0.465	0.016	0.891	0.054	0.59	0.02	TD
67	SL	4.148	0.104	4.538	0.099	0.84	0.03	...
68	SL	1.372	0.07	1.844	0.125	2.08	0.19	...
70	SL	1.023	0.069	0.575	0.042	2.73	0.33	...
71	SL	0.935	0.066	4.829	0.339	6.42	1.30	...
73	SLLL	1.153	0.068	2.191	0.315	1.712	0.083	0.738	0.097	0.60	0.05	FD
74	SL	10.4	0.183	52.190	0.380	0.48	0.01	...
75	SL	5.076	0.124	2.077	0.225	0.84	0.03	...
76	SLLL	2.691	0.086	2.896	0.319	8.915	0.196	3.422	0.302	0.69	0.03	FD
77	SL	77.67	13.47	3.611	0.286	-0.04	0.00	...
78	SL	49.813	3.359	0.538	0.064	-1.72	0.05	...
79	SLLL	2.476	0.084	2.227	0.303	4.634	0.103	1.296	0.147	0.48	0.03	FD
80	SL	2.964	0.089	1.621	0.057	0.54	0.03	...
81	SL	3.211	0.092	2.957	0.084	0.74	0.03	...
82	SL	4.402	0.107	7.828	0.247	0.39	0.02	...
83	SL	2.854	0.09	2.767	0.057	1.07	0.04	...
84	SLLL	3.704	0.1	3.255	0.324	2.627	0.044	1.056	0.094	0.35	0.02	FD
85	SL	4.876	0.116	2.229	0.046	0.65	0.02	...
86	SLLL	2.325	0.082	3.188	0.326	1.432	0.039	0.840	0.078	0.50	0.03	FD
88	SLLL	TD
89	SL	1.385	0.071	3.285	0.178	2.66	0.20	...
90	SLLL	2.115	0.079	3.684	0.334	10.890	0.283	7.078	0.527	0.45	0.03	FD
91	SL	4.323	0.107	142.400	1.837	0.42	0.02	...
92	SL	3.214	0.095	4.348	0.234	1.30	0.06	...
93	SL	1.237	0.069	5.923	0.302	0.56	0.05	...
94	SLLL	4.472	0.108	2.308	0.309	2.889	0.056	1.044	0.144	0.53	0.02	FD
95	SLLL	0.267	0.058	-0.024	0.257	0.832	0.185	-0.012	0.585	-19.53	12.01	FD
96	SL	2.676	0.085	2.305	0.071	0.77	0.03	...
97	SLLL	4.127	0.104	4.214	0.337	2.131	0.031	1.241	0.078	0.53	0.02	FD
98	SLLL	3.338	0.094	4.357	0.352	3.489	0.062	1.401	0.125	0.58	0.02	FD
99	SLLL	2.447	0.083	1.076	0.282	2.330	0.057	0.324	0.081	0.50	0.03	FD
100	SL	4.04	0.103	12.880	0.181	0.57	0.02	...
101	SL	1.681	0.077	1.781	0.091	5.64	0.52	...
102	SL	1.435	0.074	1.508	0.106	1.12	0.07	...
103	SLLL	2.935	0.09	1.33	0.282	11.380	0.217	1.669	0.287	0.40	0.02	FD

Table 8—Continued

Num.	mod	EW10 (μm)	σ_{EW10} (μm)	EW20 (μm)	σ_{EW20} (μm)	F10 ($10^{-12}\text{ erg/s/cm}^2$)	σ_{F10} ($10^{-12}\text{ erg/s/cm}^2$)	F20 ($10^{-12}\text{ erg/s/cm}^2$)	σ_{F20} ($10^{-12}\text{ erg/s/cm}^2$)	$F_{11.3}/F_{9.8}$	$\sigma_{F_{11.3}/F_{9.8}}$	TD/FD
106	SLLL	2.256	0.081	1.537	0.29	4.066	0.106	0.825	0.131	0.49	0.03	FD
108	SLLL	8.262	0.162	5.637	0.368	100.500	0.661	40.520	0.35	0.01	TD	TD
112	SLLL	1.247	0.069	1.312	0.284	10.960	0.491	2.700	0.476	0.70	0.06	FD
114	SL	1.643	0.073	9.604	0.339	1.27	0.08	...
117	SLLL	2.194	0.08	0.434	0.263	23.400	0.574	2.290	0.911	0.44	0.03	FD
119	SL	2.176	0.08	1.120	0.040	0.47	0.03	...
120	SL	2.724	0.086	2.859	0.066	0.47	0.03	...
121	SLLL	1.105	0.067	1.399	0.285	2.960	0.154	1.058	0.181	0.77	0.06	FD
122	SLLL	1.603	0.073	1.854	0.294	13.480	0.456	5.344	0.658	0.48	0.04	FD
123	SLLL	2.488	0.084	2.866	0.314	2.149	0.051	2.004	0.209	0.62	0.03	FD
125	SLLL	4.713	0.112	3.459	0.328	21.640	0.254	6.508	0.450	0.63	0.02	FD
127	SLLL	2.462	0.084	0.637	0.271	1.256	0.069	0.191	0.083	0.76	0.04	FD
128	SLLL	0.885	0.065	1.924	0.294	1.505	0.146	1.148	0.144	1.94	0.16	FD
129	SL	1.833	0.076	1.514	0.059	0.79	0.05	...
131	SLLL	2.037	0.078	2.895	0.319	5.971	0.174	2.039	0.177	0.66	0.04	FD
132	SL	1.08	0.067	18.340	0.956	1.72	0.17	...
133	SLLL	1.983	0.078	2.125	0.3	6.149	0.168	2.575	0.287	0.54	0.03	FD
134	SLLL	2.844	0.088	1.341	0.281	6.919	0.140	1.011	0.161	0.71	0.03	FD
135	SLLL	3.724	0.099	3.976	0.339	13.610	0.211	4.482	0.279	0.68	0.03	FD
136	SLLL
137	SL	527.196	53.074	2.117	0.061	-0.25	0.01	...
138	SLLL	2.93	0.089	1.249	0.282	8.779	0.170	1.645	0.309	0.50	0.03	FD
139	SL	1.643	0.075	63.640	2.214	16.29	8.15	...
140	SLLL	4.449	0.11	2.972	0.314	43.130	0.525	15.500	1.140	0.32	0.01	FD
141	SLLL	1.315	0.069	4.409	0.352	11.400	0.501	5.665	0.342	1.01	0.07	FD
142	SLLL	4.76	0.113	3.327	0.326	14.270	0.177	5.403	0.430	0.40	0.02	FD
143	SL	4.07	0.102	3.927	0.154	1.46	0.05	...
144	SLLL	1.974	0.078	1.661	0.29	45.060	1.259	20.250	2.886	0.48	0.03	FD
145	SL	2.19	0.081	3.984	0.120	1.02	0.05	...
146	SL	3.457	0.096	3.216	0.174	0.55	0.02	...
147	SL	0.773	0.065	1.315	0.164	25.24
148	SLLL
149	SLLL	2.124	0.079	1.926	0.295	22.480	0.568	14.790	2.005	0.53	0.03	TD
150	SL	3.879	0.1	14.070	0.273	0.77	0.03	...
151	SLLL	4.157	0.105	2.888	0.32	2.640	0.052	0.537	0.050	0.50	0.02	FD
152	SL	4.387	0.108	18.980	0.466	1.14	0.03	...
153	SL	2.442	0.085	1.753	0.092	3.11	0.21	...
154	SLLL	2.415	0.083	3.675	0.334	1.643	0.043	1.331	0.101	0.60	0.03	TD
155	SL	1.513	0.072	0.907	0.099	0.79	0.06	...
156	SLLL	2.116	0.08	2.152	0.299	9.292	0.238	3.536	0.356	0.50	0.03	FD
158	SL	1.206	0.07	5.668	0.380	9.00	2.22	...
159	SLLL	3.337	0.094	1.791	0.292	1.598	0.034	0.719	0.105	0.53	0.02	FD
160	SLLL	2.543	0.085	1.898	0.295	16.130	0.333	3.765	0.471	0.36	0.03	FD
161	SLLL	2.96	0.09	2.902	0.318	1.289	0.031	0.562	0.066	0.49	0.02	FD
162	SLLL	3.886	0.102	3.33	0.323	24.320	0.342	8.771	0.598	0.37	0.02	FD
163	SL	2.283	0.082	12.350	0.348	0.03	0.02	...
164	SLLL	5.185	0.119	2.996	0.316	22.260	0.239	8.089	0.636	0.39	0.01	TD
165	SLLL	2.954	0.09	1.4	0.284	3.020	0.059	0.609	0.102	0.50	0.02	FD
166	SLLL	1.076	0.067	2.537	0.311	0.958	0.052	0.778	0.088	0.65	0.06	FD
167	SLLL	1.846	0.076	3.052	0.317	2.100	0.077	1.668	0.135	0.67	0.04	FD

Table 8—Continued

Num.	mod	EW10 (μm)	σ_{EW10} (μm)	EW20 (μm)	σ_{EW20} ($10^{-12} \text{ erg/s/cm}^2$)	F10 ($10^{-12} \text{ erg/s/cm}^2$)	σ_{F10} ($10^{-12} \text{ erg/s/cm}^2$)	F20 ($10^{-12} \text{ erg/s/cm}^2$)	σ_{F20} ($10^{-12} \text{ erg/s/cm}^2$)	$F_{11.3}/F_{9.8}$	$\sigma_{F_{11.3}/F_{9.8}}$	TD/FD
168	SLLL	1.888	0.076	1.896	0.293	22.460	0.671	9.864	1.214	0.62	0.04	FD
169	SLLL	2.586	0.086	4.607	0.349	0.740	0.020	1.132	0.073	0.72	0.03	TD
170	SLLL	2.522	0.084	1.062	0.284	0.487	0.022	0.189	0.056	0.45	0.03	FD
172	SLLL	3.212	0.093	2.948	0.318	1.851	0.038	1.678	0.157	0.56	0.02	TD
173	SLLL	0.796	0.063	1.926	0.302	12.200	0.867	4.165	0.732	1.11	0.10	FD
174	SLLL	4.067	0.104	3.174	0.322	2.064	0.034	1.171	0.097	0.58	0.02	TD
175	SL	13.9227	0.242	4.547	0.123	0.55	0.02	...
176	SLLL	3.201	0.093	2.468	0.311	0.964	0.023	0.585	0.076	0.49	0.02	TD
177	SLLL	2.186	0.08	5.217	0.371	0.100	0.004	0.714	0.044	0.67	0.03	TD
178	SLLL	4.233	0.107	1.936	0.295	8.788	0.114	1.995	0.233	0.34	0.01	FD
179	SLLL	3.09	0.091	4.653	0.361	2.527	0.049	1.135	0.076	0.47	0.02	FD
180	SLLL	1.03	0.066	1.121	0.283	8.642	0.462	1.573	0.442	1.02	0.08	FD
181	SLLL	2.983	0.089	2.742	0.318	2.543	0.051	0.865	0.098	0.59	0.03	FD
182	SLLL	2.053	0.079	1.592	0.291	4.558	0.127	1.139	0.181	0.41	0.03	FD
183	SLLL	2.467	0.084	2.122	0.3	3.988	0.092	1.441	0.180	0.46	0.03	FD
184	SLLL	8.605	0.166	6.43	0.389	2.937	0.038	1.440	0.090	0.52	0.01	TD
185	SLLL	4.796	0.114	3.389	0.325	3.277	0.042	1.860	0.138	0.48	0.02	TD
186	SLLL	3.737	0.1	2.201	0.3	4.477	0.071	2.106	0.242	0.45	0.02	FD
187	SLLL	2.307	0.081	1.581	0.29	2.858	0.085	1.088	0.39	0.39	0.03	FD
188	SLLL	3.288	0.094	3.193	0.324	1.131	0.030	1.118	0.103	0.78	0.03	TD
189	SLLL	4.215	0.105	4.43	0.348	5.363	0.078	1.920	0.111	0.53	0.02	FD
190	SLLL	1.507	0.072	2.141	0.3	5.757	0.059	1.215	0.145	0.37	0.03	FD
191	SLLL	1.498	0.072	2.177	0.301	69.550	2.522	57.890	6.442	0.53	0.04	FD
192	SLLL	2.209	0.08	3.982	0.344	1.031	0.030	0.836	0.064	0.69	0.03	FD
193	SLLL	3.9	0.103	13.431	0.556	4.096	0.068	4.094	0.138	0.42	0.02	FD
194	SLLL	0.462	0.061	1.813	0.297	0.111	0.018	0.400	0.070	-4.59	0.52	FD
195	SLLL	1.38	0.07	5.598	0.386	1.002	0.042	0.985	1.535	0.52	0.05	FD
196	SLLL	2.334	0.082	1.692	0.291	9.582	0.222	2.417	0.337	0.60	0.03	FD
197	SLLL	1.875	0.076	1.567	0.29	2.197	0.066	0.947	0.154	0.56	0.03	FD
198	SLLL	4.679	0.112	6.111	0.385	2.555	0.047	1.714	0.091	0.66	0.02	TD
199	SLLL	1.19	0.068	1.544	0.289	2.281	0.120	0.624	0.100	0.53	0.05	FD
200	SLLL	1.459	0.071	1.333	0.285	3.191	0.143	0.792	0.151	0.62	0.05	FD
201	SLLL	1.631	0.074	2.479	0.309	5.652	0.199	1.747	0.183	0.40	0.03	FD
202	SLLL	1.038	0.066	1.344	0.285	5.432	0.291	2.595	0.460	0.58	0.05	FD
203	SLLL	5.864	0.126	4.193	0.341	5.294	0.049	1.679	0.102	0.46	0.02	TD
204	SLLL	3.554	0.097	5.262	0.364	0.407	0.007	0.423	0.024	0.60	0.02	FD
205	SLLL	4.285	0.106	3.204	0.32	13.450	0.175	4.266	0.309	0.39	0.02	FD
206	SLLL	2.151	0.08	1.826	0.293	44.930	1.132	10.950	1.408	0.46	0.03	FD
207	SLLL	0.775	0.063	1.089	0.277	5.781	0.416	3.921	0.799	0.45	0.05	FD
208	SLLL	0.874	0.065	1.128	0.281	6.524	0.439	3.476	0.749	0.68	0.06	FD
209	SLLL	2.836	0.089	2.362	0.304	65.540	1.233	31.420	3.118	0.34	0.02	FD
210	SLLL	0.717	0.063	0.897	0.276	2.797	0.218	1.172	0.318	0.64	0.08	FD
211	SLLL	3.277	0.093	7.001	0.408	0.304	0.006	0.520	0.033	0.72	0.03	TD
212	SLLL	3.624	0.098	2.502	0.309	3.770	0.059	1.091	1.408	0.46	0.03	FD
213	SLLL	1.566	0.073	1.481	0.287	6.847	0.244	3.921	0.799	0.45	0.05	FD
214	SLLL	4.717	0.111	3.657	0.33	4.577	0.064	1.158	0.084	0.55	0.02	FD
215	SLLL	3.375	0.095	2.528	0.308	4.752	0.081	2.001	0.198	0.46	0.02	FD
216	SLLL	1.035	0.068	-0.918	0.24	0.112	0.007	-0.995	0.031	3.44	1.56	FD
217	SLLL	0.995	0.066	0.605	0.269	3.047	0.169	0.475	0.171	0.54	0.05	FD
218	SLLL	1.867	0.076	3.538	0.334	0.135	0.005	0.291	0.031	0.74	0.04	TD

Table 8—Continued

Num.	mod	EW10 (μm)	σ_{EW10} (μm)	EW20 (μm)	σ_{EW20} (μm)	F10 (10^{-12} erg/s/cm 2)	σ_{F10} (10^{-12} erg/s/cm 2)	F20 (10^{-12} erg/s/cm 2)	σ_{F20} (10^{-12} erg/s/cm 2)	$F_{11.3}/F_{9.8}$	$\sigma_{F_{11.3}/F_{9.8}}$	TD/FD
219	SLLL	3.311	0.094	3.018	0.328	0.314	0.009	0.304	0.032	0.82	0.03	TD
220	SLLL	1.791	0.075	1.969	0.294	2.709	0.086	1.554	0.195	0.48	0.03	FD
221	SLLL	5.961	0.13	3.699	0.331	3.877	0.041	2.047	0.139	0.42	0.01	TD
222	SLLL	3.5	0.097	1.481	0.286	9.226	0.152	1.558	0.237	0.44	0.02	FD
223	SLLL	2.062	0.079	2.02	0.304	0.145	0.006	0.150	0.023	0.86	0.04	TD
224	SLLL	6.227	0.132	2.038	0.296	194.500	1.658	25.060	2.688	0.39	0.01	FD
225	SLLL	2.322	0.082	1.355	0.284	31.780	0.748	4.517	0.766	0.57	0.03	FD
226	SLLL	4.715	0.111	2.672	0.311	76.250	0.930	13.050	1.119	0.56	0.02	FD
227	SLLL	5.344	0.119	6.945	0.403	2.779	0.038	2.033	0.090	0.76	0.02	TD
228	SLLL	1.422	0.071	1.32	0.288	0.820	0.035	0.296	0.065	0.58	0.04	FD
229	SLLL	1.168	0.068	5.65	0.376	0.117	0.007	0.588	0.038	1.61	0.17	TD
230	SLLL	7.549	0.149	5.099	0.372	0.479	0.008	0.316	0.022	0.92	0.02	FD
231	SLLL	2.045	0.079	3.974	0.338	14.100	0.368	11.450	0.680	0.42	0.03	FD
232	SLLL	2.363	0.082	2.345	0.304	3.159	0.077	1.865	0.200	0.55	0.03	FD
233	SLLL	2.025	0.078	1.702	0.293	1.248	0.038	0.490	0.078	0.60	0.03	FD
234	SLLL	3.608	0.098	2	0.298	3.838	0.067	0.781	0.101	0.48	0.02	FD
235	SLLL	5.342	0.12	1.552	0.286	249.000	2.585	34.210	4.728	0.38	0.01	FD
236	SLLL	1.936	0.077	3.481	0.327	3.102	0.093	2.352	0.166	0.56	0.04	FD
237	SLLL	6.613	0.139	4.531	0.35	2.386	0.024	2.910	0.174	0.35	0.01	TD
238	SLLL	3.116	0.092	2.533	0.309	3.943	0.080	2.017	0.197	0.58	0.03	FD
239	SLLL	6.318	0.134	4.08	0.338	9.723	0.102	4.474	0.266	0.40	0.01	TD
240	SLLL	1.128	0.068	1.265	0.284	0.518	0.032	0.141	0.031	0.45	0.05	FD
241	SLLL	1.62	0.073	0.644	0.27	2.942	0.102	0.428	0.164	0.55	0.04	FD
242	SLLL	1.684	0.074	1.939	0.298	26.470	0.875	10.220	1.321	0.60	0.04	FD
243	SLLL	1.497	0.072	2.248	0.303	2.914	0.111	1.444	0.155	0.62	0.05	FD
244	SLLL	1.635	0.073	1.772	0.295	1.963	0.070	0.643	0.092	0.70	0.04	FD
245	SLLL	1.884	0.076	1.216	0.282	7.976	0.234	2.956	0.602	0.63	0.04	FD
246	SLLL	2.955	0.09	3.185	0.323	3.695	0.069	1.546	0.121	0.55	0.03	FD
247	SLLL	1.216	0.069	1.214	0.282	10.510	0.463	6.012	1.171	0.37	0.04	FD
248	SLLL	2.02	0.079	2.231	0.305	2.864	0.077	1.822	0.205	0.48	0.03	FD
249	SLLL	4.211	0.106	5.985	0.376	1.538	0.026	1.144	0.061	0.54	0.02	FD
250	SLLL	3.453	0.096	2.216	0.302	4.841	0.081	1.030	0.109	0.52	0.02	FD
251	SLLL	0.969	0.066	1.821	0.297	2.115	0.122	0.834	0.117	0.83	0.07	FD
252	SLLL	0.962	0.066	2.131	0.305	4.200	0.230	2.673	0.325	0.39	0.05	TD
253	SLLL	2.59	0.085	5.851	0.387	4.547	0.094	2.521	0.108	0.55	0.03	FD
254	SLLL	1.919	0.077	3.467	0.329	24.830	0.693	10.910	0.755	0.42	0.03	FD
255	SLLL	3.604	0.1	4.458	0.35	6.136	0.092	5.052	0.277	0.30	0.02	FD
256	SLLL	0.868	0.064	0.932	0.276	6.090	0.378	2.613	0.667	0.48	0.06	FD
257	SLLL	1.073	0.067	2.218	0.305	0.131	0.010	0.433	0.060	0.55	0.05	TD
258	SLLL	1.192	0.068	0.9	0.276	13.300	0.588	4.826	0.39	0.45	0.05	FD
259	SLLL	1.748	0.075	1.512	0.288	12.420	0.380	5.271	0.853	0.42	0.03	FD
260	SLLL	0.895	0.065	6.213	0.398	0.082	0.007	0.742	0.044	0.68	0.05	TD
261	SLLL	-0.346	0.051	1.491	0.289	-5.322	0.760	5.443	0.927	0.29	0.10	FD
262	SLLL	2.706	0.086	2.01	0.298	19.480	0.394	5.094	0.834	0.48	0.06	FD
263	SLLL	1.92	0.077	1.552	0.29	0.862	0.042	0.314	0.060	0.55	0.05	FD
264	SLLL	1.787	0.075	1.821	0.298	2.459	0.076	0.961	1.269	0.69	0.04	FD
265	SLLL	1.963	0.078	2.287	0.304	1.374	0.040	0.658	0.073	0.52	0.03	FD
266	SLLL	3.098	0.091	2.195	0.299	110.300	1.953	56.530	5.834	0.42	0.02	FD
267	SLLL	4.21	0.106	3.953	0.336	12.210	0.159	3.568	0.206	0.44	0.02	FD
268	SLLL	1.784	0.075	1.641	0.291	9.981	0.307	3.271	0.478	0.58	0.04	FD

Table 8—Continued

Num.	mod	EW10 (μm)	σ_{EW10} (μm)	EW20 (μm)	σ_{EW20} (μm)	F10 ($10^{-12}\text{ erg/s/cm}^2$)	σ_{F10} ($10^{-12}\text{ erg/s/cm}^2$)	F20 ($10^{-12}\text{ erg/s/cm}^2$)	σ_{F20} ($10^{-12}\text{ erg/s/cm}^2$)	$F_{11.3}/F_{9.8}$	$\sigma_{F_{11.3}/F_{9.8}}$	TD/FD
269	SLLL	1.437	0.071	2.375	0.306	9.079	0.363	5.898	0.617	0.64	0.04	FD
270	SLLL	0.641	0.062	4.381	0.348	0.308	0.056	1.312	0.094	14.21	0.03	TD
271	SLLL	3.591	0.097	5.003	0.365	0.402	0.008	1.467	0.083	0.64	0.03	TD
272	SLLL	1.097	0.067	2.126	0.3	0.685	0.034	0.553	0.066	0.57	0.06	FD
273	SLLL	3.833	0.1	1.516	0.287	3.187	0.050	0.455	0.078	0.54	0.02	FD
274	SLLL	0.688	0.062	3.227	0.327	0.691	0.055	1.164	0.095	0.35	0.06	FD
275	SLLL	2.545	0.084	2.868	0.318	1.879	0.044	3.028	0.266	0.70	0.03	TD
276	SLLL	1.328	0.07	2.676	0.311	10.800	0.446	7.620	0.673	0.42	0.04	FD
277	SLLL	2.139	0.08	2.229	0.302	17.500	0.435	7.514	0.805	0.41	0.03	FD
278	SLLL	2.623	0.086	2.459	0.307	2.146	0.053	0.817	0.089	0.51	0.02	FD
279	SLLL	3.412	0.096	2.652	0.312	2.593	0.049	2.374	0.226	0.52	0.02	TD
280	SLLL	3.466	0.096	1.901	0.294	20.060	0.316	6.252	0.755	0.65	0.03	FD
281	SLLL	2.071	0.079	2.852	0.316	1.717	0.050	0.920	0.088	0.60	0.03	FD
282	SLLL	1.202	0.068	1.029	0.278	24.420	1.114	7.439	1.723	0.78	0.06	FD
283	SLLL	0.815	0.064	3.486	0.331	0.051	0.006	0.264	0.024	1.42	0.14	TD
284	SLLL	3.997	0.103	4.193	0.341	3.169	0.048	1.321	0.089	0.49	0.02	FD
285	SLLL	3.015	0.09	2.296	0.304	5.294	0.099	1.458	0.154	0.56	0.03	FD
286	SLLL	1.983	0.078	3.252	0.333	0.950	0.031	0.467	0.043	0.65	0.04	FD
287	SLLL	3.954	0.103	3.101	0.318	1.566	0.029	0.680	0.055	0.51	0.02	FD
288	SLLL	3.91	0.102	1.95	0.297	2.208	0.037	0.470	0.063	0.45	0.02	FD
289	SLLL	2.536	0.085	2.777	0.313	15.440	0.330	10.180	0.878	0.52	0.03	FD
290	SLLL	4.343	0.108	2.721	0.308	4.012	0.063	1.757	0.152	0.49	0.02	TD
291	SLLL	6.355	0.132	3.557	0.335	0.570	0.009	0.709	0.067	0.57	0.02	TD
292	SLLL	2.029	0.078	2.141	0.305	1.668	0.050	0.504	0.069	0.49	0.03	FD
293	SLLL	3.201	0.093	2.975	0.317	1.373	0.026	0.646	0.062	0.39	0.02	FD
294	SLLL	2.398	0.083	6.578	0.39	1.235	0.037	3.198	0.141	0.49	0.03	TD
295	SLLL	3.186	0.092	2.344	0.304	21.350	0.363	4.423	0.441	0.58	0.03	FD
296	SLLL	0.455	0.06	0.19	0.262	143.000	15.700	21.170	0.152	0.49	0.02	FD
297	SLLL	3.774	0.101	5.155	0.366	0.513	0.008	0.624	0.032	0.32	0.14	FD
298	SLLL	3.264	0.093	2.729	0.312	11.610	0.206	2.400	0.211	0.68	0.03	FD
299	SLLL	3.183	0.093	2.265	0.302	1.543	0.031	0.508	0.064	0.38	0.02	FD
300	SLLL	1.29	0.069	4.676	0.359	0.910	0.040	1.380	0.082	0.55	0.05	FD
301	SLLL	4.372	0.108	3.845	0.334	3.334	0.023	0.729	0.054	0.50	0.02	TD
302	SLLL	1.77	0.075	6.855	0.405	0.106	0.006	0.881	0.050	2.57	0.23	TD
303	SLLL	1.127	0.068	2.82	0.317	0.143	0.008	0.580	0.061	0.53	0.05	TD
304	SLLL	0.803	0.064	1.436	0.286	7.496	0.500	4.122	0.682	0.48	0.07	FD
305	SLLL	2.511	0.083	0.745	0.278	4.264	0.100	0.448	0.191	0.35	0.02	FD
306	SLLL	8.015	0.154	5.083	0.363	6.221	0.052	6.625	0.381	0.54	0.02	TD
307	SLLL	3.574	0.098	4.901	0.381	0.282	0.009	0.379	0.043	0.71	0.03	FD
308	SLLL	0.698	0.062	0.741	0.271	27.980	2.090	9.884	2.796	0.60	0.10	FD
309	SLLL	0.121	0.056	2.89	0.326	0.605	0.154	2.033	0.179	-0.20	0.26	FD
310	SLLL	1.229	0.069	1.202	0.281	0.515	0.047	0.182	0.046	0.65	0.05	FD
311	SLLL	1.598	0.074	1.111	0.289	0.103	0.010	0.064	0.019	0.69	0.04	FD
312	SLLL	0.196	0.106	19.931	0.96	0.005	0.016	0.081	0.016	-0.13	0.01	FD
313	SLLL	2.352	0.082	1.475	0.284	1.049	0.033	0.684	0.127	0.81	0.04	FD
314	SLLL	6.146	0.131	2.614	0.309	1.472	0.020	0.725	0.073	0.54	0.02	TD
315	SLLL	1.055	0.067	1.245	0.282	17.120	0.861	6.255	1.177	0.38	0.05	FD
316	SLLL	0.841	0.064	1.567	0.289	54.600	3.471	33.910	5.164	0.61	0.07	FD
317	SLLL	1.895	0.077	1.298	0.282	1.186	0.038	0.439	0.077	0.48	0.03	FD
318	SLLL	0.608	0.061	0.99	0.277	4.186	0.392	2.421	0.570	0.54	0.08	FD

Table 8—Continued

Num.	mod	EW_{10} (μm)	$\sigma_{\text{EW}_{10}}$ (μm)	EW_{20} (μm)	$\sigma_{\text{EW}_{20}}$ (μm)	F_{10} ($10^{-12} \text{ erg/s/cm}^2$)	$\sigma_{\text{F}_{10}}$ ($10^{-12} \text{ erg/s/cm}^2$)	F_{20} ($10^{-12} \text{ erg/s/cm}^2$)	$\sigma_{\text{F}_{20}}$ ($10^{-12} \text{ erg/s/cm}^2$)	$F_{11,3}/F_{9,8}$	$\sigma_{F_{11,3}/F_{9,8}}$	TD/FD
319	SU.I.L	0.904	0.065	1.007	0.281	0.893	0.056	0.347	0.085	1.00	0.10	FD

Table 9: Median Mass Accretion Rates:
FD vs. TD

		Subgroups by spectral ranges			
		K-M	K	M	M3 and later
FD	N	56	23	33	11
	\dot{M}	10.3	45.4	3.51	1.93
TD	N	50	13	37	18
	\dot{M}	1.76	4.77	1.50	1.34

N is the number of objects. The unit of \dot{M} is $10^{-9} M_{\odot}/\text{yr}$.

Table 10: Distribution of Properties Comparison to Taurus:FD and TD

parameter	Taurus Median	K-S test									
		Ori A			ONC			L1641			
		Median	D	p	Median	D	p	Median	D	p	
FD	n_{K-6}	-1.49	-1.33	0.13	0.14	-1.33	0.16	0.11	-1.33	0.13	0.36
	n_{6-13}	-0.87	-0.64	0.20	<0.01	-0.61	0.23	<0.01	-0.64	0.18	0.06
	n_{13-31}	-0.54	-0.66	0.15	0.05	-0.67	0.16	0.12	-0.66	0.17	0.10
	EW(10 μ m)	1.56	2.21	0.32	<0.01	2.47	0.38	<0.01	1.98	0.26	<0.01
	$F_{11.3}/F_{9.8}$	0.55	0.52	0.93	<0.01	0.52	0.91	<0.01	0.53	0.97	<0.01
TD	n_{K-6}	-1.89	-2.23	0.34	0.14	-2.18	0.36	0.15	-2.39	0.36	0.15
	n_{6-13}	-0.75	-0.52	0.17	0.90	-0.47	0.21	0.77	-0.62	0.13	1.00
	n_{13-31}	0.71	0.59	0.23	0.55	0.50	0.30	0.32	0.70	0.24	0.60
	EW(10 μ m)	4.67	3.45	0.41	0.04	3.57	0.38	0.10	3.31	0.44	0.04
	$F_{11.3}/F_{9.8}$	0.50	0.57	0.69	<0.01	0.54	0.76	<0.01	0.60	0.62	<0.01

D is the maximum deviation between the cumulative distribution of two groups. p indicates the probability that there is no significant difference between the distributions

Table 11. n_{20-31} and the projected distance (d) from θ^1 Ori C

Num.	n_{20-31}	$\sigma_{n_{20-31}}$	d (arcsec)	d (pc)	Section
1	-0.31	0.43	1075.8	2.2	DN
2	0.37	0.3	1103.5	2.2	DN
3	-1.31	0.1	966.8	1.9	CS
4	-0.82	0.21	2607.3	5.2	L
5	-1.12	0.17	1164.1	2.3	DS
6	-0.49	0.18	844.0	1.7	CS
8	-0.85	0.42	1584.0	3.2	DN
9	-0.61	0.1	800.6	1.6	CS
10	0.05	0.36	985.1	2.0	CS
11	0.91	0.15	928.1	1.9	CS
12	-0.48	0.19	2264.5	4.6	DN
13	1.8	0.34	1029.6	2.1	CS
14	-0.21	0.22	1044.2	2.1	CS
15	-1.31	0.36	664.0	1.3	CS
16	2.45	0.2	869.9	1.8	CN
17	-0.67	0.31	1006.9	2.0	CS
18	-0.23	0.46	2085.4	4.2	DN
19	0.43	0.71	680.5	1.4	CS
20	-0.24	0.27	944.1	1.9	CS
21	-0.94	0.07	1000.5	2.0	CS
22	-0.36	0.17	787.2	1.6	CS
23	-1.11	0.16	1272.0	2.6	CN
24	-0.69	0.17	678.2	1.4	CS
25	0.11	0.6	2037.6	4.1	DN
26	0.81	0.3	1405.2	2.8	DN
27	-0.37	0.24	1684.3	3.4	DN
28	-0.19	0.1	508.7	1.0	CS
29	1.48	0.22	559.9	1.1	CS
30	-0.59	0.17	1945.7	3.9	DN
31	0.66	0.06	1905.2	3.8	DN
32	1.46	0.37	773.4	1.6	CS
33	0.2	0.13	780.2	1.6	CS
34	0.18	1.25	2097.1	4.2	DN
35	1.41	0.85	866.8	1.7	CN
36	-0.67	0.23	1062.7	2.1	CS
37	-1.35	0.24	337.1	0.7	B
38	0.42	0.29	1508.7	3.0	DS
39	-0.26	1.44	1931.8	3.9	DN
40	-0.07	0.25	1670.3	3.4	DN
41	0.08	0.28	1036.5	2.1	CS
42	-1.15	0.47	1104.8	2.2	CS
43	-0.59	0.09	986.3	2.0	CS
44	0.06	0.22	1140.2	2.3	CN
45	-2.23	0.11	373.7	0.8	B
46	-0.93	1.26	325.6	0.7	B
47	2.18	0.37	351.5	0.7	B

Table 11—Continued

Num.	n_{20-31}	$\sigma_{n_{20-31}}$	d (arcsec)	d (pc)	Section
48	-0.57	0.63	1216.2	2.4	CN
49	-999	-999	235.0	0.5	A
50	-1.49	0.7	431.7	0.9	B
51	-0.62	0.21	1642.6	3.3	DN
52	-0.31	0.19	733.6	1.5	CN
53	-0.27	0.27	3374.7	6.8	L
54	-1.84	0.67	1607.4	3.2	DN
55	-999	-999	178.2	0.4	A
56	-999	-999	178.5	0.4	A
57	-0.25	0.21	1119.8	2.3	CS
58	-0.81	0.43	1873.5	3.8	DS
59	0.54	0.21	2203.8	4.4	L
60	0.21	0.34	1277.3	2.6	CS
61	-0.43	0.2	1302.4	2.6	CS
62	-1.25	0.26	1365.3	2.7	CS
63	-999	-999	209.3	0.4	A
64	-999	-999	155.4	0.3	A
65	-0.13	0.47	1631.5	3.3	DS
66	0.5	0.42	833.0	1.7	CN
67	-999	-999	187.2	0.4	A
68	-999	-999	150.4	0.3	A
70	-999	-999	238.0	0.5	A
71	-999	-999	139.0	0.3	A
73	-0.24	0.76	1035.8	2.1	CS
74	-999	-999	148.6	0.3	A
75	-999	-999	133.7	0.3	A
76	-1.15	0.19	2045.9	4.1	DN
77	-999	-999	125.7	0.3	A
78	-999	-999	150.3	0.3	A
79	-0.41	0.17	1842.5	3.7	DS
80	-999	-999	226.5	0.5	A
81	-999	-999	217.8	0.4	A
82	-999	-999	114.2	0.2	A
83	-999	-999	117.5	0.2	A
84	-0.14	0.38	1498.3	3.0	DN
85	-999	-999	223.9	0.5	A
86	0.03	0.32	807.8	1.6	CS
88	2.11	0.11	523.7	1.1	B
89	-999	-999	114.6	0.2	A
90	-0.64	0.26	373.4	0.8	B
91	-999	-999	154.5	0.3	A
92	-999	-999	104.0	0.2	A
93	-999	-999	115.3	0.2	A
94	0.31	0.37	715.3	1.4	B
95	0.13	0.13	575.9	1.2	B
96	-999	-999	227.6	0.5	A

Table 11—Continued

Num.	n_{20-31}	$\sigma_{n_{20-31}}$	d (arcsec)	d (pc)	Section
97	0.98	0.2	921.9	1.9	CS
98	-1.51	0.72	566.8	1.1	B
99	-0.34	0.49	1532.7	3.1	DS
100	-999	-999	284.3	0.6	A
101	-999	-999	315.6	0.6	A
102	-999	-999	136.9	0.3	A
103	-1.38	0.19	2191.8	4.4	DN
106	-0.89	0.23	2534.0	5.1	L
108	-0.21	0.04	1391.9	2.8	CS
112	-1.21	0.13	972.4	2.0	CS
114	-999	-999	272.9	0.5	A
117	-1.01	0.24	455.4	0.9	B
119	-999	-999	324.2	0.7	A
120	-999	-999	320.8	0.6	A
121	-0.81	0.22	1194.7	2.4	CS
122	-0.56	0.12	596.1	1.2	B
123	0.09	0.33	563.6	1.1	B
125	-1.43	0.14	948.0	1.9	CS
127	1.76	0.3	811.9	1.6	CN
128	1.08	0.19	1435.2	2.9	CN
129	-999	-999	329.9	0.7	A
131	-0.79	0.1	2258.6	4.5	DN
132	-999	-999	225.7	0.5	A
133	-0.62	0.15	2103.7	4.2	DS
134	-1.6	0.28	3675.3	7.4	L
135	-1.74	0.18	1150.5	2.3	CS
137	-999	-999	323.7	0.7	A
138	-0.59	0.18	1799.7	3.6	DN
139	-999	-999	354.6	0.7	A
140	-1.96	0.2	1223.1	2.5	CN
141	-1.59	0.17	848.1	1.7	CN
142	-1.33	0.43	982.7	2.0	CN
143	-999	-999	251.6	0.5	A
144	-0.11	0.05	919.8	1.9	CN
145	-999	-999	294.1	0.6	A
146	-999	-999	196.0	0.4	A
147	-999	-999	202.8	0.4	A
149	1.19	0.03	1024.6	2.1	CN
150	-999	-999	165.6	0.3	A
151	-1.73	0.36	3380.3	6.8	L
152	-999	-999	102.9	0.2	A
153	-999	-999	264.0	0.5	A
154	-0.38	0.29	1176.7	2.4	CS
155	-999	-999	299.1	0.6	A
156	-1.22	0.34	1312.8	2.6	CN
158	-999	-999	145.7	0.3	A

Table 11—Continued

Num.	n_{20-31}	$\sigma_{n_{20-31}}$	d (arcsec)	d (pc)	Section
159	-0.17	0.34	2153.2	4.3	DS
160	-3.12	0.84	945.4	1.9	CN
161	-0.43	0.54	2159.5	4.3	DN
162	-1.49	0.16	2109.9	4.2	DN
163	-999	-999	264.1	0.5	A
164	-0.56	0.11	1433.3	2.9	CN
165	-0.78	0.33	1713.4	3.4	DS
166	0.16	0.35	4917.0	9.9	L
167	-0.41	0.21	1110.4	2.2	CN
168	-0.52	0.06	847.6	1.7	CN
169	-0.01	0.29	2225.5	4.5	DN
170	2.56	0.41	1035.3	2.1	DN
172	0.11	0.21	2150.8	4.3	DN
173	-2.75	0.66	683.0	1.4	B
174	-0.07	0.19	1122.5	2.3	CN
175	-999	-999	260.2	0.5	A
176	-0.01	0.52	1164.2	2.3	CN
177	0.91	0.38	3608.5	7.3	L
178	-1.35	0.36	1130.6	2.3	CN
179	-0.95	0.53	1437.1	2.9	CN
180	-2.66	0.63	674.6	1.4	B
181	-0.4	0.61	1030.3	2.1	CN
182	-0.62	0.35	827.1	1.7	CN
183	-0.18	0.23	1091.9	2.2	CN
184	0.54	0.41	801.4	1.6	CN
185	-0.82	0.22	1588.6	3.2	DS
186	0.14	0.12	1348.0	2.7	CN
187	2.52	0.07	429.1	0.9	B
188	-0.57	0.27	1729.0	3.5	DS
189	-1.12	0.25	1027.2	2.1	CN
190	-0.3	0.22	1648.0	3.3	DN
191	0.14	0.02	2818.4	5.7	L
192	0.24	0.39	2192.3	4.4	DN
193	-1.88	1.91	408.7	0.8	B
194	1.11	0.54	1545.5	3.1	DN
195	-1.56	1.4	1369.8	2.8	CS
196	-0.75	0.13	4774.4	9.6	L
197	-0.08	0.27	2071.8	4.2	DS
198	-1.47	0.32	4417.6	8.9	L
199	-0.96	0.28	3189.6	6.4	L
200	-0.59	0.24	4768.6	9.6	L
201	-1.11	0.16	4160.9	8.4	L
202	-0.51	0.14	5136.4	10.3	L
203	-1.07	0.24	3300.0	6.6	L
204	-0.34	0.44	3137.6	6.3	L
205	-1.26	0.16	902.3	1.8	CN

Table 11—Continued

Num.	n_{20-31}	$\sigma_{n_{20-31}}$	d (arcsec)	d (pc)	Section
206	-0.19	0.04	4971.4	10.0	L
207	-0.32	0.17	3643.4	7.3	L
208	-0.23	0.07	3310.3	6.7	L
209	-0.54	0.11	3752.9	7.6	L
210	-0.25	0.07	2759.6	5.6	L
211	-0.73	0.9	3792.7	7.6	L
212	-0.92	0.31	4813.3	9.7	L
213	-0.52	0.03	2795.3	5.6	L
214	-1.54	0.72	801.8	1.6	CN
215	-0.56	0.17	4910.7	9.9	L
216	1.23	0.22	6512.3	13.1	L
217	-0.72	0.23	4268.4	8.6	L
218	0.04	0.28	4083.2	8.2	L
219	-0.01	0.42	3111.9	6.3	L
220	-0.47	0.2	2938.7	5.9	L
221	-0.15	0.29	2972.6	6.0	L
222	-0.55	0.22	4869.8	9.8	L
223	0.29	0.34	4057.8	8.2	L
224	-1.57	0.1	2918.1	5.9	L
225	-1.69	0.2	4315.7	8.7	L
226	-1.51	0.1	4435.3	8.9	L
227	-0.63	0.31	7372.8	14.8	L
228	0.49	0.19	5415.3	10.9	L
229	0.37	0.41	4610.5	9.3	L
230	0.22	0.28	5485.8	11.0	L
231	-1.03	0.16	5246.8	10.6	L
232	0.37	0.12	5346.8	10.8	L
233	0.45	0.15	6925.5	13.9	L
234	-0.63	0.19	6950.3	14.0	L
235	-0.96	0.07	5403.4	10.9	L
236	-0.75	0.22	6419.7	12.9	L
237	0.55	0.06	6599.7	13.3	L
238	0.01	0.12	5777.3	11.6	L
239	-0.23	0.09	9012.4	18.1	L
240	-1.37	0.48	8794.9	17.7	L
241	-0.39	0.27	6061.9	12.2	L
242	-0.54	0.11	6008.9	12.1	L
243	-0.77	0.25	6019.5	12.1	L
244	-1.28	0.22	6483.6	13.1	L
245	0.42	0.05	7745.0	15.6	L
246	-0.66	0.33	6376.8	12.8	L
247	-0.25	0.05	6811.0	13.7	L
248	-0.15	0.12	7417.2	14.9	L
249	-0.26	0.5	7535.5	15.2	L
250	-1.35	0.32	7615.6	15.3	L
251	-1.31	0.27	7589.0	15.3	L

Table 11—Continued

Num.	n_{20-31}	$\sigma_{n_{20-31}}$	d (arcsec)	d (pc)	Section
252	-0.15	0.17	7689.1	15.5	L
253	-3.86	0.99	8039.8	16.2	L
254	-1.67	0.2	7906.2	15.9	L
255	-0.53	0.43	7985.7	16.1	L
256	-0.31	0.11	7796.6	15.7	L
257	0.38	0.28	9079.9	18.3	L
258	-0.45	0.09	7950.6	16.0	L
259	0.32	0.03	10641.3	21.4	L
260	0.84	0.25	7886.8	15.9	L
261	-0.09	0.08	9536.3	19.2	L
262	-0.54	0.09	10268.3	20.7	L
263	0.06	0.47	10277.1	20.7	L
264	-0.94	0.51	9591.2	19.3	L
265	-0.91	0.57	8716.7	17.5	L
266	-0.61	0.06	10100.7	20.3	L
267	-1.22	0.16	9177.7	18.5	L
268	-0.66	0.08	7781.6	15.7	L
269	-0.24	0.05	10203.6	20.5	L
270	1.52	0.09	10308.1	20.7	L
271	1.22	0.24	9141.7	18.4	L
272	-0.52	0.53	9770.0	19.7	L
273	-0.51	0.54	10430.8	21.0	L
274	-0.6	0.23	9405.8	18.9	L
275	0.04	0.14	9449.1	19.0	L
276	-0.68	0.08	12438.3	25.0	L
277	-0.13	0.04	10303.9	20.7	L
278	0	0.28	9764.3	19.7	L
279	0.1	0.15	10039.5	20.2	L
280	-0.87	0.08	12177.2	24.5	L
281	-0.34	0.35	9986.5	20.1	L
282	-0.61	0.07	10127.9	20.4	L
283	1.42	0.22	9551.8	19.2	L
284	-1.22	0.53	10070.9	20.3	L
285	-1.18	0.35	10790.7	21.7	L
286	-0.35	0.58	12320.6	24.8	L
287	-0.25	0.29	10128.5	20.4	L
288	-0.42	0.51	10716.0	21.6	L
289	-0.32	0.09	10166.0	20.5	L
290	-0.58	0.24	10748.3	21.6	L
291	-0.35	0.34	11095.4	22.3	L
292	-0.91	0.34	12522.7	25.2	L
293	-0.39	0.53	11130.7	22.4	L
294	0.97	0.13	12986.0	26.1	L
295	-1.91	0.07	12531.9	25.2	L
296	0.35	0.04	11226.9	22.6	L
297	-0.04	0.33	12242.4	24.6	L

Table 11—Continued

Num.	n_{20-31}	$\sigma_{n_{20-31}}$	d (arcsec)	d (pc)	Section
298	-1.52	0.28	12493.9	25.1	L
299	-0.93	0.31	10869.0	21.9	L
300	0.03	0.2	12541.5	25.2	L
301	-1.05	0.28	11373.1	22.9	L
302	0.86	0.34	12270.9	24.7	L
303	1.22	0.2	12117.4	24.4	L
304	-0.25	0.08	1546.1	3.1	DS
305	-0.45	0.59	1131.4	2.3	CS
306	0.73	0.39	402.5	0.8	B
307	0.24	1.01	1071.8	2.2	DN
308	-0.49	0.09	1658.4	3.3	DN
309	-0.96	0.31	7857.7	15.8	L
310	0.13	0.24	5924.4	11.9	L
311	0.68	0.19	5403.4	10.9	L
312	1.94	5.34	2974.3	6.0	L
313	0.44	0.21	3646.4	7.3	L
314	-0.26	0.15	4176.3	8.4	L
315	-0.71	0.09	12438.3	25.0	L
316	-0.44	0.06	9630.5	19.4	L
317	-0.87	0.45	8998.1	18.1	L
318	-0.22	0.06	8194.4	16.5	L
319	0.04	0.36	9256.7	18.6	L

Note. — The region for each section is indicated in Figure 1. L indicates L1641 in Figure 2.